Petrographic consideration of the impact of the Tshipise Fault on coal quality in the Soutpansberg Coalfield, South Africa.

by

Maseda Mphaphuli

Dissertation

Submitted in fulfilment for the requirement for the degree

of

Magister Scientiae

in

Geology

in the

Faculty of science

at the

University of Johannesburg

Supervisor: **Prof Nicola Wagner**

Co-supervisor: Mr John Sparrow

January 2017

ACKNOWLEDGEMENTS

"God is not a man, that He should lie, nor a son of man, that He should repent. Has He said, and will He not do? Or has He spoken, and will He not make it good?"

Numbers 23 vs 19 NKJV

I am entirely grateful to my supervisor Professor Nicola Jane Wagner for introducing me to coal petrography, which I had no previous knowledge of, and for training me. She steered me in the right direction whenever she thought I needed it. Not only did she support me with the project but also financially and emotionally.

I am also sincerely grateful to my co supervisor John Sparrow for guiding me during my sample collection and for always being willing to help when I had questions. I would like to also acknowledge Nthabiseng Masunyana and everyone at Coal of Africa Limited, who were always willing to help with data and information that I needed for the study.

This project could not have been possible without the research grant from the Eskom Tertiary Education Support Programme (TESP) and the National Research Foundation and Department of Technology and Science (NRF-DST) Innovation Award. International Committee for Coal and Organic Petrology (ICCP) travel grant is acknowledged for providing funding to attend the 9th ICCP training course hosted in Potsdam, Germany.

I would like to express my gratitude to Mr Abraham and Ms Mapilane Madiba from the Mineral Processing at the University of Johannesburg DFC for helping with sample preparation. Zama Mthabela, Patience Moyo and Tafara Chitsiga from the Carbon Research Group, from University of the Witwatersrand, are thanked for their support and help during sample preparation and chemical analysis. Special thanks to the sample preparation team, especially Thuso Ramaliba, Lisborn Mangwane, and Baldwin Tshivhiahuvhi. Dr Christian Reinke and Dr Nomvano Mketo are also thanked for all their help in the Spetrau lab.

I would like to express my love and gratitude to my family, especially my mother and best friend Tami Mphaphuli, and my siblings, Murendeni and Aluwani Mphaphuli, for

supporting me without fail and for their encouragement during my years of study. I would not be where I am today if not for you. Special mention to my sister Zwoitwa Mphaphuli, for always believing that I could reach the stars, Te amo.

Finally, special thanks to the staff and fellow postgraduate students at the University of Johannesburg, especially my officemate Mmasetena Anna Molekwa for always being there when I needed someone to share my coal ideas with even though you did not understand coal petrography at first. I am sure now you are an expert in coal petrography. Special thanks to Ndivhuho Nendouvhada for all the fun times we had exploring the Master degree together.

CONTRIBUTION TO SCIENCE

This study has been presented at four conferences, during the study period 2015/2016:

Mphaphuli, M., Wagner, N., 2016. Variation of coal petrographic composition on either side of the Tshipise Fault, Soutpansberg Coalfield, South Africa. 35th International Geological Congress (IGC), 27- 4 September, Cape Town, South Africa.

Mphaphuli, M., Wagner, N., 2016. Mineral matter in coals from the Soutpansberg Coalfield, South Africa. The International Pittsburgh Coal Conference (PCC), 8 – 12 August, Cape Town, South Africa.

Mphaphuli, M., 2015. Petrographic consideration of the impact of the Tshipise Fault on coal quality in the Soutpansberg Coalfield, South Africa. Fossil Fuel Foundation 20th South African Conference in Coal Science and Technology, 24 – 25 November 2015, Potchefstroom, South Africa.

Hlongwane, S., Mphaphuli, M., Sebola M. J., Drennan, G., 2015. Structural and weathering effects on the coal quality in the Soutpansberg and Tuli Coalfields. Limpopo Minerals Conference and Trade Show. 10 – 12 November 2015, Park Hotel, Mokopane, Limpopo, South Africa.

ABSTRACT

The Soutpansberg Coalfield is hosted in the Karoo Basin in the Limpopo Province of South Africa. The basis of this research is to understand coal quality, coal composition, petrographic variations, and depositional environments, of coal samples from the Soutpansberg Coalfield. The Soutpansberg coals are preserved within extensive horst and graben systems and faults have exerted major structural controls on the geology. There are three major faults, the Klein Tshipise, Tshipise, and Bosbokpoort Faults. On the southern side of the Tshipise Fault, which is ENE-SWS trending, the coal exhibits higher reflectance values and coking properties compared to the coals occurring on the northern side of the Tshipise Fault, where lower reflectance values and limited coking properties occur.

Thirty five samples were collected across the coalfields of Limpopo, with the focus being the Makhado area either side of the Tshipise Fault. The coal samples were sampled from the Madzaringwe Formation in the Soutpansberg and Limpopo Coalfields. Chemical analyses (including proximate analyses, CV, and total sulphur), Free Swelling Index, petrographic analyses (maceral point, vitrinite reflectance and abnormal condition), and mineral analyses (XRD, SEM, EMPA) were conducted on the samples. The petrographic analyses were carried out using Zeiss Axio Imager M2M retrofitted with Hilgers Diskus Fossil software, at a magnification of x500 under oil immersion. The samples were scanned automatically and analysed offline using Fossil Student.

According to the UNECE classification, the rank of the coal north of the Tshipise Fault ranged from bituminous medium Rank C - A coal and coal samples south of the Tshipise Fault ranged from medium rank C to A. Most coal samples were characterised by relatively high ash, total sulphur, and volatile matter contents, and low moisture and calorific values. High FSI number was found to be associated with samples that had high volatile matter, lower ash content and higher calorific values. The maceral analysis indicated that the coal horizons are rich in vitrinite, with low inertinite and very low liptinite contents, considered to be characteristic of the Soutpansberg coals. Pseudovitrinite was observed, which is not a good indicator for coking properties.

The mineral matter identified in the coals was clay, quartz, siderite and pyrite. Samples from the northern side of the Tshipise Fault reported high total sulphur and ash values, with syngenetic pyrite being the most common mineral form. On the southern side of the Tshipise Fault, the coal is rich in silicates, with slightly higher siderite content and a dominance of epigenetic pyrite. Framboidal pyrite with concentric ring overgrowths was noted on the southern side of the fault. The overgrowths of the botryoidal pyrite were enriched in As, Ni, Pb, and Co. It is proposed that the Tshipise Fault carried fluids rich in those metal elements which precipitated around the syngenetic pyrite.

The interpretation of depositional environments using coal petrographic parameters relied on the use of "facies diagnostic" vitrinite, inertinite and liptinite macerals. The maceral facies diagnostics helped determine the Gelification Index (GI) and Tissue Preservation Index (TPI). TPI and GI indices indicated a marsh and wet forest depositional environment for most samples. The syngenetic pyrite possibly indicates marine transgression influence or ground water enriched in sulphur circulating in the peat.

TABLE OF CONTENTS

LIST OF FIGURES

LIST OF TABLES

LIST OF ABBREVIATIONS

ACA – Abnormal Condition Analysis

As – Arsenic

BL – Bottom Lower

BLB – Bottom Lower Bottom

BSE – Back Scatter Electrons

BU – Bottom Upper

Cdt – Collodetrinite

CGS – Council of Geosciences

Co – Cobalt

CoAL – Coal of Africa Limited

Cpg – Corpogelinite

Ct – Collotelinite

Cut – Cutinite

EDS – Energy Dispersive Spectrometer

EMPA – Electron Probe Micro Analyzer

FSI – Free Swelling Index

Fus – Fusinite

ICCP – International Committee for Coal and Organic Petrology

MKB – Main Karoo Basin

ML – Middle Lower

Mt – Million Tonnes

Mtpa – Million Tonnes per annum

MU – Middle Upper

Ni – Nickel

PY – Pyrite

Qtz – Quartz

RoV - Vitrinite Reflectance measurement

Sec – Secretinite

SEM – Scanning Electron Microprobe

Sid – Siderite

Sm – Semifusinite

Spr – Sporinite

T – Top Seam

Tel – Telinite

TGA – Thermogravimetric analysis

UJ – University of Johannesburg

Vdt – Vitrodetrinite

WITS – University of the Witwatersrand

XRD – X-ray Diffraction

CHAPTER 1: INTRODUCTION

1.1. Introduction

According to the World Coal Association (WCA) (2014), coal is the major fuel used for generating electricity worldwide. In 2013, coal was used to generate over 40% of the world's electricity. Approximately 15% (over 1.2 billion tonnes) of total coal production is currently used by the steel industry and roughly 70% of total global steel production is dependent on coal (WCA, 2014).

Growing energy efficiency, rising pollution worries and stiffer competition from other fuels mean that in most countries the tide is turning against coal. Europe and America have already cut coal fired generation capacity by over a fifth in a decade (The Economist, 2015). However, Wilson and Clark (2011) argue that the calls to switch from coal to gas as a way of reducing emissions is a “western rich country solution”. Developing countries have easier access to coal than gas and will need to burn coal (cleanly) to continue to develop.

South Africa depends heavily on coal for electricity generation in contrast to the developed countries like the United States and Germany. The majority of South Africa’s reserves and mines are in the Main Karoo Basin (MKB) which includes the Witbank, Highveld, and Ermelo (Mpumalanga) Coalfields (Figure 1.1). Many of the Mpumalanga Coalfields are nearing depletion and additional sources for coal supply must be developed if the South African coal industry is to continue into the 21st century (Jeffrey, 2005). Recent exploration efforts have focused on the Waterberg Coalfield, located in the Limpopo Province, which could become a major coal mining centre in the future, subject to infrastructure and water constraints (Eberhard, 2015). Coal production in the Waterberg area is anticipated to double in the next 5 years. In the Limpopo Province, other coalfields (Soutpansberg and Limpopo) are also being explored, with development of the coking coal industry as the main focus (Eberhard, 2011).

The South African coking coals are fast becoming depleted to the extent that current consumers are becoming reliant on imported supplies of good quality coking coal for the coke making purposes. The Tshikondeni (coking) Coal Mine closed in 2015 due

to end of life. The year 2008 marked the highest price for coking coal, mainly because of China's dramatic increase in production of steel in recent years and demand for coking coal (The Economist, 2015). Since 2011 there has been a drop in the price of coking coal (Figure 1.2) and coal mines have been put on ice due to poor economic feasibility of opening the mines. Two such areas affected are the Limpopo and Soutpansberg Coal of Africa Limited (CoAL) deposits. However, this quiet time has enabled reflection on the coal formation and coal quality in these understudied coalfields (Pers comm., J. Sparrow).

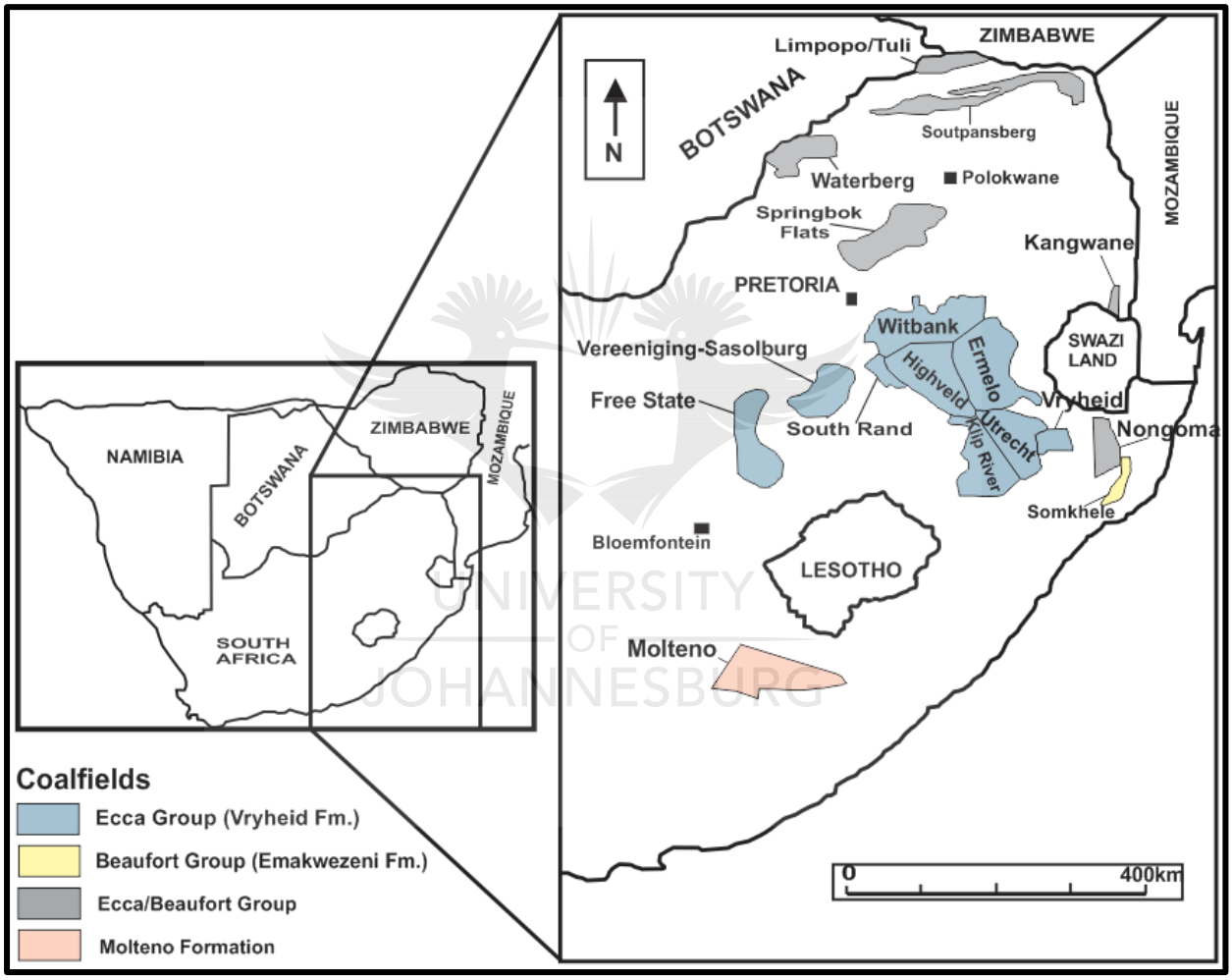

Figure 1.1: Coalfields of South Africa (modified after Hancox and Gotz, 2014).

1.2. Background to the Study area

The Limpopo Province hosts four coalfields, including: Soutpansberg, Tuli/Limpopo, Waterberg and Springbok Flats (Figure 1.1). For the purpose of this section the

background of the Soutpansberg and Limpopo Coalfields are discussed further as they are important to this study. The Waterberg and Springbok Flats Coalfields are discussed in Chapter 2 in more detail.

Figure 1.2: Drop in coal prices from 2010 to 2015 (The Economist, 2015)

Sparrow (2012) referred to the Soutpansberg Coalfield as the "forgotten basin" (Figure 1.3) situated in the north of South Africa. The Soutpansberg Coalfield has recently been explored for both thermal and coking coal markets by CoAL. Mining in the Soutpansberg Coalfield began in 1911, when the Messina Transvaal Copper Company developed the Lilliput Colliery to supply coal to the copper smelter at the mine, but closed 7 years later (Hancox and Gotz, 2014). The Council for Geosciences (CGS) prospected the coalfield from the late 1950 to late 1970's (Hancox and Gotz, 2014). Iscor carried out an extensive exploration programme, which ceased when the Tshikondeni Mine (Figure 1.3), located at the eastern side of the coalfield, was commissioned in 1983 (Saad and Pinhiero, 2001). In 2002, Rio Tinto and Kwezi started exploring in the Waterpoort area situated in western Soutpansberg. Currently CoAL has completed some 198 boreholes, a large scale exploration sample pit, and various other exploration projects in the Makhado and Vele areas, located in the central Soutpansberg and Limpopo Coalfields respectively

(Figure 1.3). CoAL's Makhado project is now at an advanced feasibility project stage (Hancox and Gotz, 2014).

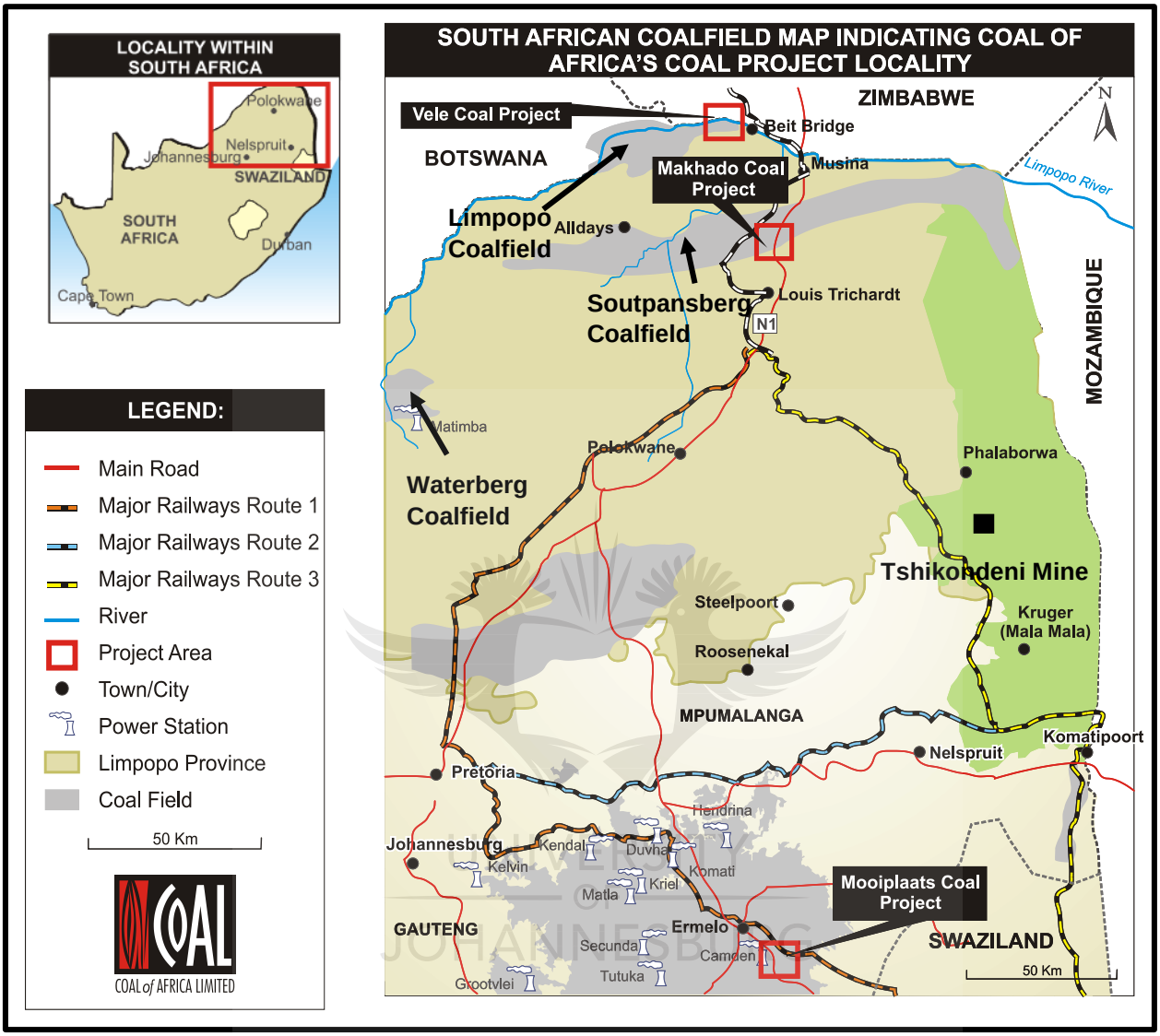

Figure 1.3: Location of the Makhado coal project (in the Soutpansberg Coalfield) and Vele Colliery (in the Tuli/Limpopo Coalfield) (Coal of Africa, 2013).

The coal deposits of the Soutpansberg Coalfield offer a rare opportunity of supplying the domestic metallurgical market with (semi-soft) coking coal. With the exception of the Tshikondeni Mine (which has recently closed), the coalfield has been neglected for many years due to the misconception that Iscor held mineral rights of the primary deposits (Saad and Pinhiero, 2001). Tshikondeni Coal Mine supplied hard coking coal to ArcelorMittal South Africa Ltd's Vanderbijlpark plant, the continent's biggest steelmaking facility (Hancox and Gotz, 2014). ArcelorMittal now needs to import "cheaper" coking coal used in steel production, because it was technically too

difficult to operate the Tshikondeni mine on a commercial basis and end of life was reached.

According to Barker (1999), the Limpopo Coalfield (Figure 1.3) (sometimes called Tuli Coalfield), is the smallest coalfield in South Africa. The coalfield was first explored by Anglo Coal in the period of 1960 and 1976 (Ortlepp, 1986). In 2008 CoAL started exploring the coalfield, and by 2010, CoAL had successfully drilled 188 slim boreholes and 28 large diameter boreholes (Hancox and Gotz, 2014). Vele Colliery, an open cast mine with a life span of 16 years was opened in 2011, with 362.5Mt mineable tonnes in situ. The mine was recently mothballed for economic reasons.

1.3. Study area

In this study, two of the Limpopo Province coalfields are considered in detail, namely the Soutpansberg and Limpopo Coalfields. The Soutpansberg Coalfield is located north of the Soutpansberg Mountain Range in Limpopo Province (Figure 1.3). According to Hancox and Gotz (2014) it extends for ± 190 km from Waterpoort (west) to Kruger National Park (east). CoAL has been exploring the area, and the study area is located in the Makhado Coal Project area (Figure 1.4). The nearest town is Makhado, situated approximately 35km to the south of the Makhado Coal Project area. Musina town is situated approximately 50km north of the Makhado Coal Project area.

The Soutpansberg Group (approximately 1850 Ma) is overlaid by the Karoo aged rocks containing the Soutpansberg coals (Hancox and Gotz, 2014). Structurally, the Soutpansberg Coalfield is a very complex area. Three major faults are recognised, that is: Tshipise, Klein Tshipise and Bosbokpoort Faults. The study will focus on the Tshipise Fault, which is an ENE SWS normal trending fault. All the faults appear to be normal and probably of post-Karoo in age (Brandl, 1981). Within the Makhado area, the study area located north of the Tshipise Fault is referred to as Voorburg, and south of the Tshipise Fault is referred to Makhado (Figure 1.4). The Voorburg area is situated in the magisterial district of Vhembe, in the Limpopo Area. For the purpose of this study is subdivided into Voorburg North and Voorburg South.

Voorburg North, located 10km north of the Tshipise Fault, represents an isolated and up-faulted block of Karoo aged sediments. Voorburg South is located between the Tshipise and Bosbokpoort Faults (Figure 1.4) (Telfer and Njowa, 2012).

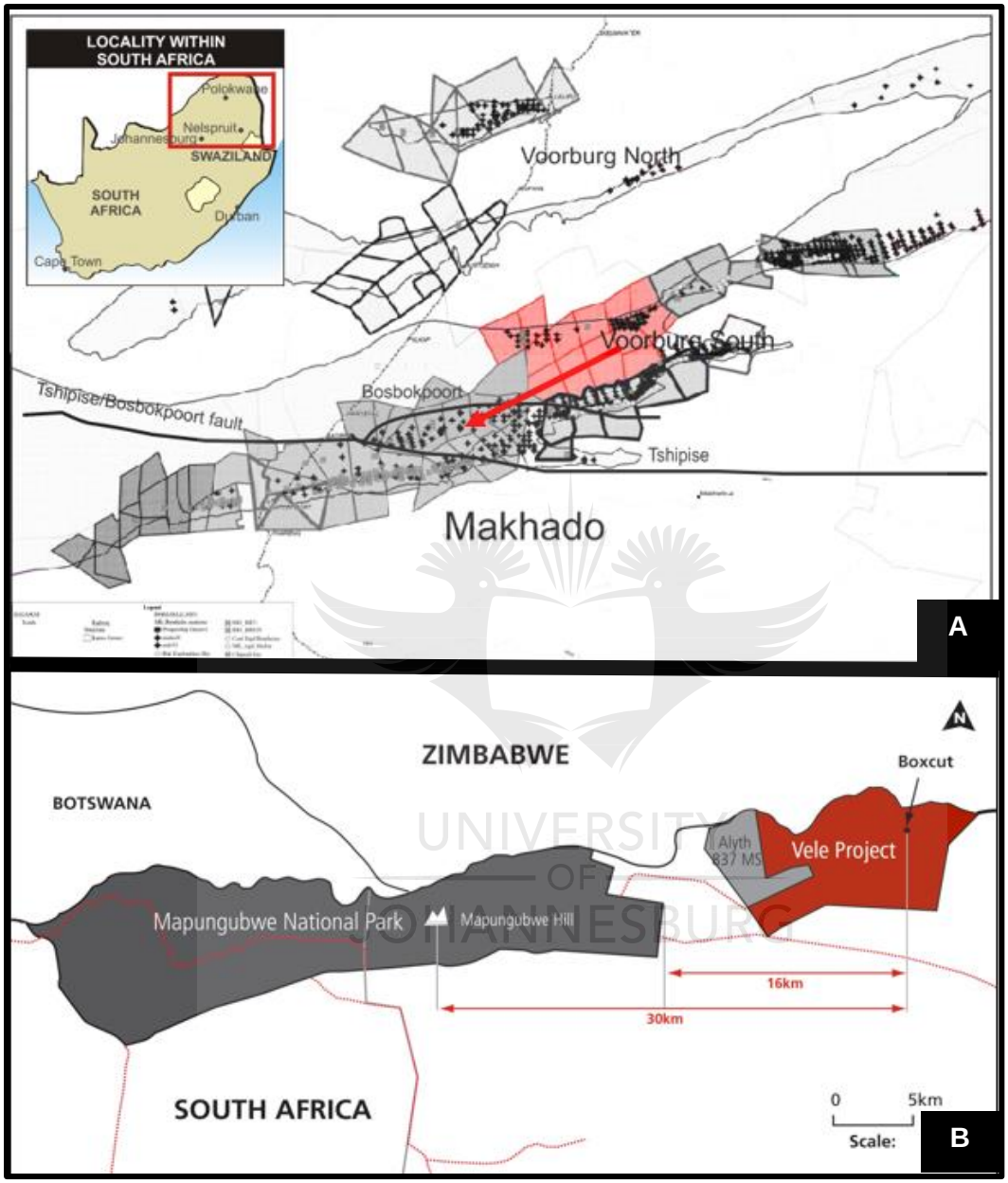

Figure 1.4: Location of A) Voorburg Area (Voorburg North, Voorburg South), and Makhado area in the Soutpansberg; and B) Vele Colliery in the Limpopo Coalfield (CoAL, 2015).

Like the Soutpansberg Coalfield, the Limpopo Coalfield is also situated in Limpopo Province, extending for ± 80km from Pont Drift in the west to Beit Bridge in the east. The Vele Colliery (Figure 1.4), located in the Limpopo Coalfield, is situated 40km south east of Musina Town and 5km east of the Mapungubwe National Park (Telfer

and Njowa, 2012). The north of the colliery is bounded by the Limpopo River, which defines the international border between South Africa and Zimbabwe. In the Limpopo Coalfield there are no major faults, although minor faulting trends east-northeast. The faults are believed to be normal (Malaza, 2013).

A sample from the Tshikondeni Mine on the eastern side of the Soutpansberg Coalfield and samples from the Waterberg Coalfield in Lephalale were included for comparative purposes.

1.4. Aim and objectives of present study

According to Hancox and Gotz (2014), there are limited studies done on the Soutpansberg Coalfield. This study will attempt to provide information on the coal quality and petrographic variation on either side of the Tshipise Fault and also attempt to explain how the Tshipise Fault has impacted the coking properties. It is also anticipated that the results acquired from the study will assist in the reconstruction of the paleoenvironment and provide a sound understanding of the coal in the coalfield. The age of the Tshipise Fault is currently undetermined but is beyond the scope of the current project; an MSc student at the University of Pretoria (South Africa) under the guidance of CoAL is researching this aspect. It is possible the Tshipise Fault system is ± 2.06 billion years old (Millonig, 2009).

As previously mentioned in Section 1.2, CoAL has been exploring the Soutpansberg Coalfield. During their exploration, they established that on the southern side of the Tshipise Fault (the area referred to as Makhado) the coal was of a higher rank with good coking properties, whereas on the northern side of the Tshipise Fault (Voorburg area), the coal was of a lower rank and the coal had limited coking properties. There is, therefore, an opportunity to investigate what caused the variations in the coal rank and the coking properties on either sides of the Tshipise Fault, and what impact the fault has had on the coal quality. The main aim of the project is therefore to understand coal quality and petrographic variations on either side of the Tshipise Fault, in the Soutpansberg Coalfield.

The objectives of the project included:

- Detailed petrographic analyses on the Limpopo Coalfield samples including a consideration of condition.
- Specific focus on reflectance analyses for the Soutpansberg samples to determine differences across the Tshipise Fault
- Characterisation of the samples using chemical analyses (proximate analyses; that is: ash, volatile matter, moisture content and fixed carbon; calorific value (CV); and total sulphur)
- The determination of the impact; if any; of the Tshipise Fault on the coking properties using Free Swelling Index (FSI)
- The consideration of mineralogical differences in the coal samples on either side of the Tshipise Fault
- An attempt to reconstruct the depositional environment of the Soutpansberg Coalfield based on samples obtained.

1.5. Scope of project

Chapter 1: Introduction chapter includes the background, study area location and aims and objective of the study.

Chapter 2: Literature review chapter provides a summary of geological setting of the study and coal geology, and considers coal petrography in detail.

Chapter 3: Methodology chapter explains were samples were collected and which methods were undertaken to meet the aim and objectives.

Chapter 4: Results and discussion in detail from analyses conducted

Chapter 5: An attempt to reconstruct the paleoenvironment using petrographic indices and references. A study by Malaza (2013) was used as a guideline.

Chapter 6: Conclusion and recommendations.

CHAPTER 2: LITERATURE REVIEW

This chapter provides information on: 1) coal utilization; 2) geological setting of the Soutpansberg and Limpopo Coalfields; 3) origin and formation of coal in South Africa; 4) coal petrography application; and 5) depositional environment. Based on the scope of the project only the coalfields to the north of the MKB will be discussed.

2.1. Coal Utilization

The principal uses of traded coals worldwide are for electricity generation and coke making. Global coal exports grew by 4.2% to reach record levels of over 1.3 billion tonnes in 2014, as steam coal exports grew by 5% and coking coal exports grew by 2.4% (WCA, 2014). In South Africa, coal remains the primary energy source for domestic power generation, and is set to dominate the energy mix for the foreseeable future. Eskom, the state-owned national electricity supply utility, generates 96% of the country's electricity from a coal base (Hancox and Gotz, 2014).

Apart from being combusted for electricity generation, coal is also a valuable source of petrochemical and non-fuel substances. By the process of liquefaction and gasification, coal can be converted to liquid fuels. The produced liquid fuels can be refined further into transport fuels and other chemical products (Horsfall, 1993). South Africa currently is one of the few countries in the world that operates commercial coal to liquid (CTL) synfuel plants, and coal is the feedstock for the production of a substantial percentage of the country's liquid fuels (Hancox and Gotz, 2014). Coal can be used for gasification to form synthetic natural gas and gas of lower specific energy (Ward, 1984).

Coal is furthermore used extensively in the metallurgical industry for steel manufacture as coking coal. For the purposes of this study, coking coal and its properties will be discussed further.

2.1.1. Coking Coal

Coking coal is coal that softens, swells, and solidifies as it is heated through the temperature range of 350^{o} C to 550^{o} C (Kruger, 2013). This gives rise to a hard,

spongy, swollen residue called coke. During the process of coking, the carbon is not oxidized while the volatile matter escapes; hence the coke is enriched in carbon (Chatterjee, 2006).

Not all coals are coking coals and only bituminous coal can produce coke. Lignite, sub-bituminous coal, semi-anthracites, anthracites, and meta-anthracites do not coke (Crelling, 2008). Coals that are to be used for conventional coke production must have three essential properties: 1) they must be within a specific range in rank, that is bituminous coal ideally in the range of 1.01 – 1.45 Rov%; 2) they must possess a high proportion of fusible macerals (> 40% vitrinite) to form a strong well-fused coke; and 3) they must have low levels of certain elements, notably sulphur and phosphorus, and be generally low in mineral matter (Thomas, 2013). According to Stach et al. (1982), coking power does not only depend on rank, but also on maceral composition.

Most of the coke produced in industrialised countries is used for metallurgical purposes, particularly in steel production as a reducing agent (Prasad, 1986). According to Taylor et al. (1998), Diez et al. (2002), and Pajares and Diez (2014), the coke produced from blends of coking coal is used to maintain the process of iron production in the blast furnace where it has three major roles, that is: 1) as a fuel, it provides heat for the endothermic requirements of chemical reactions and the melting of slag and metal; 2) to provide heat necessary for the chemical reaction that separates metal from ore; and 3) to maintain necessary permeability that allows the other two roles to function. According to Booysens (2013), South Africa has the potential to become a future coking-coal producer. As iron and steel production is expected to increase, the growth should lead to increased demand for coking coal and South Africa should be able to take advantage of the increased demand. However, this has not happened due to the decline in coking price (Figure 1.2). As a result, the anticipated Vele Colliery producing semi soft coking coal was mothballed.

In South Africa, semi soft coking coal is mined in the Waterberg Coalfield (Grootegeluk Mine) and prime coking coal was previously mined in Tshikondeni Mine in the Soutpansberg Coalfield. CoAL has been exploring semi soft coking coal and the Makhado project is in a feasibility stage. Hence, the Limpopo Province coals appear to have parameters necessary for the metallurgical industry. The next section discusses the formation of coal in South Africa.

2.2. Karoo Basin

The term Karoo is used to describe the sedimentary fill of all the basins of similar age across Gondwana; the term Karoo is extrapolated from the MKB of South Africa (Figure 2.1) (Catuneanu et al., 2005). The most complete succession of the sedimentary strata and largest coal resources are contained in the Karoo Basin (Johnson et al., 1996a; Cairncross, 2001). The coal of southern Africa ranges in age from early Permian to Mid Triassic, compared to the coals of Europe and North America which are Carboniferous in age (Falcon, 1986).

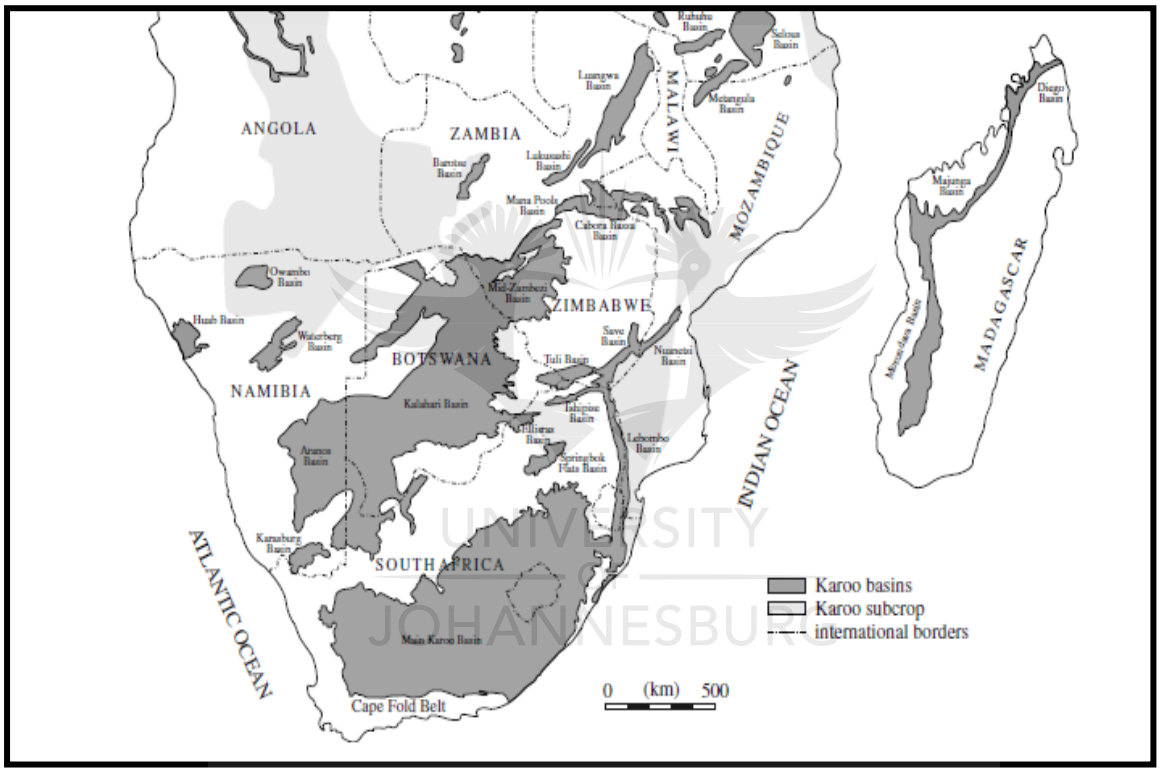

Figure 2.1: Distribution of the Karoo basin. The Karoo basins are found throughout southern Africa, with the MKB located in South Africa (Catuneanu et al., 2005).

According to Catuneanu et al. (2005), the Karoo-aged basins formed during the first order cycle of supercontinent assembly and later breakup. This occurred when Pangaea was under the influence of two different tectonic regimes sourced from the convergent margins of Gondwana. The two tectonic regimes resulted in the formation of different basin types across Africa, with accommodation generated by tectonic and dynamic loads in the south and rifting to the north. The Late

Carboniferous to Middle Jurassic Karoo Basin covers approximately one-third (that is, 700,000 km^2) of South Africa (Gotz and Ruckwied, 2013).

The MKB forms part of a major series of Gondwanan basins that developed through subduction, compression, collision, and terrane accretion along the southern margin of Gondwana (Hancox and Gotz, 2014). The MKB can be classified as a retro-arc foreland basin, situated behind a magmatic arc and associated fold-thrust belt (Johnson et al., 1996a). Apart from MKB of South Africa, all the other coal bearing southern Africa basins are extensional rift related basins, either inter or intracratonic grabens or half grabens (Cairncross, 2001). The Karoo Supergroup preserves a maximum thickness of 12 km in the south-eastern portion of the MKB (Johnson et al., 1996b).

Stratigraphically, the Karoo Supergroup can be divided into four groups, that is: 1) Dwyka, 2) Ecca 3) Beaufort and 4) Stormberg. The Vryheid Formation of the Ecca Group hosts the majority of economically extracted coals. The Volkrust Formation host coals in the northern Karoo basins (Hancox and Gotz, 2014). The Karoo basins in South Africa contain 19 different coalfields (Figure 1.1) (Barker 1999), and the MKB hosts 13 coalfields, where the major producing collieries occur. In the MKB, the depth of coal below surface is generally shallow, with most coal being less than 200m below surface; 50% of mines are open cast (Pinheiro et al., 1999). The depth increases in the south, south west and west in the Free State area. The coal seams in the Witbank, Highveld and Free State are usually low rank bituminous coals, while the Kwa-Zulu Natal and Vryheid Coalfields are anthracitic (Snyman, 1998; Pinheiro et al., 1999). Thus, the coal rank increases eastwards across the MKB (Cadle et al., 1993).

North and northeast of the MKB there are other coalfields located on the edge of the Kaapvaal Craton and the Limpopo Mobile Belt (LMB). These are the Kanganwe, Springbok Flats, Waterberg, Soutpansberg, and Limpopo Coalfields (Cairncross, 2001). Only the coalfields (that is Soutpansberg and Limpopo) pertinent to this study will be discussed in detail; a cursory review of the other coalfields follows:

- The Kangwane Coalfield (Figure 1.1) is located to the north of the Swaziland border and stretches for 70km in a north to south direction and extends for 40km. There is very limited academic work on the Kangwane Coalfield

(Hancox and Gotz, 2014). The coal hosted in the Vryheid Formation is about 10m thick and referred to as the 1 seam. The coal is of a low grade. Coal in the Volksrust Formation occurs at a depth between 300m and 400m above the 1 Seam. The seams in the Volksrust Formation are named from the bottom upwards as 2/4, 6 and 8 seams and are about 2 meters in thickness (De Jager, 1986). The strata dips between 3º and 20º towards the east and are very faulted from north to south with faults typically displacing the strata for about 100m. In addition to the faults there are dolerite dykes and sills which turned the coal into natural coke (Kwiecinska and Peterson, 2004) (Hancox and Gotz, 2014).

- The Springbok Flat is a small, fault bounded, cratonic limnic basin situated on the central Kaapvaal Craton in the Limpopo. The Springbok Flats is situated about 90 km north of Johannesburg and about 40km from Pretoria. The coal seams are best developed in the central portion of the field. The coalfield has a single coal zone which is 3m to 7m thick in the upper zone. The coal zone is located stratigraphically between the mudstone of the Beaufort Group and the siltstone of the Vryheid Formation of the Karoo sequence. The coal seams are very deep lying between 200 and 1000 m and are shale and mudstone bounded (De Jager, 1986). The Springbok Flats coals are known to contain high uranium contents (Cairncross, 2001).
- The Waterberg Coalfield is situated in the western part of the Limpopo Province of South Africa, approximately 25 km west of the town of Lephalale. The Waterberg Coalfield has an approximate 88km east to west strike length and has a north-south width of 40km. According to Cairncross (2001), the coalfield is structurally deformed, with east west and northwest southeast trending faults. The coalfield extends from the Palala shear zone in the east, to the Botswanan border in the west. The northern boundary is defined by the Melinda Fault Zone. The southern boundary is formed by the Eenzaamheid Fault Zone (Hancox and Gotz, 2014). The coal seams occur in the Vryheid and Volkrust (Grootegeluk) Formations contained in the Ecca Group. There are eleven coal zones that occur over a stratigraphic thickness of at least 110m interbedded with sandstone and mudstone. The lower five seams fall within the Vryheid Formation and the upper six within the Volksrust Formation (Faure et al., 1996). There is limited information published regarding the

overall coal qualities of the Waterberg Coalfield. However, it is known that the coal rank increases steadily from west to east with potential to produce semi soft coking coal (Jeffrey, 2005; Hancox and Gotz, 2014).

The Soutpansberg and Limpopo Coalfields are discussed in the next section in detail.

2.2.1. Geological setting of the Soutpansberg Coalfield

As indicated in Section 2.2 the deposition of the Karoo sediments occurred in two different tectonic settings. According to Catuneanu et al. (1998), the MKB sedimentary rocks are retroarc foreland fills. The basins north of the MKB are preserved in separate, fault-bounded depositories interpreted either as rift basins or intracratonic thermal sag basins (Johnson et al., 1996a; Bordy and Catuneanu, 2002).

The Soutpansberg Coalfield is preserved within a down-faulted, half graben structure, at the north-eastern edge of the Kaapvaal Craton. The shape and structure of the Soutpansberg were controlled by the east northwest and south west faults that followed the trend of the Limpopo Mobile Belt (LMB) (Hancox and Gotz, 2014). According to Malaza (2013), the Karoo rocks containing the Soutpansberg Coalfield overly the ± 1850 Ma Soutpansberg Group and Beit Bridge Complex.

The full stratigraphy of the Karoo Supergroup is preserved in the Soutpansberg Coalfield (Figure 2.2). The Tshidzi Formation of the Soutpansberg is the equivalent of the Dwyka Group in the MKB; these contain the diamictite and coarse grain sandstone. The Tshidzi Formation is overlain by the Madzaringwe Formation, which is the basal part of the Ecca Group (Hancox and Gotz, 2014). According to Sparrow (2012), Rio Tinto identified seven coal seams numbered 1 to 7 from top to bottom as indicated in Figure 2.2. The number 6 seam of the Madzaringwe Formation consists of a bright coal band, and is the economic seam. A number of coal horizons occur within a 30m to 40m thick carbonaceous zone of the Madzaringwe Formation. Six potential mining horizons (within the Number 6 seam) were identified by CoAL and are referred to as the Upper Seam, Middle Upper Seam, Middle Lower Seam, Bottom Upper Seam, Bottom Middle Seam and Bottom Lower Seam (Telfer and Njowa, 2012).

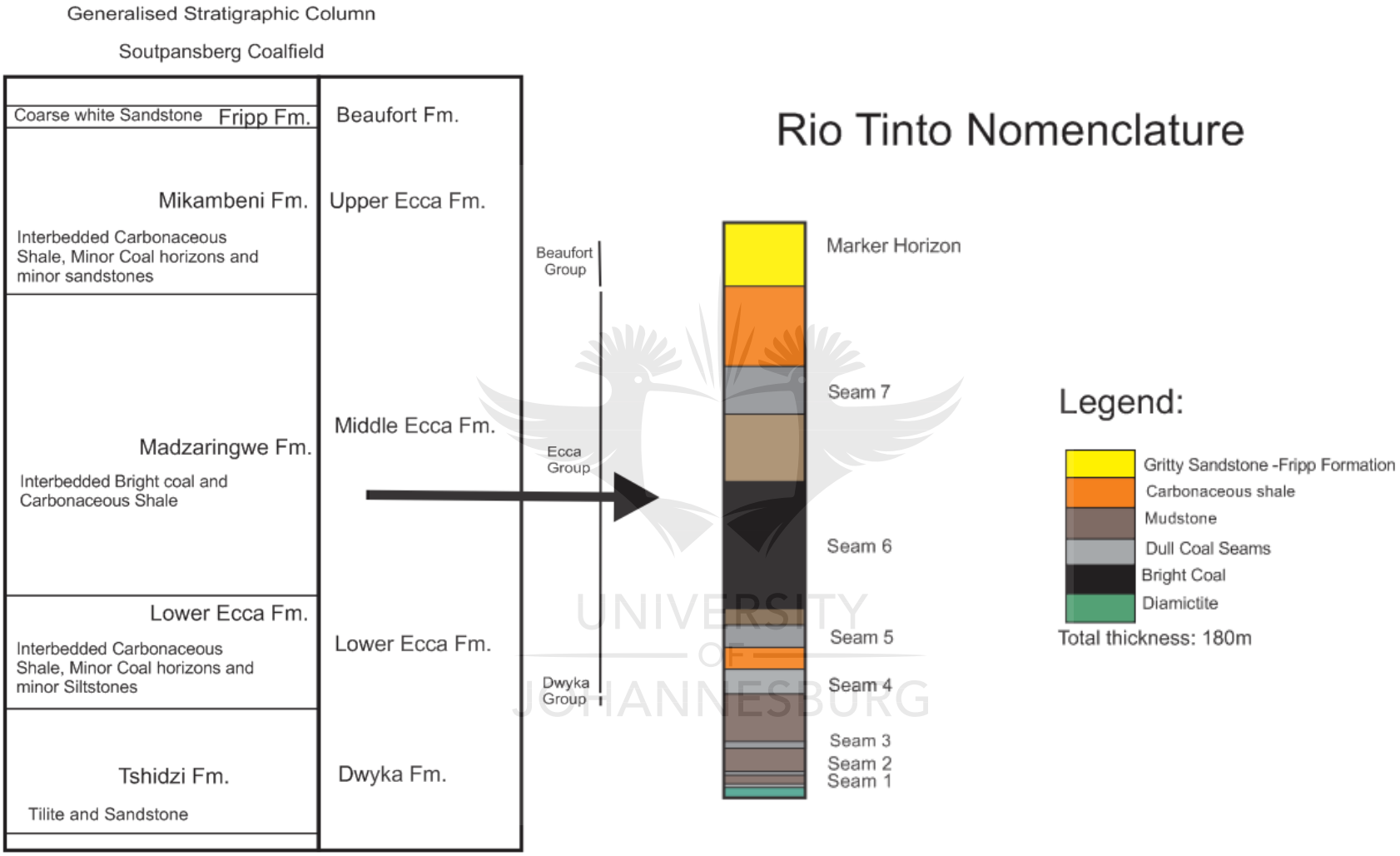

Figure 2.2: Full stratigraphy of the Soutpansberg Coalfield (modified after Sparrow, 2012).

The nature of the coal deposits gradually changes from a multi-seam coal-mudstone association, approximately 40m thick in the west and comprising up to seven discrete coal seams (Mopane Coalfield in the Waterpoort area), to two individual seams in the east (Pafuri Coalfield in the Tshikondeni area) (Telfer and Njowa, 2012). The coal is generally bright and rich in vitrinite and the coal rank increases towards the east from medium rank C to medium rank B/A. Dull coal occurs locally at the base of the multi-seam coal mudstone association in the Waterpoort area as well as in the upper part of the lower seam at Tshikondeni (Hancox and Gotz, 2014).

2.2.2. Sub-basins in the Soutpansberg Coalfield

The Soutpansberg Coalfield may be sub-divided into three separate smaller sub-basins, namely the Mopane (Western Soutpansberg), Tshipise (Central Soutpansberg) and Pafuri (Eastern Soutpansberg) sub-basins, as indicated in Figure 2.3 (Hancox and Gotz, 2014). However, Sparrow (2012) further subdivided the sub-basins into: Waterpoort, Mopane, Sand River, Mphephu, Tshipise South, Tshipise North and Pafuri sub-basin. However, the three better known sub-basins are discussed in this study. The Makhado area and Voorburg are located in the Tshipise sub-basins. Figure 2.4 provides a stratigraphy of sub-basins.

A. Mopane sub-basin

The Mopane Coalfield is 140km from east to west and 26km from north to south where it is widest (Hancox and Gotz, 2014). It comprises of a number of east-west trending half-graben structures in which the upper sedimentary rocks of the Ecca are preserved. The geology is generally broken up into fault blocks by a number of parallel strike faults (Hancox and Gotz, 2014). There has never been any commercial mining within the Mopane Coalfield. CoAL's Makhado Coal Project, once opened, would therefore represent the first mining operation in the Mopane sub-basin, and overall the second active coal mine within the Soutpansberg Coalfield, the first being the Tshikondeni Mine (Telfer and Njowa, 2012). Not much literature has been documented on seam qualities of individual sub-basins but, across the sub-basins (including the Tshipise and Pafuri) the washed coal indicate yields of 53 – 47%, with ash values of 12–10%, volatiles of 35.5–36.5%, sulphur of ~ 1.1% and swelling indices of 8.0–8.5 (Jeffrey, 2005).

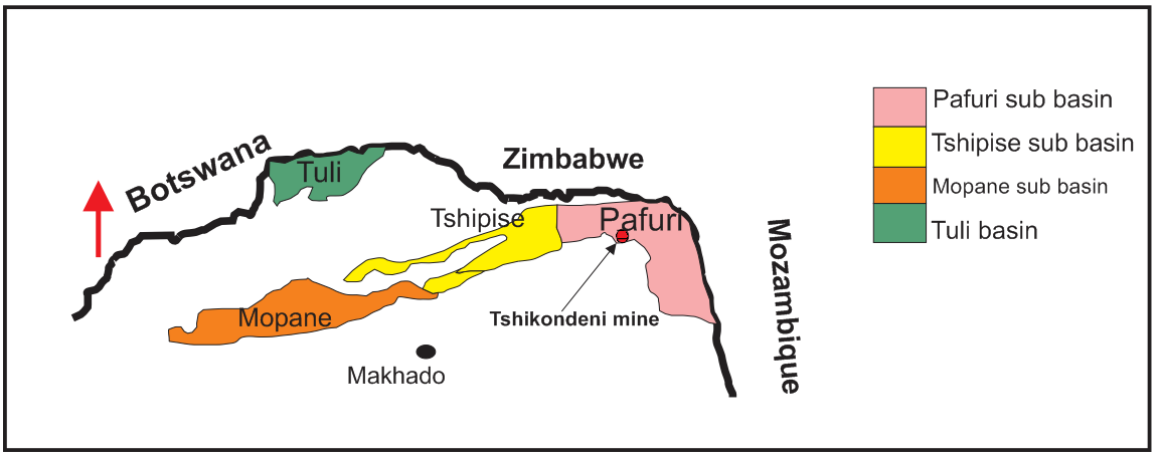

Figure 2.3: The sub-basins of the greater Soutpansberg Coalfield (modified after Meyer, 2012). Green indicating Tuli (Limpopo Coalfield); Orange = Mopane, Yellow = Tshipise and Pafuri = Pink, (making up the Greater Soutpansberg Coalfield).

B. Tshipise sub-basin

The Tshipise sub-basin lies to the north and east of the Mopani Basin (Saad and Pinhiero, 2001). Again, according to Hancox and Gotz (2014) not much work has been done in this sub-basin, and is best known from the work undertaken at CoAL's Makhado Coal Project. The stratigraphic column (Figure 2.4) of the Tshipise sub-basin is very similar to that of the Pafuri sub-basin, except that the coal-bearing interval is dominated by shale, mudstone and siltstone (Telfer and Njowa, 2012). The coal seams are also complex, consisting of alternating bands of coal and mudstone, and the coal bands display the same trend of decreasing vitrinite content (from 90% to 80%) with increasing depth. The raw coal has an ash content of approximately 25% (Hancox and Gotz, 2014).

C. Pafuri sub-basin

The Pafuri sub-basin is 109 km from east to west and is 26 km from north to south at its widest, extending from a point midway between the towns of Makhado and Musina eastwards. The Pafuri sub-basin hosted the Exxaro's Tshikondeni Mine and the geology of the area is best known from work associated with this mine (Hancox and Gotz, 2014). Tshikondeni underground coal mine, situated 140km northeast of Musina, alongside the Kruger National Park, exploited the coking quality coal of the Main Seam. Structurally, the Tshikondeni Mine was very complex, with faulting and dolerite intrusions having a significant impact on mining in terms of displacement and devolatilisation of the coal (Telfer and Njowa, 2012).The mine was a prime coking coal producer.

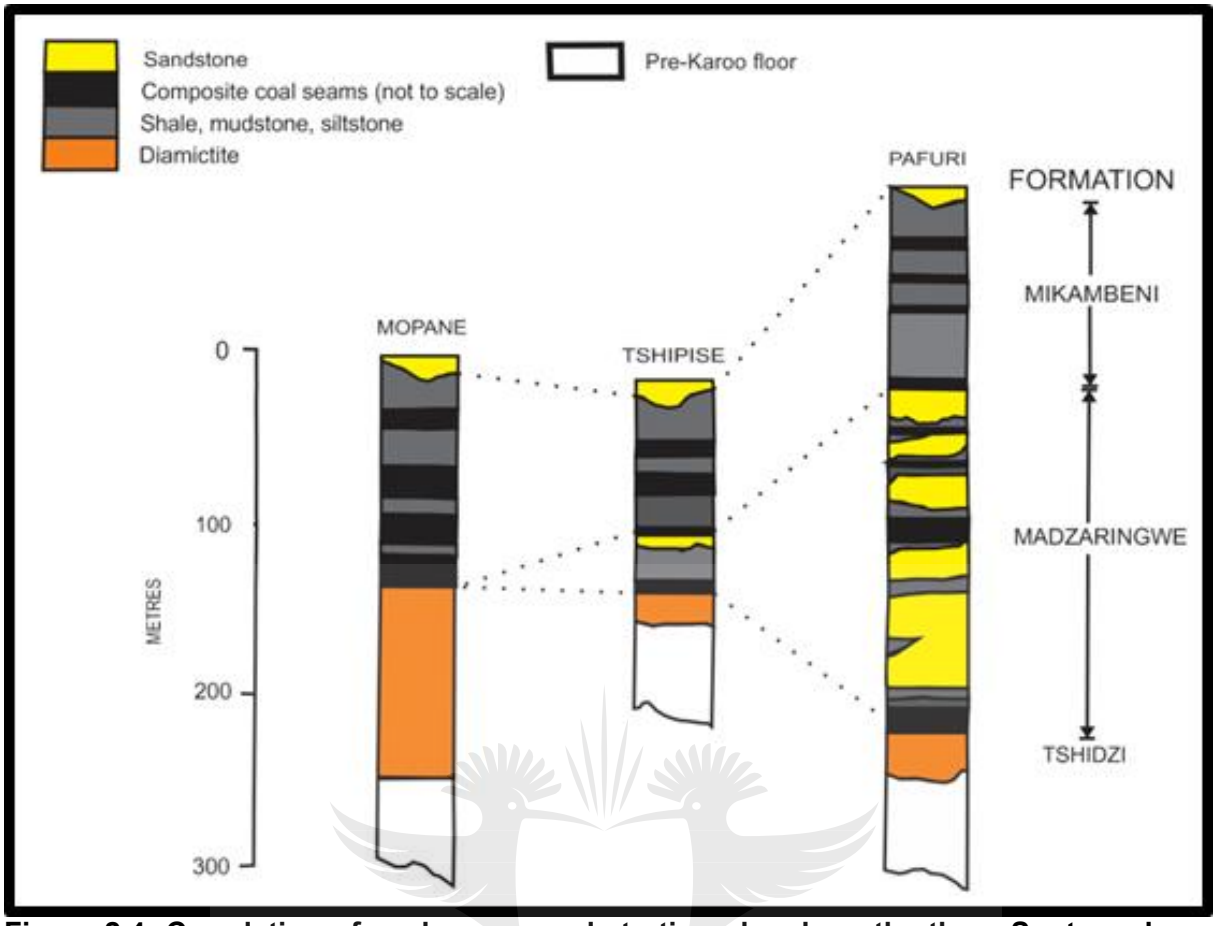

Figure 2.4: Correlation of coal seams and stratigraphy along the three Soutpansberg sub-basins (Modified after Meyer, 2012).

2.2.3. Structure of Soutpansberg Coalfield

As previously indicated, the Soutpansberg Coalfield is structurally complex. Movement along the Limpopo Mobile Belt due to continuous tension in the Karoo era, caused fault zones to occur and controlling the formation of the Karoo sediments (Malaza, 2013). Intense block-faulting caused the development of a series of stepped half-grabens and these are now seen as repeatedly occurring narrow strips of Karoo rocks mostly around the Soutpansberg Basin Karoo. The fault systems are thought to have been present before the deposition of the Karoo and a series of reactivation faults after the formation of the coal.

Within the Soutpansberg Coalfield there are two major structural systems: one system is composed of faults which trend East-North-East, parallel to the regional strike, and delineate major horst and graben structures. According to Brandl (1981) and Hancox and Gotz (2014), three notable faults occur within the Soutpansberg Coalfield, namely: Tshipise, Klein Tshipise and Bosbokpoort Faults (Figure 2.5).

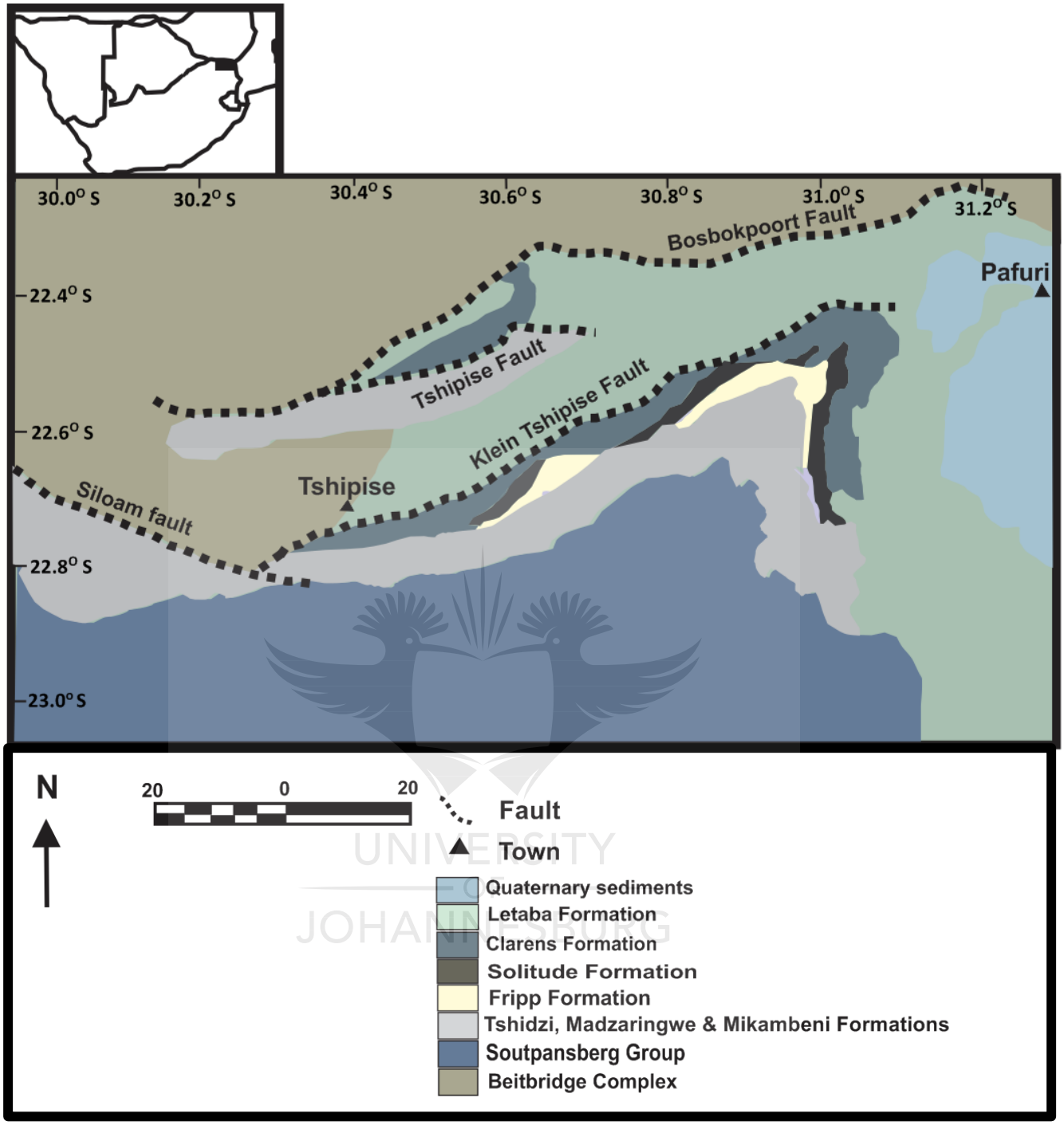

Figure 2.5: Geology of the Tshipise basin, indicating the three major fault system, i.e., Tshipise, Bosbokpoort, and Klein Tshipise Faults, tending ENE – SWS, and the Siloam Fault Trending WNW - NW (modified after Malaza et al., 2013).

Vertical throws of between 60 m and 200m occur leading to the formation of horst and graben structures. As previously mentioned, the Tshipise Fault is east-north-east (ENE) to south-west-south (SWS) trending fault. The Tshipise Fault joins up with the east north easterly trending Bosbokpoort Fault.

A second system is oblique to the regional strike and has faults trending West-North-West (WNW) to North-West (NW) and the most prominent fault is the Siloam Fault (Figure 2.5). There is not much literature on the Tshipise Fault; the age of the fault is unknown but all the faults affecting the Karoo strata appear to be normal and most are probably of post-Karoo in age (Malaza, 2013). This faulting, which controlled graben formation, continued during the deposition of the Karoo sediments and was reactivated in post-Karoo times, resulting in a very complex structural setting trending Bosbokpoort Fault.

2.2.4. Local geology of Makhado and Voorburg.

In the Makhado Coal Project area, the coal horizon/seams dip northwards at approximately 12° (Figure 2.6) (Brown, 2013). Major faults mark the western and eastern limits of the resource area along strike. The frequency of smaller scale faulting is not well understood (Telfer and Njowa, 2012). No commercial mining has taken place at Makhado, but mining in the Makhado Coal Project area was scheduled to commence production by the end of 2016 and is expected to produce 2.3 million tonnes (Mt) of coking coal and 3.2Mt of thermal coal a year, processing approximately 12.6 million tonnes per annum (Mtpa) of run-of-mine over an estimated mine life of 16 years (Brown, 2013).

The Voorburg Area is situated in the magisterial district of Vhembe, in the Limpopo Area. The nearest town is Musina, situated approximately 30km to the northeast of the Voorburg Area. The Voorburg Project represents an isolated and up-faulted block of Karoo aged sediments, which lies approximately 10km to the north of the remainder of the coalfield. The basin represents a half graben with an unconformable southern contact and a fault bounded northern contact (Telfer and Njowa, 2012).

The coal bearing sediments occur as alternating mudstone laminae and coal bands within the Upper Ecca or Mikambeni Formation. The coal bearing strata are overlain by red shales and mudstones belonging to the Beaufort Group.

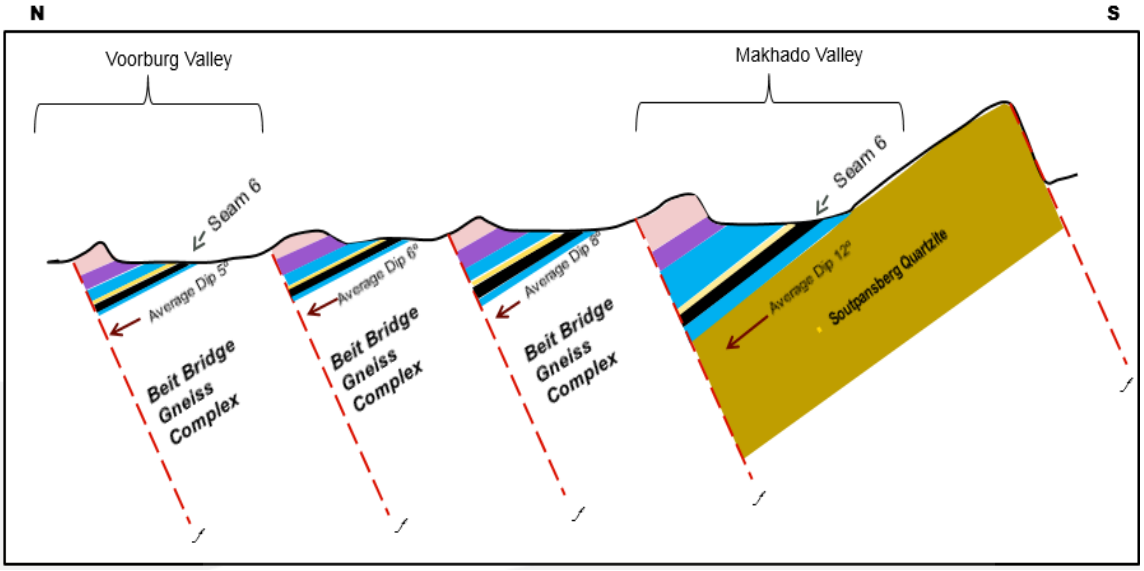

Figure 2.6: Schematic cross section through the greater Soutpansberg Coalfield (modified after Sparrow, 2012).Seam 6 represents the 6 mining horizons identified by CoAL.

2.2.5. Geological setting of the Tuli/Limpopo Coalfield

The Limpopo Coalfield forms part of the greater Tuli Basin that extends northwards into Zimbabwe and Botswana. It is represented in South Africa by only a relatively narrow deposit of Karoo Supergroup rocks on the right hand bank of the Limpopo River (Hancox and Gotz, 2014). The Limpopo Coalfield is generally fault bounded, with the southern extent of the basin controlled by erosion. Deposition of Karoo sediments occurred with concurrent movement of the pre-existing fault planes. This resulted in highly truncated sequences of lithologies. The lithologies are distinctly different to those that are encountered in the MKB, to the south in the Mpumalanga Province (Telfer and Njowa, 2012).

The structure of the Tuli Basin reflects the east west regional structural trend of the LMB. Dwyka-aged glacial deposits of the Karoo Supergroup have been deposited on the irregular Archaean basement and are overlain by Ecca equivalent arenaceous mudstones and laminated sandstones. The general stratigraphy of the area is represented by or correlated to the Molteno, Beaufort, and Ecca Formations of the Main Karoo Sequence (Bordy, 2005).

The Madzaringwe Formation hosts the Main Coal which is approximately 15m thick. There are three distinct coal horizons that occur in the Main Coal Zone of the Madzaringwe Formation. Sparrow (2012), named these horizons: Top, Middle and

Bottom Coal Horizons. All three coal horizons comprise interbedded coal and mudstone units with varying coal quantities and qualities. The coal zone can be subdivided into three sections or composite seams (Hancox and Gotz, 2014).

In Vele Colliery, the Top, Middle and Bottom horizons are recognised. The Top and Bottom Seams can be further differentiated into Top Lower, Top Middle and Top Upper, Bottom Lower and Bottom Upper Seams. The Top Middle and Top Upper Seams are not considered economic. Individual sub-seams can be correlated over the entire area. The Bottom Seam lies directly over the glacial Dwyka-aged sediments or granite-gneiss basement. The coal seams generally dip gently at not more than 2°N but this can increase to 10°N near faults. A series of dolerite dykes trend east-west over the Colliery site and the largest is over 15m thick. The dykes do not appear to have caused any displacement but have devolatilised the coal in their vicinity (Teffer and Njowa, 2012).

2.3. Coal origin and formation

Having addressed the study area in detail, attention now turns to a discussion on coal. Coal is a combustible sedimentary rock, composed essentially of lithified plant debris (Ward and Suaréz-Ruiz, 2008; Pajares and Diez, 2014).Coal consists predominantly of organic matter, largely derived from a variety of plant remains (higher plants, ferns, fungi, and algae) and different tissues (leaves, stalks, woody trunks, bark, pollen, spores, sclerotia, resins, etc.) with associated mineral constituents (Pajares and Diez, 2014). The plant debris was originally deposited in a swampy depositional environment to form soft, spongy sediment called peat (Stach et al., 1982; Suaréz-Ruiz and Ward, 2008).

Coal is found in deposits called seams that originated through the accumulation of vegetation that has undergone physical and chemical changes. These physical and chemical processes are caused by compaction and elevated temperatures with prolonged burial at depths of up to several kilometres and over periods of up to several hundred million years that changed the peat into coal through a process referred to as coalification or rank advance. For an organic rock to form there must be a source of organic matter available, and the organic matter must be preserved during the process of deposition, diagenesis and coalification. Most coal seams

originate from peat deposited in mires (Taylor et al., 1998). Mire is a swampy environment that contains the conditions necessary to allow peat to form and collect into more or less thick beds (Schweinfurth, 2009).

2.3.1. Peat formation

Miller (2005) and Ghosh and Prelas (2009) discuss two theories for the accumulation of the vegetal matter that gives rise to the coal seams. The first theory, and the one that explains the origin of most coals, is that the coal formed *in-situ*, and such a deposit is said to be autochthonous in origin. Most coal deposition commenced with thick peat bogs where the water was nearly stagnant and plant debris accumulated. Vegetation tended to grow for many generations, with plant material settling on the swamp bottom and being converted into peat by microbiological action. After some time, the swamps became submerged and were covered by sedimentary deposits (sands and muds), and a new future coal seam was formed. When this cycle was repeated, over hundreds of thousands of years, additional coal seams were formed.

These cycles of accumulation and deposition were followed by digenetic and tectonic actions and, depending upon the extent of temperature, time, and forces exerted, formed the different ranks of coal observed today. While the formation of most coals can be explained by the autochthonous process, some deposits are not easily explained by this model.

Some coals appear to have been formed through the accumulation of vegetal matter that has been transported by water (Taylor et al., 1998). According to this theory, the fragments of plants have been carried by streams and deposited on the bottom of the sea or in lakes where they build up strata, which later become compressed into solid rock. This is termed allochthonous (Miller, 2005).

2.3.2. Coalification

Coalification is the process of alteration of organic matte that takes place under conditions of raised temperature and pressure. This results in the transformation of the original peat swamp through the progressive stages of brown coal, sub-bituminous coal, and bituminous coals to anthracites and meta-anthracites. The level that coal has reached in this coalification series is termed its rank (Williams et al., 2000). The temperature changes can be achieved in two ways; that is: direct contact of the coal with igneous material either as minor intrusion or deep seated major

intrusion; and rise in temperature can also be associated with the depth of burial heat from and geothermal heat from earth's crust (Thomas, 2002).

In the early stage of accumulation and degradation (or biochemical coalification) certain factors can influence the formation of coal; these factors are (Falcon, 1986):

- tectonic control and sedimentary environments
- plant communities
- prevailing climatic conditions and
- geochemical conditions such as water level, Eh and pH conditions, and salinity.

All these factors control the rate and degree of degradation of plant matter, and the types and proportions of the organic and inorganic components which characterise the coal during the remaining stages of maturation.

2.3.3. Coal formation in South Africa

The coals in South Africa were formed during the Permian, and the Permian swamps existed under cold to cool temperature conditions associated with the waning of a massive ice age (Falcon, 1986). The majority of coals in South Africa are bituminous with some anthracite located in the KwaZulu Natal coalfields (Jeffreys, 2005).

The coal bearing sediments were deposited in a relatively stable continental depression in the form of shallow cratonic basins, intercratonic and fault bounded grabens and shorelines deposits along the margins of shallow inter-continental seas (Falcon, 1986).

Abundant river channels meandered through the peat swamps bearing abundant fine sediments from melting glaciers in the local highlands (Falcon, 1986). This resulted in marked fluctuations in the water level, changing geochemical factors (Eh, pH), rapid variations in mineral content, and in the drift and in situ sites of plant accumulation (Falcon, 1986). The Permian Karoo Basin of South Africa contains approximately 60 Gt of in situ coal and, within this; the Witbank Basin contains about 16.2 Gt. Most of this coal occurs as part of the Vryheid Formation. The number 2 seam appears to have been largely hypautochthonous or allochthonous

accumulated (Glasspool, 2003). In the Waterberg Coalfield, the Vryheid Formation is allochthonous and the Grootegeluk Formation autochthonous (Jeffrey, 2005).

The palaeoenvironment of the Permian coals changed from glacial, to marine, fluviodeltaic, fluviolacustrine, to dry–wet desert conditions (Cadle et al., 1993). In the MKB, coals accumulated in fresh to brackish mires with low subsistence rates and well-drained mires, resulting in oxidation of the peat and microbial degradation, and hence the high inertinite content on a regional scale (O'Keefe et al., 2013). North and North East of the MKB, coals are rich in vitrinite. The degradation was rapid allowing for gelification of coal (Falcon 1986).

2.4. Coal petrography

Coal is heterogeneous and it can be composed of a number of different microscopic organic constituents known as macerals (Stach et al., 1982; Falcon and Snyman, 1986; Suaréz-Ruiz and Ward, 2008; ICCP, 2011). Most coals have heterogeneous structure that is visible in hand specimen (lithotype), but the details of composition can be revealed when studied under the microscope (Stach et al., 1982). Coal petrography is defined by Falcon and Snyman (1986) as the study of microscopic organic and inorganic constituents in coal and the degree of metamorphosis (rank) of which they have been subjected to their burial. These studies may be extended to include: the physical, chemical, and technological properties of these microscopic constituents, which when combined contribute to the properties of the seam and digenetic interpretation derived from them regarding the original conditions of coal formation and the subsequent history of seams. In this section macerals and mineral matter in coal will be discussed.

2.4.1. Macerals

According to Stach et al. (1982), Ward (1984), Crelling (1989), Diessel (1992), Taylor et al. (1998), Scott (2002), and ICCP (2011, 2015), the maceral concept was first introduced by Mary Stopes in 1935. Macerals were defined by the ICCP 1994, as the smallest recognisable organo-petrographic entities in coal and other sediments using the optical microscope (ICCP, 2011). Some macerals may represent preserved forms or structure of the remains of plants that formed the coal, while other macerals

are degradation products (Taylor et al., 1998). Macerals are usually small, commonly less than a hundred microns in diameter, and well mixed together (Crelling, 1989).

According to Stach et al. (1982), reflectance, colour, shape, relief or polishing hardness are parameters that can be chosen to distinguish macerals from each other. Three maceral groups are identified, that is: vitrinite, inertinite, and liptinite. Each of the three maceral group differs from the other in terms of both chemical composition and optical properties. The ICCP 1994 defined a maceral group by level of reflectance. The maceral subgroups are defined by degree of destruction, and macerals themselves are defined by morphology (external shape and internal structure) and by degree of coalification. Hence, maceral groups are subdivided into macerals (Table 2.1) based on their reflectance, degree of destruction/preservation of original material, presence of cellular structure, gelification, and morphological features (Suaréz-Ruiz and Ward, 2008). The macerals within a maceral group have a smaller range of properties compared with the main maceral group. Each maceral group is discussed further.

i. Vitrinite

The vitrinite maceral was defined by the ICCP (1998) as grey in colour with reflectance generally between that of the associated darker grey liptinite and lighter grey inertinite over the rank range in which the three respective maceral groups can readily be recognized (ICCP, 1998). The precursor of vitrinite is huminite. Vitrinite macerals are derived from the cell wall material (woody tissue), cellulose and lignin of plants. It is a coalification product of humic substances that originated from lignin and cellulose of plant cell walls (Taylor et al., 1998). The structure is difficult to see because of the extreme processes of gelification (Falcon and Snyman, 1986).

Vitrinite is distinguished from the other maceral groups primarily on the basis of its morphology, but the morphology of vitrinite in coals varies widely. Thus, although the distinction of vitrinite from other maceral groups in coals is made primarily on morphological grounds, in practice, reflectance is commonly the most important criterion used to identify any given field. In high rank coals, the vitrinite maceral is difficult to distinguish from other maceral groups (ICCP, 1998).

Vitrinite fluorescence is dependent on the rank of the coal. Vitrinite fluoresces from 0.5 random reflectance and in coals >1.2 rov% the fluorescence declines (ICCP, 1998).

Table 2.1: Maceral groups, sub-groups, and macerals (ICCP, 1998, 2001, Pickel et al., 2017).

Maceral group	Maceral sub group	Maceral
Vitrinite	Telovitrinite	Telinite
		Collotelinite
	Detrovitrinite	Vitrodetrinite
		Collodetrinite
	Gelovitrinite	Corpogelinite
		Gelinite
Inertinite	Not sub groups : (with plant cell structure)	Fusinite
		Semifusinite
		Funginite
	(lacking plant cell structure)	Secretinite
		Macrinite
		Micrinite
	(fragmented inertinite)	Inertodetrinite
Liptinite		Cutinite
		Suberinite
		Sporinite
		Resinite
		Exsudatinite
		Chlorophyllinite
		Alginite
		Liptodetrinite
		Bituminite

The vitrinite maceral group consists of three main subgroups, namely: telovitrinite, detrovitrinite, and gelovitrinite:

- Telovitrinite subgroup comprises of vitrinites with preserved botanical cell structures which may or may not be visible (ICCP, 1998). The subgroups can further be subdivided into two macerals, that is: telinite and collotelinite (ICCP, 1998). The two are distinguished by their different degree of geochemical gelification. Telinite has clearly recognizable cell walls; collotelinite is of almost structureless (Falcon 1986).

- Detrovitrinite subgroup consists of finely fragmented vitrinitized plant remains occurring either isolated or cemented by amorphous vitrinitic matter. Two macerals, collodetrinite and vitrodetrinite belong to this group (ICCP, 1998). Collodetrinite displays the clearly visible and separate particles of vitrinite,

occurring isolated or cemented by amorphous vitrinitic matter or minerals; vitrodetrinite is characterised by aggregates or a groundmass of vitrinite in which boundaries of individual particles can no longer be distinguished without etching because of gelification (ICCP, 1998).

- Gelovitrinite is described by colloidal infillings of vitrinitic material in former voids. The subgroup is subdivided into corpogelinite and gelinite macerals. Corpogelinite describes oval discrete bodies occurring in situ or isolated within the coaly or mineral matrix; the gelinite describes secondary homogeneous infillings of microfissures, cleats or other formerly empty spaces (ICCP, 1998).

Pseudovitrinite is another less common vitrinite form observed and is used to describe vitrinite-like material of characteristic texture and optical properties (Benedict et al., 1966). Pseudovitrinite is fairly frequently observed in South African Permian-age coals (Kruszewska, 2003), identified by desiccation cracks or slit like openings in the collotelinite. Desiccation cracks observed are of different sizes or length and orientated in different directions. According to Stach et al. (1982), Gurba and Ward (1997), Taylor et al. (1998), Ryan (2003), Mastalerz and Drobniak (2005), and O'Keefe et al., (2013) pseudovitrinite has a vitrinite reflectance at least 0.025% higher than typical vitrinite.

Pseudovitrinite is thought to have formed by primary oxidation drying out or desiccation during periods of low water table in peat formation (Falcon and Snyman, 1986). The exact origin of pseudovitrinite remains uncertain although it may have originated from the same or similar woody precursors as collotelinite (O'Keefe et al., 2013). Kaegi (1985) explained that pseudovitrinite was produced during the oxidation of coal rather than precoalification. It is important to take note of pseudovitrinite in this study as it could be used to explain any anomalies in the coking properties of coal (Stach et al., 1982). Benedict et al. (1966), considered pseudovitrinite as semi inert and similar to semifusinite in the coke production process.

Coals north of the MKB (Limpopo Province area) are rich in vitrinite in comparison to the Mpumalanga coalfields that are rich in inertinite (Kruszewska, 2003).

ii. Inertinite macerals

The inertinite macerals are derived from plant material that has been strongly altered and degraded in the peat stage of coal formation (Taylor et al., 1998; ICCP, 2001).

For example, fossil charcoal is believed to form the inertinite maceral fusinite. The inertinite macerals have the highest reflectance of all the macerals in bituminous coals and are distinguished by their relative reflectance and structure (Falcon and Snyman, 1986). Inertinite has the same precursor plant material as vitrinite, but was subjected to intensive desiccation, varying degrees of oxidation and partial burning of vegetal matter (Diessel, 1992). Inertinite can be subdivided into: fusinite, semifusinite, funginite, secretinite, macrinite, micrinite, and inertodetrinite as indicated in Table 2.1.

- Fusinite displays well preserved wood cells; however, these cells are frequently broken and referred to as bogen structure (ICCP, 2001). Fusinite shows the highest reflectance of all macerals under the microscope (Diessel, 1982) and is believed to represent the charred fossilised wood resulting from ancient forest fires (Taylor et al., 1998).
- Semifusinite is a product of partial degradation of woody material as a result of complete combustion or following decomposition in sub aerobic conditions (ICCP, 2001). The term semifusinite is used for macerals that have suffered only partial fusinization (increase in carbon) (Diessel, 1982). It occurs in layers and lenses or as cell fragments.
- Funginite is derived from fungal spores, sclerotia, mycelia and other fungal tissue (ICCP, 2015). It is not common to totally absent South African coals.
- Secretinite is a maceral of the inertinite maceral group which is composed of commonly round, vesicled to non-vesicled, and equant to elongate bodies without obvious plant structure. Secretinite may be as small as 10 microns; commonly it is 60 – 400 μm. It may show characteristic fractures and may have an oxidation rim of lower or higher reflectance.
- Macrinite occurs in the form of rounded particles, or elongated pieces of groundmass, and possesses no cellular structure. Macrinite forms from a completely gelified plant material which was fusinitised. This results in a wide array of reflectance and degrees of gelification (Falcon and Snyman, 1986).
- Micrinite consists of small rounded grains less than 1 micron in diameter that may have originated in various ways (ICCP, 2001). The origin is possibly from solid residual matter that remains after devolatilisation during coalification of the liptinite macerals or during maturation hydrocarbons generated from

bituminite, leaving highly reflecting relics (mostly micrinite) as dehydrogenated residual product (Falcon and Snyman, 1986; Pickel et al., 2017).

- Inertodetrinite occurs as discrete small inertinite fragments of varying shape with particles <10 microns.

Coals in the Permian Karoo Sequence of southern Africa typically have high inertinite content, with variable semifusinite and vitrinite contents (Cadle et al., 1993). However, according to Falcon (1986), as much as 60% of the inertinite group macerals may be classified as semi-reactive macerals.

iii. Liptinite

The liptinite maceral group was previously known as exinite. The dominant petrographic feature of the liptinite group of macerals is that they all have a reflectance that is lower than the vitrinite macerals in the same coal and that they have a characteristic fluorescence when illuminated with ultraviolet blue light (Diessel, 1982; Pickel et al., 2017). Liptinite macerals show the highest content of hydrogen of the maceral groups (Suárez-Ruiz, 2012). The liptinite macerals are dark grey to black under reflected light; as the rank increases, so does the reflectance of liptinite. When illuminated with blue light, the liptinite appears greenish yellow in low rank coals to orange in high rank coals (Pickel et al., 2017).

The liptinite macerals are believed to be derived from the waxy and resinous parts of plants such as spores, cuticles, and resins (Taylor et al,. 1998), which are resistant to weathering and diagenesis. The phyteral nature of the liptinite macerals is the main basis on which they are classified into sporinite, cutinite, resinite, alginate, suberinite, exsudatinite, chlorophyllinite, liptodetrinite, and bituminite. Sporinite and cutinite are briefly discussed:

- Sporinite is the term given to spore and pollen coats. Morphologically, the material preserved most commonly is the spore or pollen exines and more rarely the entine may be preserved (Falcon and Snyman, 1986).
- Cutinite is formed from cuticles, waxy protecting cover on leaves and young shoots (Diessel, 1982). Thin cutinite shows fluorescence that is less intense than that from thick cutinite. Cutinite has long chain structures that are waxy in nature. It is probable that during coalification, waxy alkanes can be generated

from cutinite. They do not occur on plants which grow under water (Falcon and Snyman, 1986).

In southern African coals, liptinite maceral content rarely exceeds 7% (volume) of the total maceral composition under incident (white) light analysis (Kruszewska, 2003). Southern African coals rarely contain resinite, alginate, suberinite, exsudatinite, chlorophyllinite, liptodetrinite, and bituminite and hence, are not discussed.

2.4.2. Minerals

Mineral matter refers to the inorganic material in coal (Ward, 2002). Macerals in coals are accompanied by inorganic components that may appear as fine disseminations and as discrete partings (Suárez-Ruiz, 2012). According to Ward (2002), mineral matter in coal is a product of the process associated with peat accumulation as well as subsequent processes. The mineral matter in coals has been differentiated on the basis of its origin into two major categories: intrinsic inorganic matter which was present in the original plant tissues and extrinsic or introduced forms of mineral matter that can be primary or secondary (Suárez-Ruiz, 2012). Minerals are introduced into peat in the following ways: 1) fallen or blown in by gravity, 2) washed in by periods of floods, 3) transported in solution; 4) change in chemical environments in peat due to marine or fresh water influences; and 5) due to secondary alteration of minerals (Diessel, 1992). The common minerals groups found in coal seams are silicates, sulphides, and carbonates (Stach et al., 1982). Other mineral groups, such as phosphates, may occur more rarely. Trace elements are also present in coals (Suárez-Ruiz, 2012).

Ward (2002) discussed different techniques used to determine mineral matter in coal. X-Ray diffraction (XRD) can be used to identify the crystalline minerals in coal. Scanning Electron Microscope (SEM) can be used to evaluate the nature and distribution of minerals in coal as well as to determine composition of the different mineral phases.

Understanding mineral matter in coal is very important for interpreting coal conversion process. Mineral matter is also useful in understanding depositional environments (Suárez-Ruiz, 2012).

2.5. Depositional Environment

There is a considerable variety of coal properties which carry paleoenvironment signatures as coal is the result of the accumulation of vegetable debris in a specialized environment of deposition (Thomas, 2013). Generally, the coal seams form during periods of non-deposition or quiescence when plant and peat accumulation occur at the same rate (Falcon, 1986). These are the periods that separate depositional sequences which influence the nature and extent of the seams. To reconstruct the paleoenvironment of a coal deposit, the primary genetic characteristics of the coal should be studied (ICCP, 2011). These include macerals, microlithotypes and lithotypes, and mineral matter contents have been used to assess the paleoenvironments of precursor peats (Kalaitzidis et al., 2004; Silva and Kalkreuth, 2005). The study undertaken focuses on petrographic indices to deduce paleoenvironment.

The Tissue Preservation Index (TPI) and Gelification Index (GI) are widely used to study depositional environments of coal. These petrographic indices were first introduced by Diessel (1986). TPI measures the degree of humification experienced by maceral precursors and gives a proportion of wood that contributed to peat formation. GI is significant for representing the relative wetness and influence of groundwater on peat (Diessel, 1992; Silva and Kalkreuth 2005; Sahay 2011). TPI shows a ration of structured to non-structured macerals and GI depicts the ratio of gelified to non gelified material (Silva and Kalkreuth, 2005; ICCP, 2015). The TPI and GI values are calculated from the maceral indices determined by maceral point count using the following formulas (equation 1 and equation 2) as described by Diessel (1986):

$$\mathrm{TPI} = \frac{\text{telovitrinite} + \text{semifusinite} + \text{fusinite}}{\text{detrovitrinite} + \text{macrinite} + \text{inertodetrinite}} \qquad \text{..... eq 1}$$

$$\mathrm{GI} = \frac{\text{vitrinite} + \text{macrinite}}{\text{semifusinite} + \text{fusinite} + \text{inertodetrinite}} \qquad \text{..... eq 2}$$

The TPI and GI values determined are plotted into a coal facies diagram developed by Diessel (1986) indicated in Figure 2.7. According to Diessel (1986); Silva and Kalkreuth (2005); Suwara (2006); Sahay (2011); ICCP (2015); Sen et al. (2016), high GI and TPI indicate a wet condition of peat formation and a low GI and TPI would indicate a dry condition of peat formation. High TPI suggests a balanced ratio of well-preserved plant growth and peat accumulation verses rise in groundwater. Low TPI would indicate low preservation of organic matter (Diessel, 1992; ICCP, 2015; and Sen et al., 2016).

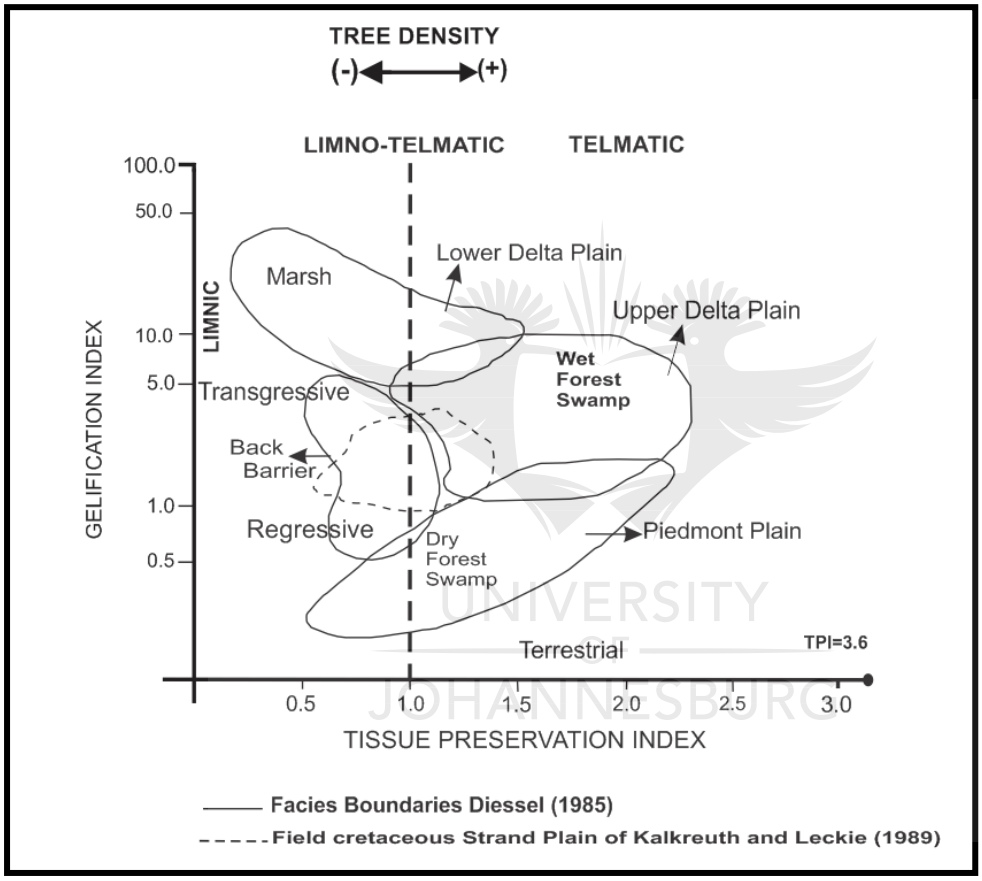

Figure 2.7: Coal facies diagram of the Tissue Preservation Index (TPI) and Gelification index (GI) in relation to the depositional environment (modified after Silva and Kalkreuth, 2005; Diessel (1985) & Kalkreuth and Leckie (1989) as cited by Silva and Kalkreuth (2005)).

Recent studies by Scott (2002); Moore and Shearer (2003); Sahay (2011); and Sen et al., (2016) have indicated limitations regarding using maceral ratios as a means to define depositional environment. They suggest that petrographic indices should be used together with palynology and geochemistry, when attempting to reconstruct paleoenvironment. For the purpose of this study, the TPI and GI indices are used

only as indicative of the sedimentological features and not a solution for depositional environment. The TPI and GI technique was invented for Northern hemisphere coal by Diessel (1986). However, Silva and Kalkreuth (2005) used the technique for southern hemisphere coal when studying the coal seams of Brazil. In this study they conclude that the coals from Candiota coal seams of Brazil were formed in limno-telmatic peat acculation in a back-barrier/strandplain setting.

2.6. Chapter summary

South African coals vary in terms of their tectonic setting. Coal in the MKB was deposited in a retro arc foreland basin. Northern Karoo coals are fault bounded deposited in intercratonic, and half graben systems. The Soutpansberg coals are believed to be vitrinite rich and hence are predicted to have formed in a waterlogged environment. The following chapters unpack these statements further.

CHAPTER 3: METHODOLOGY

This chapter provides the methods used to determine the variation in coal quality on either side of the Tshipise Fault and samples from other coalfields in Limpopo, and outlines the approach used to attempt the paleoenvironmental reconstruction. Sample collection and sample preparation are addressed, as well as detailed description of the experimental work undertaken including: chemical analyses, Free Swelling Index (FSI), petrographic analyses, Scanning Electron Microprobe (SEM) analyses, X-Ray diffraction (XRD) analyses, and Electron Microprobe analyses (EMPA). A summary of the methodology is depicted in Figure 3.1.

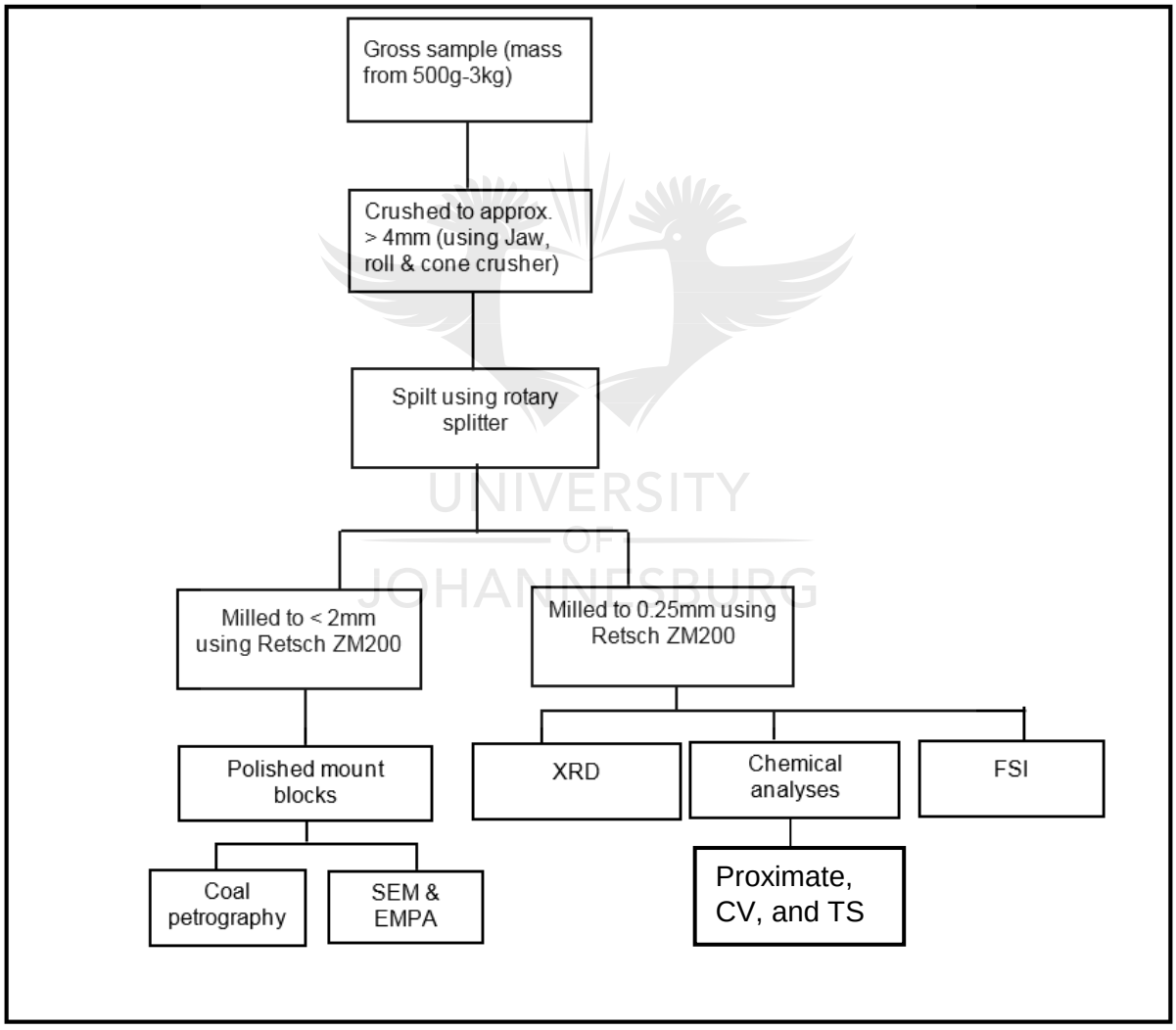

Figure 3.1: The research methodology flow chart

3.1. Sample collection

For the purpose of this study, samples were made available by John Sparrow of CoAL. Samples were collected from the Makhado Coal Project area, Voorburg, and Vele Colliery, all in Limpopo Province, South Africa; a total of 26 samples were collected, from 10 boreholes (Figure 3.2, Figure 3.3, and Table 3.1). For comparative purposes and to complete the consideration of coal from the Limpopo Province, samples from the Vele Colliery and Waterberg Coalfield were provided by Prof Nicola Wagner, and one ROM sample from Tshikondeni Colliery was provided by the University of North West. As previously mentioned, in Section 1.2, Tshikondeni Colliery produced coking coal until the mine closed in 2014.

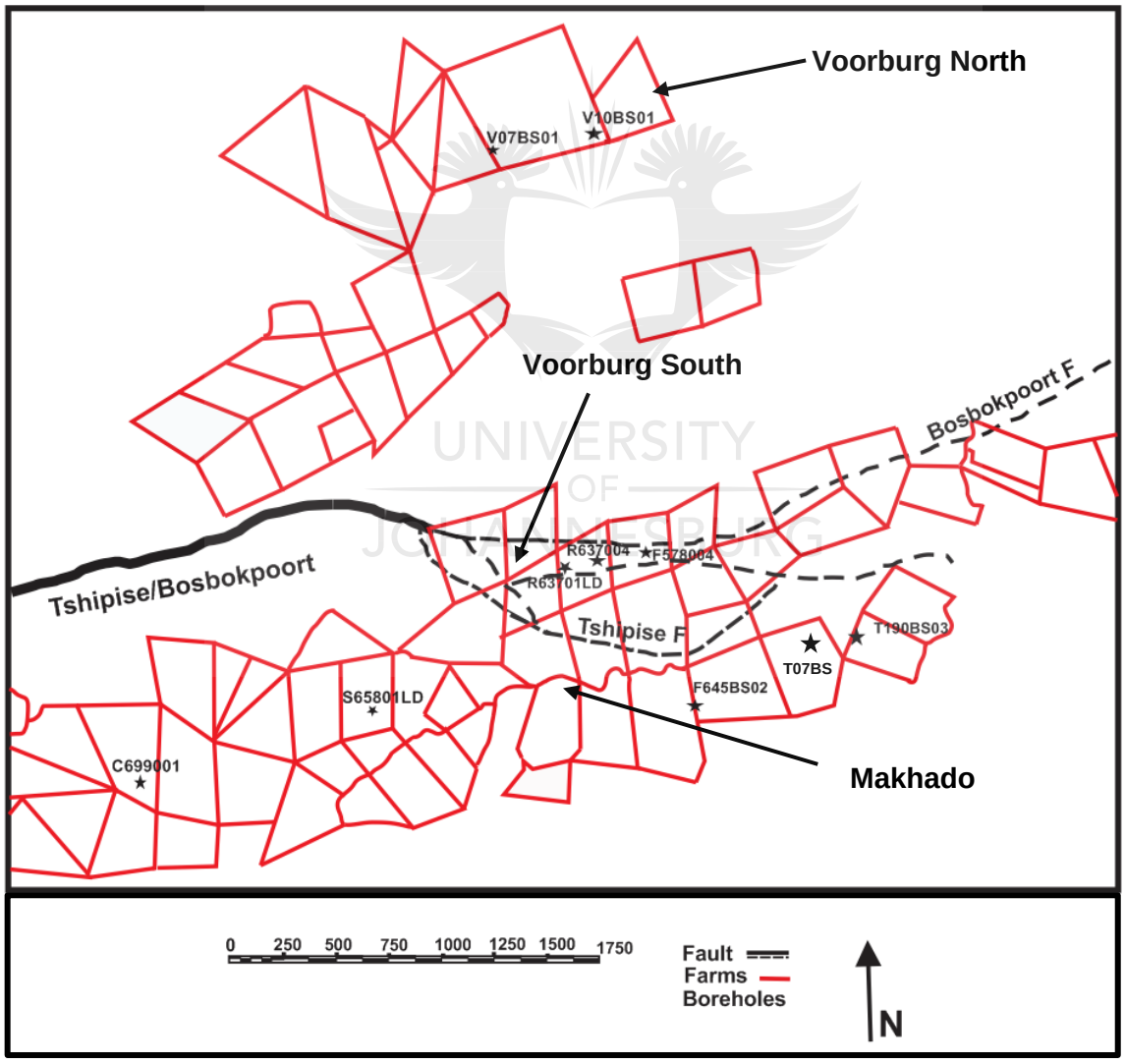

Figure 3.2: Location of the 9 borehole samples, shown in relation to the Tshipise Fault, Makhado/Voorburg area.

Table 3.1: Location and identification of all samples collected

Location	Sample ID	Borehole ID	Seams
Voorburg North (approximately 10km north of Tshipise Fault) Soutpansberg Coalfield	VB01	V07BS01	MU
	VB02	V07BS01	BU
	VB03	V07BS01	BL
	15150	V10BS01	BU
	15151	V10BS01	BL
Voorburg South (between Bosbokpoort and Tshipise Faults) Soutpansberg Coalfield	15136	R637004	MU
	15137	R637004	BU
	15138	R637004	BL
	15147	R63701LD	MU
	15148	R63701LD	ML
	15149	R63701LD	BU
	15154	F578004	MU
	15155	F578004	ML
	15156	F578004	BU
Makhado (south of Tshipise Fault) Soutpansberg Coalfield	15139	T190BS03	BU
	15140	T190BS03	BL
	15141	T07BS	MU
	15142	T07BS	BL
	15143	C699001	MU
	15144	C699001	ML
	15145	C699001	BU
	15146	C699001	BL
	15152	S65801LD	MU
	15153	S65801LD	BU
	15157	F645BS02	BU
	15158	F645BS02	BL
Vele Colliery Limpopo Coalfield	1317	CP17BS02	BU
	1318	CP17BS02	BL
	1333	OV24BS01	BLT
	1334	OV24BS01	BU
	1335	OV24BS01	Middle Seam (M)
	1336	OV24BS01	Top Seam (T)
Waterberg Coalfield	15159		Zone 8 and 9
	15160		Zone 7 and 8
Tshikondeni Colliery (Soutpansberg Coalfield)	15117		ROM

Some borehole logs were redrawn to indicate the seam depth on either side of the Tshipise Fault. The boreholes logs were provided as logs and were redrawn using Corel draw to produce stratigraphic columns provided in Figure 3.4. Only three boreholes are supplied here to indicate shallow depth in Voorburg north and Makhado; and deeper seam depth in Voorburg South.

Figure 3.3: Sample collection from the Vele site, Limpopo Province.

3.2. Sample preparation

The samples were crushed using a roll, jaw, and cone crusher at the University of Johannesburg (DFC) to obtain a particle size of approximately 4mm. The 4mm sample was split using a rotary splitter and half of the sample was kept as a reference. The other half of the 4mm sample was milled using a Retsch ZM200 to two different particle sizes at the University of the Witwatersrand Coal Laboratory in the School of Chemical and Metallurgical Engineering (WITS). The samples were milled to 1mm for petrographic and other optical studies. The second split was milled to 212µm for XRD, FSI, and chemical analyses. The samples milled to 1mm were then sieved and particles less than 38µm were removed to improve particle distribution suitable for petrographic analysis. Petrographic polished blocks were made following SABS ISO 7404 part 2 at University of Johannesburg (UJ), Department of Geology sample preparation facility. The polished blocks were prepared by mixing a representative split of 1mm coal particles with a mixture of epoxy resin and hardener. This mixture was left to solidify under vacuum overnight.

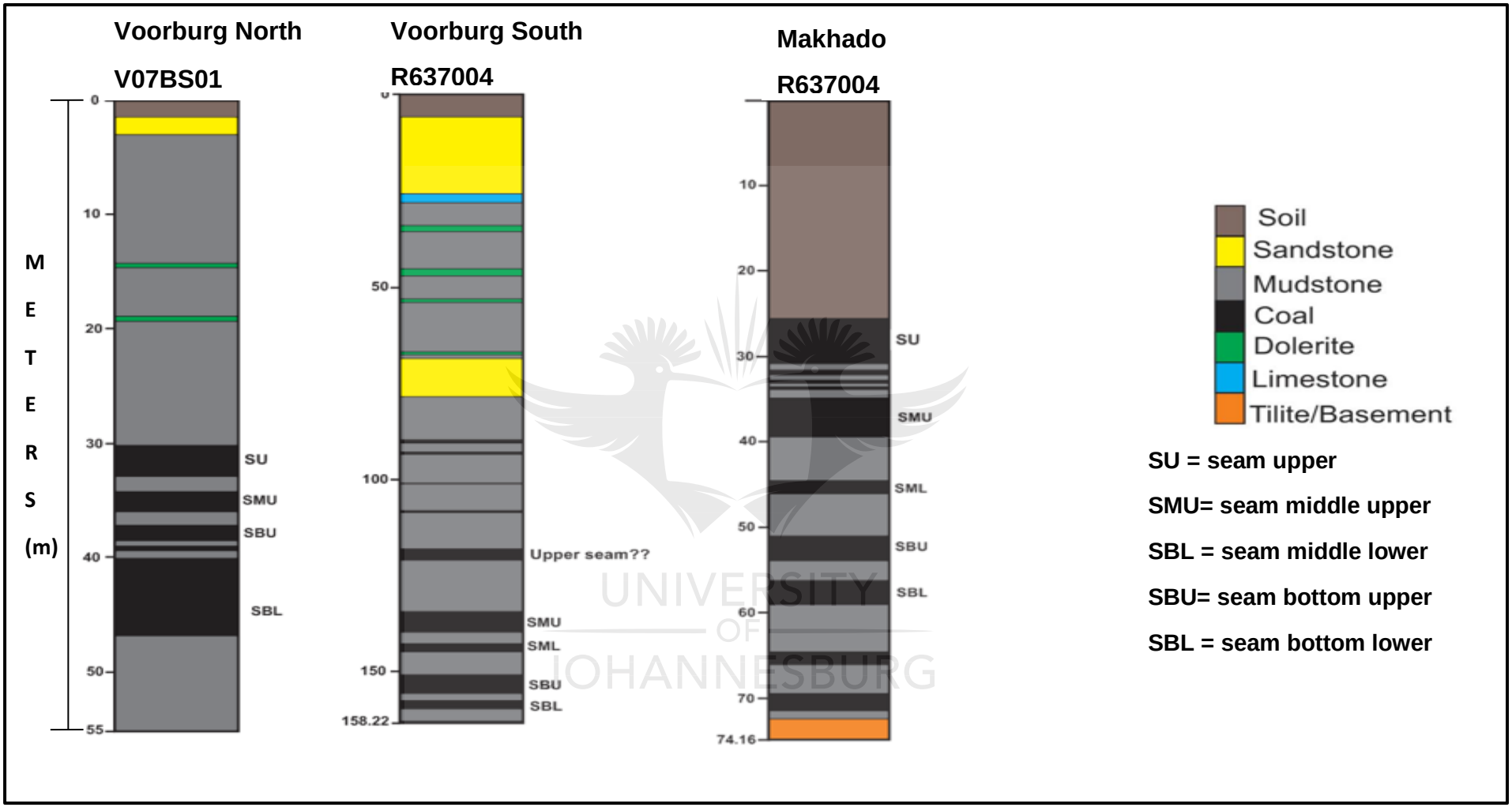

Figure 3.4: Borehole logs from representative boreholes from Voorburg and Makhado, showing different depth of seams from which coal samples were collected (borehole data provided by CoAL).

Once the blocks were set, they were polished using a Struers TegraForce–1 polisher, following the standard procedures of SABS ISO 7404 part 2 to achieve a relief free, scratch free surface. The polished mount blocks were used for petrography as well as SEM and EMPA studies.

In order to improve the conductivity the samples for SEM and EMPA, the samples were carbon coated to a brash blue index colour, using a Q150R Rotary-Pumped Sputter Coater/Carbon Coater at UJ Spectrum. Ethanol was used to clean the polished blocks from any polishing chemicals or residual oil. The coating was deposited on the sample surface in a high vacuum chamber by electrically heating a narrow carbon rod. A royal blue interference colour on the plate corresponded to a coating thickness of 25 nm. A polished brass plate was also coated as an indicator for the brass blue colour. The coating quality is important for successful analyses.

For the purpose of XRD, samples crushed to 212µm were used to make pressed pellet discs. Samples for FSI determination were submitted to ALS Laboratory, Witbank, a commercial laboratory. Chemical analyses were conducted at Wits.

3.3. Chemical analyses

3.3.1. Proximate analyses

Proximate analyses were conducted using a PerkinElmer STA 6000 Simultaneous Thermal Analyser. The analyses were done following the procedures of the School of Chemical and Metallurgical Engineering, WITS under the supervision of Mrs Zama Mthabela. The TGA proximate method determines the ash, moisture, volatile and fixed carbon content of coal. The sample (11mg of 212µm) is heated from 30ºC to over 900ºC. The first stage (30ºC - 110ºC); involves drying the sample in a nitrogen atmosphere, and determining the moisture content by mass loss. As the temperature increases from 110ºC- 700ºC, the coal is devolatilised, as measured by the weight loss, to determine the volatile matter of the coal. In the final stage (700ºC - 900ºC), the gas is switched from nitrogen to oxygen to allow for the combustion of the coal, measuring the fixed carbon content. When oxygen is introduced to the TGA furnace, and the sample is burned to constant weight, the ash content is determined. The ash is the remaining residue determined by weight. Data was interpreted using the 2007 edition of the Pyris Software producing a curve as indicated in Figure 3.5. Results are reported as weight

percent (wt. %). The moisture content was calculated as weight loss between 30ºC to 110ºC, volatile matter between 110ºC - 700ºC, fixed carbon between temperature range 700ºC - 900ºC. The ash was recalculated using formula = 100 – (moisture + Volatile + fixed carbon).

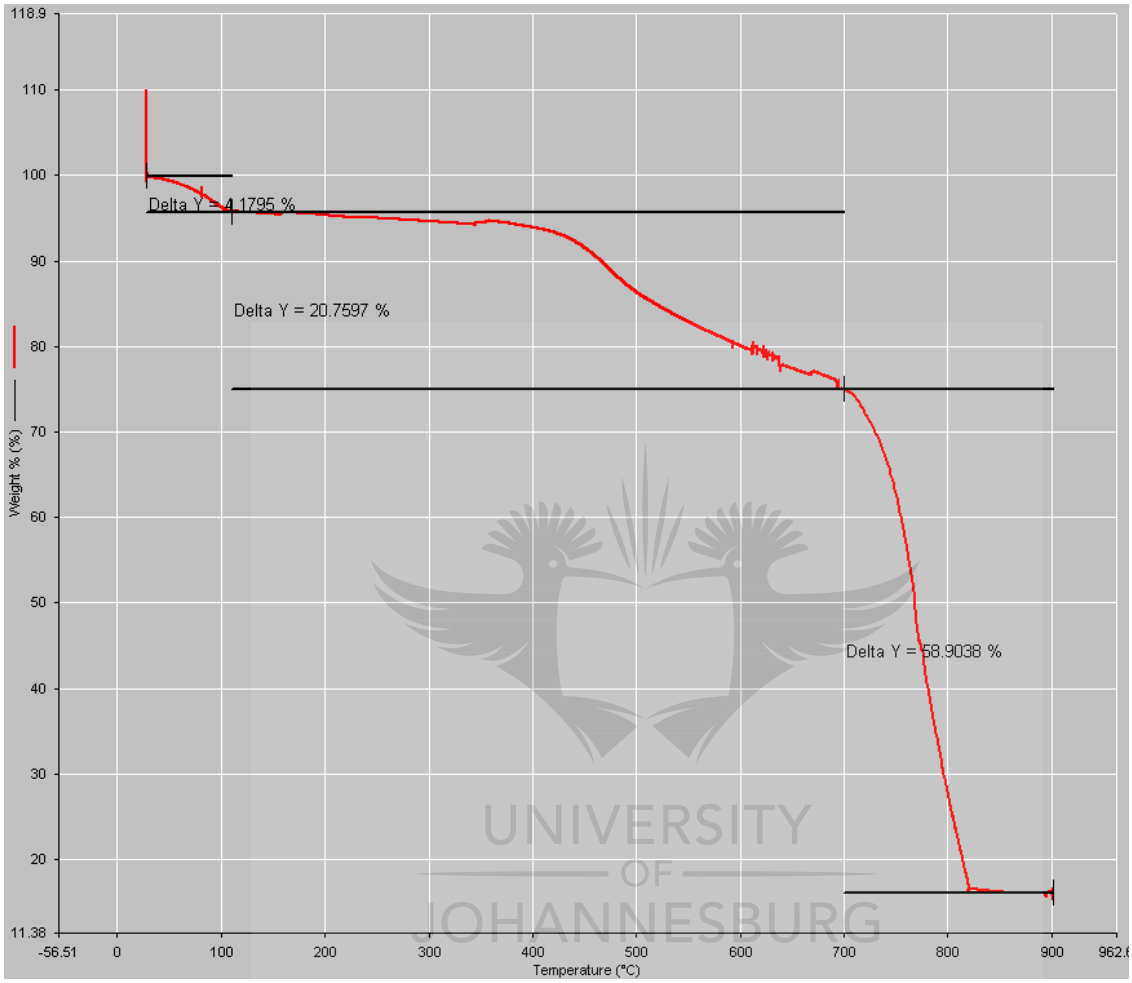

Figure 3.5: Proximate analysis curve showing weight loss in weight percentage (wt. %) against temperature (ºC).

3.3.2. Calorific Value (CV)

The calorific value (CV) of each sample was determined by the use of a Dry Cal bomb calorimeter at WITS. A bomb calorimeter is used for the determination of the total amount of heat produced from completely burning one unit mass or volume of fuel in a high pressure oxygen atmosphere. The sample, weighed to 0.40g of 212µm, was loaded into a crucible which was placed on a sample holder in the bomb. The bomb was charged with oxygen at a pressure of 2500 KPa. The bomb was lowered into the calorimeter, and the analysis started when the lid of the bomb was closed. The calorimeter measured the heat energy produced per unit mass when burning the loaded

sample in the bomb. The calibration was conducted using a tablet with a CV of 25MJ/kg, run after every three coal samples to ensure consistency. Results are reported as gross CV (MJ/kg).

3.3.3. Total Sulphur

Total sulphur analyses were conducted on all samples at WITS using a Leco SC632. This analysis was used to obtain the mass fraction of total sulphur in the coal samples. Each sample was weighed to 0.25 grams (212µm) in a crucible before being totally combusted in pure oxygen in the oxidation furnace (at 1350ºC). SO_2 is collected by the analyser and infers the amount of sulphur present in each sample. The calibration was checked after three samples to ensure no drift occurred using a certified reference material (LECO PN: 502-388) with total sulphur value of 5.40%. Results are presented as % total sulphur.

3.4. Free Swelling Index (FSI)

FSI analyses were conducted by ALS Laboratory, Witbank. The analyses were done following the standard ISO 501. This is a simple test to indicate coking properties (Speight, 2005). A coking coal will, to some extent, melt when heated and the test to determine caking will aim to quantify the degree of melting (Speight, 2005). Thus, FSI is applied to measure the plasticity of coal characteristic required to assess the caking properties. The test is a measure of the increased volume of coal when heated at 800ºC. When the coal is heated, the volatile matter is released, leaving a button of coke as a residue. After heating the sample under the specified conditions, the resulting coke button is compared to the standard index profiles to find the best fit (Figure 3.6). If the residue is powder, the swelling is recorded as zero. The cross section of the button is compared to a profile, were 1 is no swelling and 9 is maximum swelling matching standard profiles as indicated in Figure 3.5. According to this standard, coal with FSI between 0 – 2 are weakly caking coals, 2 – 4 medium caking and 4 – 9 strongly caking coals (Table 3.2) (Khorami et al., 2011).

Table 3.2: Plastic properties of coal (after Speight, 2005).

Coal type	Swelling Index
Non caking	0
Weakly caking	1 – 2
Medium caking	2 – 4
Strongly caking	>4

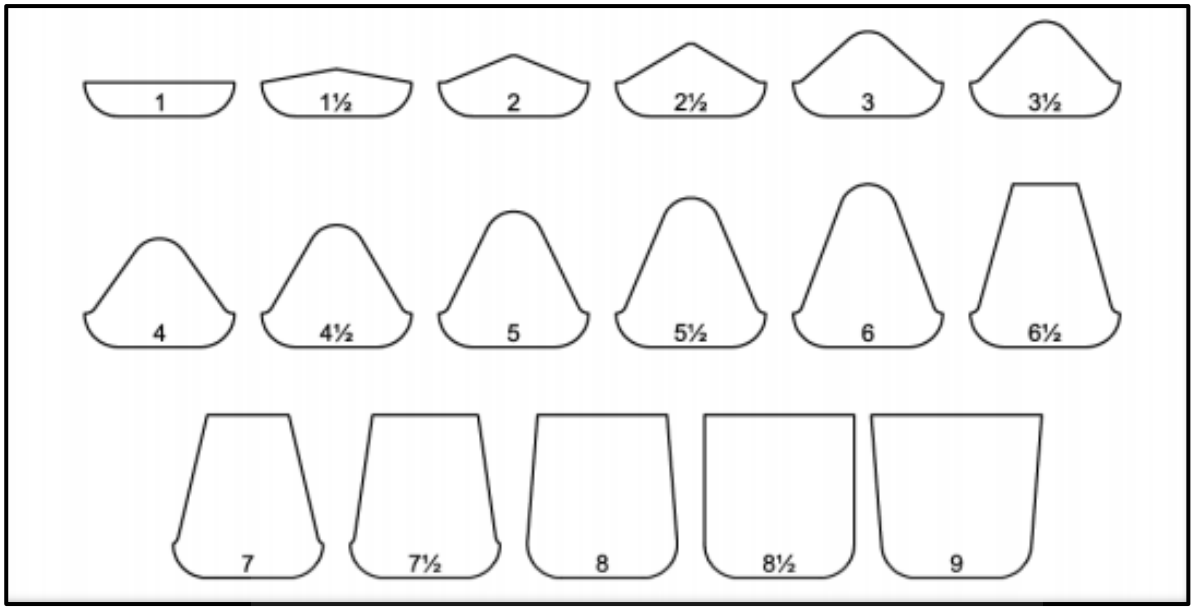

Figure 3.6: Full scale standard profiles and corresponding Free Swelling Index Number (Speight, 2005).

3.5. Petrographic analyses

Petrographic analyses were conducted using a Zeiss Axio Imager M2 polarized reflected light microscope with an oil immersion objective, retrofitted with a Hilgers Diskus Fossil component and software (Figure 3.7). The system is housed in the Department of Geology, UJ. The use of a monochromatic digital camera together with an automated stage enables scanning and analyses of polished blocks with subsequent offline assessment via Student Fossil software installed on a separate PC. The technique applied using the Fossil software is elaborated on Appendix A. Three analyses were conducted during this research: 1) detailed maceral analysis; 2) vitrinite reflectance measurements; and 3) abnormal condition analysis. Maceral analyses and vitrinite reflectance measurements were conducted largely following SABS ISO 7404 part 3 and SABS ISO 7404 part 5 respectively. The abnormal condition analysis follows procedure proposed by Wagner (2007). The petrographic analyses were done under the supervision (and training) of Professor Nicola Wagner.

3.5.1. Maceral Analysis

A detailed maceral point count analysis was conducted in order to determine the composition of the coal samples. As discussed in Section 2.3, coal consists of macerals as a result of the coalification process, and the maceral composition infers the

depositional environment, as well as predicting performance behaviour of the coal on utilisation. Twenty one (21) macerals and three mineral groups making a total of 24 were selected (Table 3.3). Five hundred (500) points were counted for each sample (excluding the resin) and the results were displayed as volume percentage (vol %).

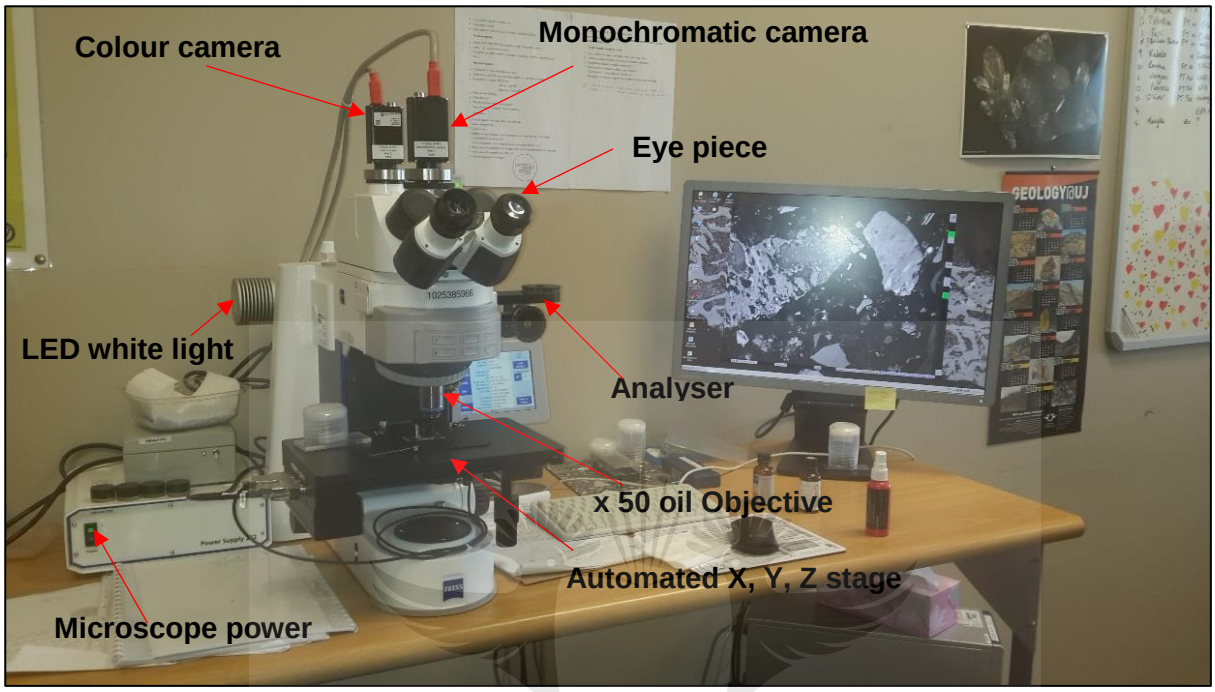

Figure 3.7: Zeiss Axio Imager M2 polarized reflected light microscope retrofitted with Hilgers diskus Fossil components.

Table 3.3: Macerals and minerals groups selected for maceral analysis

Vitrinite	Inertinite	Liptinite	Mineral groups
Telinite	Fusinite	Sporinite	Silicates
Collotelinite	Semifusinite*	Cutinite	Sulphides
Vitrodetrinite	Funginite	Resinite	Carbonates
Collodetrinite	Secretinite	Alginite	
Corpogelinite	Macrinite	Liptodetrinite	
Gelinite	Micrinite	Suberinite	
Pseudovitrinite	Inertodetrinite	Exsudatinite	

***Semifusinite was not subdivided into reactive and inert semifusinite components during the current research**

3.5.2. Vitrinite reflectance analyses

Vitrinite reflectance analyses were conducted using the calibrated Hilgers system and measurements were made off-line on the scanned images. This analysis was imperative for this study as it determined the rank of the samples; coal rank is important when determining the sustainability of a coal for coking purposes. The analysis on all

samples was conducted largely following SABS ISO 7404 part 5.

All reflectance readings were taken on collotelinite. The reflected light from the microscope was calibrated using the Yttrium-Aluminium Garnet (YAG) standard from Klein and Bekker, with a certified value of 0.90 and a black hole of 0.01 and cross checked with an internal standard. The calibration was checked after every third sample to ensure no drift occurred. Histograms were plotted and the standard deviation considered to understand the distribution of the reflectance values. The total numbers of measurements per sample were 100, except for some samples where suitable particles were not readily available.

3.5.3. Abnormal condition Analysis (ACA)

The abnormal condition analysis (ACA) proposed by Wagner (2007) was initially developed to identify and quantify the various weathering features observed in stockpiled coal discards, and is applied here to determine abnormal features in the borehole core samples. The purpose of conducting this analysis was to assess any physical changes in the coals potentially caused by the fault. The cross hair quadrilateral of 50 x 50 microns field of view was used to examine the conditions observed. 500 point counts were recorded for each sample. The same samples prepared for petrography were used for the ACA. The features reported for ACA are indicated in Table 3.4.

Table 3.4: Abnormal Condition Analysis

Features identified by the ACA (volume % basis)
Fresh particles
Fissures few and extensive
Cracks few and extensive
Desiccation cracks few and extensive
Discoloured particles
Heat affected particles
Alteration mineral

Fresh particles define particles that are in their original state, indicating no alteration, weathering. Fissures are <1µm in width, the ACA will consider if they are few or extensive in a particle under the crosshair. Cracks are > 1µm in width. Cracks may contain mineral matter in them. In this study extensive cracking would indicate impact of the faults. Dessication cracks would typically indicate pseudovitrinite. Pseudovitrinite in this study as it could be used to explain any anomalies in the coking properties of coal

(Stach et al., 1982). Heat effects consider heat that may be from intrusion of dykes and sills that may affect the rank of coal.

3.6. Mineralogical analyses

During the course of the petrographic analyses, some interesting minerals were encountered. Hence further analyses were conducted.

3.6.1. XRD analyses

XRD analyses were conducted to understand the mineral matter in the samples. A Philips PANanalytical X-PertPro X-Ray Diffractometer located at the UJ Spectrum facility was used. The X-ray diffractometer was operated at 40kV and 40mA for 2 hours using a monochromatic anti scatter slit over a range of 2θ from 0° to 80º and a step size of 0.04. The prepared pellet discs were placed into a sample holder within the XRD. As each mineral has a unique diffraction phase, when X-rays are bombarded into the powder sample, they interact with each mineral phase present, resulting in a variety of diffraction patterns. The High Score Plus software was used for identification and interpretation of the diffraction patterns. The analysis was done qualitatively. Unfortunately no standards were available for quantification of values received, thus only qualitative studies were done. Two samples were also assessed by Professor Sabine Veryn of XRD Analytical and Consulting for comparative purposes.

3.6.2. SEM

Scanning Electron Microscope back scattered electron (SEM-BSE) and energy dispersive analysis (SEM-EDS) using a Tescan Vega, were conducted at the UJ Spectrum facility. The backscattered electron detector is primarily used for imaging samples. The SEM analyses permits resolution of finer detail than is possible with reflected light microscopy. These analyses were conducted to study the interrelations and morphology of mineral matter in the coal samples. Six samples were selected based on mineral matter composition. The EDS is equipped with Aztec software, which was used to acquire element maps and spectrum peaks of different minerals in the coal samples.

3.6.3. EMPA

The Electron Microprobe Analyser (EMPA) enables the quantitative analysis of minerals, and was conducted at UJ Spectra facility using a Cameca SX-100

microprobe. Operating conditions include: accelerating voltage 15 kV, and 20nA beam for sulphide mineral analysis. This analysis was conducted to assess only the carbonates and pyrite in the coal seams, providing more detail than possible with SEM. Carbonates, in particular calcite, aragonite, and to some degree dolomite, degrade under normal electron microprobe operating conditions. The degradation can be reduced by increasing the beam size depending on the size of sample being analysed (Jarosewich and Macintyre, 1983). Hence different operating conditions were used for carbonate analysis; they were accelerated at 15kV, 6nA and electron beam diameter of between 5 - 20µm.

3.7. Data interpretation

To enhance the understanding of the coals of Soutpansberg and Limpopo Coalfields, the data obtained from analyses were used in order to meet the outlined objectives. The data obtained from the maceral group analysis was used in an attempt to reconstruct the depositional environment. This was conducted using petrographic indices, discussed in Section 2.4. Table 3.5 obtained from Steyn and Minnitt (2010) were used to classify the coal in terms of proximate and CV analyses.

Table 3.5: Steyn and Minnitt (2010) coal classification

1. Domestic coal specifications

Parameter	Units	A grade	B grade	C grade	D grade
Calorific value	MJ/kg	> 27.5	>26.5	>25.5	>24.5
Total sulphur	Maximum %(AR)	12.0	12.0	8.0	8.0
Ash	Maximum %(AR)	15.0	16.0	18.0	21.0
Volatile matter	Maximum %(AR)	24.0	23.0	23.0	23.0
Sulphur	Maximum %(AR)	1.0	1.0	1.0	1.5

2. Thermal coal product specifications

Parameter	Units	Eskom	Domestic	Export
Calorific value	(NAR)	21-24 MJ/kg	24.5-27.5MJ/kg	5850-6000cal/kg (27.5 Mjkg)
Total sulphur	(AR)	8-12	8-12	8-12
Ash	(AR)	25-34	15-21	15
Volatile matter	(AR)	20-30	23-30	22-20
Sulphur	(AR)	0-2	0-1.5	0-1.0
Handgrove Index			45-70	45-70
Ash fusion temp				1.25
Phosporus			0.001-0.01	0.001-0.01
Calcium oxide in ash	%(DB)			12
Sizing	mm	0x40mm	0x60mm 6x25mm 25x40mm	0x50mm

CHAPTER 4: RESULTS AND DISCUSSION

The results of analyses conducted on all the samples are presented and discussed in this chapter in the following order: 1) chemical analyses (including proximate analyses, CV, and total sulphur); 2) FSI; 3) petrographic analyses (maceral point count, vitrinite reflectance and abnormal condition analysis; and 4) mineral analyses (XRD, SEM, and EMPA). Results presented in this chapter aim to give insight into the coal quality, the rank of the samples, the mineralogy, interrelations of the minerals and organic matter, as well as to provide data for the interpretation of the paleoenvironment. The Voorburg area was subdivided into: 1) Voorburg North (four samples) referring to boreholes approximately 10km north of the Tshipise Fault; and 2) Voorburg South (nine samples) referring to boreholes between the Tshipise and Bosbokpoort Faults. Coal quality across the Tshipise Fault is the main focus of this research.

4.1. Chemical analyses

The data presented in this section includes results from proximate, CV and total sulphur analyses. The results of the chemical analyses are reported in Table 4.1a, with average values presented in Table 4.1b and Figure 4.1. The percentage components (moisture, volatile matter, ash and fixed carbon) were calculated as illustrated in Section 3.4.

Samples from Voorburg North were characterised by high ash ranging from 34.92 – 49.73%, and high volatile matter (16 – 25.97%) (Table 4.1a) and CV decreases with increasing ash contents. The highest total sulphur of 9.49% (Figure 4.3) was noted for sample VB01. Based on Steyn and Minnitt (2010) domestic coal classification, the Voorburg North samples would be classified as below grade D for domestic coal utilization.

Voorburg South samples reported varied ash contents, and as expected by the variations in ash the CV of the coal is varied. Voorburg South samples were classified as below grade D based on Steyn and Minnitt 2010 classification with the exception of sample 15149 with CV of 28.24 MJ/kg implying grade A and suitable for export (Table 4.1a and Figure 4.2). The sulphur content of Voorburg South is low compared to Voorburg North (Figure 4.3).

Table 4.1a: Chemical analyses of samples from all localities (adb) (MC= moisture content; VM = volatile matter; FC = fixed carbon; and TS= total sulphur). Note VB03 and Vele FSI is not available.

Location	Borehole ID	Seams	Sample ID	Ash (wt. %)	MC (wt. %)	VM (wt. %)	FC (wt. %)	CV (MJ/kg)	TS (wt. %)	FSI
Voorburg North	V07BS01	MU	VB01	34.92	0.60	25.97	38.51	20.34	9.49	5.5
		BU	VB02	36.60	1.26	24.60	37.55	25.42	2.79	3.0
		BL	VB03	34.99	0.56	21.75	42.70	22.06	3.93	-
	V10BS01	BU	15150	42.55	0.80	20.41	36.24	16.94	1.60	3.0
		BL	15151	49.73	1.30	16.44	32.53	13.65	0.52	0.5
Voorburg South	R637004	MU	15136	27.71	0.62	26.14	45.52	23.27	1.57	7.5
		BU	15137	24.75	0.59	21.88	52.78	22.83	0.54	6.5
		BL	15138	47.34	0.52	15.18	36.96	15.69	0.24	1.0
	R63701LD	MU	15147	28.99	2.82	20.92	47.26	22.69	0.93	6.5
		ML	15148	34.59	0.87	24.71	39.84	18.54	1.16	4.5
		BU	15149	16.02	0.67	21.20	62.11	28.24	0.88	8.0
	F578004	MU	15154	29.21	0.82	20.44	49.53	21.64	1.38	0.0
		ML	15155	48.33	0.96	14.25	36.46	15.20	0.54	0.0
		BU	15156	49.62	1.02	13.96	35.40	14.24	0.50	0.0
Makhado	T190BS03	BU	15139	49.54	0.56	16.31	33.59	14.66	0.49	1.0
		BL	15140	25.75	0.68	20.22	53.35	24.26	0.73	3.5
	T07BS	MU	15141	18.00	0.80	24.81	56.38	30.20	1.23	7.5
		BL	15142	58.11	0.98	15.69	25.22	10.05	0.31	0.0
	C699001	MU	15143	36.17	0.64	22.41	40.78	17.07	2.16	2.5
		ML	15144	20.06	1.01	27.55	51.38	26.87	1.45	7.0
		BU	15145	42.87	0.55	24.57	32.01	11.51	0.47	1.0
		BL	15146	46.55	0.78	20.22	32.44	14.71	1.14	1.0
	S65801LD	MU	15152	30.20	0.70	19.93	49.17	22.28	1.40	1.5
		BU	15153	26.11	0.89	26.65	46.35	23.91	0.67	7.5
	F645BS02	BU	15157	57.22	0.70	15.66	26.42	10.36	0.31	0.0
		BL	15158	49.86	0.88	16.22	33.04	12.11	0.40	0.0
Vele	OV24BS01	BU	1333	27.40	1.80	29.70	41.10	24.10	1.10	-
		BL	1334	62.00	1.50	16.80	19.70	12.10	1.10	-
		BLB	1335	47.90	1.80	22.80	27.50	17.00	0.80	-
		T	1336	47.50	2.30	22.90	27.30	16.90	1.10	-
Waterberg		Zone 8+9	15159	48.22	0.65	16.86	34.27	13.38	2.00	0.0
		Zone 7+8	15160	50.22	0.89	15.74	33.15	12.59	1.43	0.0
Tshikondeni			15117	14.85	0.88	23.55	60.72	28.24	0.91	8.0

Table 4.1b: Chemical analyses (average) from different locations in Limpopo Province (adb) (Run of mine coal)

Location	Ash (wt. %)	MC (wt. %)	VM (wt. %)	FC (wt. %)	CV (MJ/kg)	TS (wt. %)
Voorburg North	39.76	0.90	21.83	37.51	19.68	3.67
Voorburg South	34.06	0.99	19.85	45.10	20.26	0.86
Makhado	38.37	0.76	20.85	40.01	18.17	0.90
Vele	46.20	1.85	23.05	28.90	17.53	1.03
Waterberg	49.22	0.77	16.30	33.71	12.99	1.72
Tshikondeni	14.85	0.88	23.55	60.72	28.24	0.91

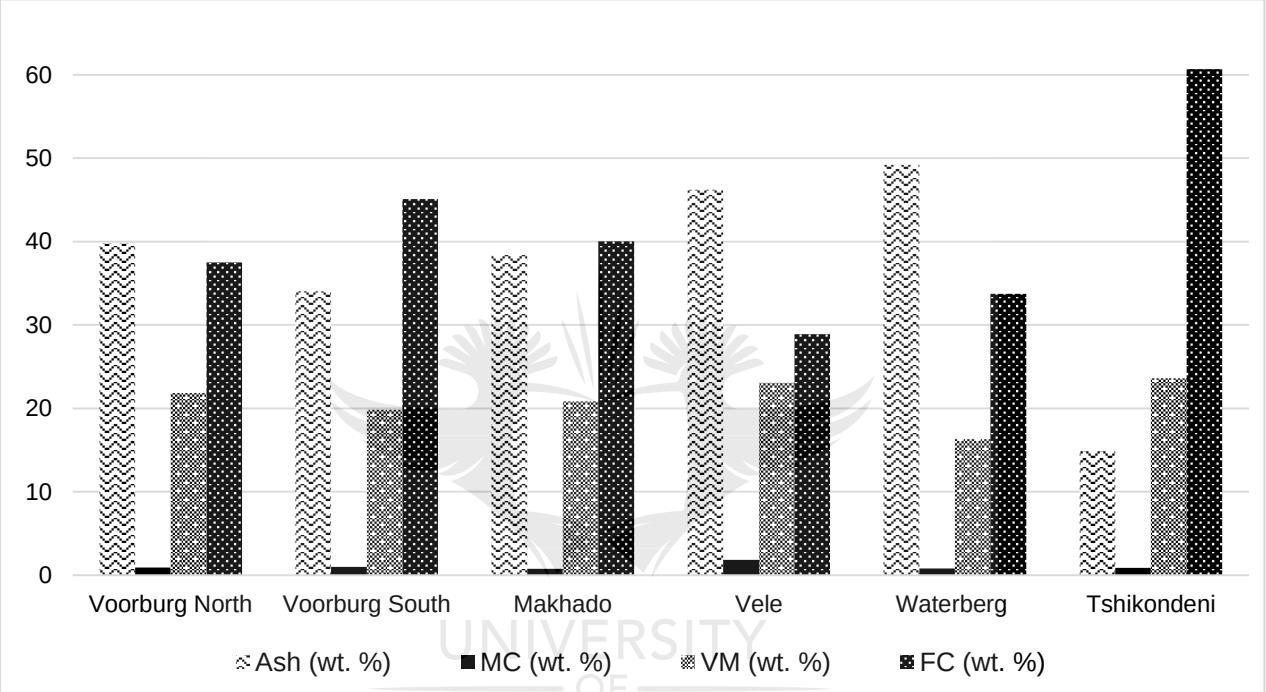

Figure 4.1: Comparison of proximate analyses (average) obtained from different locations in Limpopo Province (adb).

The Makhado samples reported variable ash and volatile matter contents. Two samples (15142 and 15157) from Makhado had ash content greater than fifty percent (> 50 %). Samples with ash content > 50 % were considered as carbonaceous rocks. Based on Steyn and Minnitt (2010), the coal in Makhado is classified as below grade D for domestic application. However, samples 15141 and 15144 reported CV above 27.5 MJ/kg therefore classified as grade A and suitable for export.

Four samples from Vele area had proximate analyses provided by CoAL (Table 4.1a). Vele samples reported very high ash content except sample 1333. These

samples are classified as below grade D on the Steyn and Minnitt (2010) domestic coal classification, but again could be upgraded by beneficiation.

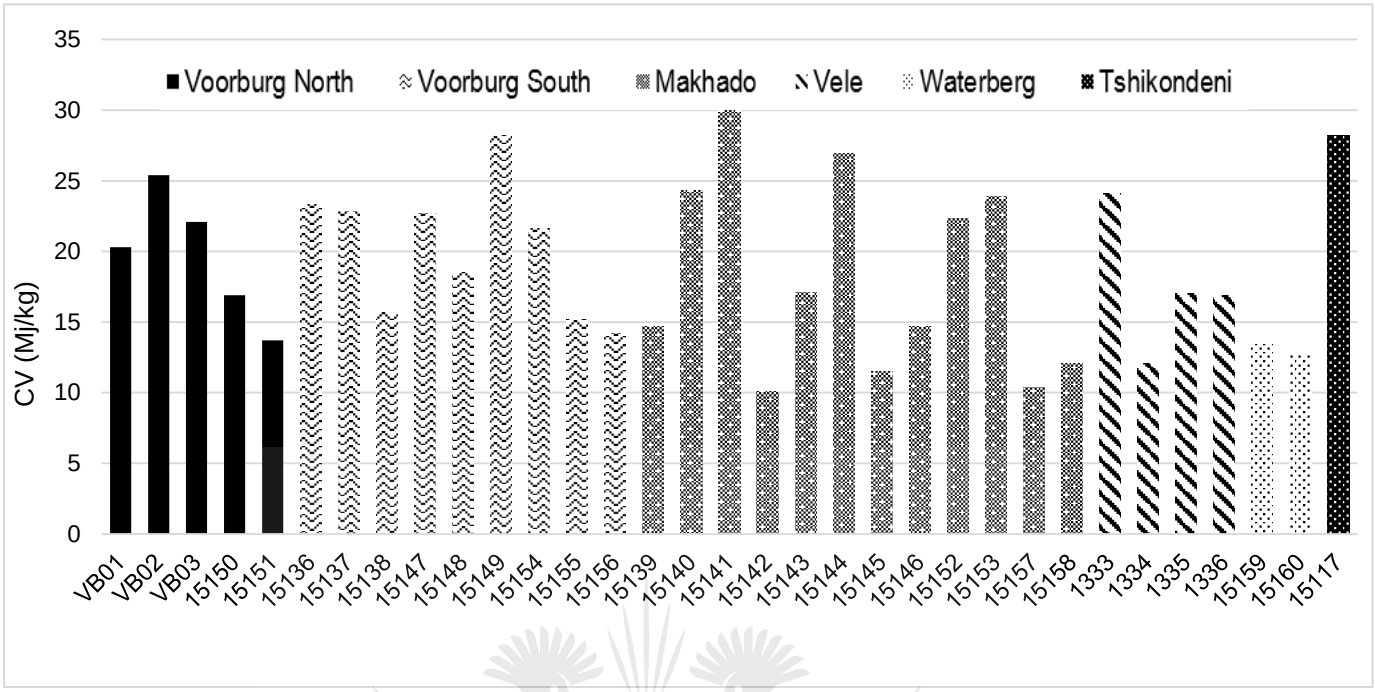

Figure 4.2: Calorific Value for each sample collected (MJ/kg).

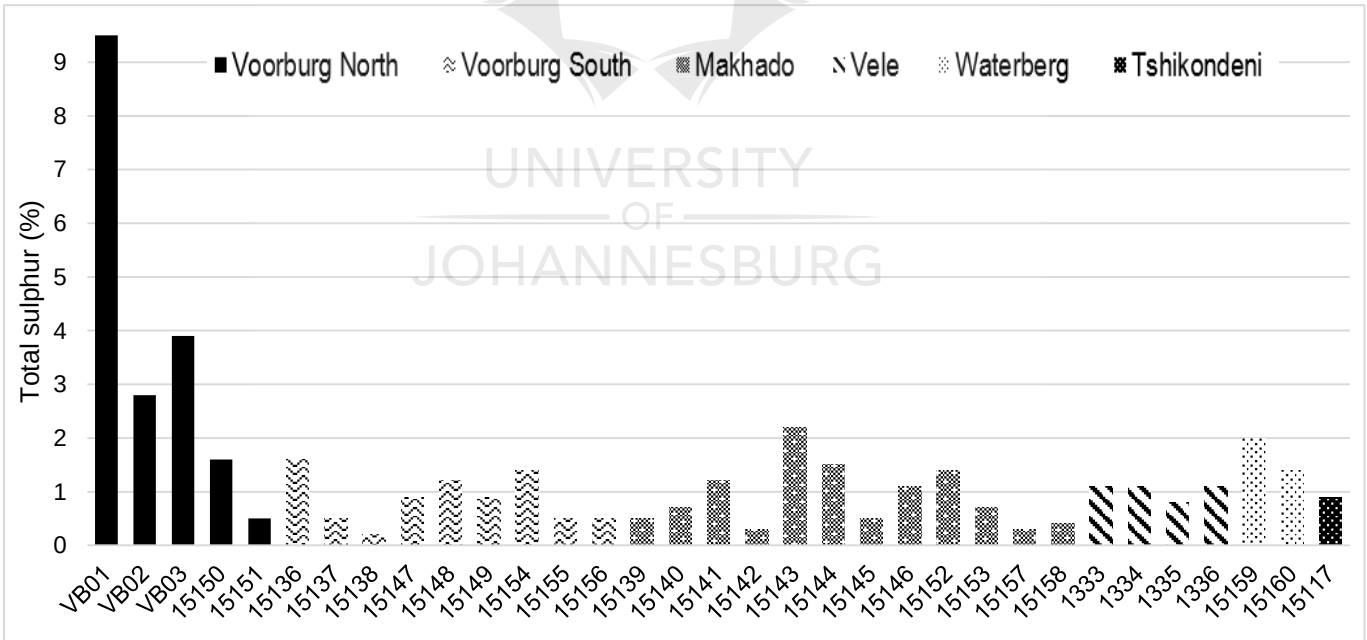

Figure 4.3: Comparison of total sulphur content for all coal sample (%).

Only two samples from Waterberg Coalfield were provided, for comparative purposes for this study, and they reported high ash and low volatile matter contents. Based on Steyn and Minnitt (2010), the coal in Waterberg Coalfield is classified as below grade D, but this coal and the Soutpansberg coals can all be upgraded by coal

beneficiation. The Tshikondeni sample reported low ash, high volatile and high CV contents. This was anticipated as the Tshikondeni mine was a prime coking coal producer.

Assessing the lateral variation across the Voorburg and Makhado areas, the MU seam coal samples were comparable, with the exception of sample 15141, but a difference in the sulphur distribution was noted (Figure 4.3). The MU seams of Voorburg area were characterised by higher CV contents in comparison to those of Makhado. However, the ML seam of Makhado had higher CV than Voorburg. The BU and BL seams had no comparable trend because the ash and CV are quite varied.

On average (Table 4.1b, Figure 4.1), the Voorburg North samples are comparable to Makhado samples in terms of the ash, volatile matter and CV contents. Voorburg South reported a higher CV and lower ash compared to the other Soutpansberg Coalfield locations. Vele samples reported high ash content averaging 46.20% and a low CV with an average of 17.50 MJ/kg. The Waterberg samples reported the highest ash content on average (49.22 %). On average the CV of all the coal samples is low (due to the high ash content), with the exception of the Tshikondeni sample. The Tshikondeni sample reported the best coal quality of the Limpopo coals studied.

Generally, high ash and high volatile contents are noted (Figure 4.4A). The high ash content can be related to the high mineral matter content. The high volatile matter content can be related to the (anticipated) high vitrinite contents in petrography (Section 4.3). A trend between the ash and CV was noted, where ash increased with a decrease in CV (Figure 4.4B). According to Telfer and Njowa (2012), the Soutpansberg coal has a coal mudstone association; this is evident in the proximate analysis, where the high ash content can be attributed to the mudstone coal association.

However, according to Saad and Pinhiero (2001), coals from the Soutpansberg Coalfield are characterised by low ash content, high CV, and volatile matter content. They reported: moisture content (1.8 – 2%); volatile matter (32.9 - 33.6%); ash (18.0 - 21.2%), CV (26.4 – 27.5MJ/kg). The samples assessed for this study are ROM and

therefore they differ from Saad and Pinhiero (2001) samples which are processed products.

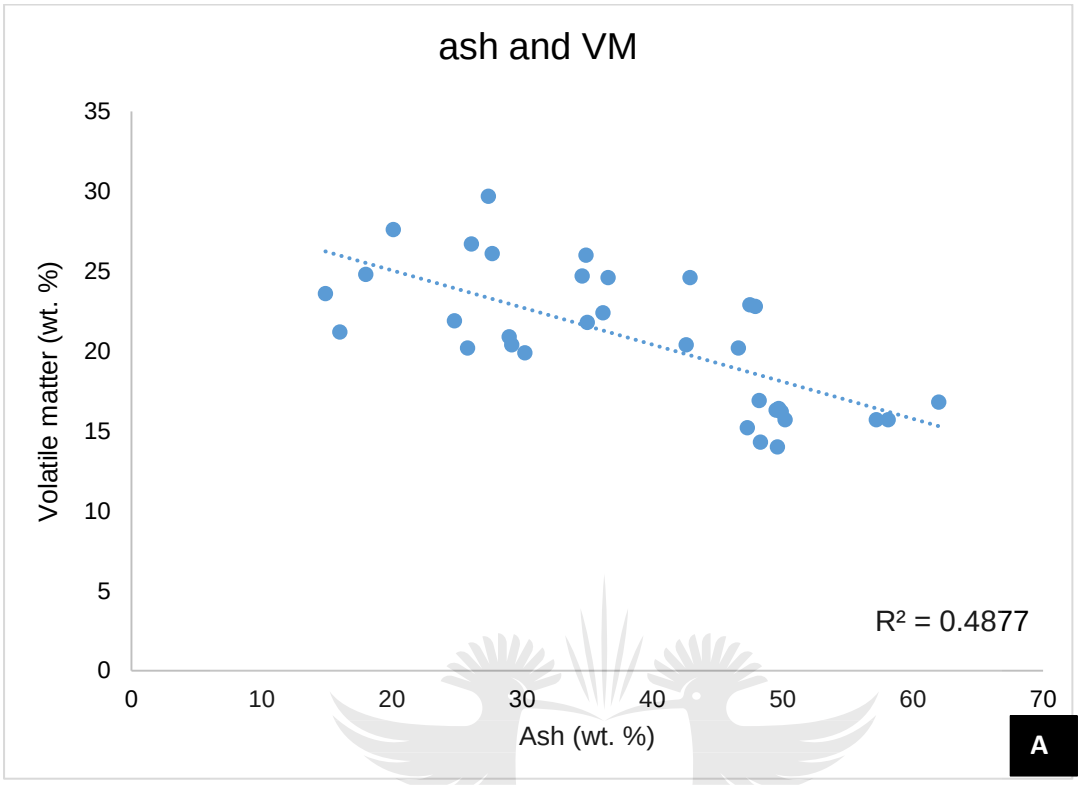

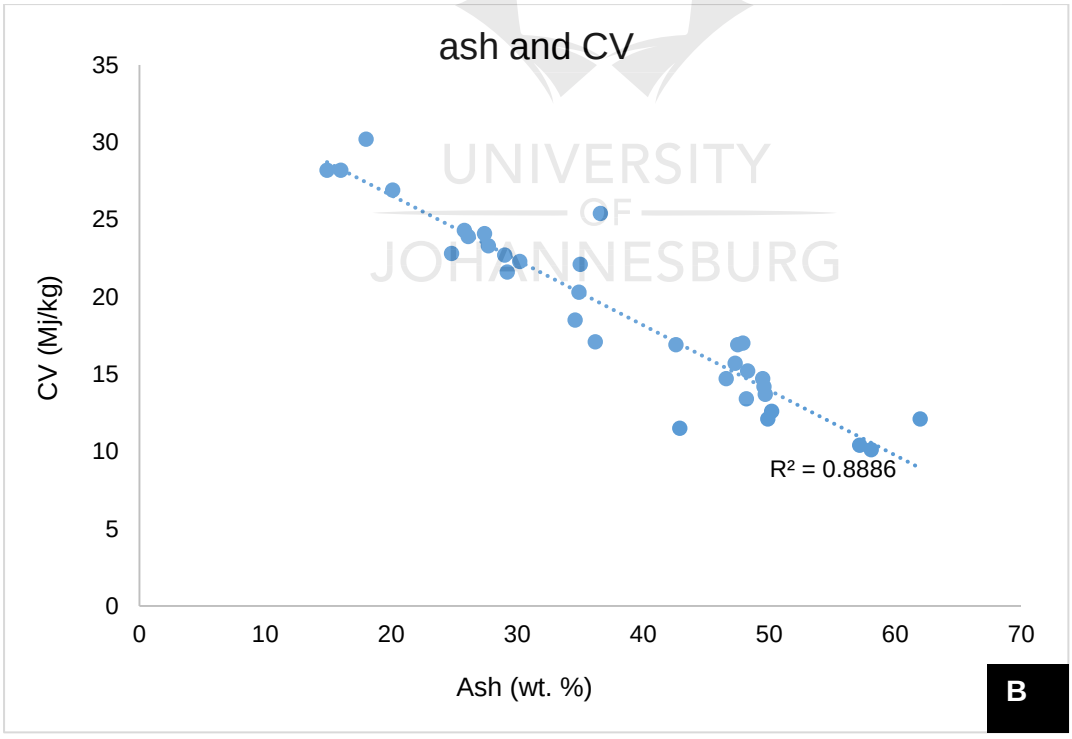

Figure 4.4: Relationship between A) ash and volatile matter and B) ash and CV

According to Webber et al. (2000), Waterberg coal samples reported values of: moisture content (2.00 – 3.96%); volatile matter (17.44 – 31.30%); ash (9.73 –

31.20%), CV (23.59 – 29.70MJ/kg). The values reported here again differ from these values obtained being high in ash. Saad and Pinhiero (2001) and Makgato et al. (2009), reported values of: moisture content (0.4-0.9); volatile matter (23.3 - 30.4%); ash (9.4 – 18.0%), CV (29.3 – 30.4MJ/kg), which is similar to the Tshikondeni sample used in this study.

In summary, the raw coals of the Limpopo Province have high ash contents and high volatile matter, associated with the coal mudstone intercalations. According to Table 3.5 provided in section 3.9 from Steyn and Minnitt (2010), (domestic coal classification table), the CV in D grade coals is >24.5MJ/kg. On the basis of the data in Table 4.1a, only coal VB02, 15144 fulfil that condition. However, sample 15117, 15149 and 15141 can be classified as grade A based on the CV, which is greater than 27.5 MJ/kg. All the remaining coals, based on their CV, can be classified as below grade D. Table 3.4 also indicates thermal coal product specifications, samples 15117, 15141, and 15149 would be suitable for export based on their CV. All the Soutpansberg Coals could be upgraded and may be suitable for a range of applications, including thermal and metallurgical.

4.2. Free Swelling Index (FSI)

As described in Section 3.4, the FSI for each coal sample will give an indication of the swelling potential for the samples, which then infers the ability of coal to produce coke. Results obtained for each coal sample are presented in Table 4.1a.

In the Voorburg area, not all samples reported a FSI number. Samples between the Tshipise and Bosbokpoort Faults had slightly higher FSI values except borehole F578004 (15154, 15155 and 15156) in comparison to samples 10km north of the Tshipise Fault. In Voorburg North, sample VB01 is classified as strongly caking with the other samples classified as non-caking to medium caking. Voorburg South samples that reported a FSI can be classified as strongly caking, with sample 15138 classified as weakly caking; sample 15154, 15155 and15156 (F578004) classified as non-caking. Samples in Makhado reported a variation in FSI with samples 15157 and 15158 (borehole F654BS02) reporting no FSI. Makhado coals varied from non-caking to strongly caking. Samples from Waterberg yielded no FSI and can be classified as non-caking. The Tshikondeni sample reported a FSI of 8, which was

expected and can be classified as strongly caking.

A trend noted was that high FSI is reported for samples with low ash and high CV. As indicated in Figure 4.5, a positive correlation is reported between CV and FSI (where higher CV yields higher FSI). In terms of ash and FSI, a negative correlation was noted; high ash and low FSI.

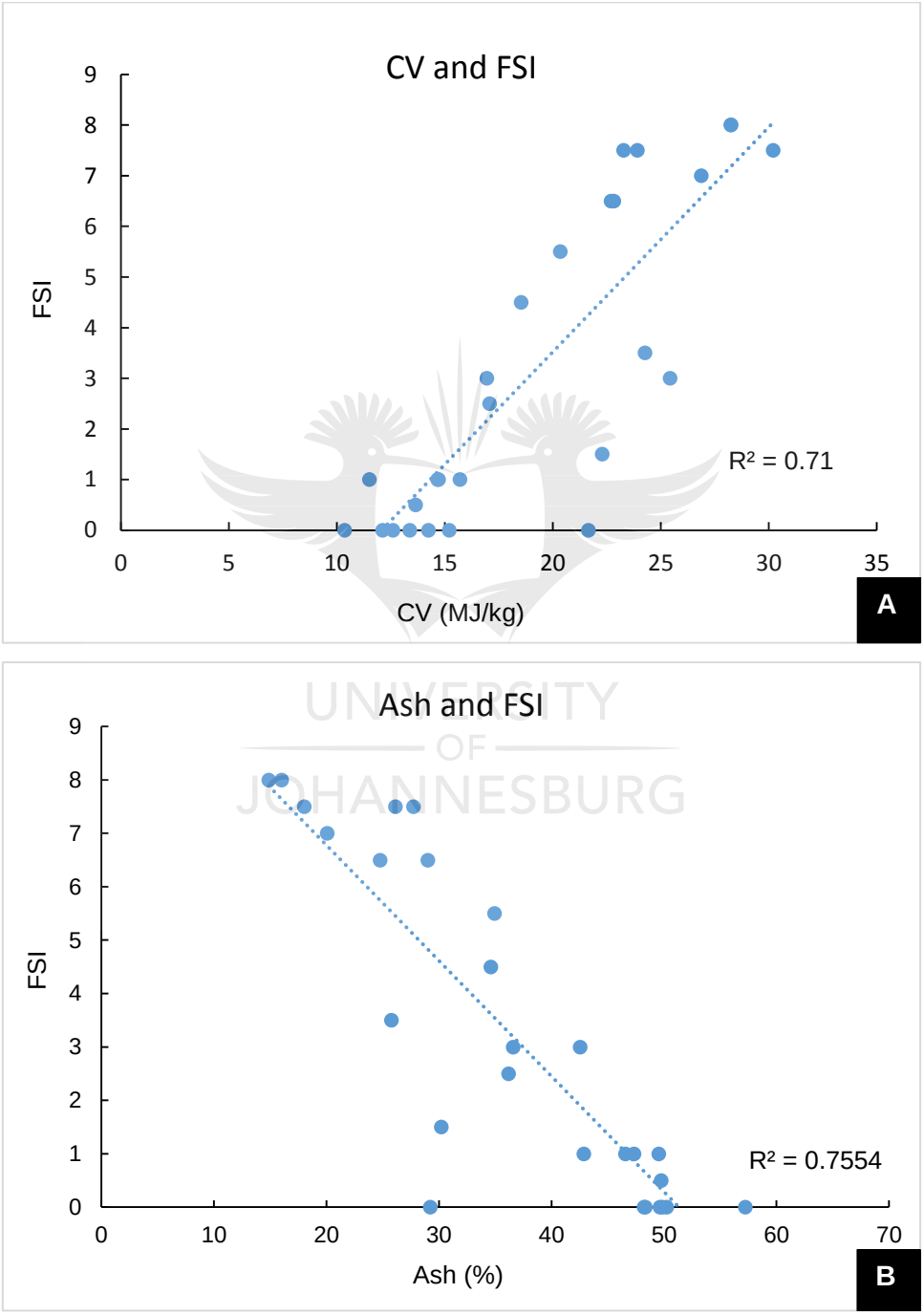

Figure 4.5: Relationship between A) CV and FSI of coal indicating a positive correlation; and B) ash and FSI indicating a negative correlation.

4.3. Petrographic analyses

This section presents petrographic results for localities studied across the Limpopo Province.

4.3.1. General Maceral Descriptions for Limpopo Province Coals

The coals of the Limpopo Province are generally rich in vitrinite, low in inertinite and low in liptinite, as indicated in Table 4.2 and Figure 4.6. The full maceral dataset is included in Appendix B1. On average, the coals have vitrinite contents greater than (>) 60 vol% mmf, with the exception of the Waterberg samples. In comparison coals from the Mpumalanga Province coalfields are characterised by higher inertinite than vitrinite (Figure 4.7) (Falcon, 1986, Pinhiero et al., 1999). As indicated in Section 2.2, the Witbank Coalfield is part of the MKB and is believed to be deposited in a retroarc foreland basin in comparison to coals north and north east of the MKB that were deposited in half graben structures.

Table 4.2: Average maceral group data (vol %) for coals in Limpopo Province (inc.mm = including mineral matter, mmf = mineral matter free).

	Voorburg N		Voorburg S		Makhado		Vele		Waterberg		Tshikondeni	
	inc. mm	mmf	inc. mm	mmf	inc. mm	mmf	inc. mm	mmf	inc. mm	mmf	inc. mm	mmf
Vitrinite	46.38	77.99	55.71	77.04	48.12	67.42	90.52	93.1	36.65	52.75	84.4	86.50
Inertinite	12.00	20.25	15.97	22.17	21.6	31.15	2.72	2.78	33.70	43.70	12.40	12.70
Liptinite	0.98	1.71	0.53	0.78	1.45	2.28	3.97	4.10	2.50	3.50	0.80	0.80
Mm	40.52		27.79		26.33		2.80		27.15		2.40	

Vitrinite occurred mostly as thick bands, light grey to dark grey in colour. Different types of vitrinite encountered are shown in Figure 4.8. According to Kruszewska (2003), the coals from the Soutpansberg are rich in vitrinite, with collotelinite dominating over collodetrinite. This is also noted for samples in this study (Figure 4.9). There were also cracks associated with vitrinite, some infilled with mineral matter (Figure 4.8E). This is because vitrinite is very brittle in comparison to other maceral groups. Extensive cracks were noted in sample 15136 (Figure 4.8F). Pseudovitrinite occurred in all samples, as identified by desiccation cracks or slit like openings in collotelinite (Figure 4.8B). Desiccation cracks observed are of different sizes or length and are orientated in different directions. No mineral inclusions were noted associated with pseudovitrinite particles in contrast to cracked collotelinite.

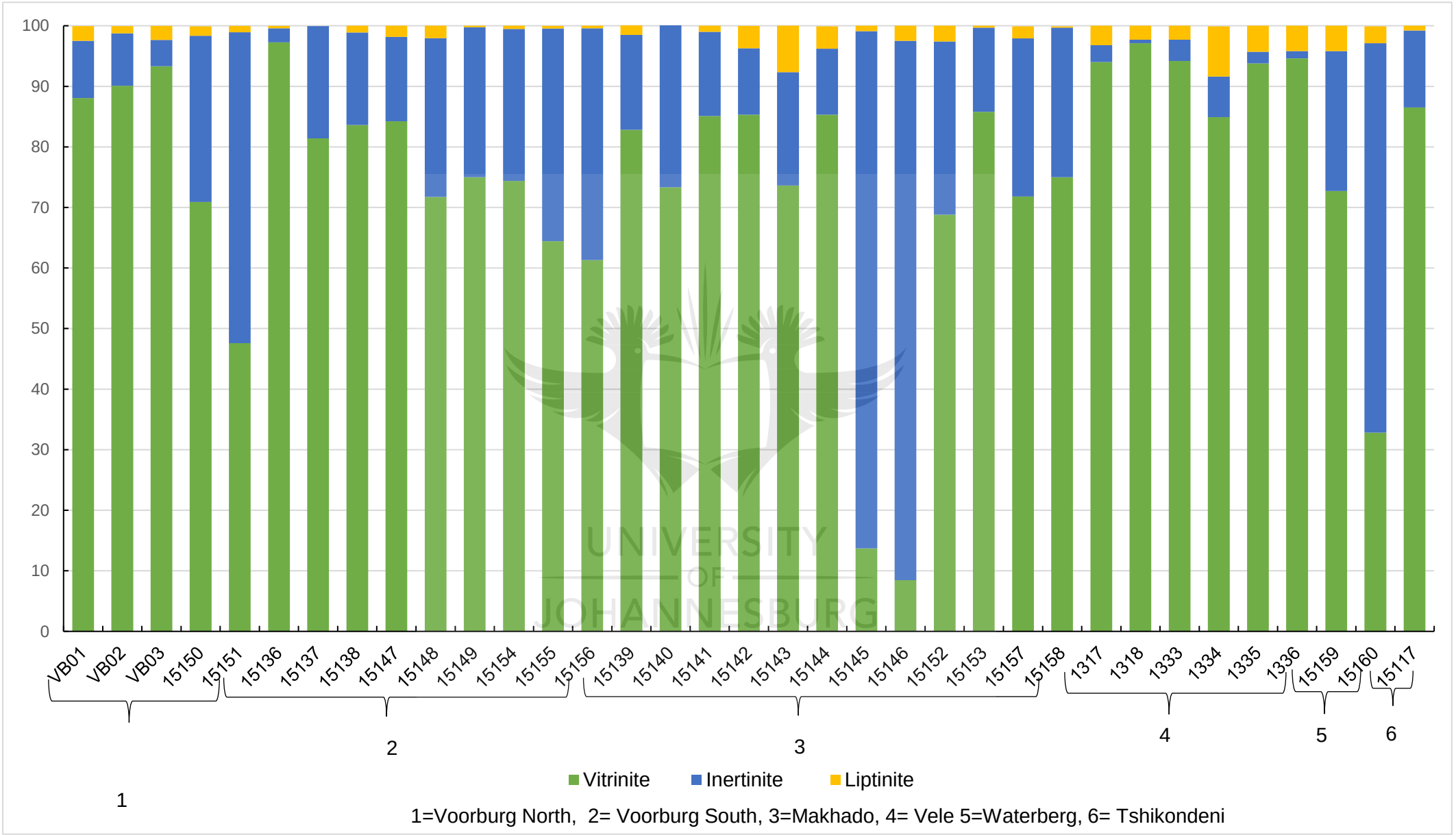

Figure 4.6: Maceral group contents for coals from Limpopo Province (mmf).

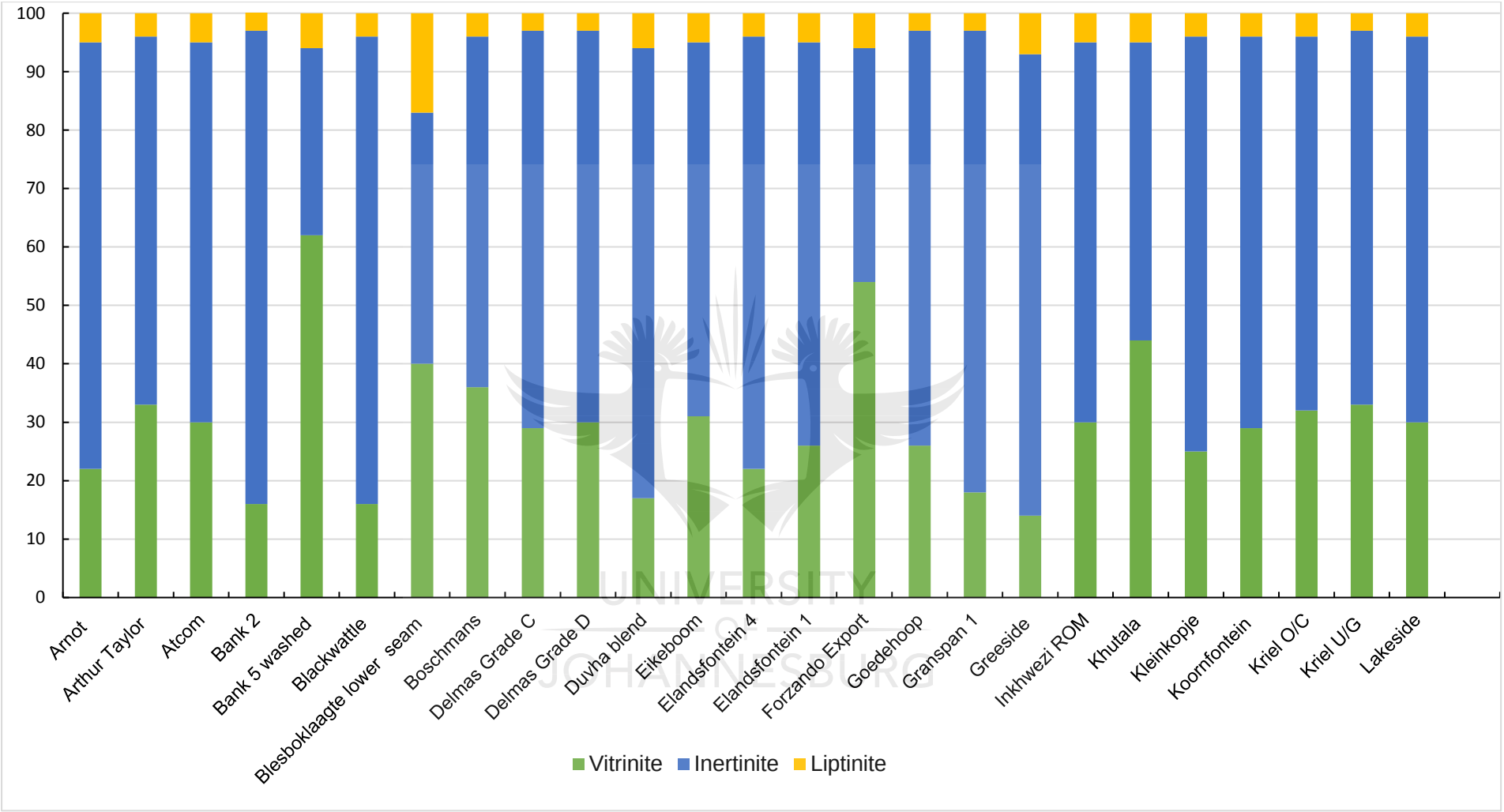

Figure 4.7: Maceral group contents in the coals from selected Witbank mines, Mpumalanga Province (mmf). (Data compiled from Pinheiro et al., 1999).

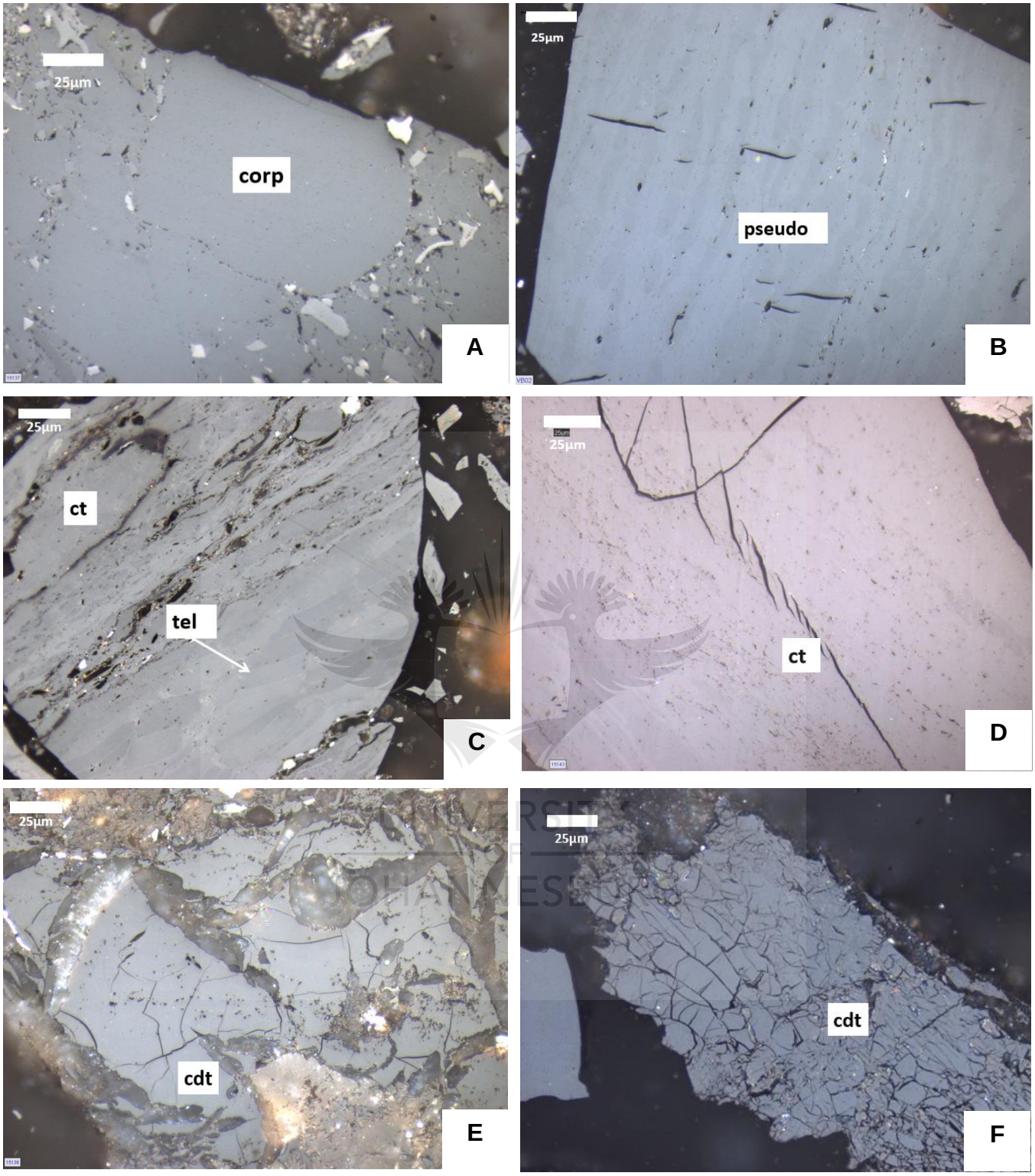

Figure 4.8: Photomicrographs of various forms of vitrinite observed in the coal samples. A) large corpogelinite (15137); B) pseudovitrinite (indicated by desiccation cracks); C) telinite with cell walls preserved and corpogelinite (1317); D) collotelinite with crack ;E) cracks and fissures associated with vitrinite and some impregnation by carbonates (15136); and F) extensive cracks in vitrinite (15136) (Reflected white light, oil immersion, x500). corp=corpogelinite; ct=collotelinite; tel=telinite; cdt=collodetrinite; pseudo=pseudovitrinite.

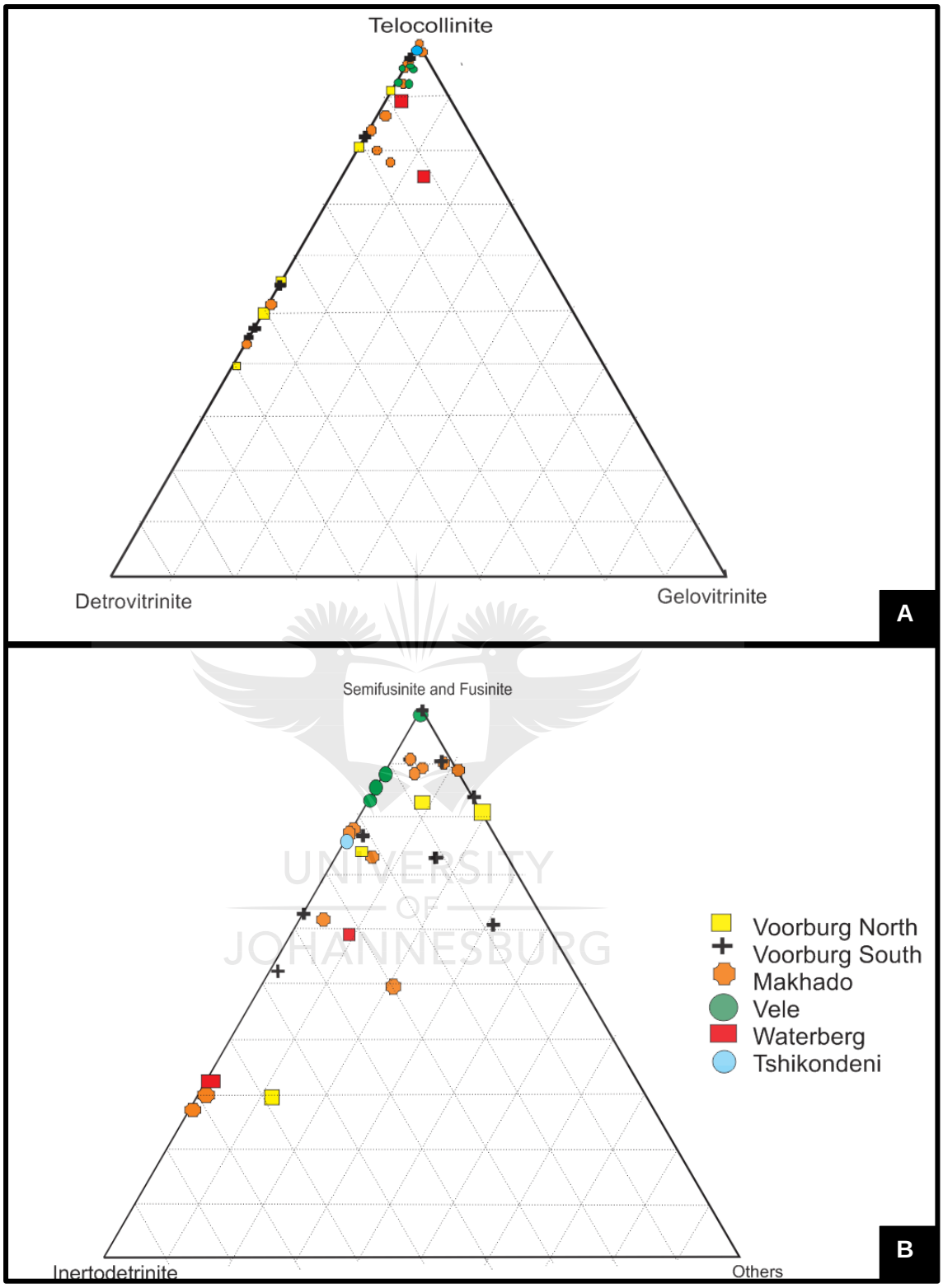

Figure 4.9: A) Vitrinite sub groups and B) inertinite macerals distributions in Limpopo Coals

Inertinite contents ranged between 0.6 - 89.1 (mmf) vol % in these Limpopo Province coal samples. Fusinite and semifusinite are the common inertinite macerals (Figure 4.9B).

The fusinite has a yellowish white tint with the highest reflectance compared to all other macerals (Figure 4.10A). It is characterised by well-preserved cell structures and also bogen structures (Figure 4.10B), where thin wall fragments occur in aggregates. The cell lumina preserved were empty or filled with mineral matter, especially clays and calcite, preventing compression of the cell walls. Where the brittle cell walls were broken, this can be attributed to overburden or tectonic pressure forming fragmented bogen structure (Diessel, 1992).

Semifusinite is characterised by poorly preserved cell structure that are barely visible. Most semifusinite displayed empty cavities (Figure 4.10C). As previously mentioned, some vitrinite particles shows higher reflectance which can be confused with semifusinite. To distinguish between reactive semifusinite and higher reflecting vitrinite, the polarizer and analyser were used; vitrinite remains isotropic, with, semifusinite being weakly anisotropic. Pale grey large bodies with preserved cell wall structures of higher reflectance were noted in samples 15150 and 15151 (Figure 4.10D); these were termed semifusinite based on reflectance although they resembled telinite and gelinite in terms of recognizable cell walls intact in plant tissue.

Secretinite occurred as sub-spherical to oblate bodies with no plant structure. Three different types of secretinite were observed: 1) secretinite bodies that preserved vesicular-like structures; (Figure 4.10E top left) 2) secretinite bodies preserved line-like features (Figure 4.10E right); and 3) secretinite bodies indicated no internal structure (Figure 4.10F). The sizes of the different secretinite ranged from <10 - 2000µm. There were secretinite grains that appeared yellowish grey, and Falcon and Snyman (1986) referred to this as being fusinitised. Secretinite with oxidation rims were identified in samples 15150 and 15151 (Figure 4.10F). The oxidized rim had a significantly lower reflectance compared to the core. The dark rims noted in Figure 4.9 were most likely formed by oxidation under subaerial conditions (ICCP, 2015).

Inertodetrinite (Figure 4.11A) occurred in some samples in the Limpopo Province coals, ranging from 0 – 64.7 vol % (in sample 15146). It occurred as fine fragments of vitrinite and some inertinite macerals and was generally associated with silicates.

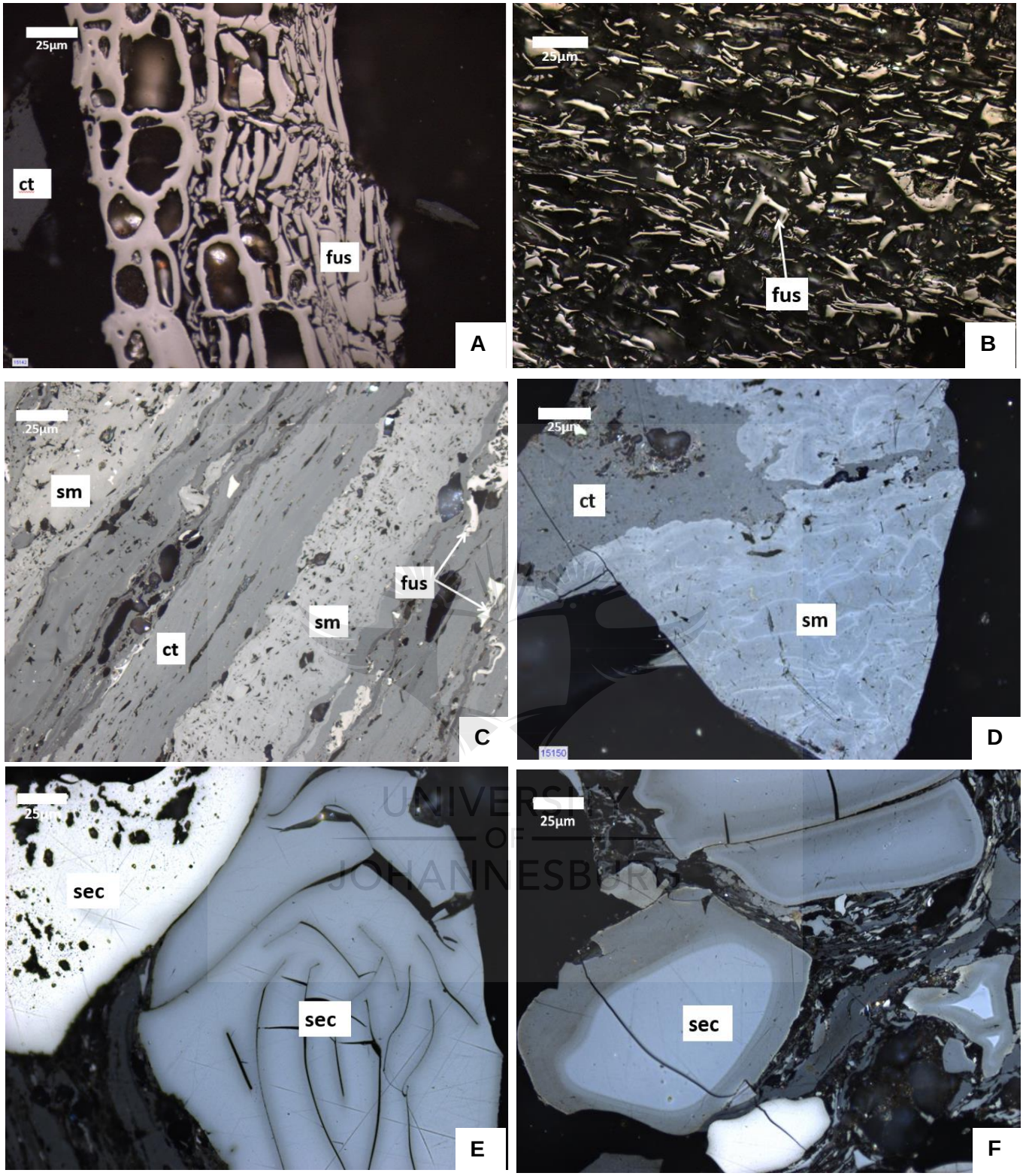

Figure 4.10: Photomicrographs of various forms of inertinite. A) fusinite (15159); B) fusinite with fragmented bogen structure (15146); C) alternating bands of vitrinite with rare fusinite fragments (15140); D) semifusinite with a preserved cell walls (15150); E) different types of secretinite (15150); and F) secretinite with oxidation rims (15151) (Reflected white light, oil immersion, x500). fus=fusinite, sm=semifusinite, ct= collotelinite, sec= secretinite).

Partially burned coal with devolatilisation features in vitrinite grains was observed in samples 15150; these particles were referred to as char but counted as fusinite (Figure 4.11B). Char is characterised by a random distribution of pores as noted in Figure 4.11B. Due to the morphology of char, it cannot be grouped together with one of the established inertinite group macerals but will behave as an inert maceral during coal conversion (ICCP 2001; Kwiecinska and Peterson, 2004). The presence of char could indicate as influence of heat from fire on (1) coal or (2) gelified organic matter in a peat (Kwiecinska and Peterson, 2004).

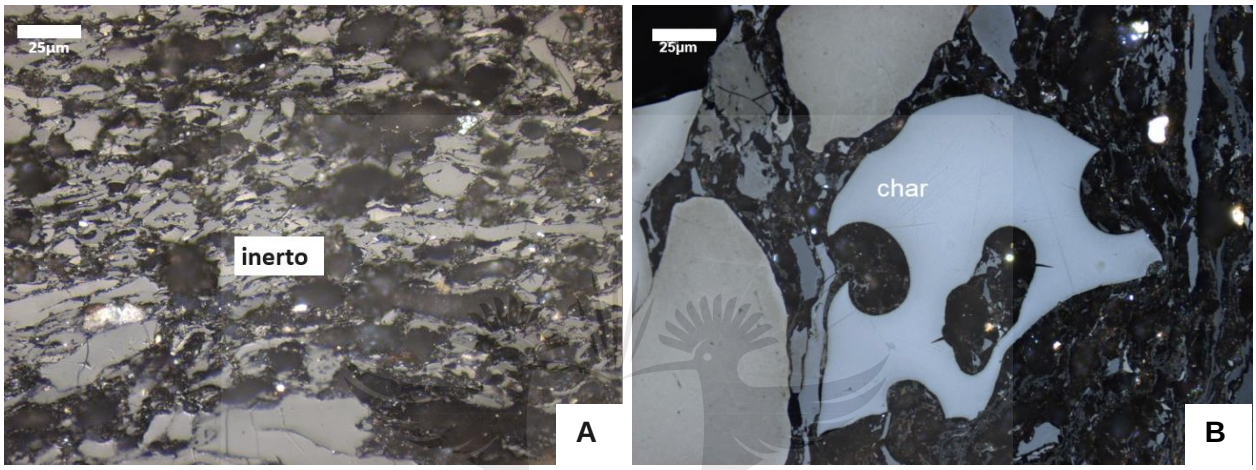

Figure 4.11: Photomicrographs of A) inertodetrinite; and B) char with porous spherical char morphology (Reflected white light, oil immersion, x500) inerto=inertodetrinite.

Liptinite appeared dark grey to black in the coal samples as it is the darkest reflecting maceral group in coal (Pickel et al., 2017). The liptinite content was generally very low in all the Limpopo coal samples assessed, possibly on average lower than the Mpumalanga Coals (Figures 4.6 and 4.7) The most common liptinite was sporinite which occurred as spores. It was mostly trapped in the vitrinite groundmass and parallel to the bedding plane, or associated with clay minerals. Liptinite can be hard to identify, so fluorescent light was used to show the presence of liptinite (Figure 4.12). However, this was not always effective as some of the liptinite appeared not to fluoresce. When fluorescing, liptinite appear yellowish, to brownish orange (Figure 4.12). In sample 15144 and 15152, sporangia (Figure 4.12A) was encountered, that is, spores were contained in the sporangia. Another interesting feature noted was the presence of exine surrounding the corpogelinite maceral (Figure 4.12B).

Cutinite was found in close association with vitrinite macerals rarely exceed 2% in the samples studied. Vele samples had the highest liptinite of all localities. The

presence of cutinite might indicate a different environment in which the liptinite was preserved or produced. Southern African coal rarely contains resinite, and from the study none was found in this study.

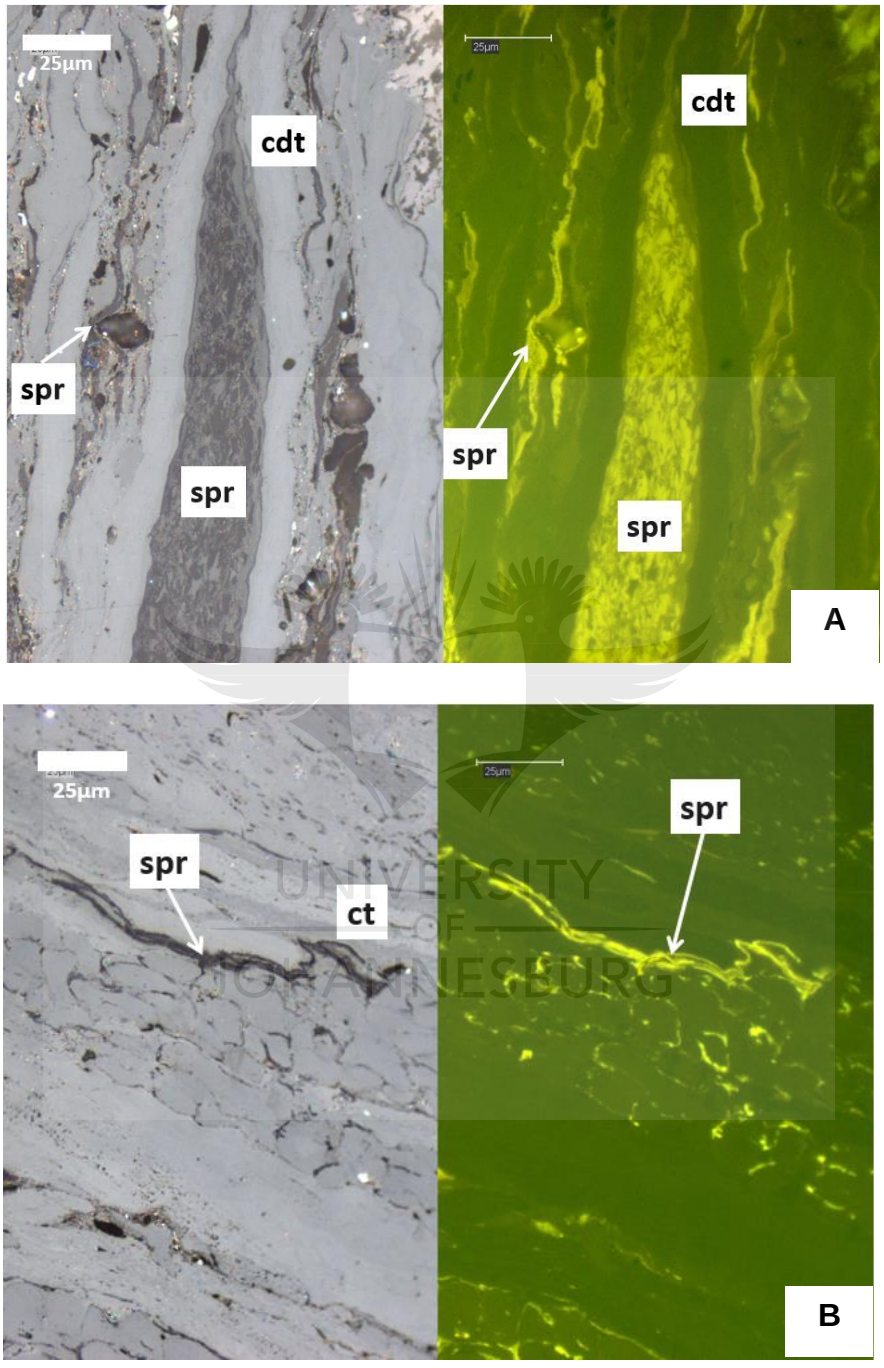

Figure 4.12: Photomicrographs of liptinite. A) sporangia (spores grouped together to form one large spore) (15152); and B) exine preserved surrounding corpogelinite (vitrinite) maceral (15151). (Reflected white and fluorescence light, oil immersion, x500). Left=white light and right=fluorescent light. cut=cutinite, spr=sporinite, ct=collotelinite, cdt=collodetrinite.

4.3.2. Detailed maceral analyses

Following the generalized maceral descriptions for the Limpopo coals samples, attention will now move to detailed maceral analyses. The discussion on reflectance and abnormal conditions analyses will follow in Section 4.3.3 and 4.3.4 respectively.

4.3.2.1. Maceral analyses: Voorburg

Fourteen coal samples from different areas and seams in the Voorburg area were assessed as indicated in Table 3.1 and Figure 3.2. Presented in Table 4.3 are the maceral group contents from point count analysis of the Voorburg coal samples; the full set of results for each borehole sample is located in Appendix B1 (B.1.1 – B.1.2).

Table 4.3: Maceral group content (vol %) for Voorburg coal samples

Location	Borehole ID	Seams	Sample ID		Vitrinite vol %	Inertinite vol %	Liptinite vol %	Mineral matter vol %
Voorburg North	V07BS01	MU	VB01	inc. mm	32.8	3.5	0.9	62.8
				mmf	88.1	9.5	2.4	
		BU	VB02	inc. mm	67.7	6.6	0.9	24.8
				mmf	90.1	8.7	1.2	
		BL	VB03	inc. mm	68.4	3.2	1.7	26.7
				mmf	93.3	4.4	2.3	
	V10BS01	BU	15150	inc. mm	31.7	12.3	0.7	55.3
				mmf	70.9	27.4	1.6	
		BL	15151	inc. mm	31.9	34.4	0.7	33.0
				mmf	47.6	51.3	1.0	
Voorburg South	R637004	MU	15136	inc. mm	72.0	1.7	0.3	26.0
				mmf	97.3	2.3	0.4	
		BU	15137	inc. mm	57.0	13.0	0.0	30.0
				mmf	81.4	18.6	0.0	
		BL	15138	inc. mm	52.6	9.6	0.7	37.1
				mmf	83.6	15.3	1.1	
	R63701LD	MU	15147	inc. mm	64.0	10.6	1.4	24.0
				mmf	84.2	14.0	1.8	
		ML	15148	inc. mm	41.9	15.3	1.2	41.6
				mmf	71.7	26.2	2.0	
		BU	15149	inc. mm	69.0	22.8	0.2	8.0
				mmf	75.0	24.8	0.2	
	F578004	MU	15154	inc. mm	56.6	19.1	0.4	23.9
				mmf	74.4	25.1	0.5	
		ML	15155	inc. mm	44.2	24.1	0.3	31.4
				mmf	64.4	35.1	0.4	
		BU	15156	inc. mm	44.1	27.5	0.3	28.1
				mmf	61.3	38.3	0.4	

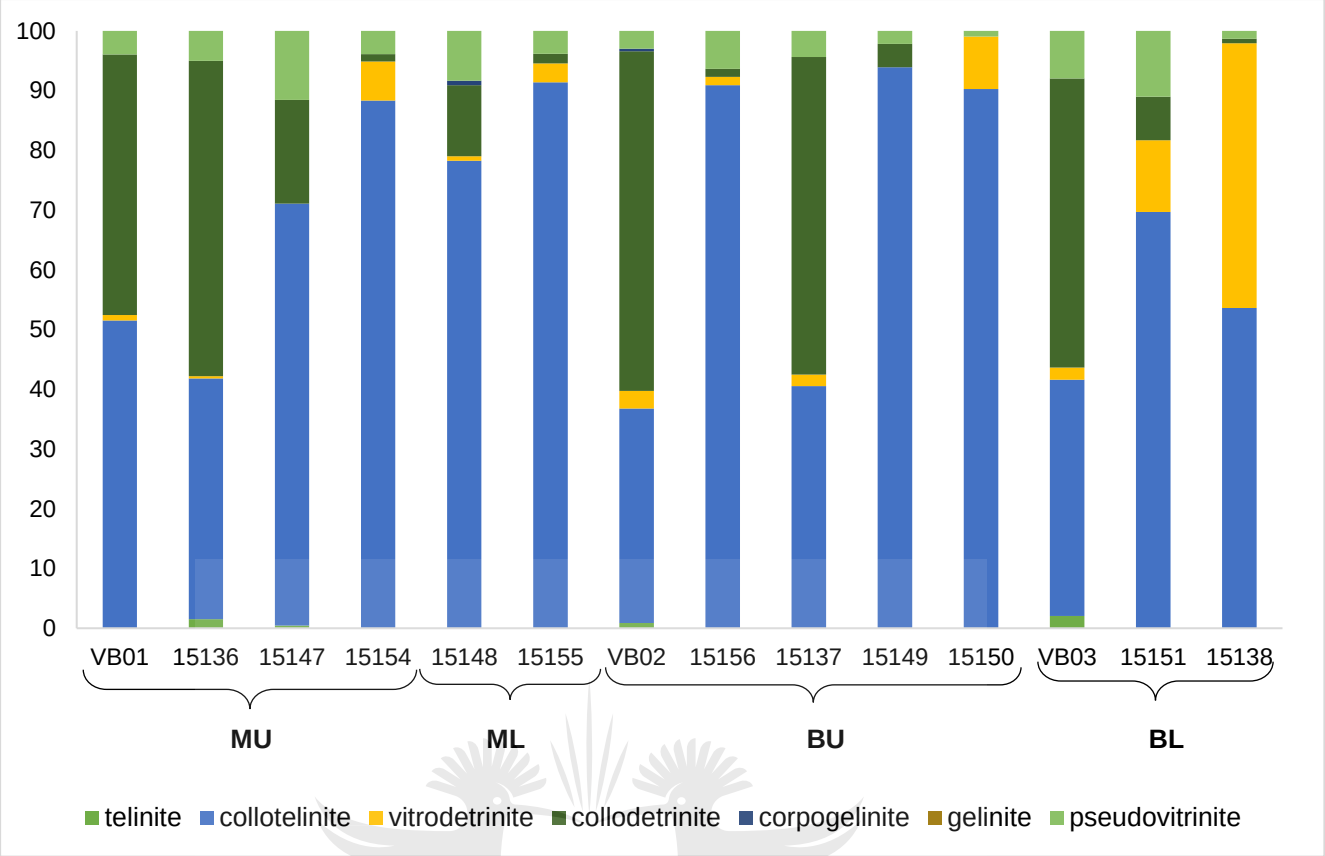

Figure 4.13: Different vitrinite macerals from the Voorburg area (vol %, grouped by seams).

As indicated in Table 4.3, the Voorburg samples generally reported very high vitrinite content, low inertinite and very low liptinite contents on mineral matter free basis (mmf). The dominant maceral group is vitrinite that comprised > 60 vol % in most samples, dominated by collotelinite and collodetrinite macerals, as indicated in Figure 4.13. Pseudovitrinite occurs in most coal samples in low proportions (Table B1). Sample 15151 is dominated by inertinite, specifically inertodetrinite, and also has the lowest volatile matter content.

According to Kruszewska (2003), in South African coals, the liptinite rarely exceeds 7 vol %; this is noted in these samples. The liptinite content is very low for all samples (below 2.5 vol % mmf) indicating that spores and pollens were limited or preservation conditions destroyed the exines.

Generally, the Voorburg North and South samples are comparable petrographically on mmf basis. However, Voorburg North reports higher observable mineral matter

content, supported by proximate analyses where the ash content was also high. The petrographically identified minerals were silicates, carbonates and sulphides (pyrite). According to Miller (2005), the presence of mineral matter is significant in coke production because of the diluting effect of ash. In Voorburg North, the high mineral matter content reported is mostly due to pyrite and siderite inclusions, with the high pyrite content correctable to the high total sulphur contents. Sample VB01 reported the highest total sulphur content (9.49%), which is substantiated by high pyrite content determined from petrography (46.5 vol %). It could be that this sample was obtained from a portion of the core containing a pyrite lens or major cleat. Conversely sample 15151 had low total sulphur content and no pyrite noted in petrography. Mineral matter observed is discussed further in Section 4.6.

4.3.2.2. Maceral analyses: Makhado

Twelve coal sample representing different seams from five boreholes from Makhado as indicated in Figure 3.2 and Table 3.2, were assessed. Maceral group analyses results from Makhado are presented in Table 4.4, with the detailed results presented in Appendix B1 (B.1.3).

Similar to Voorburg, the coal samples in the Makhado project area are rich in vitrinite, with collotelinite being the most common vitrinite maceral in the majority of samples (Figure 4.14). Again, this is in agreement with Kruszewska (2003), where the coking coals from the Soutpansberg Coalfield are rich in vitrinite, having collotelinite dominating over collodetrinite. Samples of Makhado were characterised by vitrinite content > 68.8 vol % mmf with the exception of samples 15145 and 15146 (C699001) (Figure 4.14), which reported 13.7 and 8.4 vol % of vitrinite respectively; total inertinite content was 85.9 and 89.1 vol %. The two inertinite-rich samples were dominated by inertodetrinite indicating reworked environment at this location.

Observable mineral matter samples were silicates (clays and quartz) in most samples, with minor amounts of sulphide (pyrite) and carbonate (siderite and calcite). Sample 15143 reported the highest mineral matter content (53 vol %), also reflected by the proximate analyses. Samples 15142 reported high ash content, but this was, however, not confirmed petrographically. This could be attributed to the highly dispersed fine clay content in the coals, were the particles were omitted from

the point count. As indicated in Section 3.2, samples were milled to 1mm and 32µm were screened out.

Table 4.4: Maceral group content (vol %) from Makhado

Borehole ID	Seam	Sample ID		Vitrinite vol %	Inertinite vol %	Liptinite vol %	Mineral vol %
T190BS03	BU	15139	inc. mm	53.0	10.0	1.0	36.0
			mmf	82.9	15.7	1.6	
	BL	15140	inc. mm	48.0	18.0	0.0	34.0
			mmf	73.3	26.8	1.0	
T07BS	MU	15141	inc. mm	78.6	13.0	0.9	7.5
			mmf	85.1	13.9	1.0	
	BL	15142	inc. mm	79.9	10.3	3.5	6.3
			mmf	85.3	11.0	3.7	
C699001	MU	15143	inc. mm	34.6	8.8	3.6	53.0
			mmf	73.6	18.7	7.7	
	ML	15144	inc. mm	75.3	9.6	3.3	11.8
			mmf	85.3	10.9	3.7	
	BU	15145	inc. mm	9.8	63.8	0.7	25.7
			mmf	13.2	85.9	0.9	
	BL	15146	inc. mm	4.8	64.3	1.2	29.7
			mmf	8.44	89.1	2.5	
S65801LD	MU	15152	inc. mm	42.8	17.8	1.6	37.8
			mmf	68.8	28.6	2.6	
	BU	15153	inc. mm	64.8	10.5	0.2	24.5
			mmf	85.8	13.9	0.3	
F645BS02	BU	15157	inc. mm	41.9	15.3	1.2	41.6
			mmf	71.8	26.1	2	
	BL	15158	inc. mm	43.9	17.8	0.2	38.2
			mmf	66.0	33.7	0.3	

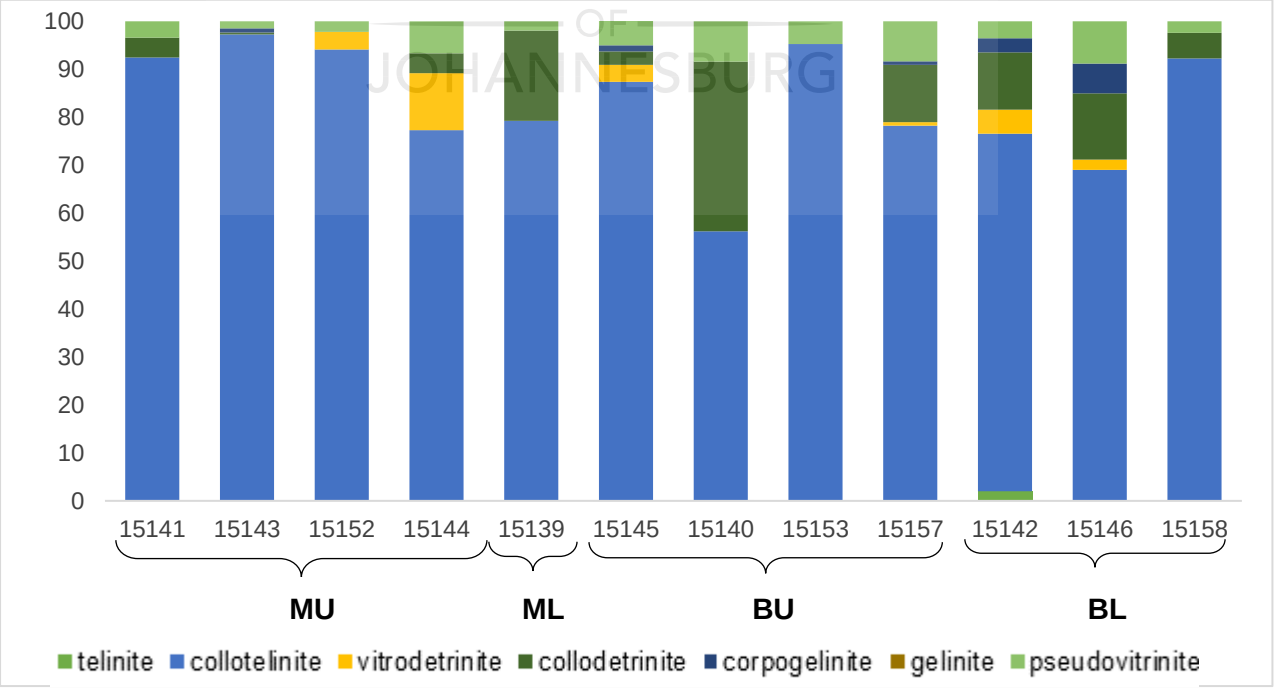

Figure 4.14: Different vitrinite macerals from the Makhado area (vol %, grouped by seam).

The samples with high mineral matter exhibited a low FSI. It important to note that although sample 15145 and 15146 reported low petrographically determined mineral content they still reported a low FSI. This is attributed to the high inertinite content. Inertinite (with the exception of reactive semifusinite – RSF) does not soften and melt when transforming coke to coal (ICCP, 2011).

4.3.2.3. Maceral analysis: Vele, Waterberg, and Tshikondeni

Results of the maceral point count analysis for the Vele, Waterberg, and Tshikondeni samples are presented in Table 4.5 and Appendix B1 (B.1.4).

Table 4.5: Maceral group contents (vol %) from Vele, Waterberg and Tshikondeni.

Location	Borehole ID	Seams	Sample ID		Vitrinite vol %	Inertinite vol %	Liptinite vol%	Mm vol%
Vele	CP17BS02	BU	1317	inc. mm	92.6	2.8	3.2	1.4
				mmf	94.0	2.8	3.2	
		BL	1318	inc. mm	93.8	0.6	2.2	3.4
				mmf	97.1	0.6	2.3	
	OV24BS01	BLT	1333	inc. mm	91.4	3.4	2.2	3.0
				mmf	94.2	3.5	2.3	
		BU	1334	inc. mm	81.8	6.4	8.0	3.8
				mmf	84.9	6.7	8.3	
		M	1335	inc. mm	92.5	1.9	4.2	1.4
				mmf	93.8	1.9	4.3	
		T	1336	inc. mm	91.0	1.2	4	3.8
				mmf	94.6	1.2	4.2	
Waterberg		zone 8+9	15159	inc. mm	46.3	14.7	2.7	36.3
				mmf	72.7	23.1	4.2	
		zone 7+8	15160	inc. mm	27	52.7	2.3	18.0
				mmf	32.8	64.3	2.8	
Tshikondeni		ROM	15117	inc. mm	84.4	12.4	0.8	2.4
				mmf	86.5	12.7	0.8	

The Vele coal samples from two boreholes reported very high vitrinite (dominated by collotelinite), low inertinite and low liptinite contents, a trend noted throughout the Limpopo coals assessed. Higher pseudovitrinite content was noted for Vele samples in comparison to Voorburg and Makhado (Figure 4.15). The Vele coal samples are generally comparable with vitrinite contents above 90%, except for sample 1334. Although still vitrinite-rich, sample 1334 contains a slightly higher proportion of liptinite and inertinite. Observable mineral matter contents noted were very low, with silicates, sulphides (pyrite) and carbonates in minor percentages (Appendix B.1.3).

The two Waterberg samples representing two different zones were variable in composition, with sample 15159 composed of higher vitrinite and mineral matter, and sample 15160 with higher inertinite, and a lower mineral matter content. The carbonate content is low with silicates dominating the minerals, as expected. According to Wagner and Tlotleng (2012), the coal bearing sequence in the Waterberg Coalfield is divided into 11 zones which are equivalent to coal seams. Zones 1 to 5 belong to the Grootegeluk Formation, typically containing bright coals at the base and grade upwards into shale. The samples in this study are from Zone 8 and 9 and Zone 6 and 7, which were anticipated to be high in vitrinite. Sample 15159 followed this trend although sample 15160 had relatively low vitrinite content.

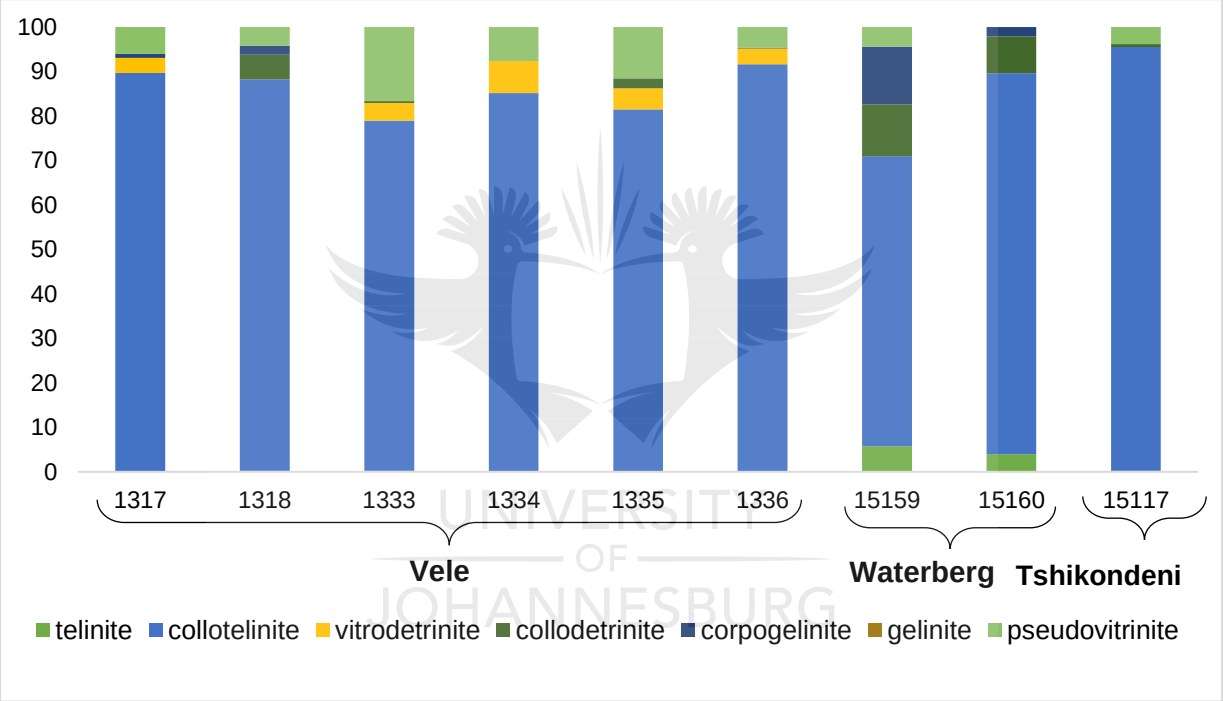

Figure 4.15: Different vitrinite macerals in Vele, Waterberg and Tshikondeni areas (vol %).

Only one Tshikondeni sample was included for comparative purposes, and as expected, the results indicated high vitrinite (collotelinite), low inertinite, low liptinite and low mineral matter. Pyrite was observed petrographically, but not counted as these particles did not fall under the crosshair. The Vele and Tshikondeni sample are more comparable in composition when compared to the Waterberg samples. All coals are suitable for thermal and metallurgical applications, possibly with processing required for the Waterberg samples.

4.3.2.4. Seam correlations

Lateral variation in petrographic content of the seams was considered for seams from the Voorburg and Makhado area in the Soutpansberg Coalfield.

In Voorburg, the MU seams contained the highest mineral matter contents. The BU and BL seams were varied in composition; sample 15145 and 15146 had elevated levels of inertinite.

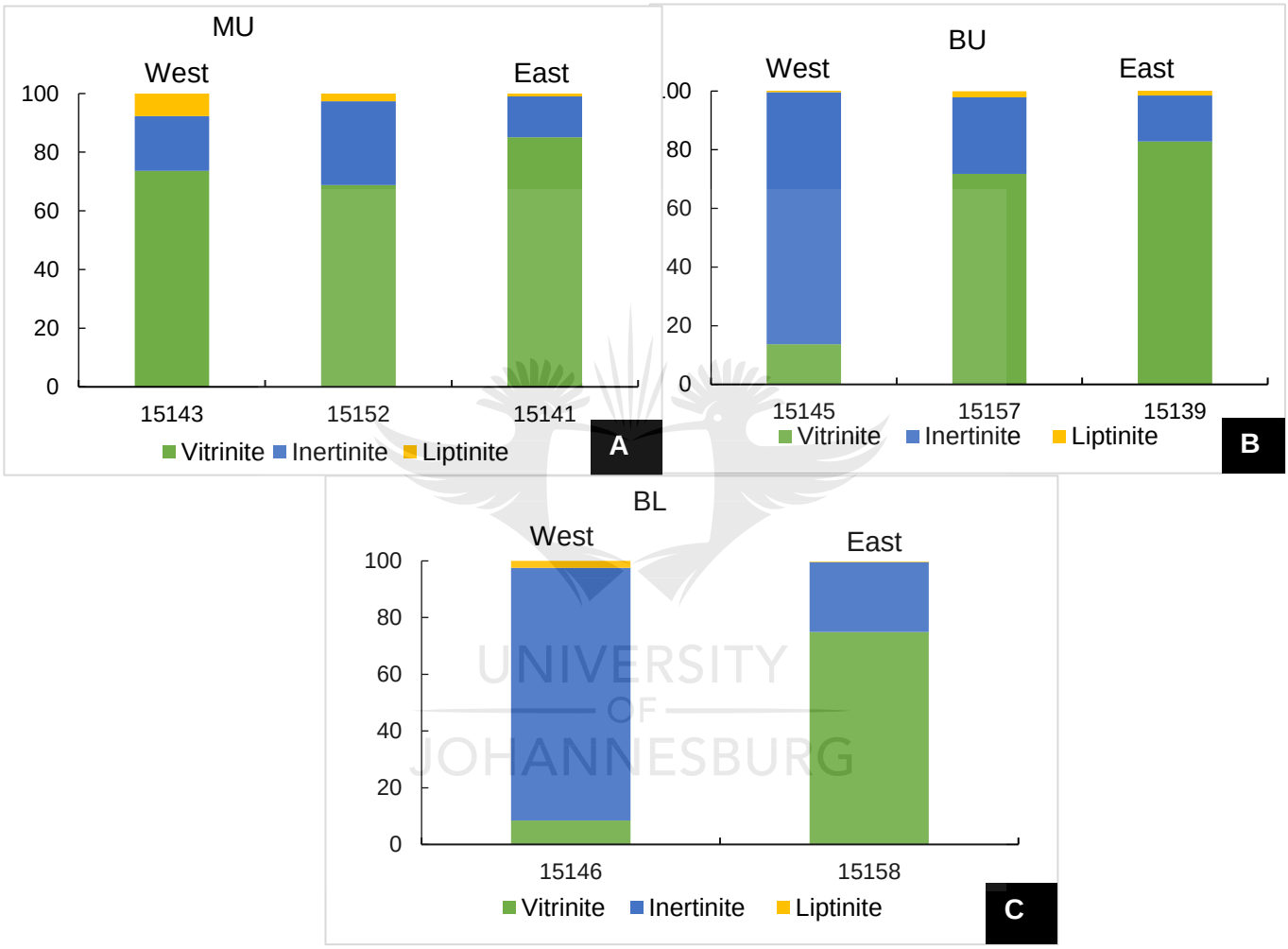

Figure 4.16: Correlation of coal horizons in Makhado indicating an increase in vitrinite content from west to east: A) MU seam; B) BU seam; and C) BL seam (vol %).

In the Makhado seams (MU, BU and BL), the vitrinite contents were noted to be lower in samples in the west in comparison to samples in the east (Figure 4.16C), indicating a trend where vitrinite contents increase from west to east. Hence, it appears to have been a slight change in depositional environment between the east and west. Tshikondeni (to the East) has very high vitrinite content and the Waterberg to the west has lower vitrinite content.

4.4. Vitrinite reflectance

The vitrinite reflectance was measured on collotelinite. Reflectance readings were not taken on pseudovitrinite. The mean reflectance results are presented in Table 4.6. Two examples of reflectance histograms are provided in Figure 4.17, indicating a unimodal and a bimodal distribution; further histograms for each coal sample are located in Appendix B2. The histograms indicated a unimodal distribution for the majority of samples. Samples 15138 and 15154 samples show a bimodal distribution. The bimodal distribution for sample 15154 could be due to elevated reflectance in certain particles that have been affected by the proximity of the fault zones. From petrography collotelinite particles of different shades of grey were observed (Figure 4.18) which could account for the bimodal distribution.

Voorburg North coal samples have a mean RoV % between 0.76 – 0.84%, with an average of 0.79%. This implied the rank of the coal to be a medium rank C classified according to UNECE (1998). Voorburg North samples have a lower reflectance compared to Voorburg South and Makhado. In Voorburg North, the Bottom Seam samples appear to have a slightly higher reflectance compared to the Middle Seam horizon.

Voorburg South reported higher reflectance values compared to Voorburg North. The coal samples reported a mean RoV% of between 0.80 - 1.26%. The rank of the coal ranges from medium rank C to medium rank A. Voorburg South samples are located between the Tshipise and Bosbokpoort Faults and the trend of the Bottom Seam having a higher reflectance does not apply. Sample 15154 to 15156 (F57800) are closer to the Bosbokpoort Fault and reported the highest reflectance values and bimodal distributions indicating that the fault played a role increased rank.

The mean vitrinite reflectance values of the Makhado coal samples (Table 4.6) range from 0.70 - 0.95 %, averaging 0.86%. This suggests a bituminous medium rank C coal, classified according to the UNECE (1998). The Bottom Seam (Sample 15140, 15142, 15453, 15157) reports higher reflectance and exhibits values a trend similar to Voorburg North; this can be attributed to an increase in the geothermal gradient.

Table 4.6: Vitrinite reflectance (RoVmr %) for the Limpopo coal samples

Location	Borehole ID	Seams	Sample ID	RoVmr %	St. dev	Min%	Max%
Voorburg North	V07BS01	MU	VB01	0.77	0.057	0.67	0.92
		BU	VB02	0.78	0.065	0.65	0.92
		BL	VB03	0.76	0.053	0.64	0.86
	V10BS01	BU	15150	0.79	0.061	0.63	0.99
		BL	15151	0.84	0.052	0.63	0.98
Voorburg South	R637004	MU	15136	0.88	0.056	0.80	1.09
		BU	15137	0.95	0.074	0.82	1.17
		BL	15138	0.80	0.160	0.59	1.14
	R63701LD	MU	15147	0.90	0.058	0.77	1.06
		BU	15148	0.92	0.050	0.81	1.01
		BL	15149	0.94	0.045	0.84	1.08
	F578004	MU	15154	1.26	0.126	0.96	1.53
		ML	15155	0.99	0.069	0.89	1.30
		BU	15156	1.02	0.062	0.93	1.28
Makhado	T190BS03	BU	15139	0.80	0.169	0.51	1.26
		BL	15140	0.95	0.076	0.77	1.09
	T07BS	MU	15141	0.83	0.044	0.73	0.94
		BL	15142	0.86	0.056	0.74	1.03
	C699001	MU	15143	0.71	0.059	0.56	0.84
		ML	15144	0.70	0.062	0.56	0.89
		BU	15145	0.79	0.074	0.65	0.97
		BL	15146	0.81	0.061	0.68	1.01
	S65801LD	MU	15152	0.89	0.061	0.74	1.07
		BU	15153	0.95	0.127	0.75	1.23
	F645BS02	BU	15157	0.93	0.079	0.76	1.22
		BL	15158	0.92	0.060	0.81	1.11
Vele	CP17BS02	BU	1317	0.74	0.065	0.60	0.89
		BL	1318	0.78	0.047	0.65	0.89
	OV24BS01	BLT	1333	0.74	0.071	0.59	0.90
		BU	1334	0.71	0.065	0.56	0.87
		M	1335	0.74	0.062	0.57	0.83
		T	1336	0.66	0.060	0.52	0.77
Waterberg		Zone 8+9	15159	0.65	0.060	0.51	0.74
		Zone 7+8	15160	0.63	0.042	0.53	0.77
Tshikondeni		ROM	15117	1.23	0.114	0.96	1.51

The mean vitrinite reflectance values for the Vele, Waterberg and Tshikondeni samples are also noted in Table 4.6. The Vele coal samples reported a mean RoV% between 0.66 – 0.78% and an average of 0.73%. According to the UNECE (1998), the coal is medium rank C coal. The two Waterberg samples reported a mean RoV% of 0.65 and 0.63. This also suggests a bituminous medium rank C coal, classified according to the UNECE (1998). The Tshikondeni sample reported a higher rank than the other Limpopo coals, with a mean RoV% of 1.23, with a standard deviation of 0.114%. According to UNECE (1998), the coal is bituminous medium rank B.

Typically Tshikondeni reflectance values occur between1.23 – 1.41 %.

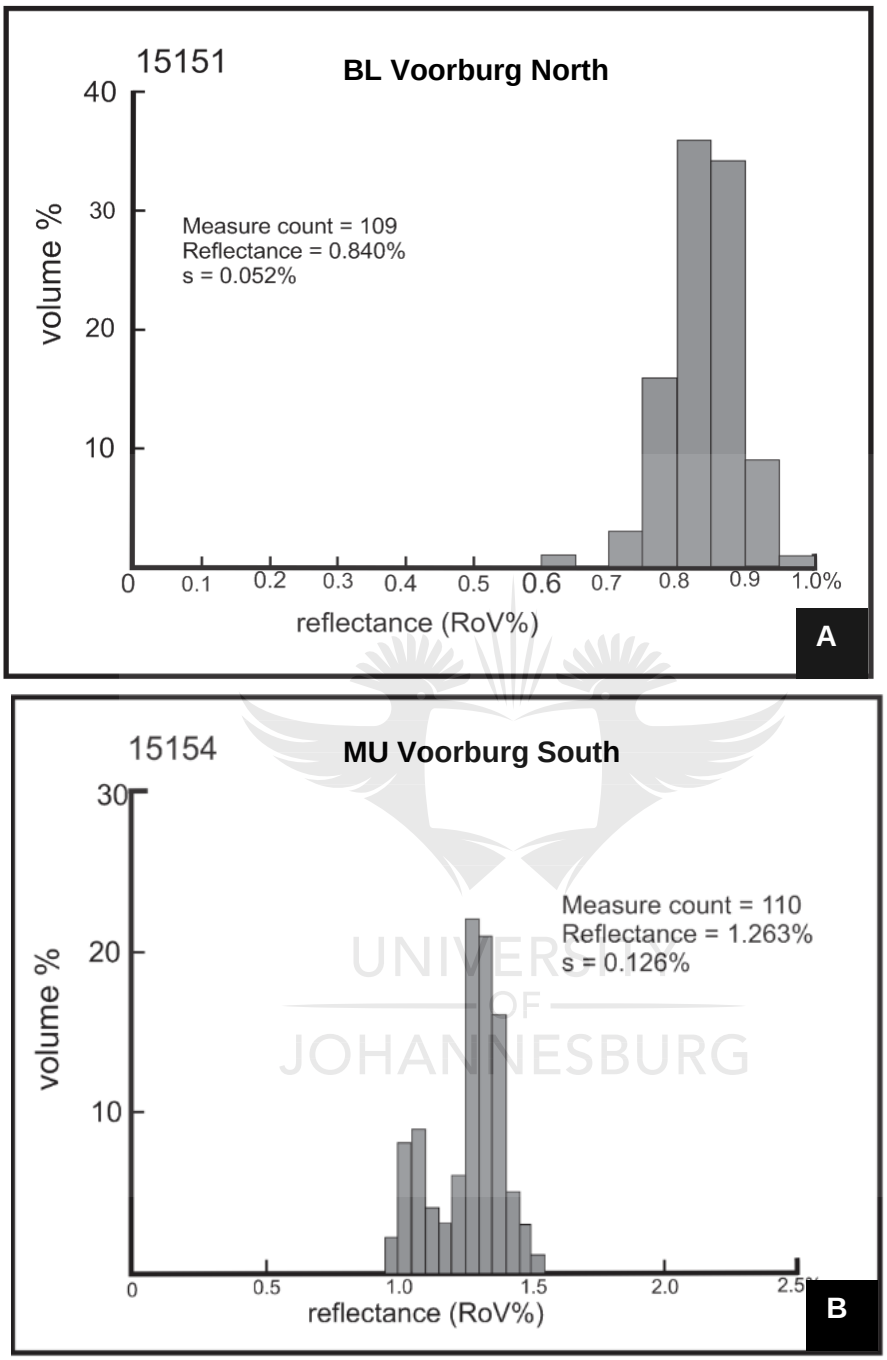

Figure 4.17: Vitrinite histograms A) unimodal distribution; and B) bimodal distribution.

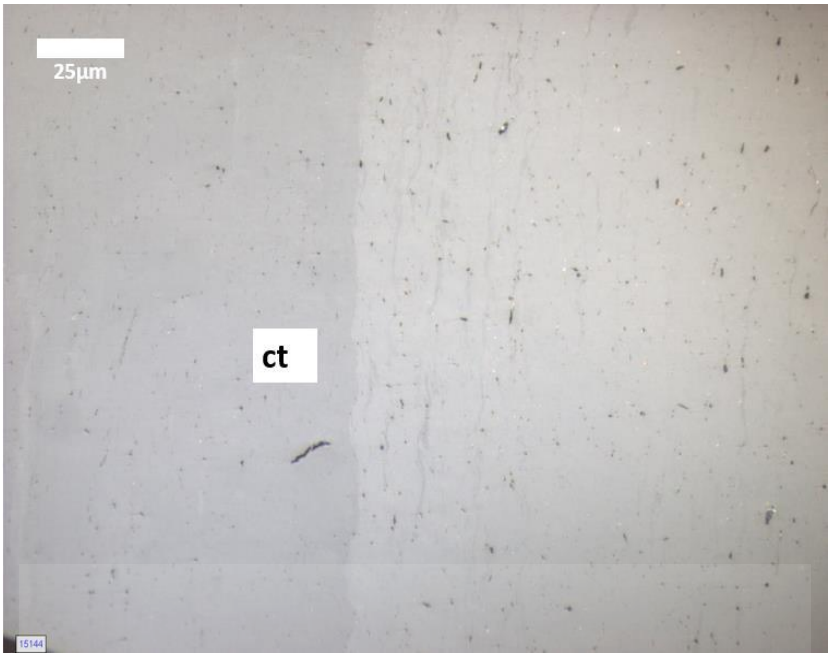

Figure 4.18: Photomicrographs of collotelinite on the left showing a slight higher reflectance compared to collotelinite on the right (15154). (Reflected white light, oil immersion, x500).

According to Sparrow (2012) and Hancox and Gotz (2014), the coal rank increases from the west to the east across the Limpopo Province. This is noted in Figure 4.19 were Waterberg samples in the west had a low reflectance of 0.63 and 0.65 in comparison to Tshikondeni in the east with a mean reflectance of 1.23 %. Across Makhado samples 15139 and 15140 (BH T190BS03) are located in the east (Figure 3.1) and have a higher vitrinite reflectance compared to samples 15143 to 15146 (BH C699001) which are located in the west. The samples contained between the Tshipise and Bosbokpoort Faults have higher reflectance values than Mkhado and Voorburg North..

The reflectance values obtained showed that samples in Voorburg North have a lower vitrinite reflectance compared to samples in Voorburg South and Makhado. The difference in the vitrinite reflectance can be explained by the geothermal gradient. As previously mentioned in Section 2.2.2, Voorburg North is an up faulted block of Karoo aged sediments with shallow seams, as indicated by borehole V07BS01 in Figure 3.4. Voorburg South samples are deeper (Figure 3.4). A 100m displacement is noted between the boreholes in Voorburg North and Voorburg South. It is well documented that the reflectance of vitrinite increases as coal becomes more thermally altered (Stach et al., 1982). Dolerite dyke and sill intrusions

observed in some boreholes. However, the vitrinite reflectance did not indicated rapid changes that can be attributed to devolatilisation by igneous intrusions (dolerite dykes and sills). The intrusions may have had a limited effect, with geothermal gradient heat probably being more dominant.

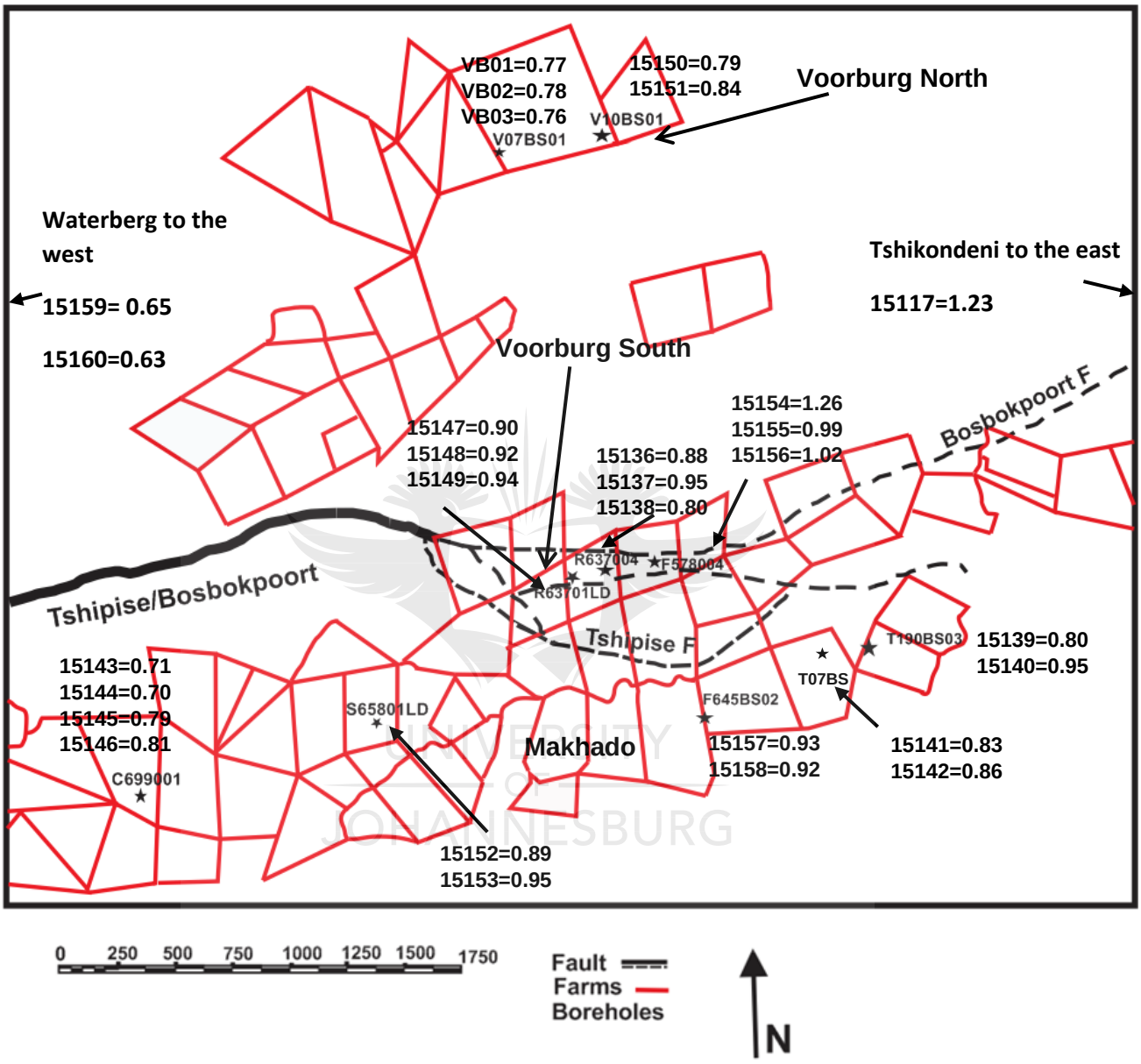

Figure 4.19: Mean vitrinite reflectance across the Waterberg, Voorburg, Makhado and Tshikondeni areas. All values are mean RoV%. 15xxx =sample ID, 0.xx= reflectance value

According to ICCP (2015), to produce prime coke the optimum rank range of coking coal is from 1.10% to1.45% vitrinite reflectance. Coals with vitrinite reflectance below the range 0.85% range form cokes with progressively weaker structures. The coals assessed in this study (except from Tshikondeni) are likely to be suitable to produce a weaker coke referred to as semi soft coke. A weaker coke results in a marked

decrease in strength indices but coke hardness may remain high (ICCP, 2011). Khorami et al. (2011), noted that FSI increased with increasing rank (determined as vitrinite maximum reflectance). Voorburg North samples have a reflectance range lower than the range aforementioned. Voorburg South coal samples have a potential to produce coke as the RoV% is within the semi coke range. It is important to note that sample 15154, 15155, and 15156 have a RoV% > 0.9 but FSI number is 0. However, the proximate analyses and maceral point count analyses revealed that samples 15155 and 15156 have high ash and CV, and are rich in mineral matter and inertinite.

4.5. Abnormal condition analysis (ACA)

The purpose of this analysis was to determine any impact the Tshipise and Bosbokpoort Faults may have on the coal in terms of abnormal features. As discussed, categories proposed Wagner (2007) were applied (Section 3.5.3).

Data obtained from the ACA are presented in Table 4.7 with a full set of results presented in Appendix B3. The Soutpansberg and Limpopo (Vele) Coalfields samples appeared fresh, as the particles indicated no major fissures or cracks. Sample 15136 had the highest total abnormal condition (23.4%). Other coal samples had a few fissures. Fissures are described as < 1µm in width. The fissures in these coals were found propagating through different types of macerals. Fissures were not extensive, with borehole 15149 reporting the most extensive fissures (4.4 %). Most samples were reported to have inherent cracks in minor proportions.

Samples in Vele had high values due to desiccation cracks associated with the high pseudovitrinite content. Cracks infilled with pyrite mineral and calcite were noted in sample 15136. This could be related to the Tshipise and Bosbokpoort Faults introducing an influx of hydrothermal fluids. From the ACA, there is no apparent concern regarding oxidation or weathering in these samples and friability should not be an issue except possibility in samples 15136, 1333 and 1335.

Table 4.7: ACA results for Limpopo Province coals (vol %)

Location	Borehole ID	Seams	Sample ID	Fresh	Total abnormal condition
Voorburg North	V07BS01	MU	VB01	85.7	14.3
		BU	VB02	94.9	5.1
		BL	VB03	90.9	9.1
	V10BS01	BU	15150	91.0	9.0
		BL	15151	90.9	9.1
Voorburg South	R637004	MU	15136	76.6	23.4
		BU	15137	90.0	10.0
		BL	15138	91.7	8.3
	R63701LD	MU	15147	89.3	10.7
		BU	15148	86.0	14.0
		BL	15149	82.2	17.8
	F578004	MU	15154	90.6	9.4
		ML	15155	89.3	10.7
		BU	15156	92.1	7.9
Makhado	T190BS03	BU	15139	87.9	12.1
		BL	15140	88.7	11.3
	T07BS	MU	15141	87.0	13.0
		BL	15142	91.1	8.9
	C699001	MU	15143	91.8	8.2
		ML	15144	88.9	11.1
		BU	15145	87.5	12.5
		BL	15146	85.1	14.9
	S65801LD	MU	15152	91.8	8.2
		BU	15153	89.8	10.2
	F645BS02	BU	15157	86.4	13.6
		BL	15158	87.9	12.1
Vele	CP17BS02	BU	1317	87.3	12.7
		BL	1318	87.3	12.7
	OV24BS01	BLT	1333	77.0	23.0
		BU	1334	87.4	12.6
		M	1335	76.8	23.2
		T	1336	88.3	11.7
Waterberg		Zone 8+9	15159	87.0	13.0
		Zone 7+8	15160	83.2	16.8
Tshikondeni		ROM	15117	83.2	16.8

4.6. Mineral Matter in Limpopo Province coals

In this section, results from mineralogical analyses for the Limpopo coal samples are discussed. Mineralogical analysis was based on the results obtained from, XRD, SEM, and EMPA. The analyses were carried out to study the mineralogy and morphology of mineral matter in coal. Ash analyses are important in determining the total amount of mineral mater and petrographically determined mineral groups provides information regarding the distribution or mode of occurrence of the mineral matter. Total observable mineral matter content and ash content (Table 4.8 and Figure 4.20) were plotted but no clear correlation was possible. However, there are limitations due to the resolution of the petrographic microscope, and minerals below 5µm could not be identified. Generally samples from the Limpopo Province are rich in mineral matter/ash. As previously mentioned, there were three main mineral matter groups identified petrographically, and each group's characteristics are discussed below. The data presented in Table 4.9 represents data acquired from XRD analyses and will be discussed together petrography observations, as well as the SEM and EDS data. The common minerals identified were quartz and kaolinite. Dolomite was not identified petrographically.

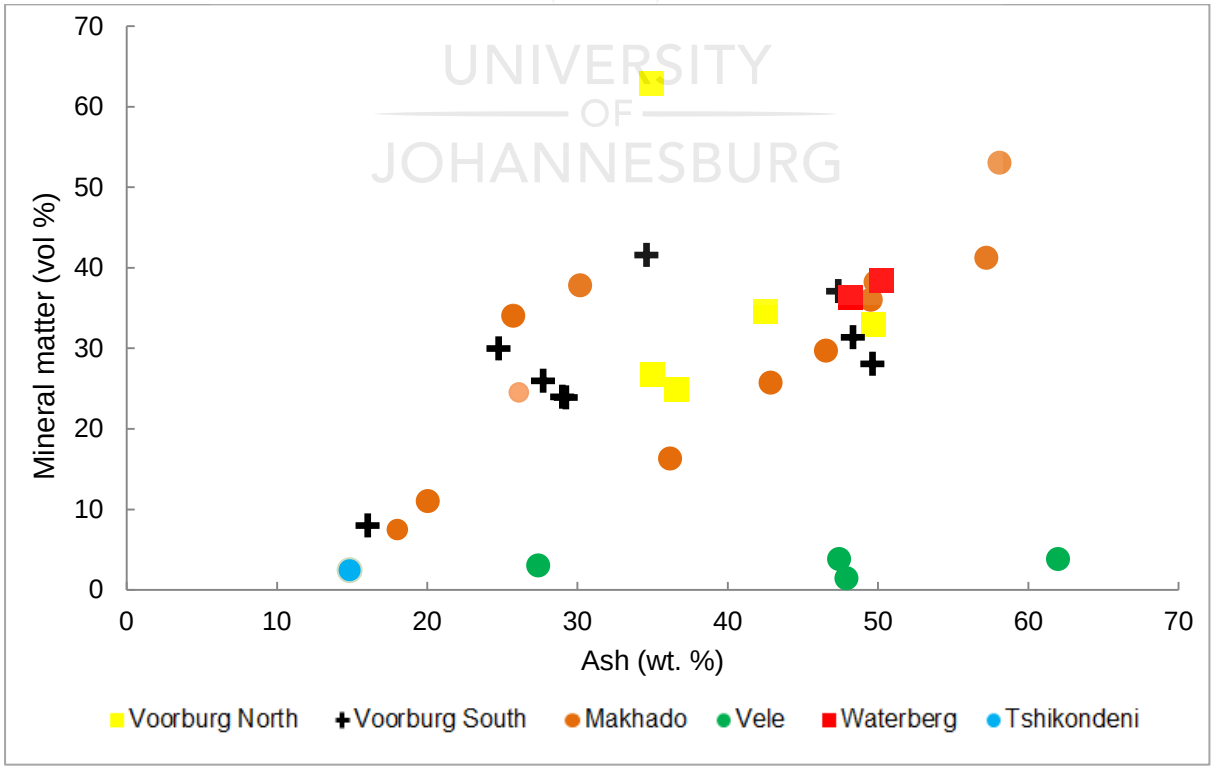

Figure 4.20: Relationship between ash (db) and observable mineral matter content (vol %).

Table 4.8: Ash (wt. %), total sulphur (%) and observable mineral matter (vol %) in the coals from Limpopo Province.

Location	Borehole ID	Seams	Sample ID	Ash (wt. %)	TS (%)	Mineral matter (vol %)
Voorburg North	V07BS01	MU	VB01	34.92	9.49	62.8
		BU	VB02	36.60	2.79	24.8
		BL	VB03	34.99	3.93	26.7
	V10BS01	BU	15150	42.55	1.60	34.5
		BL	15151	49.73	0.52	33.0
Voorburg South	R637004	MU	15136	27.71	1.57	26.0
		BU	15137	24.75	0.54	30.0
		BL	15138	47.34	0.24	37.1
	R63701LD	MU	15147	28.99	0.93	24.0
		BU	15148	34.59	1.16	41.6
		BL	15149	16.02	0.88	8.0
	F578004	MU	15154	29.21	1.38	23.9
		ML	15155	48.33	0.54	31.4
		BU	15156	49.62	0.50	28.1
Makhado	T190BS03	BU	15139	49.54	0.49	36.0
		BL	15140	25.75	0.73	34.0
	T07BS	MU	15141	18.00	1.23	7.5
		BL	15142	58.11	0.31	53.0
	C699001	MU	15143	36.17	2.16	16.3
		ML	15144	20.06	1.45	11.0
		BU	15145	42.87	0.47	25.7
		BL	15146	46.55	1.14	29.7
	S65801LD	MU	15152	30.20	1.40	37.8
		BU	15153	26.11	0.67	24.5
	F645BS02	BU	15157	57.22	0.31	41.2
		BL	15158	49.86	0.40	38.2
Vele	CP17BS02	BU	1317	27.40	1.10	3.0
		BL	1318	62.00	1.10	3.8
	OV24BS01	BLT	1333	47.91	0.80	1.4
		BU	1334	47.43	1.10	3.8
Waterberg		Zone 8+9	15159	48.22	2.00	36.3
		Zone 7+8	15160	50.22	1.43	38.4
Tshikondeni		ROM	15117	14.85	0.91	2.4

Table 4.9: XRD determined minerals from Limpopo coals (excludes Vele as samples were not available).

Location	Borehole ID	Seams	Sample ID	XRD determined minerals
Voorburg North	V07BS01	MU	VB01	Dolomite, Pyrite, Quartz, and Kaolinite
		BU	VB02	Dolomite, Pyrite, Quartz, and Kaolinite
		BL	VB03	Dolomite, Pyrite, Quartz, and Kaolinite
	V10BS01	BU	15150	Quartz and Kaolinite
		BL	15151	Quartz, Kaolinite and Dolomite
Voorburg South	R637004	MU	15136	Quartz, Siderite, Pyrite, Kaolinite, and Dolomite
		BU	15137	Quartz, Kaolinite, Dolomite, and Quartz
		BL	15138	Quartz and Kaolinite
	R63701LD	MU	15147	Quartz, Kaolinite, Siderite and Pyrite
		BU	15148	Quartz, Kaolinite, Siderite and Pyrite
		BL	15149	Quartz, Kaolinite and Dolomite
	F578004	MU	15154	Quartz and Kaolinite
		ML	15155	Quartz and Kaolinite
		BU	15156	Quartz and Kaolinite
Makhado	T190BS03	BU	15139	Quartz, Kaolinite and Dolomite
		BL	15140	Siderite, Kaolinite and Pyrite
	T07BS	MU	15141	Quartz and Kaolinite
		BL	15142	Quartz, Kaolinite and Siderite
	C699001	MU	15143	Quartz, Kaolinite, Ankerite, Pyrite
		ML	15144	Quartz, Kaolinite, Siderite and Pyrite
		BU	15145	Quartz and Kaolinite
		BL	15146	Quartz and Kaolinite
	S65801LD	MU	15152	Quartz, Kaolinite and Dolomite
		BU	15153	Quartz, Kaolinite, and Ankerite
	F645BS02	BU	15157	Quartz and Kaolinite
		BL	15158	Quartz, Kaolinite and Dolomite
Waterberg		Zone 8+9	15159	Quartz, Kaolinite
		Zone 7+8	15160	Quartz, Kaolinite
Tshikondeni		ROM	15117	Quartz, Kaolinite

4.6.1. Silicates

Silicate group minerals in this context include clays and quartz as different clays could not be differentiated petrographically. However, the XRD data indicates that the clay form is kaolinite. Clay minerals were the predominant minerals determined in all samples. Clay minerals (Figure 4.21) were typically sugary in texture, and occurred as groundmass between other macerals, as cells infilling/voids, or trapped in macerals as small grains. This indicates that most clay is primarily deposited during the peat stage. Clay minerals were generally intimately associated with vitrinite and

inertodetrinite macerals, and less commonly with semifusinite. The intimate association of clays and organic matter may reduce the high efficiency of coal beneficiation, but samples with high minerite (rock) could certainly be improved (microlithotypes analysis would be useful in this case).

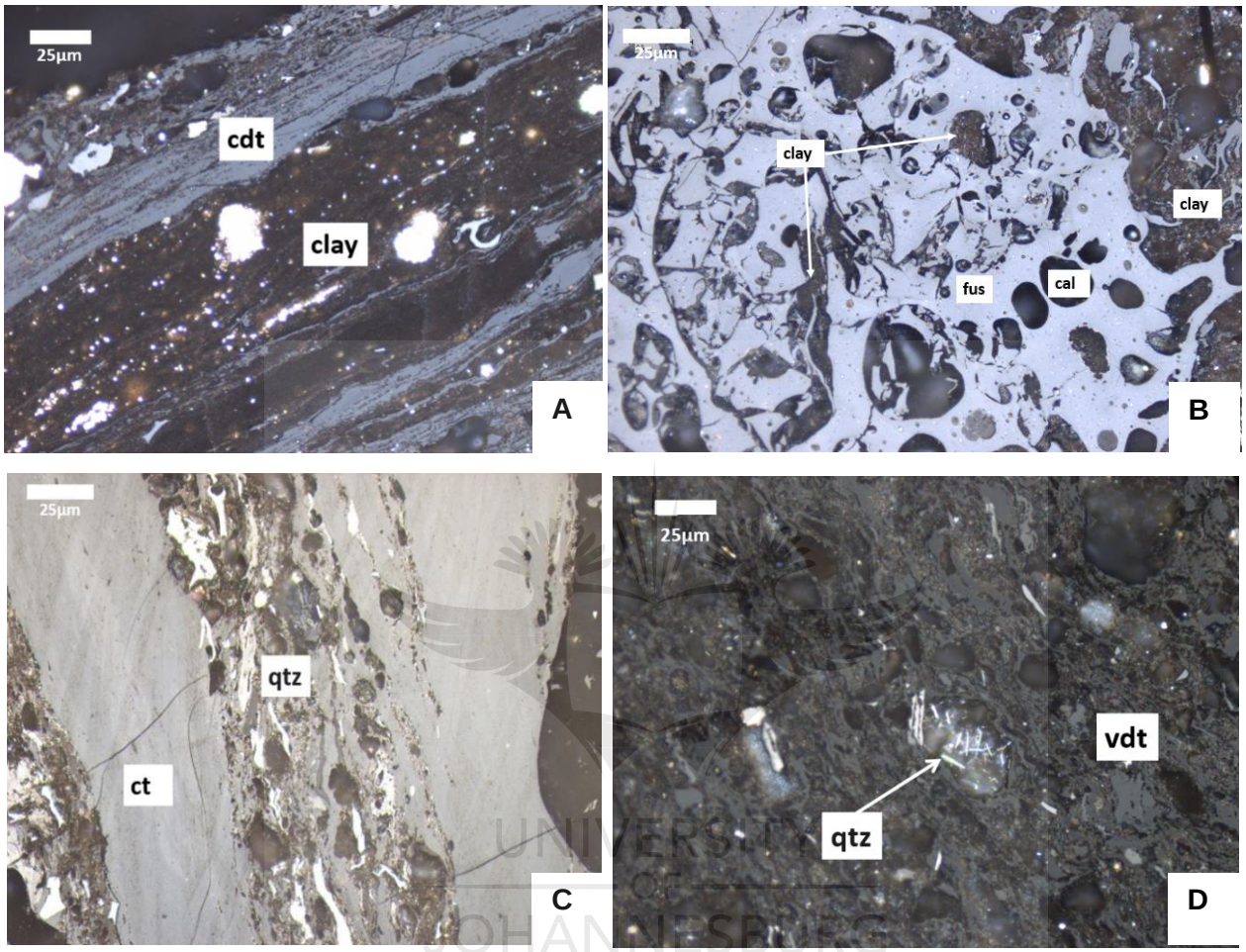

Figure 4.21: Photomicrographs of clay and quartz minerals: A) and B) clay minerals; and C) and D) quartz grains trapped in vitrinite matrix. (Reflected white light, oil immersion x500). qtz = quartz, fus = fusinite, cdt = collodetrinite, vdt = vitrodetrinite and ct = collotelinite.

Quartz typically occurred in close association with collodetrinite. Most grains were found bound in vitrinite maceral as cell or pore structure infilling also indicating an authigenic precipitation. There were quartz grains that were embedded in vitrodetrinite with colourful rods of rutile crystals (Figure 4.21D).

4.6.2. Sulphides

Based on petrographic observation using the reflected microscope, and XRD studies, the sulphide mineral was identified as pyrite. The pyrite is yellowish in colour and has a very high reflectance. It was noted to appear in a variety of modes in

these samples, as studied under the petrographic microscope, and by SEM and EMPA.

Petrographically different types of pyrite were identified: infilling cell or pore structures, disseminated euhedral, massive, infilling cracks and replacing other minerals, and framboidal pyrite sometimes preserving irregular forms (Figure 4.22). The infilling cell and pore structure pyrite is very common in the seams of Voorburg, but there are some particles were the pore/cell lumena was once filled with pyrite and the pyrite has been removed, leaving a void in the pore (Figure 4.22A). Pyrite occurs as lenses that are parallel to the bedding plane. The euhedral hexagonal (Figure 4.22B) pyrite is well shaped and has sharp crystal face, often occurring in the vitrinite matrix. This type of pyrite was rare and occurred in some coal samples of Makhado. Massive pyrite (Figure 4.22C) was common in sample Voorburh North samples VB01 to VB03 (borehole V07BS03). Pyrite infilled cracks, veins (Figure 4.22D). Pyrite was also observed replacing the associated siderite (15136). The veins and replacement pyrite occurred commonly in samples closer to the Bosbokpoort Fault as noted for sample 15136 in Voorburg South.

Framboidal pyrite is spherical concentrations of fine euhedral crystals that range in size from <1 - 20 microns (Figure 4.22E). The framboids were normally clustered together and typically occurred associated with vitrinite. Framboidal pyrite surrounded by a secondary botryoidal texture were also identified (Figure 4.22F). The botryoidal pyrite contains single dispersed framboids and also clusters of framboids. The core of the framboid is light yellow compared to the rim of the pyrite (concentric ring), which is slightly yellowish brown. Botryoidal pyrite was only observed in two samples (15143 and 15152) from Makhado. In these samples other forms of pyrite were not common.

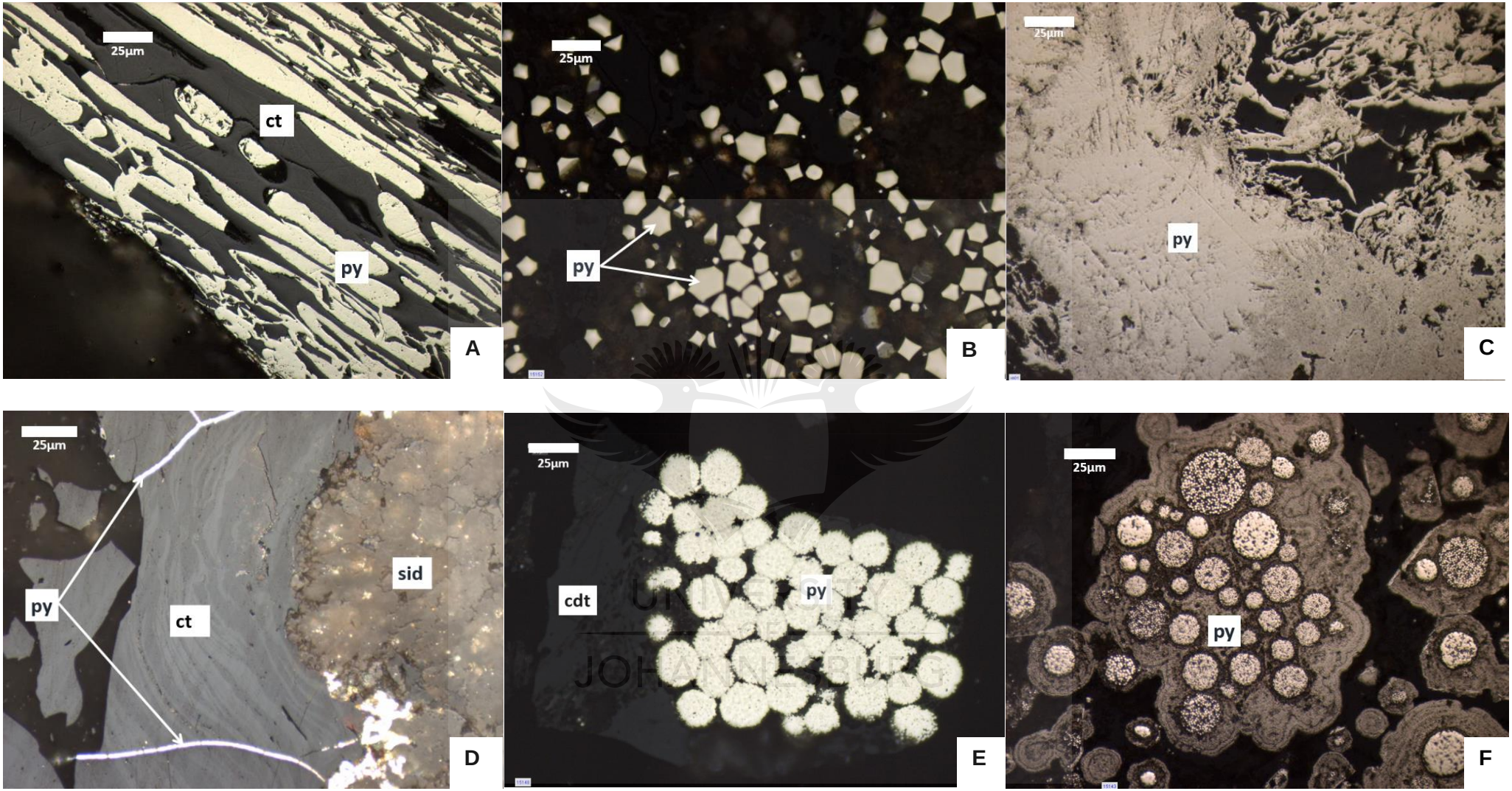

Figure 4.22: Photomicrographs of different forms of pyrite in different samples: A) infilling cell and pore structures (VB01); B) subhedral to euhedral pyrite crystals (15152); C) massive pyrite (VB01); D) pyrite infilling cracks in vitrinite (15136); E) syngenetic framboidal pyrite (15150); and F) framboidal pyrite with concentric rings formations (15143). (Reflected white light, oil immersion x500). py = pyrite, cdt = collodetrinite, ct = collotelinite and sid = siderite.

It is important to note that sample 15143 and 15152 are both the MU Seam (Table 3.1) and hence could indicate a specific event occuring at this horizon in the Makhado area. The botryoidal pyrite in sample 15143 is more concentric in comparison to sample 15152, where the overgrowth appears to act as a cement for the framboidal pyrite (Figure 4.23). Cleats (Figure 4.23A) are associated with sample 15143 (although not visible in the image due to the high reflectance of the pyrite). Sample 15152 indicated no cleats association to the botryoidal pyrite. According to Widodo et al. (2010), framboidal pyrite is syngenetic in origin due to the texture. However, the botryoidal pyrite overgrowth cannot be considered as sygenetic. The overgrowth is thought to have precipitated after the formation of the framboidal pyrite. Thus, the mineralisation of the botryoidal pyrite can be considered to be multigenerational.

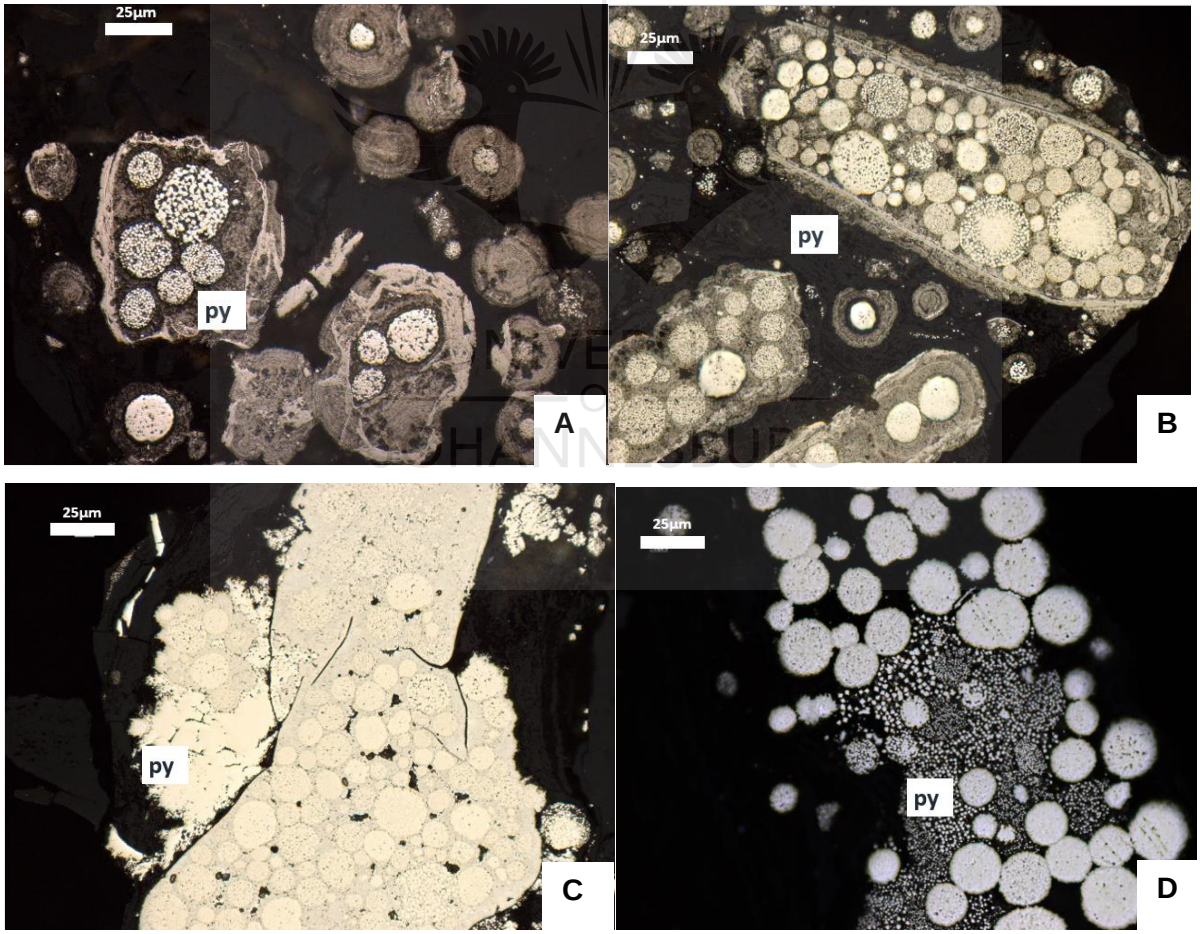

Figure 4.23: Photomicrographs of different types of pyrite in samples 15143 and 15152. A) and B) indicating a concentric ring overgrowth in sample 15143. C) and D) massive and euhedral pyrite cement in sample 15152 (Reflected white light, oil immersion x500).

In order to understand the elemental composition of the different pyrite forms, EMPA and SEM studies were undertaken. Different types of pyrite grains identified were analysed by EMPA for major and minor elements and the data acquired from the EMPA is presented in Table 4.10 with more data presented in Appendix C1. Framboidal, massive, euhedral, pyrite core and cell and crack infilling pyrite were characterised by high sulphur (S) contents (ranging from 52.88 - 53.85 wt.) and high iron (Fe) (45.07 - 46.14 wt. %). These forms contained low abundances of nickel (Ni) (0 – 0.23%), Arsenic (As) (0 – 0.19%), and lead (Pb) (0 - 0.24%), with other elements at 0 or below the detection limits. However, the botryoidal pyrite overgrowth (pyrite rim) is characterised by lower S (43.46 wt. %) and Fe (35.36 wt. %) and enriched in Ni, As, Co, Se and Pb.

Table 4.10: EMPA data for selected pyrite grains in wt. %

Sample ID	15143	15143	15143	15143	VB01	VB01	VB01	VB01
Description	pyrite rim	pyrite rim	pyrite core	pyrite core	euhedral	cell filling	framboidal pyrite	massive pyrite
S	43.46	43.3	53.19	50.24	53.85	53.4	52.88	53.34
Mn	0.00	0.01	0.00	0.00	0.00	0.00	0.00	0.01
Fe	35.36	36.21	46.45	43.71	46.14	45.96	45.07	46.08
Co	0.57	0.58	0.02	0.13	0.01	0.01	0.01	0.01
Ni	1.51	1.44	0.00	0.23	0.01	0.00	0.00	0.00
Cu	0.00	0.02	0.04	0.01	0.00	0.00	0.02	0.00
Zn	0.00	0.00	0.00	0.01	0.02	0.00	0.00	0.01
As	1.39	1.29	0.01	0.19	0.03	0.01	0.01	0.00
Se	0.19	0.19	0.00	0.03	0.00	0.00	0.00	0.00
Pb	1.40	1.25	0.02	0.24	0.01	0.01	0.05	0.00
Total	83.89	84.27	99.72	94.8	100.07	99.4	98.04	99.46

To obtain images and spectrum of individual sites of the pyrite grains, SEM studies were conducted. Figure 4.24 shows different types of pyrite as studied under the SEM. SEM-EDS spectrum peaks on the botryoidal pyrite results are presented in Figure 4.24 and 4.25. More EDS and BSE data can be found in Appendix C2.

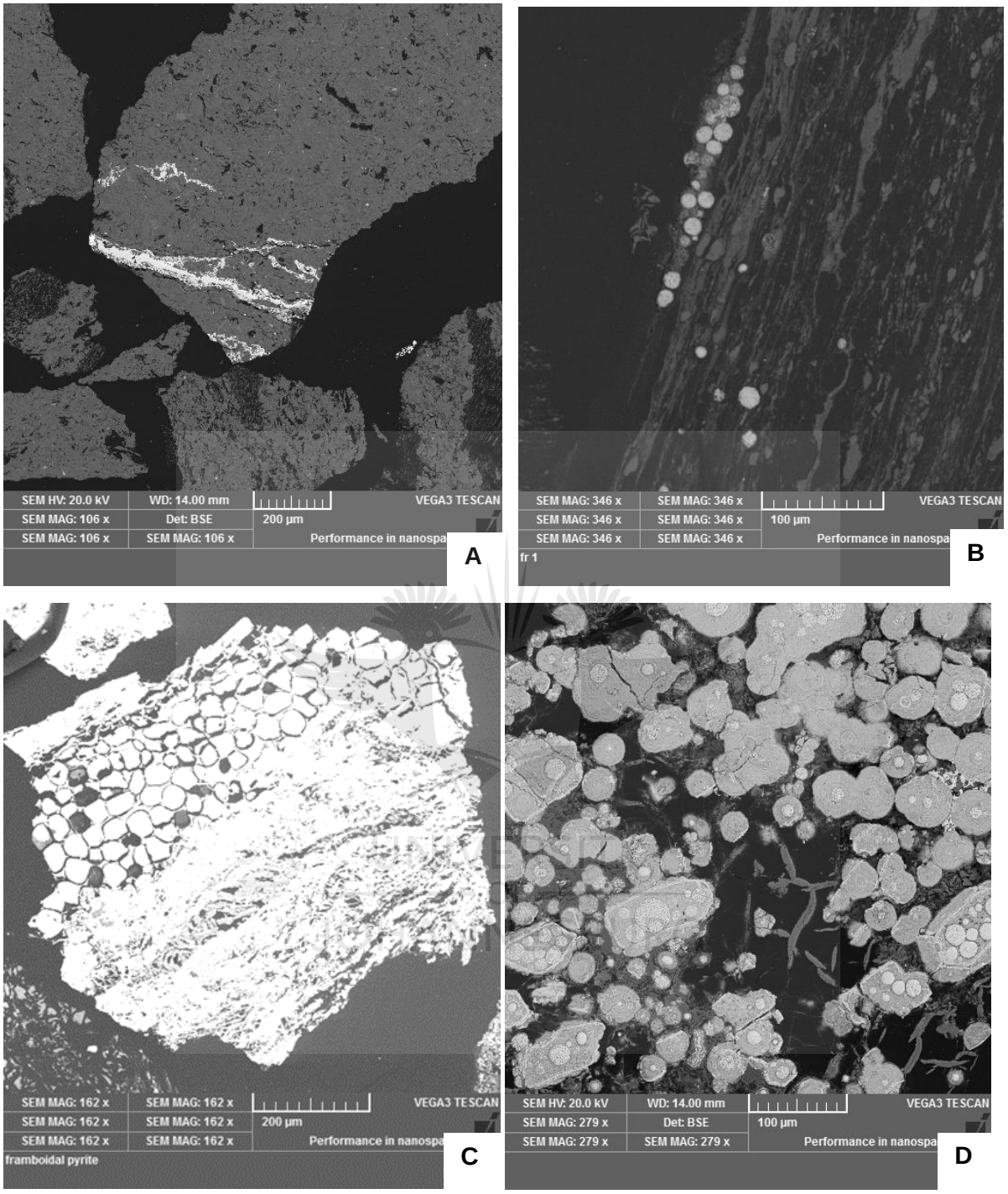

Figure 4.24: SEM – BSE images of different types of pyrite A) pyrite infilling cracks; B) framboidal pyrite; C) cell and pore infilling pyrite that grade into massive pyrite; and D) framboidal pyrite with concentric ring overgrowth. Note the scale at the base of image.

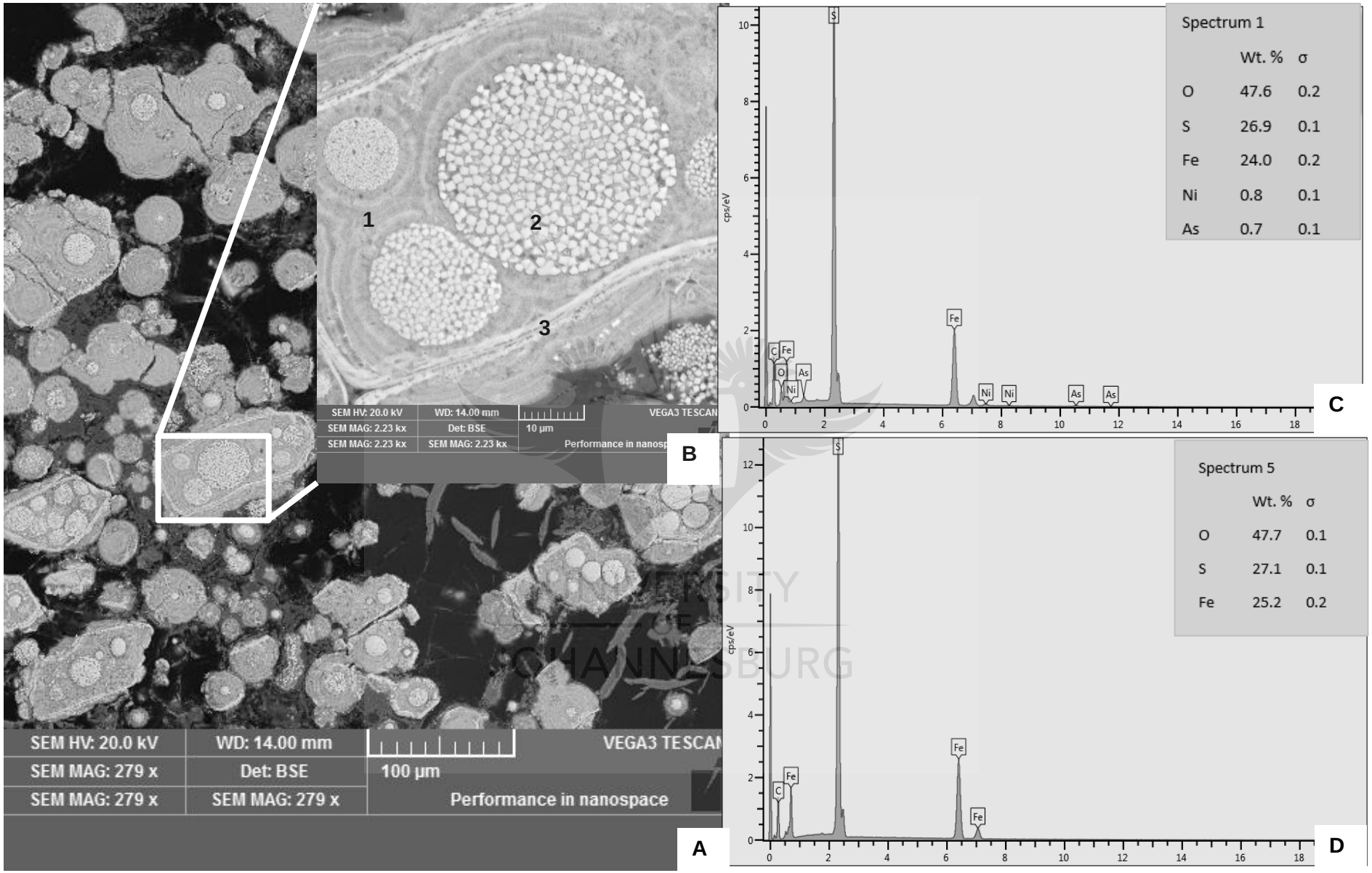

Figure 4.25: SEM – BSE and EDS images from sample 15143. A) framboidal pyrite with concentric ring overgrowth; B) zoomed image indicating clear euhedral pyrite in framboids; C) spectra for the framboidal pyrite indicated as 1 on Figure 4.24 B; and D) spectra for euhedral pyrite indicated as 2 on Figure 4.24B.

SEM-EDS indicated that Fe concentration increases from the overgrowth of the botryoidal pyrite to the core. These analyses also validated results obtained from the EMPA, as Ni, As, and Pb were detected in the overgrowth pyrite (Figure 4.25C). The concentric ring overgrowth (Figure 4.25) contains a relatively high concentration of Ni, and As, substantiating data acquired from the EMPA. However, no Pb was detected which can be detected by EMPA. Sample 15152 had a secondary overgrowth pyrite, but no metal enrichment (that is: Ni, As and Pb) were noted when studied on the SEM and EMPA.

Botryoidal pyrites with similar metal rich overgrowth has been reported by Belkin et al. (2010), who suggested that metal enrichment reflected deposition from hydrothermal fluids. Zhao et al. (2013), studied similar botryoidal pyrite and characterised the overgrowth as cemented massive pyrite. The overgrowth was characterised as later formed pyrite on earlier formed framboids. No metal enrichment was noted in the study by Zhao et al. (2013), and the overgrowth pyrite described by Zhao et al. (2013), may be similar to the overgrowth in sample 15152 in this study as it indicated no enrichment. Based on petrographic observations, SEM and EMPA studies conducted on the botryoidal pyrite, it can be inferred that three different generations of pyrite occurred (Figure 4.25B): 1) framboidal (syngenetic) pyrite; 2) massive pyrite enriched in metals (As, Ni, and Pb); 3) massive pyrite with no metal enrichment (although absent in some particles). The different pyrite generations are identified by abrupt changes in the chemistry and textural differences.

The overgrowth enriched in Ni, Pb, and As is thought to have formed from a different source than the framboidal pyrite. If the overgrowth was formed from the same source as the framboidal pyrite, then the chemical composition of both the overgrowth and framboid would be similar. This indicates an external source introduced into the system carrying the metal rich elements that precipitated around the framboidal pyrite. The metal rich elements are thought to be from rock fluid interaction in the epigenetic stages, with the introduction of hydrothermal fluids instigating the pyrite to precipitate around the syngenetic framboidal pyrite. It is therefore proposed that the Tshipise Fault

and Bosbokpoort Fault could have carried multiple fluids. It is known that these faults were active during and after coalification (Pers comm., J Sparrow).

The above figures were beyond the scope of the current investigations and, further investigations are underway to expand the understanding of the unusual mineral observations. Botryoidal pyrite has also been observed in a few samples in the Springbok Flats Coalfield (Pers comm., N. Wagner).

4.6.3. Carbonates

A variety of carbonate minerals were identified petrographically and by XRD, ranging from syngenetic siderite to epigenetic calcite (Figure 4.26). Dolomite and ankerite were determined by XRD although not observed in petrographically. Siderite occurred as brown spherical nodules with sizes ranging between 50µm - 2mm. The rims of the nodules are dark brown relative to the core, which is light brown as indicated in Figure 4.26A.

The siderite nodules appeared to be trapped in vitrinite. Nodular siderite can be interpreted to be of syngenetic origin, as bedding planes either side of the nodules show draping and compaction around the nodules. Siderite was also observed as a rhombus shape, preserving the trigonal crystal system (Figure 4.26B). The trigonal siderite was identified in samples 15148 and 15153. In other samples, trigonal siderite crystals were observed growing on the margins of pre-existing siderite nodules. Calcite occurred as a minor component in all of the coal samples, possibly not detected by XRD due to low concentrations.

Calcite showed two modes of occurrence under reflected microscopy: as cleats infilling cracks, mostly in the vitrinite, and also as cell lumena filling fusinite maceral. Calcite appears to shatter, branch and cross cut vitrinite grains. Different generations are noted by the different shades, shown in Figure 4.26, possibly attributed to different fluids events associated with the faults.

From XRD analyses, the presence of dolomite and ankerite were identified, although not identified petrographically. The EMPA studies (Table 4.11 and Appendix C4) were conducted on different types of carbonates in samples 15148, 15136 and 15143.

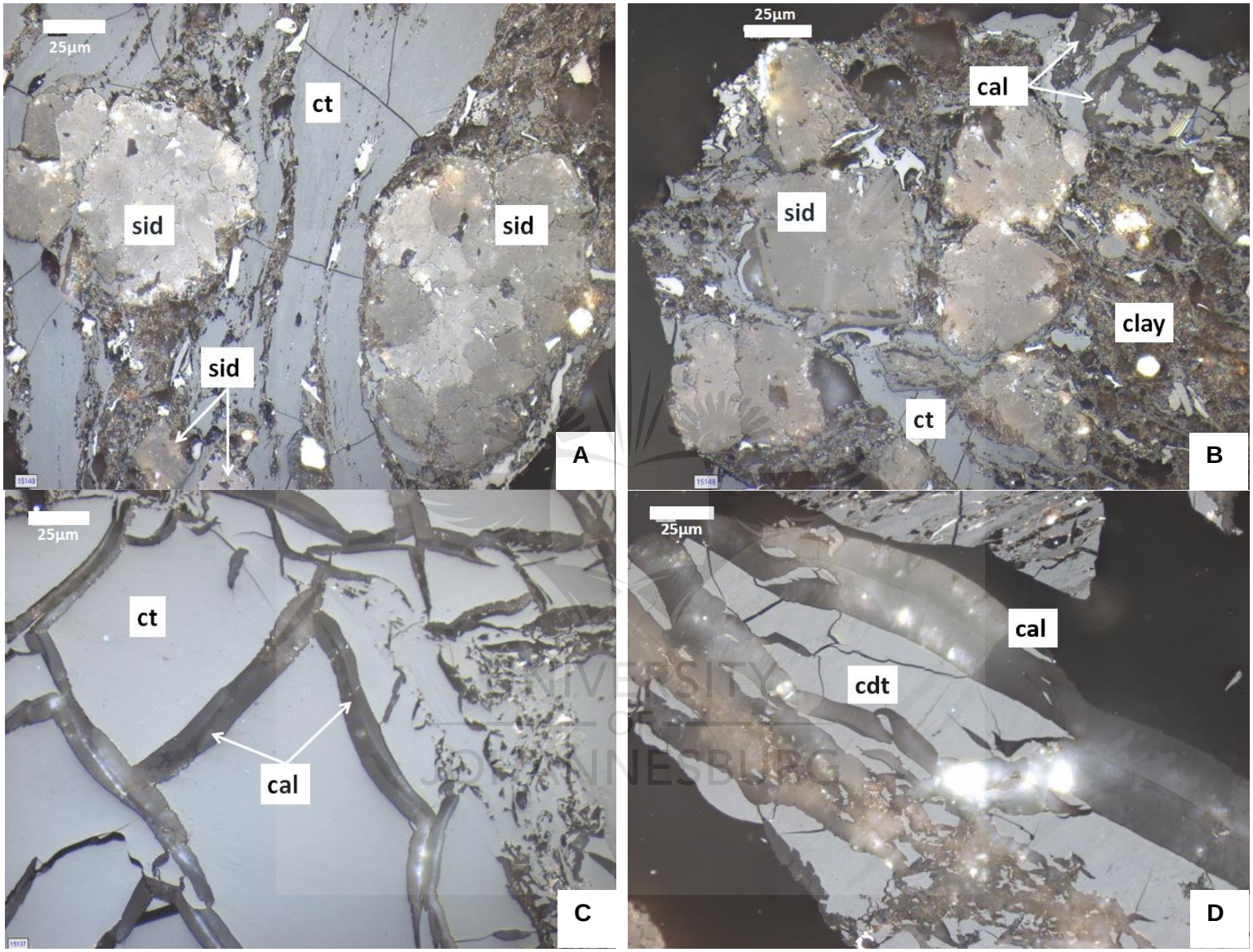

Figure 4.26: Photomicrographs of various forms of carbonates observed petrographically. A) nodular siderite trapped between vitrinite bands and associated clay (15148); B) trigonal siderite (15148); C) Calcite in association with cracks in collotelinite (15137); and D) Calcite associated with vitrinite (15136). (Reflected white light, oil immersion x500). sid = siderite, ct = collotelinite and cal = calcite.

More results from EMPA are located in Appendix C3. Results obtained revealed that nodular siderite had higher FeO content, with low CaO, MgO contents in comparison to trigonal siderite that had higher CaO and MgO contents. The results indicated that Fe content in siderite nodules varied from the core to rim by less than 3% by weight. The rims (dark brown) of nodular siderite are characterised by lower FeO and higher CaO and MgO contents when compared to the core (light brown) which has higher FeO and lower CaO and MgO contents.

From the EMPA results, the trigonal siderite indicated enrichment in FeO which is typical of siderite. Ankerite is found as cleats associated with concentric rings surrounding framboidal pyrite, as identified by the EMPA (Table 4.11). The cleats are discussed in more detail later in this section. SEM studies were also conducted on samples 15148, 15136 and 15143 (Figures 4.27 and 4.28). It was observed that the nodular siderite has slightly higher Fe and low Ca and Mg concentration in comparison to the trigonal siderite, which reported lower Fe and higher Ca and Mg concentrations. This substantiated the results from the EMPA in Table 4.11.

Table 4.11: EMPA data for carbonates minerals in wt. % from selected samples

Sample ID	15148	15148	15148	15148	15148	15148	15136	15143	15143
Description	Siderite diamond shape	Siderite diamond shape	Nodular siderite darker	Nodular siderite darker	Nodular siderite light	Nodular siderite light	Calcite	Cleats with pyrite	Cleats with pyrite
CaO	4.18	5.21	2.78	2.06	0.96	1.39	51.10	30.73	31.24
MgO	2.66	3.56	2.05	1.34	0.31	0.29	1.95	13.34	13.09
SrO	0.01	0.01	0.00	0.02	0.01	0.00	0.09	0.09	0.08
SiO2	0.29	0.32	0.04	0.11	0.09	0.08	0.05	0.24	0.22
Al2O3	0.08	0.16	0.05	0.06	0.03	0.03	0.00	0.13	0.15
FeO	51.89	49.63	53.72	52.7	58.59	58.28	3.68	9.42	9.49
MnO	1.22	0.30	1.53	1.43	1.42	1.54	0.15	0.15	0.08
BaO	0.03	0.04	0.04	0.09	0.04	0.00	0.06	0.09	0.08
ZnO	0.00	0.00	0.01	0.07	0.04	0.00	0.03	0.04	0.00
CO2	39.61	40.76	39.78	42.13	38.5	38.35	42.87	45.77	45.56
Total	99.97	100	99.99	100	100	99.95	99.99	100	100
Number of ions on the basis of 6O									
Ca	0.17	0.20	0.11	0.08	0.04	0.06	1.84	1.06	1.08
Mg	0.15	0.19	0.11	0.07	0.02	0.02	0.10	0.64	0.63
Sr	0.00	0.00	0.00	0.00	0.00	0.00	0.00	0.00	0.00
Si	0.01	0.01	0.00	0.00	0.00	0.00	0.00	0.01	0.01
Al	0.00	0.01	0.00	0.00	0.00	0.00	0.00	0.01	0.01
Fe	1.61	1.51	1.67	1.60	1.87	1.86	0.10	0.25	0.26
Mn	0.04	0.01	0.05	0.04	0.05	0.05	0.00	0.00	0.00
Ba	0.00	0.00	0.00	0.00	0.00	0.00	0.00	0.00	0.00
Zn	0.00	0.00	0.00	0.00	0.00	0.00	0.00	0.00	0.00
C	2.01	2.03	2.02	2.09	2.01	2.00	1.97	2.01	2.01
Total	3.98	3.96	3.97	3.90	3.99	3.99	4.03	3.98	3.99

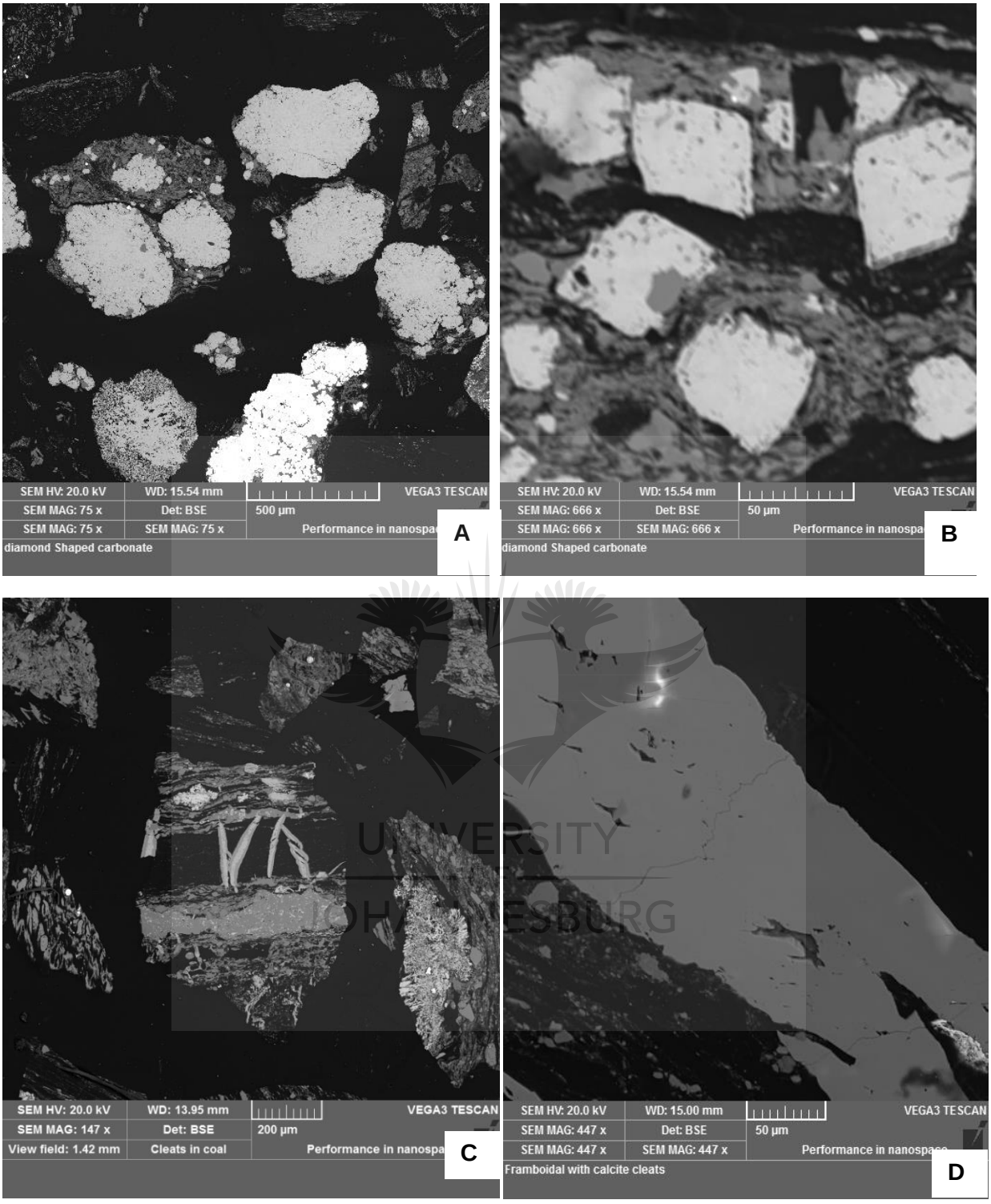

Figure 4.27: SEM – BSE images of different types of carbonates A) nodular siderite (15148); B) trigonal siderite (15148); C) calcite Cleats (15143); and D) calcite (15136).

An interesting observation was made where siderite nodules have different calcium concentrations (Figure 4.28). The Ca and Mg concentration of the nodular siderite decreases from the rim to core. Elemental maps from the EDS displayed dense

concentrations of Ca (shown as white in Figure 4.28) and Mg (blue) in the rims, in comparison to the cores that have slightly lower concentration. Spectrum peaks were determined from rim to core. The peaks showed a decrease of Ca from 6.6 wt. % in the rim to 1.4 wt. % in the core (Figure 4.29 B, C). The concentration of the Ca on the rim, could be related to the faults. The faults could have carried the Ca that precipitated on the rims of the siderite nodules. The trigonal siderites have similar concentrations of Ca and Mg as the core of the nodular carbonates. The siderite is also characterised by inclusions of quartz and pyrite grains.

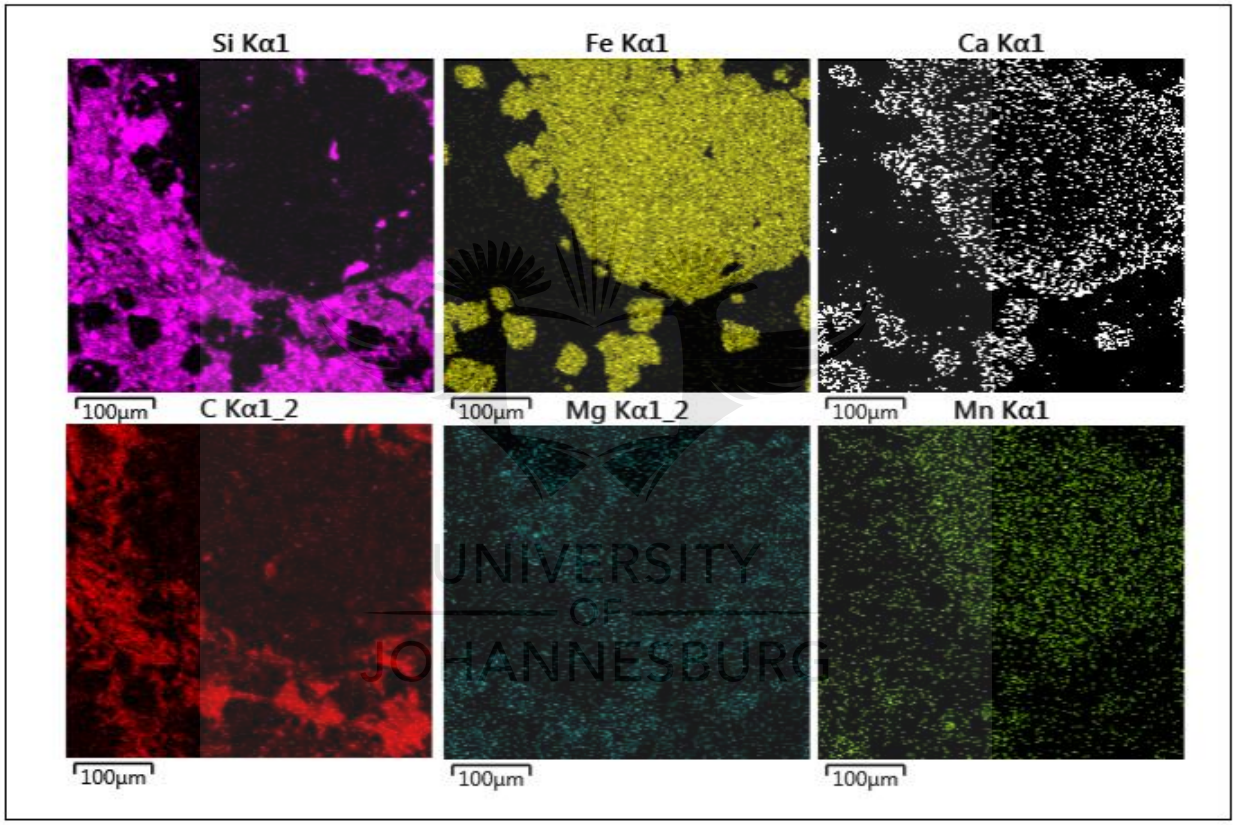

Figure 4.28: SEM – EDS elemental maps of siderite nodule indicating enrichment of Caα and Mgα in the rim in comparison to the core where less concentration of these elements are noted.

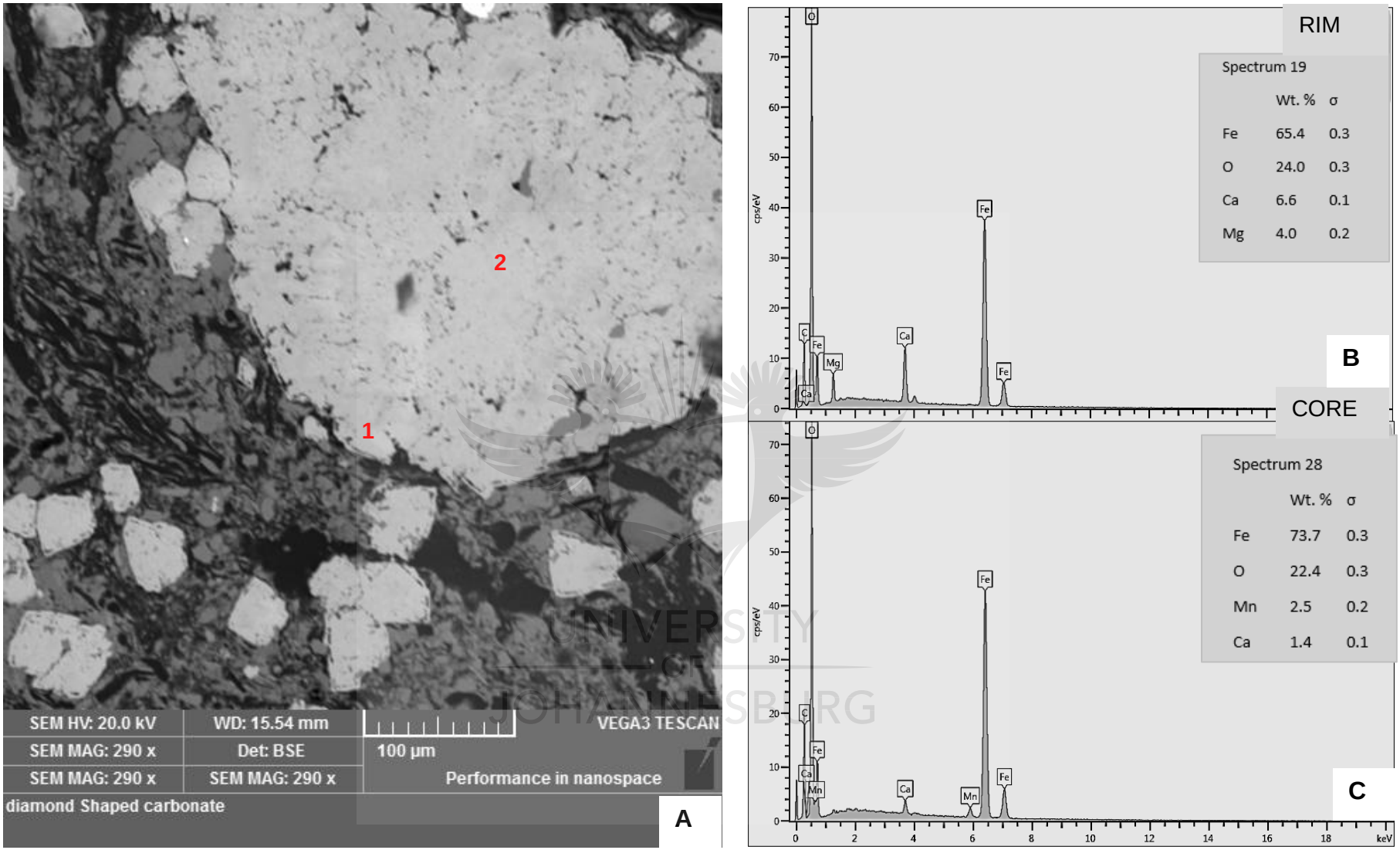

Figure 4.29: SEM - BSE and EDS image of siderite A) nodular siderite; B) shows SEM-EDS spectrum from the siderite indicated as 1 (rim) from Figure 4.30 A; and C) SEM-EDS spectrum from the siderite indicated as 2 (core) from Figure 4.29A.

When studied under the SEM, the “ankerite” cleats (as identified by EMPA) revealed zooning (Figure 4.30). The different zones are labelled 1 - 4 in (Figure 4.30): 1) ankerite; 2) ankerite with higher Fe; 3) siderite; and 4) siderite with higher Fe. It is proposed that the different compositions noted from ankerite to siderite could reflect multiple generations of Ca-rich hydrothermal fluids. Calcite cleats were also found associated with some botryoidal pyrite.

Massive pyrite (sample 15148) was observed enclosed in a siderite grain (Figure 4.30B). Parzentny and Lewinska-Preis (2005) reported similar relationship between pyrite and siderite. This relationship can be used to explain replacement between siderite and pyrite. In petrography, it was noted that the siderite is being replaced by pyrite. As this aspect was beyond the scope of the current research, further work will be undertaken on these minerals.

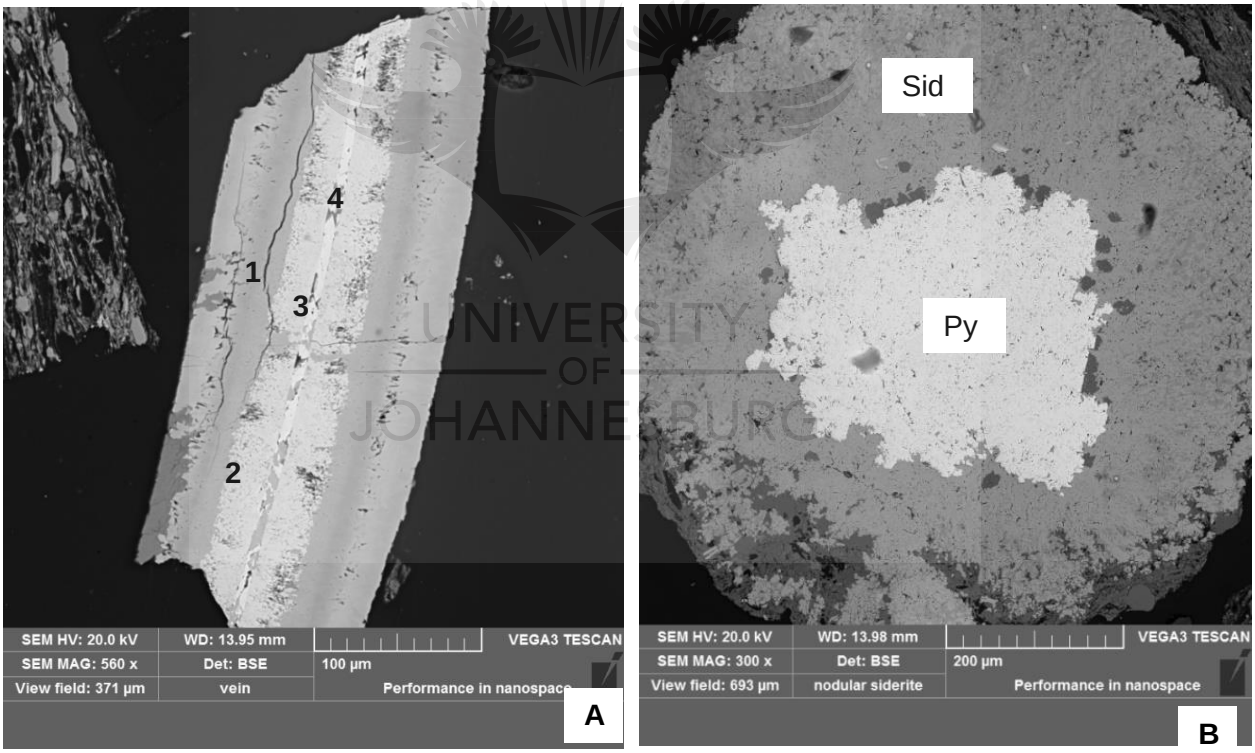

Figure 4.30: SEM – BSE images of A) carbonate zooning from ankerite on the rim of a siderite rich core; and B) Siderite nodule appearing to be replacing pyrite

CHAPTER 5: PALEOENVIRONMENT RECONSTRUCTION

This chapter uses the petrographic indices to infer the depositional environment of the coals of the Soutpansberg Coalfield with some consideration of the other Limpopo Province coalfields. The reconstruction of the depositional environment using petrographic indices (TPI and GI) was explained in Section 2.5. Macerals identified were plotted in the TPI verses GI plot after Silva and Kalkreuth (2005) to infer the possible environments of deposition. Mineral matter identified in coal was also considered in the attempt to reconstruct the depositional environment.

5.1. Tissue Preservation Index and Gelification Index as depositional environment indicators

The abundance of the maceral type plays a significant role in the reconstruction of the depositional environments. Vitrinite, inertinite and liptinite maceral groups were identified in the coal samples, as discussed in Section 4.3. The discussion pertaining to the paleoenvironment will be performed based on these macerals groups. Results of the petrographic indices are presented in Table 5.1. From Table 5.1, it is important to note that some samples reported high TPI (greater than 3.6), and therefore the TPI versus GI model of Diessel (1992) cannot be applied to those samples.

Results obtained from the maceral analysis were plotted onto the Diessel facies model (TPI and GI), as indicated in Figure 5.1. The TPI and GI values indicated that the coal samples from Voorburg were deposited in a marsh transitioning to a wet forest swamp. However, sample 15151 (Voorburg) plotted in the dry forest swamp conditions, where there is a positive tree density, indicating the presence of woody plants. Sample 15136 and VB02 were deposited in a limnic environment. This suggests that the water table during peat development occurred closer to the ground surface. TPI-GI values for samples VB01 and 15136 plot in the limnic to limno-telmatic depositional environment. This suggests that the ground surface was covered by shallow water during peat development stages.

Table 5.1: TPI and GI values from coal samples

Location	Borehole ID	Seams	Sample ID	TPI	GI
Voorburg North	V07BS01	MU	VB01	1.42	10.25
		BU	VB02	0.79	12.59
		BL	VB03	1.06	26.08
	V10BS01	BU	15150	3.90	2.66
		BL	15151	1.63	1.09
Voorburg South	R637004	MU	15136	0.92	42.35
		BU	15137	1.02	6.38
		BL	15138	1.45	6.49
	R63701LD	MU	15147	5.57	7.19
		BU	15148	8.49	2.99
		BL	15149	20.71	3.11
	F578004	MU	15154	7.60	3.05
		ML	15155	5.15	1.83
		BU	15156	4.09	1.62
Makhado	T190BS03	BU	15139	1.07	6.75
		BL	15140	1.13	2.67
	T07BS	MU	15141	22.31	6.45
		BL	15142	5.38	8.78
	C699001	MU	15143	13.27	4.14
		ML	15144	5.50	8.88
		BU	15145	0.66	0.15
	S65801LD	BL	15146	0.50	0.09
		MU	15152	7.82	2.51
		BU	15153	4.89	6.48
	F645BS02	BU	15157	8.49	2.99
		BL	15158	20.71	3.11
Vele	CP17BS02	BU	1317	25.28	33.07
		BL	1318	16.81	156.33
	OV24BS01	BLT	1333	20.55	26.88
		BU	1334	12.16	12.78
		M	1335	13.52	48.68
		T	1336	24.61	75.83
Waterberg		Zone 8+9	15159	4.32	3.46
		Zone 7+8	15160	1.10	0.51
Tshikondeni		ROM	15117	27.47	6.81

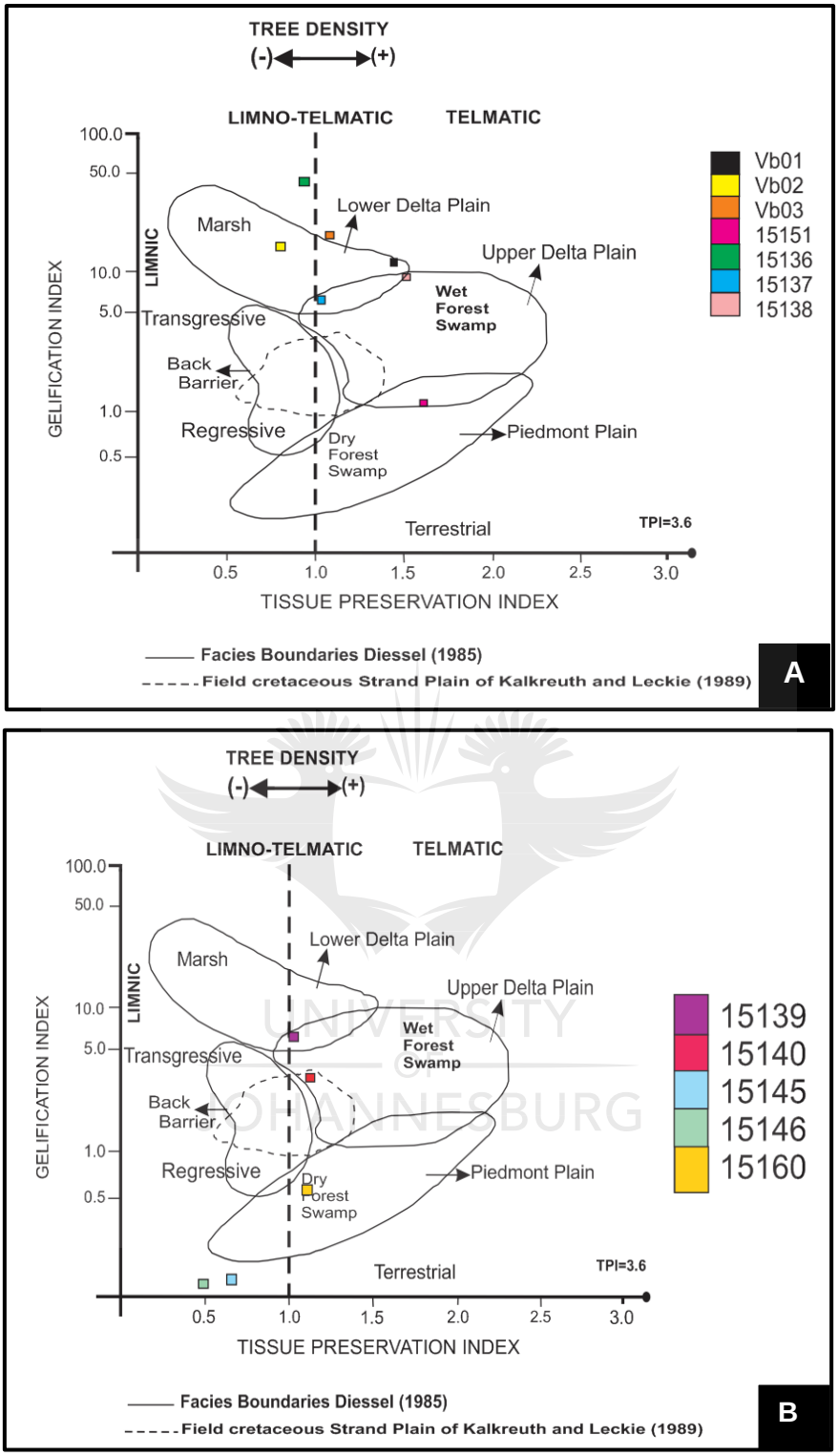

Figure 5.1: Coal facies diagram for the A) Voorburg North and South samples; B) Makhado, and Waterberg coal samples (after Silva and Kalkreuth, 2005). Samples with TPI > 3.6 (Table 5.1) cannot plot in these facies model.

Most samples plot in the wet forest swamp conditions. These samples have high vitrinite contents indicating presence of woody plants supported on the coal facies plot by a positive tree density. Suwara (2006) explained that coals rich in vitrinite are

thought to have been deposited in wet and more anoxic environments. A waterlogged environment allows for the gelification process and extensive tissue conversion, hence the high vitrinite contents are associated with wet environments. Falcon (1986) associated vitrinite-rich coals with wet or waterlogged conditions such as seashore, fluviatile, lacustrine environments.

In the Makhado area, only four samples reported values that plot on the TPI versus GI model. The Sample 15139 (BU) and 15140 (BL) indicated a wet forest swamp forest. The elevated inertodetrinite content found in samples 15145 (BU) and 15146 (BL) in Makhado resulted in these sample plotting out of the area with extremely low TPI and GI values. According to Diessel (1992), this indicates that the semifusinite and fusinite is wood-derived. It also signifies an occasionally dry forested swamp with mild gelification and humification of plant tissues. Inertinite is believed be derived from the same precursors as the vitrinite, which was woody plants (ICCP, 2001). These samples (15145 and 15446) are characterised by high inertodetrinite, which is formed from the reworking of pre-existing organic macerals (ICCP, 2001).

Sample 15160 (Waterberg) plotted in the dry forest swamp environment. This can be explained by the higher inertinite content noted petrographically. Falcon (1986) also associated samples with high inertinite content with dry forest swamp environments. High inertodetrinite indicates high energy environment and organic matter circulation during peat formation (Silva and Kalkreuth 2005). Falcon (1986) stated that coals found in dry environments were a result of reworking of the peat or early Coalfield material, which was then transported by water and deposited by river channels, or as flood deposits in the deltaic or lacustrine environments.

According to ICCP (2015), the presence of inertinite would suggest a drop in water level. The presence of inertinite can also suggest oxidation occurring in the low water table and also wildfire as indicated by the dry forest swamp depositional setting. Inclusion of fusinite in the coal samples may have been due to wind or water deposition of fossilised charcoal, but it can also be attributed to in situ burning (ICCP, 2015). Low water levels would form inertinite-rich coal, because of high degrees of oxidation of the plant matter.

The Diessel facies model was not applicable to some samples from the Voorburg, Makhado, Vele and Tshikondeni samples. This was due to high content of vitrinite content that led to TPI values greater than 3.6.

Detailed analysis of lithofacies type and facie assemblages of the Soutpansberg and Limpopo Coalfields were conducted by Malaza (2013), where it was suggested that the depositional environment of the coalfields can be interpreted as fluvio glacial to fluvial palaeo channel. The coal bearing Madzaringwe Formation, which occurs in Soutpansberg and Limpopo Coalfields, was interpreted to have formed in a clastic fluvial depositional environment. These interpretations concur with observation of this study that the high vitrinite contents indicated a wet environment and can be interpreted as deposited in a fluvial environment.

Coal samples from the MKB (Witbank, Ermelo and Highveld) are characterised by high inertinite, indicating largely oxidative conditions; the depositional environment is said to be glacio fluvial and upper delta plain. As indicated in Section 2.1.1 the Soutpansberg Coalfield is structurally controlled. As discussed above, Malaza (2013) proposed that the depositional environment of the Soutpansberg is similar to that of the MKB; in terms of both being fluvial as the coal bearing sequence of Madzaringwe Formation can be interpreted to have formed in a fluvial environment.

5.2. Mineral matter as indicators of depositional environment

The coal samples of this study, as noted in chemical analyses and petrography, are generally characterised by high ash and mineral matter. As indicated in Section 2.3.2, mineral matter in coal can provide information on the depositional conditions and geological history of the coal. This sections focuses on the sulphides (pyrite) and carbonates, present in these coal samples.

The coal samples of the Voorburg North area reported high ash, high sulphur and pyrite values. Such coals are typically associated with brackish and marine sediments (Lopez-Buendia et al., 2007; Chou, 2012). Marine influenced coals are usually characterised by high sulphur, hydrogen and nitrogen contents. The high sulphur content is caused by increased availability of sulphate in sea water and anaerobic bacteria activity (Stach et al., 1982). Peat formed in marine or brackish

environment is rich in H_2S and mineral matter, especially pyrite. Different types of pyrite were noted, as discussed in Section 4.6, namely: framboidal, cell and pore infilling pyrite, massive, euhedral and crack infilling pyrite.

Syngenetic pyrite generally is produced in a sulphobacteria mediated anoxic environment, with a sulphate rich water supply (Lopez-Buendia et al., 2007). It can be assumed that the formation of pyrite (i.e. massive, framboid, and euhedral) is generally induced by seawater during peat accumulation or early diagenesis. Epigenetic mineralisation, such as crack or fracture or cell filling pyrite and calcite, could be explained by the occurrence of hydrothermal fluids associated with the Tshipise and Bosbokpoort Faults. The fault may have acted as a conduit for the fluids, thus invading the coal sequences. According to Ward (1984), syngenetic pyrite may also be abundant in coal formed in lacustrine and similar environments having no obvious connection to the sea. This suggests that sulphate rich lakes and sulphate rich ground water can also be involved in pyrite production. It may be this theory is more applicable to the Limpopo coals as the depositional environment proposed as fluvial, most likely without marine transgressions.

Carbonates, especially siderite, were common in coals in the Voorburg South and Makhado samples. The origin of siderite is considered to be related to the latest stage of bacterial sulphate reduction, when the H_2S is too low to form pyrite in anoxic conditions (Lopez-Buendia et al., 2007). Siderite nodules occurred during deposition as the organic bedding planes are deformed around siderite grains. Siderite nodules have also been reported as forming in fresh water environments (Ward, 2016). The epigenetic carbonates forms (cleat infilling etc.) were derived from precipitated fluids that permeated through the coal (Ward, 2016), which in this study can be attributed to fluids moving through the Tshipise and Bosbokpoort Faults.

CHAPTER 6: CONCLUSION AND RECOMMENDATIONS

The main aim of the project was to understand coal quality and petrographic variations in coals on either side of the Tshipise Fault, in the Soutpansberg Coalfield, as well as across the Limpopo Coalfields. Recent coal exploration indicated that vitrinite reflectance and coking properties differed across the Tshipise Fault (Pers comm., J Sparrow). The project assessed coal quality in terms of maceral, vitrinite reflectance, FSI, abnormal condition, and mineralogical differences in coal samples taken either side of the Tshipise Fault. An attempt was made to reconstruct the depositional environments of the Soutpansberg and Limpopo Coalfields. The study focused on samples from the Voorburg, Makhado and Vele areas. For comparative purposes samples from Tshikondeni Mine to the east (former coking coal producer) and two samples from the Waterberg Coalfield to the west of the Limpopo Province were included in the study, thus covering the coalfields in the north of the Limpopo Province (excluding the Springbok Flats Coalfield). A total of 35 samples were collected across the Limpopo Province. A Zeiss Axio Imager M2M retrofitted with Hilgers Diskus Fossil software was used for petrographic analyses at a magnification of x500 under oil immersion. The samples were scanned automatically and analysed offline using the Fossil Student Software. Detailed petrography revealed interesting occurrence of minerals, therefore the investigation was expanded to include XRD, SEM, and EMPA analyses.

From this study, the following conclusions can be drawn:

- In terms of coal quality, the coal samples from the Limpopo Province were characterised by high ash contents. The high ash content can be attributed to the multiple intercalations of mudstone and coal. The volatile matter in the coal samples was variable, with low to medium to high volatile contents. According to Steyn and Minnitt (2010), as indicated in Table 3.4, the coal samples of the Limpopo Coalfield can be classified as below grade D based on the CV and ash contents reported. Plant trials have indicated that the coals can be upgraded with careful processing (Pers comm., J. Sparrow).
- Samples from Voorburg North reported higher sulphur values in comparison to the other samples. This was supported by the petrographic analyses, where higher concentrations and unusual types of pyrite were identified.

- The samples with high CV reported high FSI and samples with high ash reported low FSI as indicated in Figure 4.4. The coal samples ranged from non-caking to strongly caking when classified according to Speight (2005). Certain coals of the Soutpansberg Coalfield have the potential to produce coke based on the FSI data.
- Petrographically, the coals across the Limpopo Province coalfields are comparable, with all samples typically being rich in vitrinite, low in inertinite and low in liptinite. This is in contrast to the coals from the Witbank Coalfield, which are typically rich in inertinite. Coals in the Limpopo coalfields clearly formed under different depositional environments compared to the MKB coals. The Witbank Coalfields are thought to have formed in retroarc foreland basin and the northern coalfields preserved in structurally controlled half grabens (Johnson et al., 1996a). These environments played a role with regards to peatification and water levels and subsequent vitrinite formation.
- The most common vitrinite maceral in the Soutpansberg and Limpopo Coalfields is collotelinite. The collotelinite content is greater than collodetrinite in most samples.
- Pseudovitrinite occurred in all samples, with the highest values reported for samples from Vele (Limpopo Coalfield). This is important to note as pseudovitrinite negatively affects coking properties.
- Maceral anomalies were observed for samples 15151 (BL Seam) from Voorburg, 15145 (BU) and 15146 (BL) from Makhado, where high inertinite contents were determined, possibly indicating a dry stage in peat accumulation. These samples had low FSI, as expected as inertinite acts as an inert maceral during carbonisation.
- Abnormal Condition Analysis was conducted on all samples to determine if the Tshipise Fault impacted the coal by identifying abnormal features. From the analyses, samples studied were relatively fresh. Minor abnormal conditions like cracks, fissures, and cracks infilled by minerals could be attributed to faulting. Sample 15136 which in a borehole was closest to the Bosbokpoort Fault reported the highest abnormal conditions.
- In the Soutpansberg Coalfield, samples from Voorburg North reported a mean RoV% of 0.76 – 0.84 indicating a bituminous rank C coal. Samples from

Voorburg South reported a mean RoV% ranging from 0.80 – 1.26; hence the coal rank ranged from bituminous medium rank C to B when classified according to UNECE (1998). The Makhado samples reported mean RoV% ranging from 0.71 – 0.95, thus falling within bituminous medium rank C. The coal samples from the other Limpopo locations ranged from 0.66 – 0.78 mean RoV% (Vele in Limpopo Coalfield), 0.63 – 0.65 mean RoV% (Waterberg Coalfield) indicating a bituminous medium rank C, and 1.23 mean RoV% (Tshikondeni Colliery) classified as bituminous medium rank B. The change in reflectance values from the west to the east was determined.

- The samples from Voorburg South lie between the Bosbokpoort and Tshipise Faults. These samples reported a slightly higher reflectance than samples from Voorburg North, only 10km away. The differences in coal rank between the Voorburg North and South samples could potentially be linked to the geothermal gradient as Voorburg North coals occur in an up faulted block with shallow seams in comparison to Voorburg South and Makhado where the seams are preserved at a greater depth. As discussed in Section 2.2.1, the Tshipise Fault is believed to have been active prior to the deposition of the Karoo rocks. This faulting, which controlled graben formation, continued during the deposition of the Karoo sediments and was reactivated in post-Karoo times. This could have influenced the thermal maturity of the coals.
- This study has demonstrated there are mineralogical differences in the coals on either side of the Tshipise Fault. Silicates, sulphides and carbonates were the three main mineral groups identified in different proportions in all samples, with pyrite being the most common sulphide mineral. The Voorburg North area, north of the fault, was dominated by both syngenetic and epigenetic pyrite. Samples closer to the Tshipise Fault had more epigenetic pyrite, noted to be infilling cracks and replacing carbonates nodules. The syngenetic pyrite more dominant in sample VB01 (framboidal and euhedral in shape), is thought to have formed from marine influence or enrichment of sulphur in groundwater during peatification. The epigenetic pyrite is associated with hydrothermal fluids introduced along the Tshipise or Bosbokpoort Faults.
- In comparison to Voorburg, the Makhado area (south of the fault) contained syngenetic siderite, observed as nodules; trigonal siderite was also noted.

Although siderite was noted in samples in the Voorburg area, it was not as common as in samples from Makhado. In Makhado the siderite appears to have been mostly replaced by pyrite.

- When studied under the SEM, and EMPA, siderite nodules in sample 15143 (Makhado) indicated an enrichment of Ca on the rim in comparison to the core. It is thought that the calcium enrichment on the rim/margin could be associated with fluids carried by the fault.
- An interesting form of pyrite, termed botryoidal pyrite, was encountered in samples 15143 and 15152, both of which were sampled from the MU Seam in Makhado. The overgrowth of the botryoidal pyrite in sample 15143 were enriched in As, Ni, Pb, and Co as determined using SEM and EMPA. The botryoidal pyrite in sample 15152 had no apparent enrichment of trace elements. It is proposed that the Tshipise and Bosbokpoort Faults carried fluids rich in these elements that subsequently precipitated around the syngenetic pyrite. This study demonstrates that the mineralogy in the coal is affected by the fault subsequent to coalification.
- Calcite cleats were observed to infill cracks in vitrinite and also to shatter the vitrinite in the sample. Different generations of calcite cleats were noted and can be associated with fluid influxes along the Tshipise and Bosbokpoort Faults.
- Based on studies conducted by Malaza (2013), the coals of Soutpansberg and Limpopo Coalfields where deposited in a fluvial environment. In this study, this finding is supported by the high vitrinite content, indicative of deposition in a wet forest swamp environment. The presence of syngenetic pyrite in samples from Voorburg North and sample 15143 and 15152 (in Makhado) can also be inferred as indicating a marine transgression or, more likely, sulphate rich ground water circulation.
- The coal quality and petrography of the coal is comparable with major differences being the mineral matter. The Tshipise and Bosbokpoort Faults could have influenced the thermal maturity of the coals causing differences in rank. Mineral variations in the coals were also linked to the fault.
- The new Hilgers Fossil system petrographic software worked well. The software allowed for rapid scanning of the coal blocks and offline analyses following calibration. It made it easier to conduct repeated maceral and reflectance

analyses. The only disadvantage of working offline was that the software did not allow for switching between fluorescent and white light to identify liptinite and clay minerals and images were monochromatic light rather than in colour. However, the microscope was used to verify issues of concern.

RECOMMENDATIONS

The author recommends the following:

- The borehole closest to the Tshipise Fault used in this study was in fact 900m (Voorburg South) away from the Tshipise Fault closer to the Bosbokpoort Fault. It is therefore recommended to sample closer (less than 100m) to the fault to determine clear impacts of the fault on the coal quality. Unfortunately these samples were not available for this project.
- Detailed geochemistry, palynology and microlithotype analysis could be conducted to help enhance the understanding of the depositional environment. Palynology studies to complement standard petrographic studies will allow for a better determination of palynofacies and paleoenvironmental interpretations.
- The minerals identified in the coal seams were interesting and require more detailed studies. Detailed petrographic, SEM, and EMPA studies are recommended to study the carbonates and sulphide minerals, especially the botryoidal pyrite as it is not common in South African coals.
- In terms of coking tests, only FSI was conducted during this research as the focus was on the petrographic compositions of the coals. Studies concerning coal processing to increase coking potential would be beneficial, as well as actual coking tests. CoAL has obviously undertaken these studies internally, but the information is not published.

REFERENCES

Barker, O.B., 1999. Analyses of coal product samples of South African Collieries. In: Pinheiro, H. J. (Ed). A Tectono-economic and historical review of the South African coal industry in the 19th and 20th centuries. SABS, South Africa, pp. 1 - 63.

Belkin, H.E., Tewalt, S.J., Hower, J.C., Stucker, J.D., O'Keefe, J.M.K., Tatu, C.A., Buia, G., 2010. Petrography and geochemistry of the Oligocene bituminous coals from the Jiu Valley, Petrosani basin (southern Carpathian Mountains), Romania. International Journal of Coal Geology, 82, 68 – 80.

Benedict, L.G., Thompson, R.R., Shigo III, J.J., Aikman, R.P., 1966. Pseudovitrinite in Appalachian coking coals abstract. The Geological Society of America, pp 14.

Booysens, Y., 2013. SA has the potential to become future coking-coal producer. Minning weekly. www.miningweekly.com/articles. [Accessed 18 September 2016].

Bordy, E.M., Catuneanu, O., 2002. Sedimentology of the Beaufort – molteno karoo fluvial strata in the Tul basin, South Africa. Journal of African Earth Sciences, 105, 51 – 66.

Bordy, E.M., 2005. Sedimentary of the lower Karooo Supergroup fluvial strata in the Tuli Basin, South Africa. Journal of African Earth Sciences, 35, 503 – 521.

Brandl G., 1981. The geology of the Messina area. Explanation sheet 2230 (Messina). Geological Survey South Africa, 35 pp.

Brown, D., 2013. Makhado definitive feasibility study. www.coalofafrica.com/makhado [Accessed September 2015].

Cadle, A.B., Cairncross, B., Christie, A.D.M., Roberts, D.L, 1993. The Karoo Basin of South Africa: type basin for the coal-bearing deposits of southern Africa. International Journal of Coal Geology, 23, 117 - 157.

Cairncross, B., 2001. An overview of the Permian (Karoo) coal deposits of southern Africa. African Earth Sciences, 33, 529 – 562.

Catuneanu, O., Wopfner, H., Eriksson, P.G., Cairncross, B., Rubidge, B.S., Smith, R.M.H., Hancox, P.J., 2005. The Karoo basins of south-central Africa, Journal of African Earth Sciences, 43, 211–253.

Crelling, J., 1989. Separation and characterisation of coal macerals: Accomplishments and future possibilities. Fuel Reprint, 34, 249 – 255.

Crelling, J.C., 2008. Coal carbonization. In: Suaréz-Ruiz, I., Crelling, J.C. (Eds.), Applied Coal Petrology – The role of petrology in coal utilization. Elsevier. Chapter 7, 173 – 192.

Chatterjee, K. K., 2006. Uses of energy minerals and changing techniques. New age international limited. India.

Chou, C.L., 2012. Sulfur in coals: a review of geochemistry and origin. International Journal of Coal Geology, 100, 1 – 13.

CoAL., 2015. Vele operation. www.coalofafrica.com/our business/operations/operation-vele [Accessed 4 March 2015].

De Jager, F.S.J., 1986. Coal occurrences of the central, north-western, northern and eastern Transvaal. In: Anhaeusser, C.R., Maske, S. (Eds.), Mineral Deposits of Southern Africa. Geological Society of South Africa, pp. 2047 – 2055.

Diessel, C.F.K., 1982. An appraisal of coal facies based on maceral characteristics. In: Mallett, C.W. (Ed.), Australian Coal Geology, 2, pp. 474 – 484.

Diessel, C.F.K., 1986. On the correlation between coal facies and depositional environments. 20th Newcastle Symposium on ‘‘Advances in the Study of the Sydney Basin’’, Proceedings. Publication 246, Department of Geology, University of Newcastle, Australia, pp. 19 – 22.

Diessel, C.F.K., 1992. Coal-bearing depositional systems. Springer-Verlag, Berlin, 721pp.

Diez, M.A., Alvarez, R., Barriocanal, C., 2002. Coal for metallurgical coke production: predictions of coke quality and future requirements for coke making. International Journal of Coal Geology, 50, 389 – 412.

Eberhard, A., 2011. The future of South African coal: Market, investment, and policy challenges. Working Paper No. 100 Programme on Energy and Sustainable Development. Encina Hall East, Stanford University. CA 94305-6055, 44 pp.

Eberhard, A., 2015. Market, investment, and policy challenges for South African coal. In: Thurber, M.C., and Morse, R.K. The global coal markets. Supplying the Major fuel for emerging economies. Cambridge, pp. 164 – 203.

Falcon, R.M.S., 1986. A brief review of the origin, formation and distribution of coal in southern Africa. In: Anhaeusser, C. R. and Maske, S (Eds.). Mineral deposits of southern Africa. Vol 1 & 2, Geological Society of South Africa, Johannesburg, pp. 1879 – 1898.

Falcon, R.M.S., Snyman, C.P., 1986. An introduction to coal petrography: Atlas of petrographic constituents in the bituminous coals of southern Africa. The Geological Society of South Africa, Johannesburg. 107 pp.

Faure, K., Willies, J.P., Dreyer, J.C., 1996. The Grootegeluk Foemation in the Waterberg Coalfield, South Africa: facies, paleoenvironment and thermal history – evidence from organic and clastic matter. International Journal of Coal Geology, 29, 147 – 186.

Ghosh, T. K., Prelas, M. A., 2009. Coal in S. Science (Ed.), Energy Resources and Systems: Fundamentals and Non-Renewable Resources. Vol. 1, Springer Science + Business Media, pp. 159 – 279.

Glasspool, I.J., 2003. Hypautochthonous-allochthonous coal deposition in the Permian, South Africa, Witbank Basin no. 2 seam; a combined approach using sedimentology, coal petrology and palaeontology. International Journal of Coal Geology, 53, 81–135.

Gotz, A.E., Ruckwied, K., 2014. Palynological records of the Early Permian postglacial climate amelioration (Karoo Basin, South Africa). Paleoaerobics. Paleoenvironment, 94, 229 – 235.

Gurba, L.W., Ward, C.R., 1997. Vitrinite reflectance anomalies in the high volatile bituminous coals of the Gunnedah Basin, New South Wales, Australia. International Journal of Coal Geology, 36, 111 – 140.

Hancox, J.P., Gotz P.E., 2014. South African coalfields. International Journal of Coal Geology, 132, 170 – 254.

Horsfall, D.W., 1993. Coal Preparation and Usage. Parklands: Coal Publications (Pty) Ltd. 64 pp.

International Committee for Coal and Organic Petrology, 1998. The new vitrinite classification (ICCP System 1994). Fuel, 77, 349–358.

International Committee for Coal and Organic Petrology, 2001. New inertinite classification (ICCP system 1994). Fuel, 80, 459–471.

International committee for Coal and Organic Petrology, 2011. International handbook of coal petrography.

International committee for Coal and Organic Petrology, 2015. Fundamentals of organic Petrology. 8th ICCP course, Vol 1, 301 pp.

ISO 7404-2., 2009. Methods for the Petrographic Analysis of Coals — Part 2: Methods of Preparing Coal Samples. International Organization for Standardization, Geneva, Switzerland, 12 pp.

ISO 7404-3., 1994. Methods for the petrographic analysis of bituminous coal and anthracite. Part 3: Method of determining maceral group composition. International Organization for Standardization, Geneva, Switzerland, 6 pp.

ISO 7404-5., 2009. Methods for the Petrographic Analysis of Coals — Part 5: Methods of Determining Microscopically the Reflectance of Vitrinite. International Organization for Standardization, Geneva, Switzerland, 14 pp.

Jarosewich, E., Macintyre, I. G., 1983. Carbonate reference samples for electron microprobe and scanning electron microscope analysis. National Museum of Natural History Smithsonian Institution. Washington, D.C, 53, 677 – 678.

Jeffrey, L.S., 2005. Characterization of the coal resources of South Africa. Journal of the Southern African Institute of Mining and Metallurgy, 95–102.

Johnson, M.R., van Vuuren, C.J., Hegenberger, W.F., Key, R., Shoko, U., 1996a. Stratigraphy of the Karoo Supergroup in southern Africa: an overview. Journal of African Earth Sciences, 23, 3 - 15.

Johnson, M.R., van Vuuren, C.J., Visser, J.N.J., Cole, D.I., Wickens, H. de V., Christie, A.D.M., Roberts, D.L., Brandl, G., 1996b. Sedimentary rocks of the Karoo Supergroup. In: Johnson, M. R., Anhaeusser, C. R. and Thomas, R. J. (Eds.), The geology of South Africa, Geological Society of South Africa/Council for Geoscience, Pretoria, pp. 469 - 499.

Kaegi, D.D., 1985. On the identification and origin of pseudovitrinite. International Journal of Coal Geology, 4, 309 – 319.

Kalaitzidis, S., Bouzinos, A., Papazisimou, S., Christanis, K., 2004. A short-term establishment of forest fen habitat during Pliocene lignite formation in the Ptolemais Basin, NW Macedonia, Greece. International Journal of Coal Geology, 57, 243 – 263.

Kalkreuth, W., Leckie, D.A., 1989. Sedimentological and petrographical characteristics of Cretaceous strandplain coals: a model for coal accumulation from the North American Western Interior Seaway. International Journal of Coal Geology, 12, 381 – 424.

Khorami, M.T., Chelgani, S.C., Hower, J.C., Jorjani, E., 2011. Studies of relationships between Free Swelling Index (FSI) and coal quality by regression and adaptive Neuro Fuzzy Influence System. International Journal of Coal Geology, 85, 65 – 71.

Kruger, H., 2013. Coking Coal. Fossil Fuel Foundation Coal Coke & Carbon in Metallurgy Industry. 13-14 June 2013.

Kruszewska, K.J., 2003. Fluorescing macerals in South African coals. International Journal of Coal Geology, 54, 79 – 94.

Kwiecinska, B., Petersen, H.I., 2004. Graphite, semi-graphite, natural coke and natural char classification – ICCP system. International Journal of Coal Geology, 57, 99 – 116.

Lopez- Buendia, A.M., Whateley, M.K.G., Bastida, J., Urquiola, M.M., 2007. Origins of Mineral Matter in Peat Marsh and Peat Bog Deposits, Spain. International Journal of Coal Geology, 71, 246 - 262.

Makgato, M.H., Moikheki, L.J., Shoko, L., Kgobane, B.L., Morgan, D.L., Focke, W.W., 2009. Alkali-assisted coal extraction with polar aprotic solvents. Fuel proceeding Technology, doi:10.1016/j.fuproc.2008.12.016.

Malaza, N., 2013. Basin Analysis of the Soutpansberg and Tuli Coalfields, Limpopo Province of South Africa. Unpublished PhD Thesis, University of Fort Hare, 380pp.

Malaza N., Liu K., Zhao B., 2013. Paleostress analysis of Karoo Supergroup of the Tshipise-Pafuri Basin, South Africa. South African Journal of Geology, 118, 173–184.

Mastalerz, M., Drobniak, A., 2005. Optical properties of pseudovitrinite; implications for its origin. International Journal of Coal Geology, 62, 250–258.

Meyer, P.C., 2012. Prospectively for coking coal: Tshipise 2 Project in the Tshipise sector of the Soutpansberg Coalfield. P.C. Meyer Consulting

Miller, B.G., 2005. Coal energy systems. Elsevier Academic Press. London, 526 pp.

Millonig, L.J., 2009. The Neoarchean and Palaeoproterozoic metamorphic evolution of the Limpopo Belt's Central Zone in southern Africa. Unpublished PhD Thesis, University of Würzburg, 136 pp.

Moore, T.A., Shearer, J.C., 2003. Peat/coal type and depositional environment – are they related? International Journal of Coal Geology. 56, 233 - 252.

O'Keefe, J.M.K., Bechtel, A., Christanis, K., Dai, S., DiMichele, W.A., Eble, C.F., Esterle, J.S., Mastalerz, M., Raymond, A.L., Valentim, B.V., Wagner, N.J., Ward, C.R., Hower, J.C., 2013. On the fundamental difference between coal rank and coal type. International Journal of Coal Geology, 118, 58 – 87.

Ortlepp, G.J., 1986. Limpopo Coalfield. In: Anhaeusser, C.R., Maske, S. (Eds.), Mineral Deposits of Southern Africa, vol. II. Geological Society of South Africa, Johannesburg, pp. 2057–2061

Pajares, J.A., Diez, M.A., 2014. Coal and coke. Reference module in chemistry, molecular sciences and chemical engineering. Http://dx.doi.org/10.1016/B978-0-12-409547-2.10968-0

Parzentny, H.R., Lewin´ska-Preis, L., 2005. The role of sulphide and carbonate minerals in the concentration of chalcophile elements in the bituminous coal seams of a paralic series (Upper Carboniferous) in the Upper Silesian Coal Basin, Poland. Chermi der Erde Geochemistry, 66, 227 – 247.

Pinheiro, H.J., Pretorius, C.C., Boshoff, H.P., 1999. Analysis of coal and product samples from South African collieries 1999–1999. Bulletin 113 Coal and Miner Services, South African Bureau of Standards, pp. 64–97.

Pickel, W., Kus, J., Flores, D., Kalaitzidis, S., Christianis, K., Cardott, B.J., Misz-Kennan, M., Rodrigues, S., Hentschel, A., Hamor-Vido, M., Crosdale, P., Wagner, N., ICCP., 2017. Classification of Liptinite – ICCP system 1994. International Journal of Coal Geology, 169, 40 – 61.

Prasad, A.R., 1986. Coal industry in India. Ashish publishing house. New Delhi -110 026.

Ryan, D., 2003. Pseudovitrinite: Possible implication for gas saturation in coals and surrounding rocks. British Colombia Geological Survey, pp. 203 – 211.

Saad, A.E., Pinhiero, H.J., 2001. The Tshipise and Mopane Coalfields Soutpansberg District. Baobab Coal (PTY) LTD.

Sahay, V.K., 2011. Limitation of petrographic indices in depositional environmental interpretation of coal deposits. Central European Journal of Geosciences, 3, 287-290

Schweinfurth, S.P., 2009. An introduction to coal quality. In: Pierce, B.S., Dennen, K.O. (Eds.). The National Coal Resource Assessment Overview: U.S. Geological Survey Professional Paper 1625–F, Chapter C, 16pp.

Scott, A.C., 2002. Coal petrography and origin of macerals: a way ahead? International Journal of Coal Geology. 50, 119–134

Sen, S., Naskar, S., Das, S., 2016. Discussion on the concepts in paleoenvironmental reconstruction from coal macerals and petrographic indices. Marine and Petroleum Geology, 73, 371-391.

Silva, M.B., Kalkreuth, W., 2005. Petrological and geochemical characterization of Candiota coal seams, Brazil - Implication for coal facies interpretations and coal rank. International Journal of Coal Geology, 64, 217– 238.

Snyman, C.P., 1998. Coal. In: Wilson, M. G. C. and Anhaeusser, C. R. (Eds.). The mineral resources of Southern Africa. Handbook, Council of Geoscience, 16, 136 – 205.

Sparrow, J., 2012. The Soutpansberg Coalfield “The Forgotten Basin”. Presentation at the Inaugural FFF Limpopo Conference, October 2012.

Speight, J.G., 2005. Handbook of Coal Analysis, Wiley and Sons. 240 pp.

Stach, E., Chandra, D., Mackowsky, M., Taylor, G. H., Teichmuller, M., Teichmuller, R., 1982. Stach’s textbook of coal petrology. Gebruder Borntraeger, Berlin, 533pp.

Steyn, M., Minnitt, R.C.A., 2010. Thermal coal products in South Africa. Journal of Southern African Institute of Mining and Metallurgy, 110, 593 – 559.

Suaréz-Ruiz, I., Ward, C.R., 2008. Coal Combustion. In: Suaréz-Ruiz, I., Crelling, J.C. (Eds.), Applied Coal Petrology. Elsevier Academic Press. Chapter 4, 85 – 117.

Suaréz-Ruiz. I., 2012. Organic Petrology: An Overview, Petrology - New Perspectives and Applications, Prof. Ali Al-Juboury (Ed.), ISBN: 978-953-307-800-7, InTech, Available from: http://www.intechopen.com/books/petrology-new-perspectives-and-applications/organic-petrology-an-overview [Accessed August 2015].

Suwara, N., 2006. Permian Mengkarang coal facies and environment, based on organic petrology study. Journal Geologi Indonesia, 1, 1 – 8.

Taylor, G.H., Teichmuller, M., Davis, A., Diessel, C.F.K., Littke, R., Robert, P., 1998. Organic petrology. Gebrüder Borntraeger. Berlin. 704 pp.

Telfer, C.A., Njowa, G., 2012. Independent Geologist Specialist Report on the Principal South African Operating and Non-operating Mineral Assets of Coal of Africa Limited. Unpublished Report by Venmyn Deloitte for Coal of Africa Limited, 346 pp.

The Economist, 2015. Coal mining. http://www.economist.com/node/21647287/print [Accessed June 2015].

Thomas, L., 2002. Coal Geology. John Wiley & Sons. 384 pp.

Thomas, L., 2013. Coal geology. Dargo associates Ltd Wiley-Blackwell. UK. 456 pp.

UNECE, 1998. International classification of in-seam coals. Economic Commission for Europe, Committee on Sustainable Energy United Nations, New York. Document ENERGY/1998/19, 41 pp.

Wagner, N.J., 2007. The Abnormal Condition Analysis used to characterize weathered discard coals. International Journal of Coal Geology, 72, 177–186

Wagner, N.J., Tlotleng, M.T., 2012. Distribution of selected trace elements in density fractionated Waterberg coals from South Africa. International Journal of Coal Geology. 94, 225–237.

Ward, C.R., 1984. Coal geology and coal technology. Blackwell Scientific Publications. 345 pp.

Ward, C.R., 2002. Analysis and significance of mineral matter in coal seams. International Journal of Coal Geology, 50, 135 – 168.

Ward, C.R., 2016. Analysis and significance of mineral matter in coal. An updated review. International Journal of Coal Geology, 165, 1– 27.

World Coal Association, 2014. Coal statistics. http://www.worldcoal.org/coal-facts-2014 [Accessed March 2015]

Webber, S.L., Cairncross, B., Falcon, R.M.S., 2000. Mineralogical, petrographic and geological controls on the coal ash fusion temperature from New Cyclesdale Colliery, Witbank Coalfield, South Africa. The Journal of the South African Institute of mining and metallurgy, pp. 181 – 190.

Widodo, S., Oschmann, W., Bechtel, A., Sachsenhofer, R.F., Anggayana, K., Puettmann, W., 2010. Distribution of sulfur and pyrite in coal seams from Kutai Basin (East Kalimantan, Indonesia): implications for paleoenvironmental conditions. International Journal of Coal Geology, 91, 151–162.

Williams, A., Pourkashanian, M., Jones, J.M., Skorupska, N., 2000. Combustion and gasification of coal. Applied energy technology series. USA. 336 pp.

Wilson, J., Clark, P., 2015. BHP chief: stop saying gas is cleaner than coal. http://on.ft.com/1EBa6bT [Accessed April 2015].

Zhao, L., Ward, C.R., French, D., Graham, I.T., 2013. Mineralogical composition of Late Permian coal seams in the Songzao Coalfield, southwestern China. International Journal of Coal Geology. 116-117, 208–226.

APPENDICES

Appendix A: Fossil Software description.

The Zeiss Axio Imager m2m is retrofitted with Fossil software. Fossil is a software for microscopic reflectance analysis with a digital camera. It supports microscopic observations, and reflectance and point count analysis in reflected white light and fluorescence mode. The automated stage and keyboard replaces the 'swift pointer counter' system. To initialise the stage, you enter the parameters: number of position vertical, horizontal, and the distance to the next position. The stage moves to the first position, and the camera shows the live image in full resolution. The fossil software allows microscopic view, where you observation are done in white light reflectance and fluorescence mode. Maceral analyses can be done to identify different macerals and up to 27 classes can be distinguished. Before running the analysis there is a calibration done using the Klein and Bekker standard. Due to the fact that the complete image range is calibrated, allows the user to choose the point of measurement with the mouse pointer at any position of the displayed image.

Fossil student is a software that allows to analyse samples that have been previously scanned with a microscope. The data from reflectance and maceral analysis can be exported as comma separated values file or excel spreadsheet or portable document format (PDF) files. Fast scans images allows for random reflectance images.

Fossil student gives an option to use the eyepiece and computer screen. Because the measurements are carried out also using the screen, allowing the user therefore, to maintain a physically relaxed operating position which makes fossil less strenuous to operate.

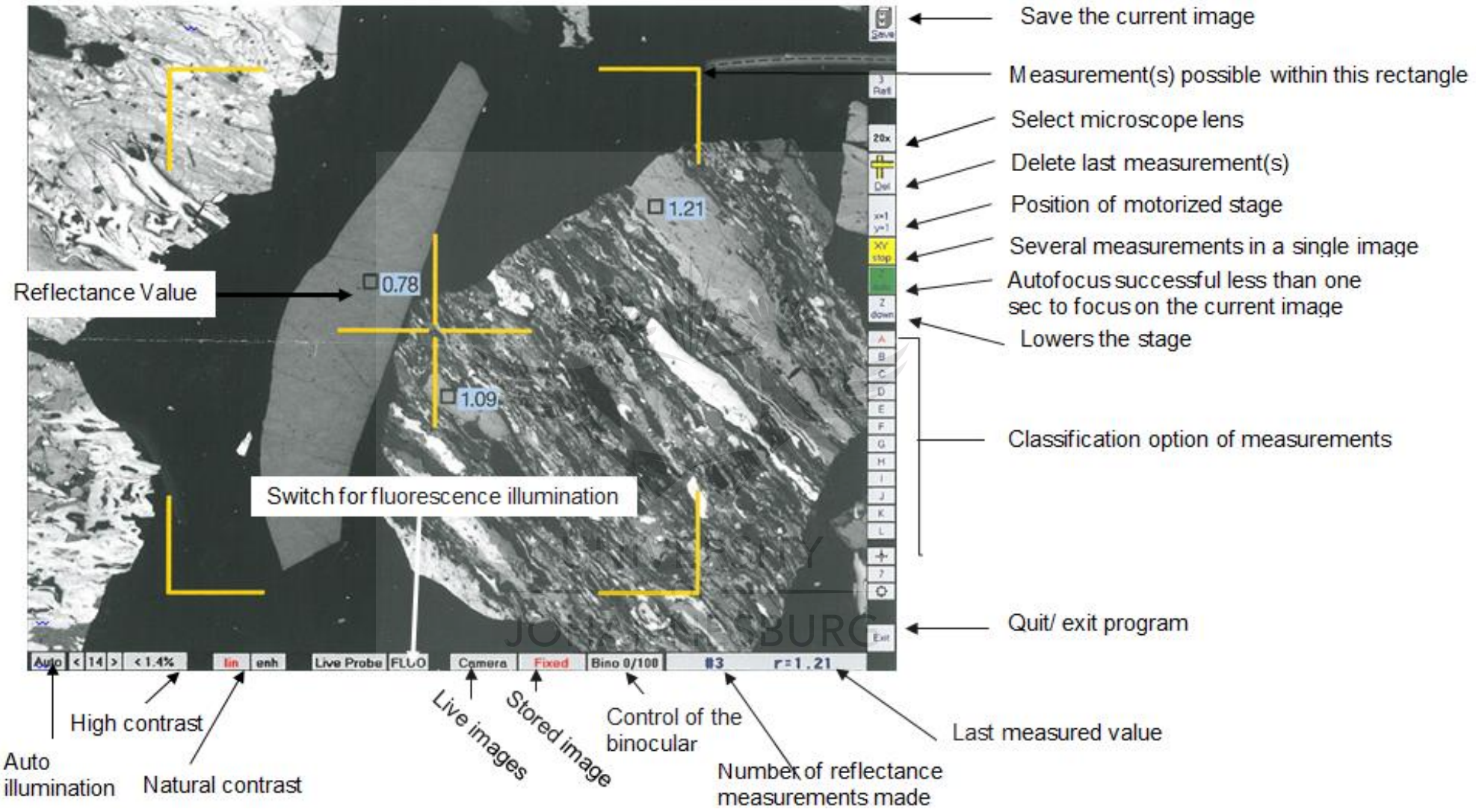

Figure A.1: Main screen Vitrinite reflectance measurement

Appendix B: Petrographic Analyses

B.1. Maceral analyses

Table B.1.1: Maceral analysis of Voorburg North

BH ID	V07BS01						V10BS01			
Sample ID	VB01		VB02		VB03		15150		15151	
Seam	MU		BU		BL		BU		BL	
	inc. mm	mmf	inc. mm	mmf	inc. mm	mmf	inc. mm	mmf	inc. mm	mmf
MACERAL	vol%	vol%	vol%	vol%	vol%	vol%	vol%	vol%	vol%	vol%
telinite	0.0	0.0	0.6	0.8	1.4	1.9	0.0	0.0	0.0	0.0
collotelinite	26.9	74.4	54.3	71.6	50.8	68.6	22.1	49.3	28.8	43.0
vitrodetrinite	0.3	0.8	2.0	2.7	1.4	1.9	3.8	8.5	2.8	4.2
collodetrinite	4.3	9.4	8.5	12.0	9.2	13.7	2.3	5.3	0.0	0.0
corpogelinite	0.0	0.0	0.3	0.3	0.0	0.0	0.0	0.0	0.0	0.0
gelinite	0.0	0.0	0.0	0.0	0.0	0.0	0.0	0.0	0.0	0.0
pseudovitrinite	1.3	3.5	2.0	2.7	5.6	7.3	3.5	7.8	0.3	0.4
Total Vitrinite	32.8	88.1	67.7	90.1	68.4	93.3	31.7	70.9	31.9	47.6
fusinite	1.3	3.5	3.1	4.0	0.9	1.2	3.5	7.8	0.0	0.0
semifusinite	1.6	4.4	2.3	3.1	1.7	2.3	5.6	12.5	10.1	15.1
micrinite	0.0	0.0	0.6	0.8	0.0	0.0	0.2	0.4	0.0	0.0
macrinite	0.0	0.0	0.3	0.4	0.0	0.0	0.0	0.0	1.0	1.5
secretinite	0.0	0.0	0.3	0.4	0.6	0.8	0.2	0.4	3.1	4.6
funginite	0.3	0.8	0.0	0.0	0.0	0.0	0.0	0.0	0.0	0.0
inertodetrinite	0.3	0.8	0.0	0.0	0.0	0.0	2.8	6.2	20.2	30.1
Total Inertinite	3.5	9.5	6.6	8.7	3.2	4.4	12.3	27.4	34.4	51.3
sporinite	0.6	1.6	0.9	1.2	1.7	2.3	0.7	1.7	0.7	1.0
cutinite	0.3	0.8	0.0	0.0	0.0	0.0	0.0	0.0	0.0	0.0
resinite	0.0	0.0	0.0	0.0	0.0	0.0	0.0	0.0	0.0	0.0
alginite	0.0	0.0	0.0	0.0	0.0	0.0	0.0	0.0	0.0	0.0
liptodetrinite	0.0	0.0	0.0	0.0	0.0	0.0	0.0	0.0	0.0	0.0
suberinite	0.0	0.0	0.0	0.0	0.0	0.0	0.0	0.0	0.0	0.0
exsudatinite	0.0	0.0	0.0	0.0	0.0	0.0	0.0	0.0	0.0	0.0
Total Liptinite	0.9	2.4	0.9	1.2	1.7	2.3	0.7	1.7	0.7	1.0
Total Reactive*	33.7	90.5	68.6	91.3	70.1	95.6	32.4	72.6	32.6	48.6
silicate (clay+quartz)	4.6		4.0		3.5		51.0		31.3	
sulfide	46.5		10.0		16.9		3.8		0.7	
carbonate	11.7		10.8		6.3		0.5		1.0	
other	0.0		0.0		0.0		0.0		0.0	
Total Mineral matter	62.8		24.8		26.7		55.3		33.0	

*Total reactive macerals = Total vitrinite + total liptinite; RSF was excluded from the analysis as it was rarely encountered (This applicable to all tables in Appendix B1).

Table B.1.2: Maceral analysis for Voorburg South

BH ID	R637004						R63701LD								F578004			
Sample ID	15136		15137		15138		15147		15148		15149		15154		15155		15156	
Seam	MU		BU		BL		MU		ML		BU		MU		ML		BL	
	inc. mm	mmf	inc. mm	mmf	inc. mm	mmf	inc. mm	mmf	inc. mm	mmf	inc. mm	mmf	inc. mm	mmf	inc. mm	mmf	inc. mm	mmf
telinite	1.1	1.5	0.0	0.0	0.0	0.0	0.3	0.4	0.0	0.0	0.0	0.0	0.0					
collotelinite	29.0	39.2	23.1	33.0	38.2	44.8	45.2	59.5	32.8	56.2	64.8	70.4	50.0	65.7	40.4	58.9	40.1	55.8
vitrodetrinite	0.3	0.4	1.1	1.6	13.3	37.0	0.0	0.0	0.3	0.5	0.0	0.0	3.7	4.9	1.4	2.0	0.6	0.8
collodetrinite	38.0	51.3	30.3	43.3	0.4	0.6	11.1	14.6	5.0	8.5	2.7	2.9	0.7	0.9	0.7	1.0	0.6	0.8
corpogelinite	0.0	0.0	0.0	0.0	0.0	0.0	0.0	0.0	0.3	0.5	0.0	0.0	0.0	0.0	0.0	0.0	0.0	0.0
gelinite	0.0	0.0	0.0	0.0	0.0	0.0	0.0	0.0	0.0	0.0	0.0	0.0	0.0	0.0	0.0	0.0	0.0	0.0
pseudovitrinite	3.6	4.9	2.5	3.6	0.7	1.1	7.4	9.7	3.5	6.0	1.5	1.6	2.2	2.9	1.7	2.5	2.8	3.8
Total Vitrinite	72.0	97.3	57.0	81.4	52.6	83.6	64.0	84.2	41.9	71.7	69.0	75.0	56.6	74.4	44.2	64.4	44.1	61.3
fusinite	1.1	1.5	1.8	2.6	4.2	6.7	2.9	3.8	6.2	10.6	10.9	11.8	12.5	16.4	11.7	17.1	4.0	5.6
semifusinite	0.6	0.8	6.1	8.7	2.8	4.5	6.0	7.9	7.6	13.0	9.8	10.6	2.2	2.9	3.4	5.0	10.7	14.5
micrinite	0.0	0.0	0.0	0.0	0.4	0.6	0.3	0.4	0.0	0.0	0.0	0.0	0.0	0.0	0.0	0.0	0.0	0.0
macrinite	0.0	0.0	0.4	0.6	0.0	0.0	0.0	0.0	0.3	0.5	0.0	0.0	0.4	0.5	0.0	0.0	0.0	0.0
secretinite	0.0	0.0	3.6	5.1	1.1	1.7	1.4	1.8	0.9	1.5	0.6	0.7	0.0	0.0	0.0	0.0	0.0	0.4
funginite	0.0	0.0	0.0	0.0	0.0	0.0	0.0	0.0	0.0	0.0	0.0	0.0	0.0	0.0	0.0	0.0	0.0	0.0
inertodetrinite	0.0	0.0	1.1	1.6	1.1	1.7	0.0	0.0	0.3	0.5	1.5	1.6	4.0	5.3	9.0	13.1	12.8	17.8
Total Inertinite	1.7	2.3	13.0	18.6	9.6	15.3	10.6	13.9	15.3	26.2	22.8	24.8	19.1	25.1	24.1	35.1	27.5	38.3
sporinite	0.3	0.4	0.0	0.0	0.7	1.1	1.4	1.8	1.2	2.0	0.2	0.2	0.4	0.5	0.3	0.4	0.3	0.4
cutinite	0.0	0.0	0.0	0.0	0.0	0.0	0.0	0.0	0.0	0.0	0.0	0.0	0.0	0.0	0.0	0.0	0.0	0.0
resinite	0.0	0.0	0.0	0.0	0.0	0.0	0.0	0.0	0.0	0.0	0.0	0.0	0.0	0.0	0.0	0.0	0.0	0.0
alginite	0.0	0.0	0.0	0.0	0.0	0.0	0.0	0.0	0.0	0.0	0.0	0.0	0.0	0.0	0.0	0.0	0.0	0.0
liptodetrinite	0.0	0.0	0.0	0.0	0.0	0.0	0.0	0.0	0.0	0.0	0.0	0.0	0.0	0.0	0.0	0.0	0.0	0.0
suberinite	0.0	0.0	0.0	0.0	0.0	0.0	0.0	0.0	0.0	0.0	0.0	0.0	0.0	0.0	0.0	0.0	0.0	0.0
exsudatinite	0.0	0.0	0.0	0.0	0.0	0.0	0.0	0.0	0.0	0.0	0.0	0.0	0.0	0.0	0.0	0.0	0.0	0.0
Total Liptinite	0.3	0.4	0.0	0.0	0.7	1.1	1.4	1.8	1.2	2.0	0.2	0.2	0.4	0.5	0.3	0.4	0.3	0.4
Total Reactive	72.3	97.7	57.0	81.4	53.3	84.7	65.4	86.1	43.1	73.7	69.2	75.2	57.0	74.9	44.5	64.8	44.4	61.7
silicate	2.0		21.0		32.9		18.0		22.0		4.4		19.1		28.6		20.8	
sulfide	10.9		6.5		2.8		1.1		2.6		1.5		2.6		1.4		1.5	
carbonate	13.1		2.5		1.4		4.9		17.0		2.1		2.2		1.4		5.8	
other	0.0		0.0		0.0		0.0		0.0		0.0		0.0		0.0		0.0	
Total Mineral	26.0		30.0		37.1		24.0		41.6		8.0		23.9		31.4		28.1	

Table B.1.3: Maceral analysis for Makhado

BH ID	T190BS03				T07BS							
Sample ID	15139		15140		15141		15142		15152		15153	
Seam	BU		BL		MU		BL		MU		BU	
MACERAL	inc. mm vol%	mmf vol%	inc. mm vol%	mmf vol%	inc. mm vol%	mmf vol%	inc. mm vol%	mmf vol%	inc. mm vol%	mmf vol%	inc. mm vol%	mmf vol%
telinite	0.0	0.0	0.0	0.0	0.0	0.0	1.6	1.7	0.0	0.0	0.0	0.0
collotelinite	26.0	40.6	17.0	26.1	72.8	78.7	59.6	63.6	41.6	66.9	50.1	66.3
vitrodetrinite	0.0	0.0	0.0	0.0	0.0	0.0	4.0	4.3	0.0		7.7	10.2
collodetrinite	26.0	40.6	27.0	40.2	3.2	3.5	9.6	10.2	0.2	0.3	2.7	3.6
corpogelinite	0.0	0.0	0.0	0.0	0.0	0.0	2.3	2.5	0.4	0.6	0.0	0.0
gelinite	0.0	0.0	0.0	0.0	0.0	0.0	0.0	0.0	0.0	0.0	0.0	0.0
pseudovitrinite	1.0	1.6	4.0	6.0	2.6	2.9	2.8	3.0	0.6	1.0	4.3	5.7
Total Vitrinite	53.0	82.7	48.0	72.3	78.6	85.1	79.9	85.3	42.8	68.8	64.8	85.8
fusinite	0.0	0.0	2.0	3.0	4.3	4.6	6.3	6.7	5.6	9.0	1.6	2.1
semifusinite	5.0	7.8	12.0	17.8	7.2	7.8	2.8	3.0	5.4	8.7	6.1	8.1
micrinite	0.0	0.0	0.0	0.0	0.5	0.5	0.5	0.5	0.0	0.0	0.0	0.0
macrinite	1.0	1.6	0.0	0.0	0.0	0.0	0.0	0.0	0.4	0.6	0.0	0.0
secretinite	1.0	1.6	0.0	0.0	0.2	0.2	0.7	0.7	0.0	0.0	0.5	0.7
funginite	0.0	0.0	0.0	0.0	0.0	0.0	0.0	0.0	0.2	0.3	0.0	0.0
inertodetrinite	3.0	4.7	4.0	6.0	0.7	0.8	0.0	0.0	6.2	10.0	2.3	3.0
Total Inertinite	10.0	15.7	18.0	26.7	12.9	13.9	10.3	10.9	17.8	28.6	10.5	13.9
sporinite	1.0	1.6	0.0	1.0	0.9	1.0	3.5	3.7	1.6	2.6	0.2	0.3
cutinite	0.0	0.0	0.0	0.0	0.0	0.0	0.0	0.0	0.0	0.0	0.0	0.0
resinite	0.0	0.0	0.0	0.0	0.0	0.0	0.0	0.0	0.0	0.0	0.0	0.0
alginite	0.0	0.0	0.0	0.0	0.0	0.0	0.0	0.0	0.0	0.0	0.0	0.0
liptodetrinite	0.0	0.0	0.0	0.0	0.0	0.0	0.0	0.0	0.0	0.0	0.0	0.0
suberinite	0.0	0.0	0.0	0.0	0.0	0.0	0.0	0.0	0.0	0.0	0.0	0.0
exsudatinite	0.0	0.0	0.0	0.0	0.0	0.0	0.0	0.0	0.0	0.0	0.0	0.0
Total Liptinite	1.0	1.6	0.0	1.0	0.9	1.0	3.5	3.7	1.6	2.6	0.2	0.3
Total Reactive	54.0	84.3	48.0	73.3	79.5	86.1	83.4	89.0	44.4	71.4	65.0	86.1
silicate	31.0		11.0		5.6		3.3		7.4		18.6	
sulfide	3.0		6.0		0.5		1.6		1.2		1.8	
carbonate	2.0		17.0		1.4		1.4		29.2		4.1	
other	0.0		0.0		0.0		0.0		0.0		0.0	
Total Mineral matter	36.0	0.0	34.0	0.0	7.5	0.0	6.3	0.0	37.8	0.0	24.5	0.0

Table B.1.3: Maceral analysis of Makhado continued

BH ID	C6699001								F645BSO2			
Sample ID	15143		15144		15145		15146		15157		15158	
Seam	MU		ML		BU		BL		BU		BL	
MACERAL	inc. mm vol%	mmf vol%	inc. mm vol%	mmf vol%	inc. mm vol%	mmf vol%	inc. mm vol%	mmf vol%	inc. mm vol%	mmf vol%	inc. mm vol%	mmf vol%
telinite	0.0	0.0	0.0	0.0	0.0	0.0	0.0	0.0	0.0	0.0	0.0	0
collotelinite	30.2	64.3	52.0	58.9	9.6	12.4	4.5	8.0	32.8	56.2	39.7	60.9
vitrodetrinite	1.2	2.6	1.6	1.8	0.0	0.5	0.0	0.0	0.3	0.5	0.0	0
collodetrinite	1.0	2.1	10.4	11.8	0.0	0.0	0.0	0.0	5.0	8.6	2.7	3.5
corpogelinite	0.4	0.9	4.7	5.3	0.0	0.0	0.0	0.0	0.3	0.5	0.0	0
gelinite	0.0	0.0	0.0	0.0	0.0	0.0	0.0	0.0	0.0	0.0	0.0	0
pseudovitrinite	1.8	3.8	6.6	7.5	0.2	0.3	0.3	0.4	3.5	6.0	1.5	1.6
Total Vitrinite	34.6	73.6	75.3	85.3	9.8	13.2	4.8	8.4	41.9	71.8	43.9	66.0
fusinite	2.4	5.1	2.8	3.2	2.1	2.8	2.1	3.9	6.2	10.6	5.9	12.8
semifusinite	5.4	11.5	5.7	6.5	17.3	23.3	14.0	20.5	7.6	13.0	9.8	18.6
micrinite	0.0	0.0	0.0	0.0	0.0	0.0	0.0	0.0	0.0	0.0	0.0	0
macrinite	0.2	0.4	0.2	0.2	0.0	0.0	0.0	0.0	0.3	0.5	0.0	0
secretinite	0.2	0.4	0.9	1.0	0.2	0.3	0.0	0.0	0.9	1.5	0.6	0.7
funginite	0.0	0.0	0.0	0.0	0.0	0.0	0.0	0.0	0.0	0.0	0.0	0
inertodetrinite	0.6	1.3	0.0	0.0	44.2	59.5	48.2	64.7	0.3	0.5	1.5	1.6
Total Inertinite	8.8	18.7	9.6	10.9	63.8	85.9	64.3	89.1	15.3	26.1	0.0	33.7
sporinite	3.6	7.7	3.3	3.7	0.7	0.9	1.2	2.5	1.2	2.0	0.2	0.3
cutinite	0.0	0.0	0.0	0.0	0.0	0.0	0.0	0.0	0.0	0.0	0.0	0.0
resinite	0.0	0.0	0.0	0.0	0.0	0.0	0.0	0.0	0.0	0.0	0.0	0.0
alginite	0.0	0.0	0.0	0.0	0.0	0.0	0.0	0.0	0.0	0.0	0.0	0.0
liptodetrinite	0.0	0.0	0.0	0.0	0.0	0.0	0.0	0.0	0.0	0.0	0.0	0.0
suberinite	0.0	0.0	0.0	0.0	0.0	0.0	0.0	0.0	0.0	0.0	0.0	0.0
exsudatinite	0.0	0.0	0.0	0.0	0.0	0.0	0.0	0.0	0.0	0.0	0.0	0.0
Total Liptinite	3.6	7.7	3.3	3.7	0.7	0.9	1.2	2.5	1.2	2.0	0.2	0.3
Total Reactive	38.2	81.3	78.6	89.0	10.5	14.1	6.0	10.9	43.1	73.8	44.1	66.3
silicate	48.8		8.5		25.3		28.5		22.0		28.2	
sulfide	3.4		0.9		0.2		0.8		2.6		5.3	
carbonate	0.8		2.4		0.2		0.4		17.0		4.1	
other			0.0		0.0		0.0		0.0		0.0	
Total Mineral Matter	53.0		11.8		25.7		29.7		41.6		38.2	

Table B.1.4: Maceral analysis for Vele, Waterberg, and Tshikondeni areas.

	VELE COALFIELD											
BH ID	CP17BS02				OV24BS01							
Sample ID	1317		1318		1333		1334		1335		1336	
Seam	BU		BLB		BLT		BU		M		T	
MACERAL	inc. mm vol%	mmf vol%	inc. mm vol%	mmf vol%	inc. mm vol%	mmf vol%	inc. mm vol%	mmf vol%	inc. mm vol%	mmf vol%	inc. mm vol%	mmf vol%
telinite	0.0	0.0	0.2	0.2	0.2	0.2	0.0	0.0	0.0	0.0	0.0	0.0
collotelinite	83.0	84.3	82.6	85.5	72.0	74.2	69.6	72.3	75.3	76.4	83.4	86.7
vitrodetrinite	3.2	3.2	0.0	0	3.6	3.7	5.9	6.1	4.4	4.5	3.2	3.3
collodetrinite	0.0	0.0	5.2	5.4	0.4	0.4	0.0	0.0	2.1	2.1	0.2	0.2
corpogelinite	0.8	0.8	1.8	1.9	0.0	0.0	0.0	0.0	0.0	0.0	0.0	0.0
gelinite	0.0	0.0	0.0	0.0	0.0	0.0	0.0	0.0	0.0	0.0	0.0	0.0
pseudovitrinite	5.6	5.7	4.0	4.1	15.2	15.7	6.3	6.5	10.7	10.8	4.2	4.4
Total Vitrinite	92.6	94.0	93.8	97.1	91.4	94.2	81.8	84.9	92.5	93.8	91.0	94.6
fusinite	1.8	1.8	0.2	0.2	1.6	1.7	3.2	3.4	1.1	1.1	0.4	0.4
semifusinite	0.6	0.6	0.4	0.4	1.4	1.4	2.4	2.5	0.8	0.8	0.6	0.6
micrinite	0.0	0.0	0.0	0.0	0.0	0.0	0.0	0.0	0.0	0.0	0.0	0.0
macrinite	0.0	0.0	0.0	0.0	0.0	0.0	0.0	0.0	0.0	0.0	0.0	0.0
secretinite	0.0	0.0	0.0	0.0	0.0	0.0	0.0	0.0	0.0	0.0	0.0	0.0
funginite	0.0	0.0	0.0	0.0	0.0	0.0	0.0	0.0	0.0	0.0	0.0	0.0
inertodetrinite	0.4	0.4	0.0	0.0	0.4	0.4	0.8	0.8	0.0	0.0	0.2	0.2
Total Inertinite	2.8	2.8	0.6	0.6	3.4	3.5	6.4	6.7	1.9	1.9	1.2	1.2
sporinite	2.8	2.8	1.2	1.3	2.2	2.3	4.3	4.5	1.3	1.3	2.4	2.5
cutinite	0.4	0.4	1.0	1.0	0.0	0.0	3.7	3.8	2.9	3.0	1.6	1.7
resinite	0.0	0.0	0.0	0.0	0.0	0.0	0.0	0.0	0.0	0.0	0.0	0.0
alginite	0.0	0.0	0.0	0.0	0.0	0.0	0.0	0.0	0.0	0.0	0.0	0.0
liptodetrinite	0.0	0.0	0.0	0.0	0.0	0.0	0.0	0.0	0.0	0.0	0.0	0.0
suberinite	0.0	0.0	0.0	0.0	0.0	0.0	0.0	0.0	0.0	0.0	0.0	0.0
exsudatinite	0.0	0.0	0.0	0.0	0.0	0.0	0.0	0.0	0.0	0.0	0.0	0.0
Total Liptinite	3.2	3.2	2.2	2.3	2.2	2.3	8.0	8.3	4.2	4.3	4.0	4.2
Total Reactive	95.8	97.2	96.0	99.4	93.6	96.5	89.8	93.2	96.7	98.1	95.0	98.8
silicate (clay+quartz)	0.4		0.6		1.8		3.0		0.8		2.8	
sulfide	0.2		0.8		0.0		0.6		0.0		0.2	
carbonate	0.6		2.0		1.2		0.2		0.6		0.8	
other	0.2		0.0		0.0		0.0		0.0		0.0	
Total Mineral matter	1.4		3.4		3.0		3.8		1.4		3.8	

Table B.1.4: Maceral analysis for Vele, Waterberg, and Tshikondeni areas continued....

Location	WATERBURG COALFIELD				TSHIKONDENI MINE	
BH ID	Zone 8+9		Zone 7+8		ROM	
Sample ID	15159		15160		15117	
MACERAL	inc. mm	mmf	inc. mm	mmf	inc. mm	mmf
telinite	2.7	4.2	1.1	1.3	0.2	0.2
collotelinite	30.2	47.4	23.1	28.1	80.4	82.4
vitrodetrinite	0.0	0.0	0.0	0.0	0.0	0.0
collodetrinite	5.4	8.5	2.2	2.7	0.6	0.6
corpogelinite	6.0	9.4	0.6	0.7	0.0	0.0
gelinite	0.0	0.0	0.0	0.0	0.0	0.0
pseudovitrinite	2.0	3.2	0.0	0.0	3.2	3.3
Total Vitrinite	46.3	72.7	27.0	32.8	84.4	86.5
fusinite	2.7	4.2	1.1	1.3	2.2	2.3
semifusinite	6.0	9.4	16.1	19.6	7.4	7.5
micrinite	0.0	0.0	0.0	0.0	0.0	0.0
macrinite	0.0	0.0	0.0	0.0	0.0	0.0
secretinite	1.3	2.0	0.0	0.0	0.0	0.0
funginite	0.0	0.0	0.0	0.0	0.0	0.0
inertodetrinite	4.7	7.4	35.5	43.4	2.8	2.9
Total Inertinite	14.7	23.0	52.7	64.3	12.4	12.7
sporinite	2.7	4.2	1.7	2.1	0.8	0.8
cutinite	0.0	0.0	0.6	0.7	0.0	0.0
resinite	0.0	0.0	0.0	0.0	0.0	0.0
alginite	0.0	0.0	0.0	0.0	0.0	0.0
liptodetrinite	0.0	0.0	0.0	0.0	0.0	0.0
suberinite	0.0	0.0	0.0	0.0	0.0	0.0
exsudatinite	0.0	0.0	0.0	0.0	0.0	0.0
Total Liptinite	2.7	4.2	2.3	2.8	0.8	0.8
Total Reactive	49.0	76.9	29.3	35.6	85.2	87.3
silicate (clay+quartz)	28.3		17.4		1.2	
sulfide	6.7		0.6		0.0	
carbonate	1.3		0.0		1.0	
other	0.0		0.0		0.2	
Total Mineral matter	36.3		18.0		2.4	

B.2. Vitrinite reflectance Histograms

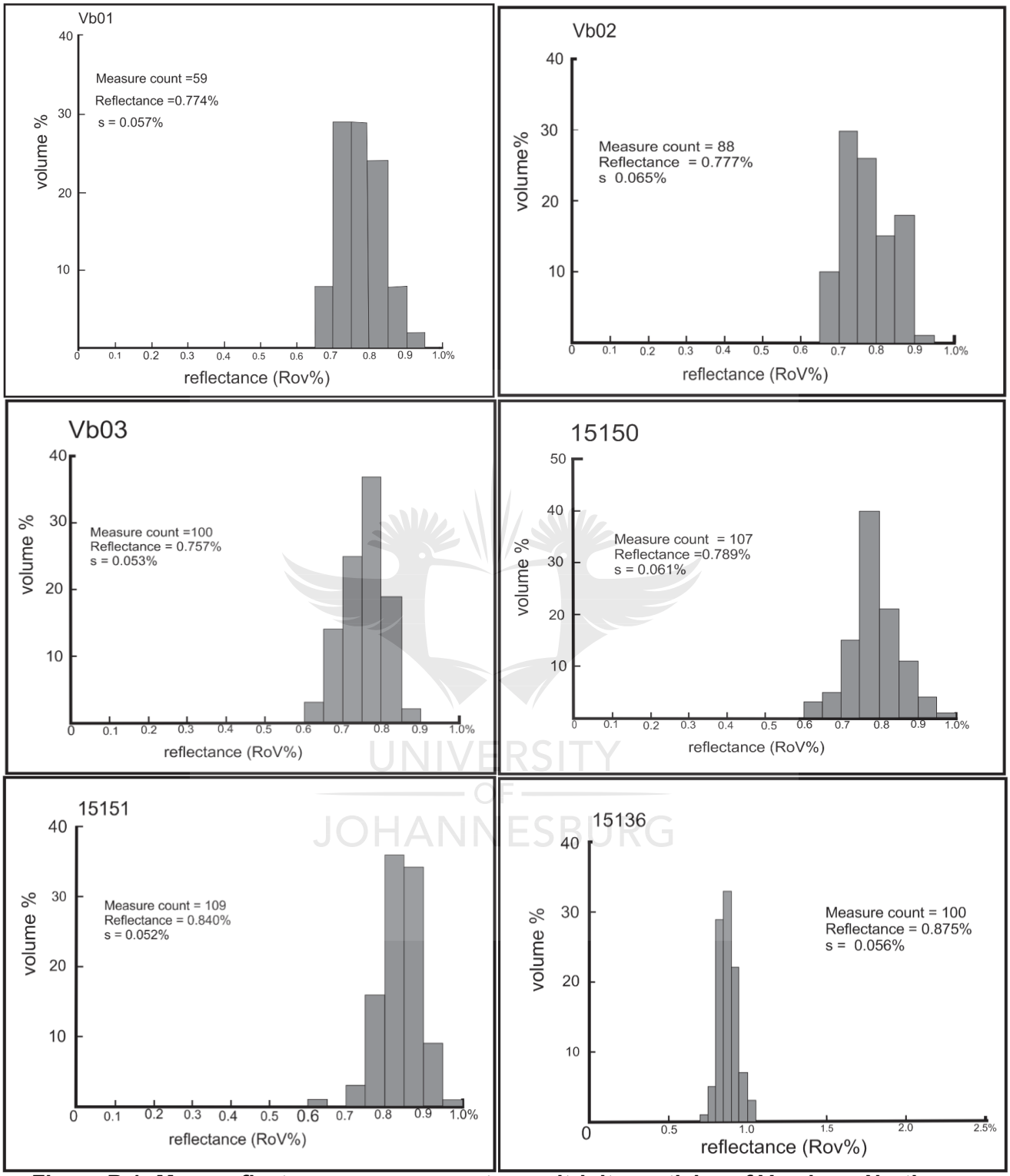

Figure B.1: Mean reflectance measurements on vitrinite particles of Voorburg North, samples indicating a unimodal distribution.

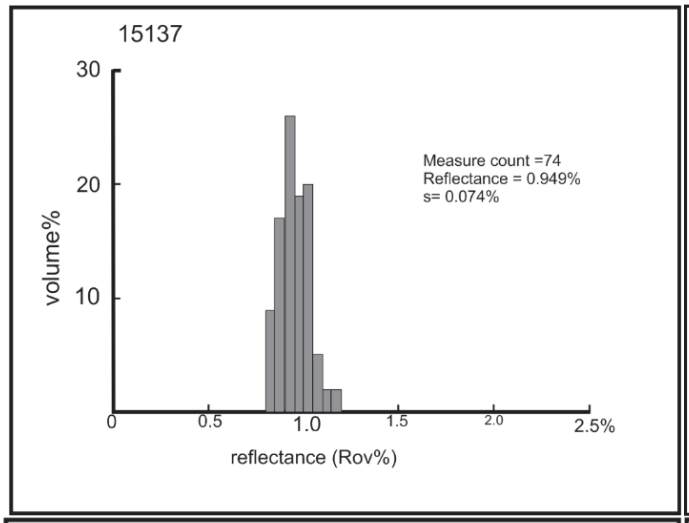

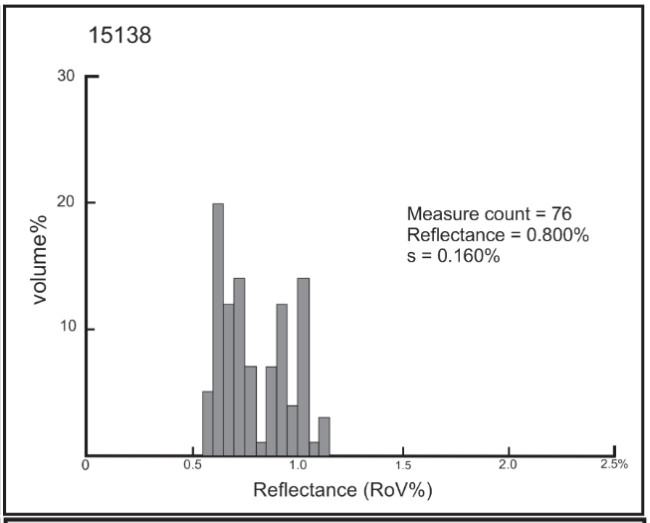

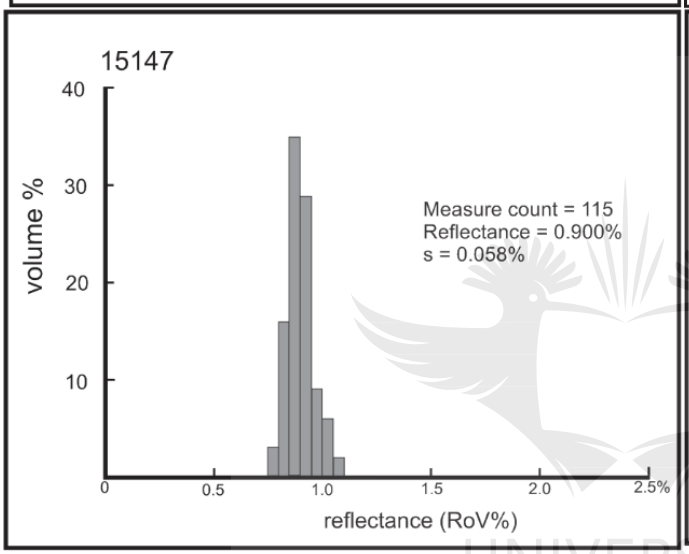

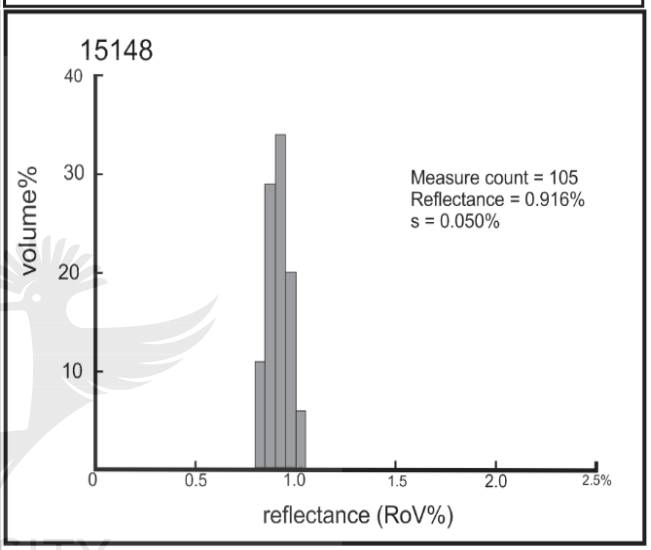

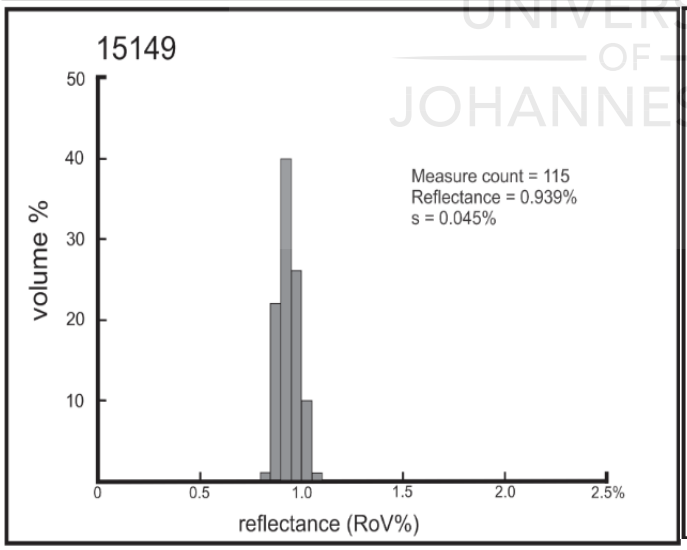

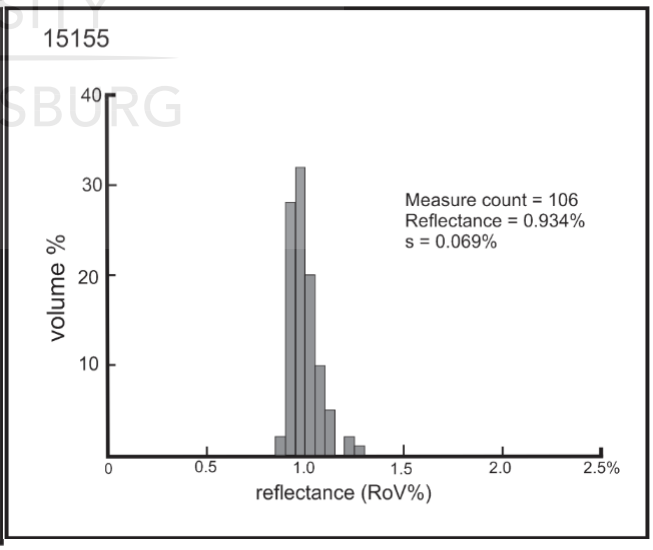

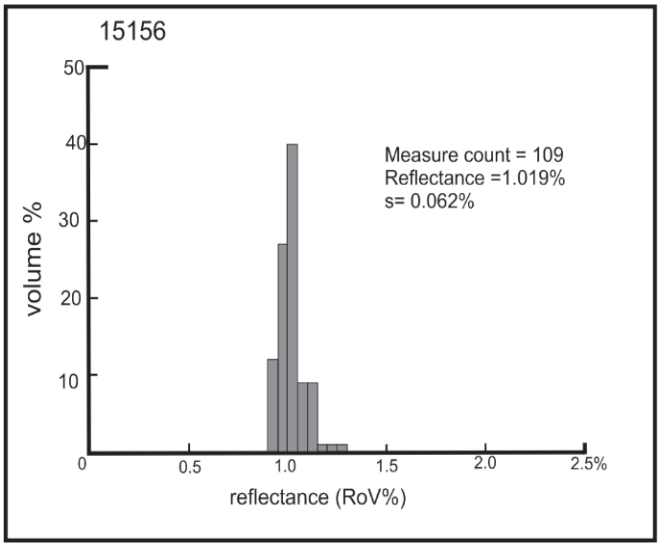

Figure B.2: Mean reflectance measurements on vitrinite particles of Voorburg South, with most samples indicating a unimodal distribution with the exception of sample 15139 which indicated a bimodal distribution.

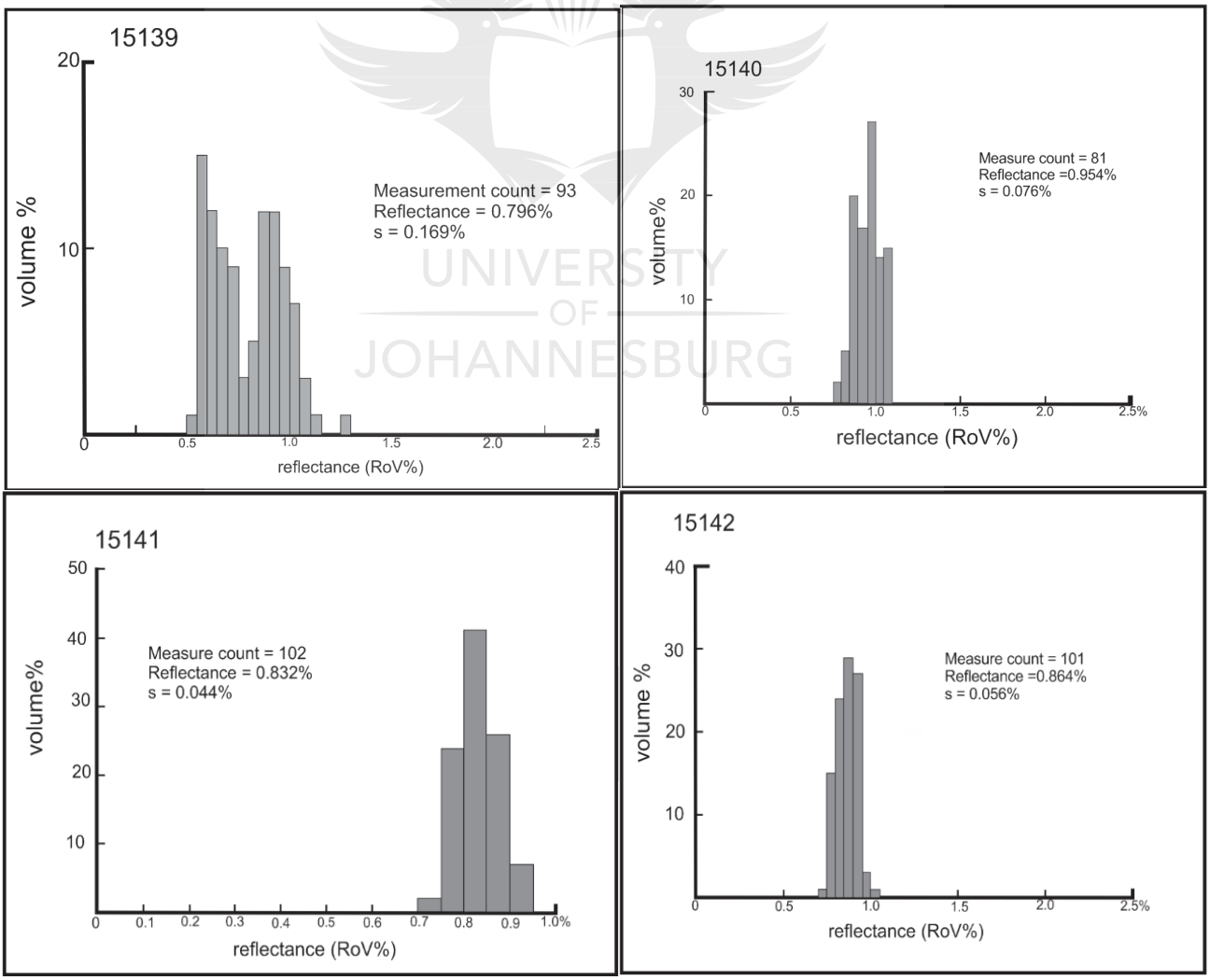

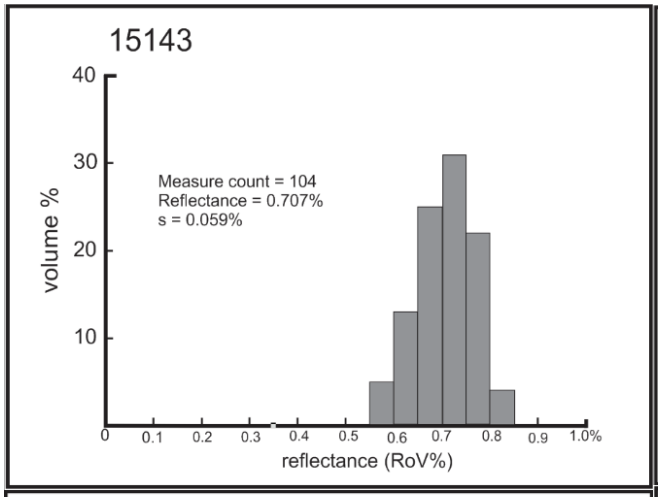

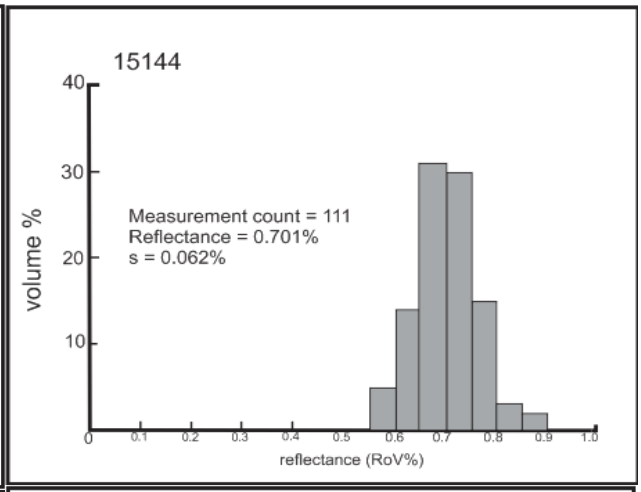

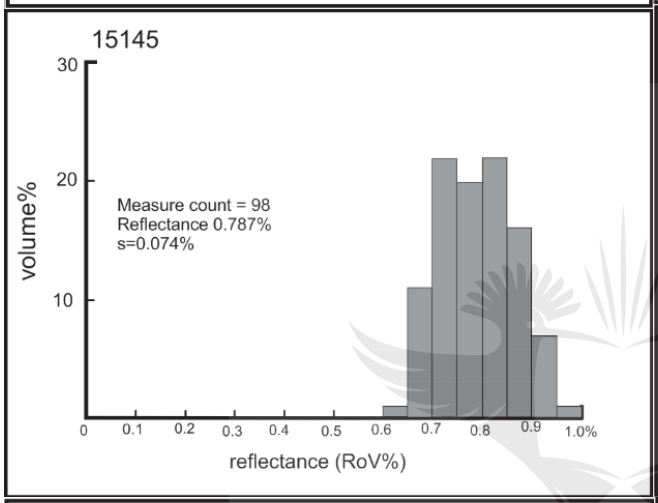

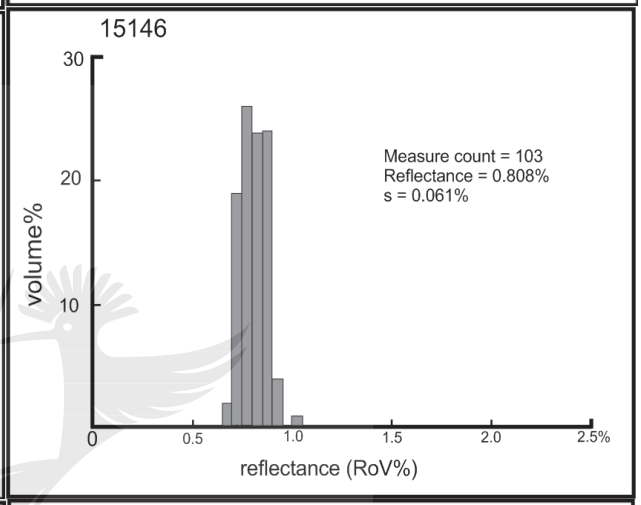

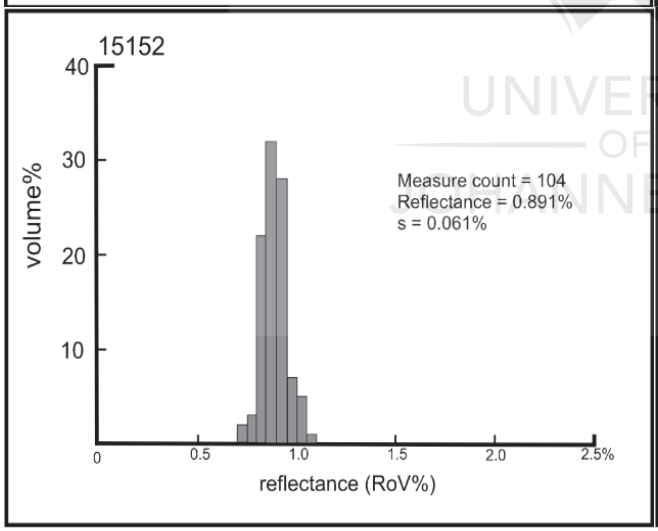

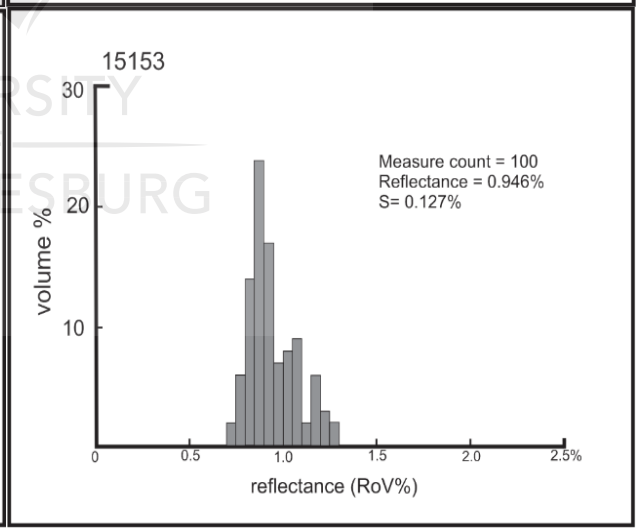

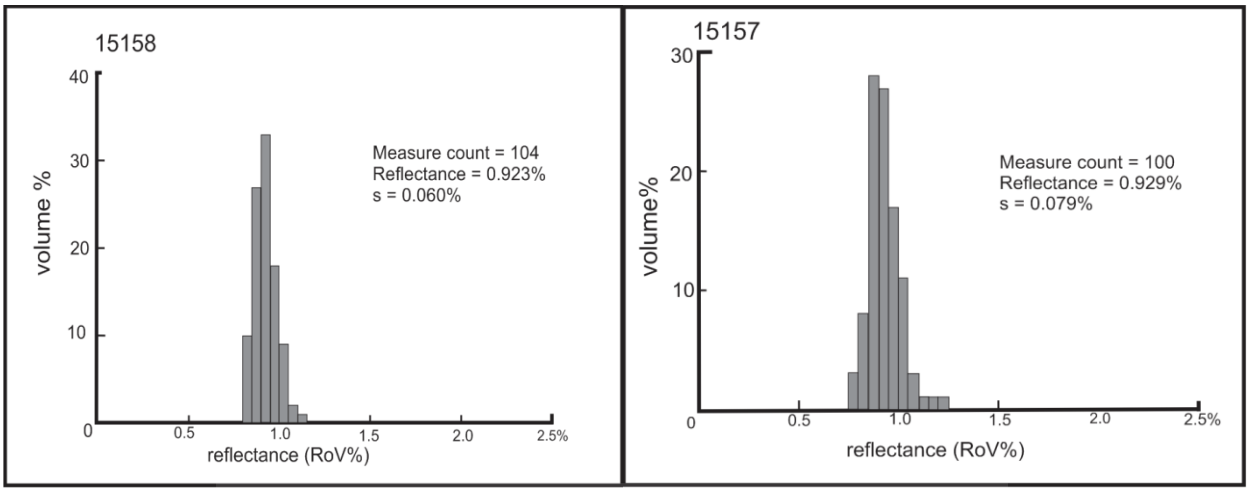

Figure B.3: Mean reflectance measurements on vitrinite particles of Makhado are. Both unimodal and bimodal distribution (samples 15139 and 15153) were noted.

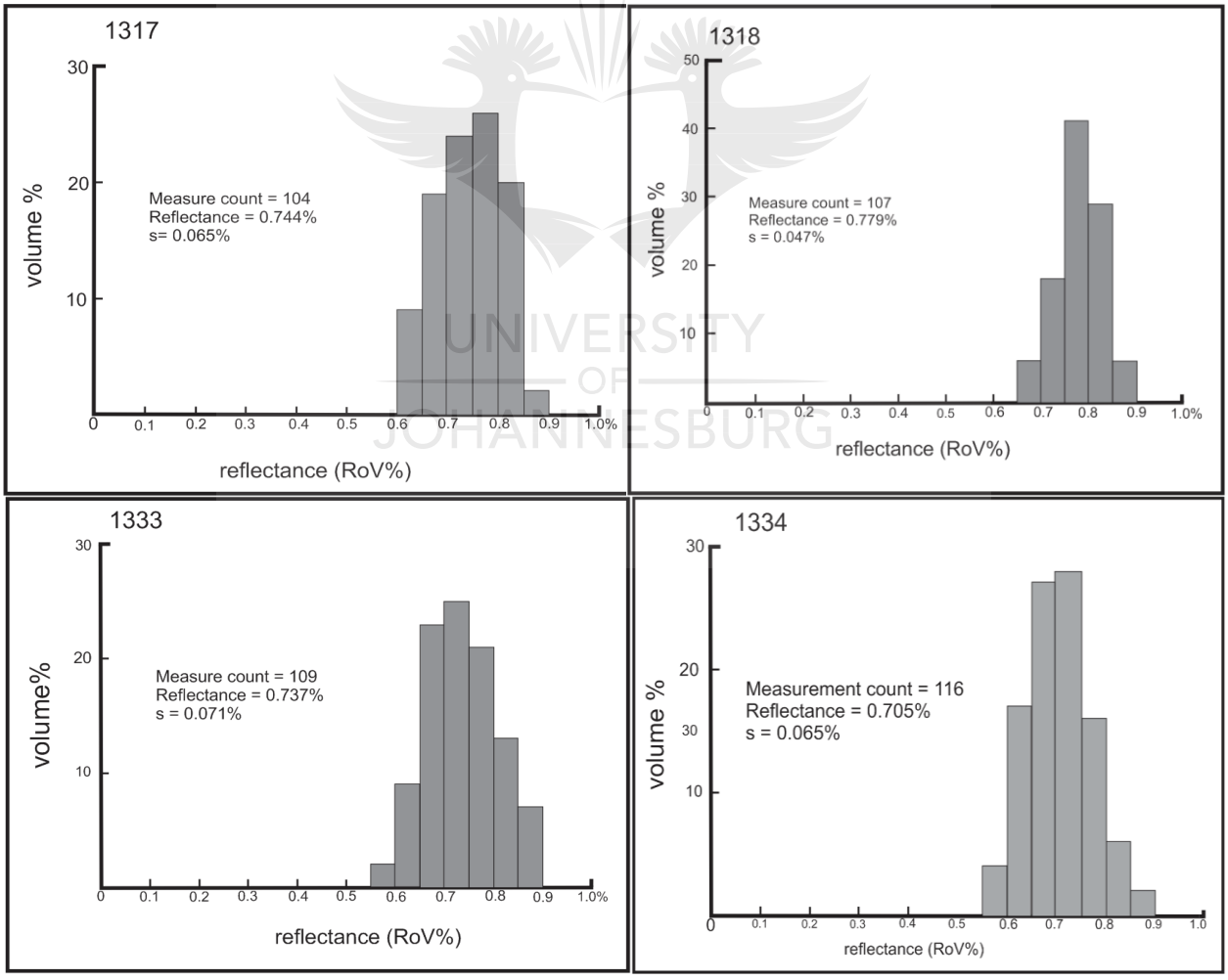

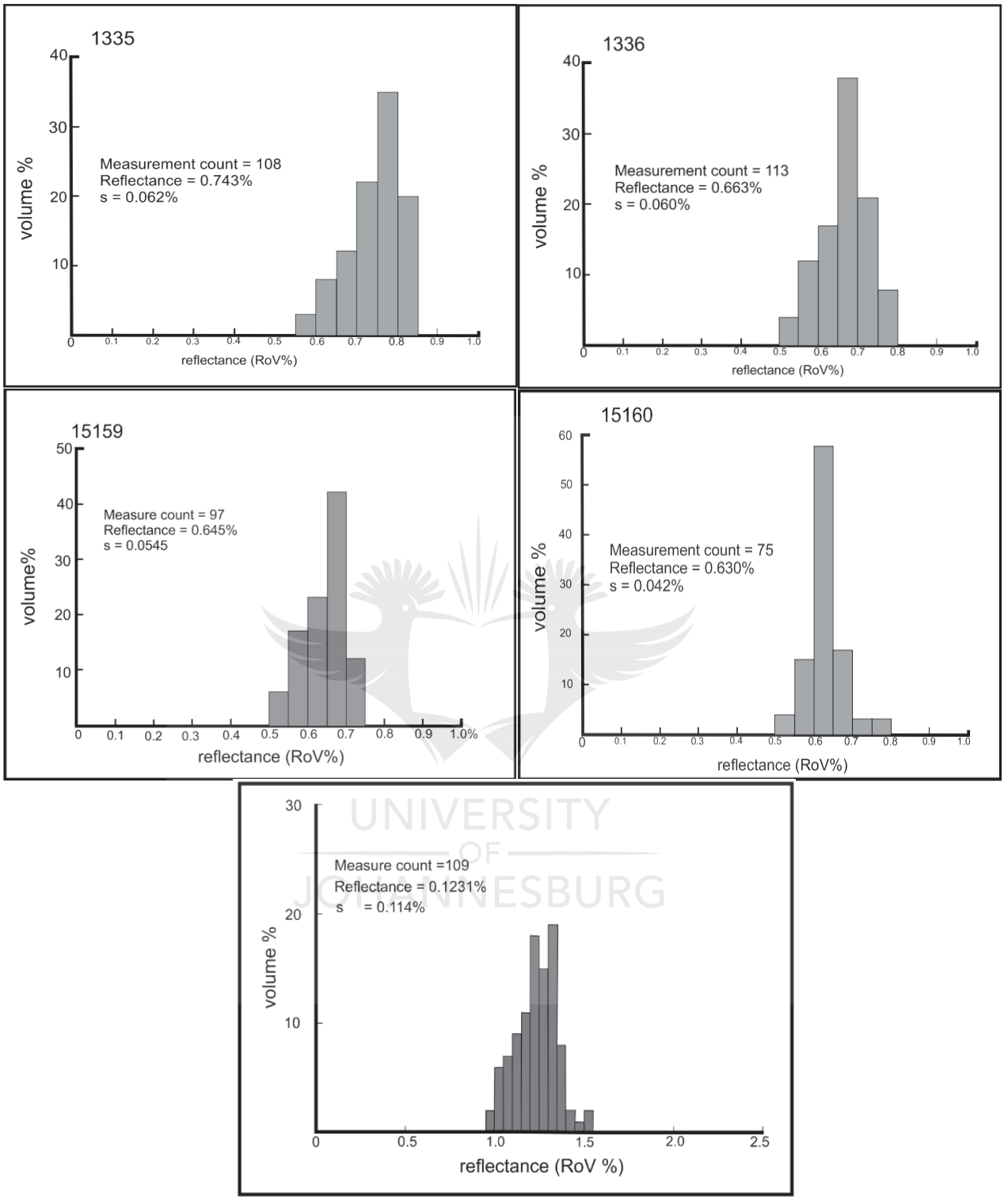

Figure B.4: Mean reflectance measurements on vitrinite particles of Vele, Waterberg and Tshikondeni. Both unimodal and bimodal distribution (15117) were noted.

B.3. Abnormal conditions analysis

Table B.1.5: Data from ACA

Location	Voorburg North					Voorburg South									Makhado			
Borehole ID	V07BS01			V10BS03		R637005			R63701LD			F578004			T190BS03		SD65801LD	
Sample no.	VB01	VB02	VB03	15150	15151	15136	15137	15138	15147	15148	15149	15154	15155	15156	15139	15140	15152	15153
Fresh	85.7	94.9	90.9	91.0	90.9	76.6	90	91.7	89.3	86	82.2	90.6	89.3	92.1	87.9	88.7	91.8	89.8
Fissures few	5.6	2.2	4.7	6.3	7.9	15.0	6.6	7.6	6.3	8.1	12.6	3.8	6.8	2.7	10.4	4.6	4.2	6.8
Fissure many	0.5	0.0	0.0	0.2	0.0	0.4	0.0	0.0	0.4	0.2	4.6	1.1	1.0	0.0	0.0	0.4	0.2	0.2
Crack few	4.8	0.7	2.0	1.5	0.6	2.6	2.0	0.5	2.0	5.0	0.0	4.5	2.3	4.9	1.3	4.3	3.6	2.7
Crack many	0.8	0.0	0.7	0.0	0.3	0.0	0.2	0.0	0.2	0.0	0.0	0.0	0.0	0.0	0.0	0.6	0.2	0.0
Cracks with mineral	2.6	2.2	0.5	0.0	0.0	4.4	1.0	0.2	0.9	0.5	0.0	0.0	0.0	0.0	0.4	1.2	0.0	0.0
Desiccation few	0.0	0.0	1.2	1.0	0.3	1.0	0.2	0.0	0.9	0.2	0.6	0.0	0.6	0.3	0.0	0.2	0.0	0.5
Desiccation many	0.0	0.0	0.0	0.0	0.0	0.0	0.0	0.0	0.0	0.0	0.0	0.0	0.0	0.0	0.0	0.0	0.0	0.0
Discoloured	0.0	0.0	0.0	0.0	0.0	0.0	0.0	0.0	0.0	0.0	0.0	0.0	0.0	0.0	0.0	0.0	0.0	0.0
Heat affected	0.0	0.0	0.0	0.0	0.0	0.0	0.0	0.0	0.0	0.0	0.0	0.0	0.0	0.0	0.0	0.0	0.0	0.0
Alteration mineral	0.0	0.0	0.0	0.0	0.0	0.0	0.0	0.0	0.0	0.0	0.0	0.0	0.0	0.0	0.0	0.0	0.0	0.0
Total abnormal condition	14.3	5.1	9.1	9.0	9.1	23.4	10.0	8.3	10.7	14.0	17.8	9.4	10.7	7.9	12.1	11.3	8.2	10.2

Location	Makhado								Vele						Waterberg		Tshikondeni
Borehole ID	T07BS		C699001				F645BS02		CP17BS02		OV24BS01				Z0ne 8+9	Zone 7+6	ROM
Sample no	15141	15142	15143	15144	15145	15146	15157	15158	1317	1318	1333	1334	1335	1336	15159	15160	15117
Fresh	87.0	91.1	91.8	88.9	87.5	85.1	86.4	87.9	87.3	87.3	77	87.4	76.8	88.3	87.0	83.2	83.2
Fissures few	10.1	6.3	5.4	6.4	7.1	10.7	7.8	5.9	2.5	4.4	4.5	3.0	7.8	5.0	9.1	9.8	10.4
Fissure many	0.0	0.0	0.0	0.0	1.3	0.0	0.0	0.3	0.0	0.0	0.3	0.0	0	0.0	0.0	3.7	0.8
Crack few	2.7	1.9	1.6	2.5	3.8	4.2	5.8	5.9	1.0	1.7	0.5	3.0	4.2	2.0	2.8	2.8	5.0
Crack many	0.2	0.0	0.0	0.0	0.3	0.0	0.0	0.0	0.3	1.2	0.5	0.2	1.2	0.0	0.0	0.0	0.0
Cracks with mineral	0.0	0.0	1.2	1.2	0.0	0.0	0.0	0.0	0.0	0.0	0.0	0.0	0.0	0.0	0.0	0.0	0.0
Desiccation few	0.0	0.7	0.0	1.0	0.0	0.0	1.0	0.0	8.9	5.4	15.5	5.2	10.0	4.5	1.1	0.5	0.6
Desiccation many	0.0	0.0	0.0	0.0	0.0	0.0	0.0	0.0	0.0	0.0	0.0	0.0	0.0	0.0	0.0	0.0	0.0
Discoloured	0.0	0.0	0.0	0.0	0.0	0.0	0.0	0.0	0.0	0.0	0.0	0.0	0.0	0.0	0.0	0.0	0.0
Heat affected	0.0	0.0	0.0	0.0	0.0	0.0	0.0	0.0	0.0	0.0	0.0	0.0	0.0	0.0	0.0	0.0	0.0
Alteration mineral	0.0	0.0	0.0	0.0	0.0	0.0	0.0	0.0	0.0	0.0	0.0	0.0	0.0	0.0	0.0	0.0	0.0
Total abnormal condition	13	8.9	8.2	11.1	12.5	14.9	13.6	12.1	12.7	12.7	23	12.6	23.2	11.7	13	16.8	16.8

Appendix C: EMPA and SEM analyses of pyrite and carbonates

C.1. EMPA data for pyrite

Table C.1 1: EMPA for different pyrite grains (wt. %)

Sample No	15143	15143	15143	15143	15143	15143	15143	15143	15143	15143
Sample ID	Pyrite overgrowth	Pyrite overgrowth	Pyrite overgrowth	Pyrite overgrowth	Pyrite overgrowth	Pyrite overgrowth	Framboid	Framboid	Framboid	Framboid
S	43.46	43.80	44.30	43.60	50.24	43.30	50.14	53.19	50.14	53.14
Mn	0.00	0.00	0.00	0.00	0.00	0.01	0.00	0.00	0.01	0.00
Fe	35.36	35.21	35.02	35.96	43.71	36.21	41.62	46.45	43.69	46.11
Co	0.57	0.56	0.60	0.57	0.13	0.58	0.60	0.02	0.01	0.01
Ni	1.51	1.53	1.54	1.56	0.23	1.44	0.82	0.00	0.00	0.00
Cu	0.00	0.00	0.00	0.01	0.01	0.02	0.04	0.04	0.04	0.00
Zn	0.00	0.00	0.00	0.00	0.01	0.00	0.01	0.00	0.00	0.00
As	1.39	1.40	1.42	1.40	0.19	1.29	0.67	0.01	0.02	0.00
Se	0.19	0.20	0.18	0.19	0.03	0.19	0.08	0.00	0.00	0.00
Pb	1.40	0.00	0.00	0.00	0.24	1.25	0.63	0.02	0.02	0.00
Total	83.89	82.7	83.06	83.29	94.8	84.27	94.61	99.72	93.93	99.26

Table C.1.1: EMPA for different pyrite grains (wt. %) continued…

Sample No	15136	15136	15136	15136	15136	VB01	VB01	VB01	VB01
Sample ID	Massive	Massive	Infilling	Infilling	Infilling	Cell filling	Cell filling	Cell filling	Cell filling
S	52.90	53.60	53.12	53.40	53.19	53.85	53.40	52.88	53.34
Mn	0.00	0.00	0.00	0.00	0.00	0.00	0.00	0.00	0.01
Fe	45.87	46.08	45.89	45.95	46.45	46.14	45.96	45.07	46.08
Co	0.02	0.01	0.00	0.00	0.02	0.01	0.01	0.01	0.01
Ni	0.00	0.00	0.00	0.01	0.00	0.01	0.00	0.00	0.00
Cu	0.00	0.00	0.00	0.00	0.04	0.00	0.00	0.02	0.00
Zn	0.00	0.00	0.00	0.00	0	0.02	0.00	0.00	0.01
As	0.00	0.00	0.00	0.00	0.01	0.03	0.01	0.01	0.00
Se	0.00	0.00	0.00	0.00	0	0.00	0.00	0.00	0.00
Pb	0.01	0.02	0.01	0.00	0.02	0.01	0.01	0.05	0.00
Total	98.8	99.71	99.02	99.36	99.73	100.07	99.4	98.04	99.46

Sample No	VB01	VB01	VB01	VB01	VB01
Sample ID	cell filling	Massive	Massive	Massive	Massive
S	53.84	53.59	53.65	52.87	53.13
Mn	0.00	0.00	0.01	0.00	0.00
Fe	46.36	46.28	46.12	45.95	46.57
Co	0.00	0.01	0.00	0.00	0.00
Ni	0.00	0.00	0.01	0.01	0.00
Cu	0.00	0.01	0.00	0.02	0.00
Zn	0.00	0.00	0.00	0.00	0.00
As	0.03	0.02	0.06	0.01	0.04
Se	0.01	0.01	0.00	0.00	0.00
Pb	0.01	0.00	0.01	0.02	0.02
Total	100.26	99.92	99.86	98.89	99.76

C.2. SEM data for pyrite

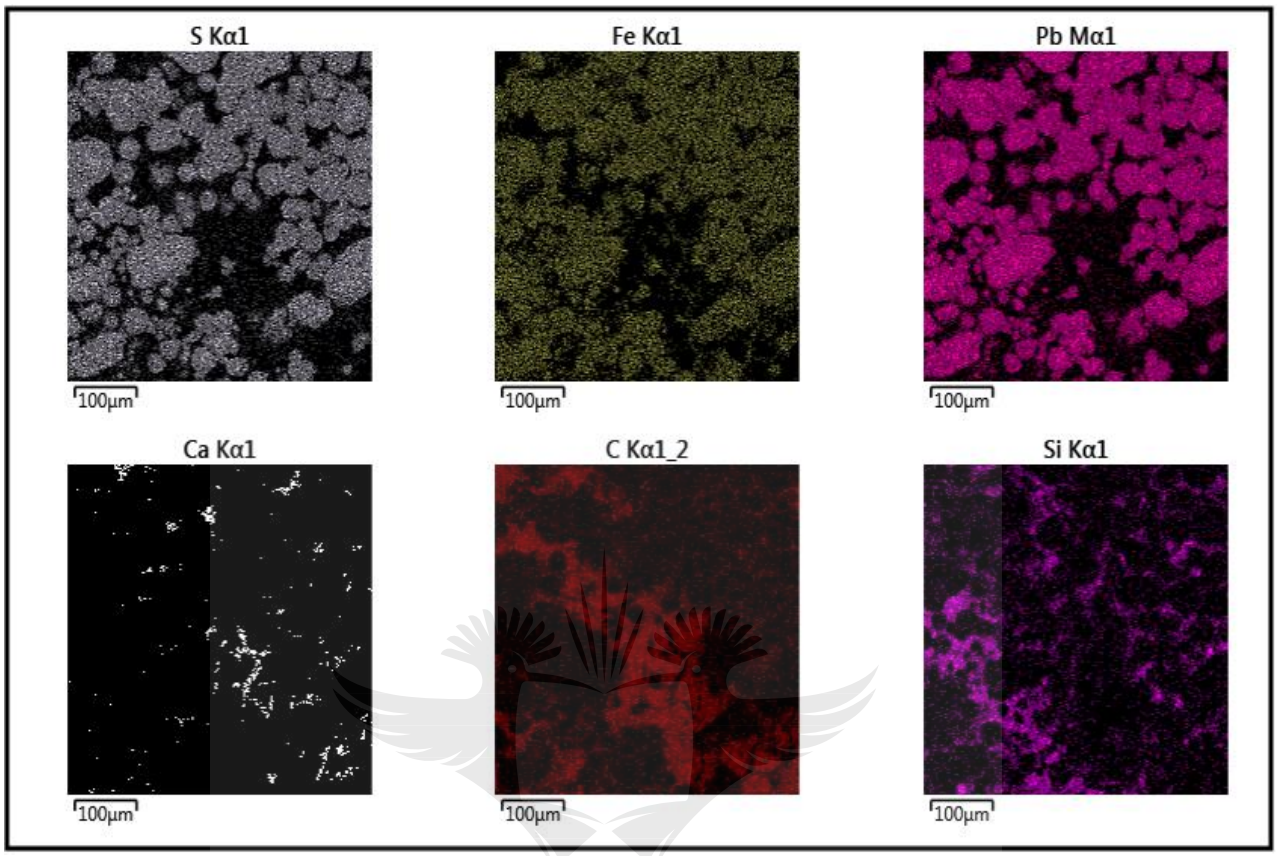

Figure C.1: SEM – EDS elemental maps of botryoidal pyrite. The pyrite shows enrichment of Pb element. The caα shows the cleats associated with the botryoidal pyrite.

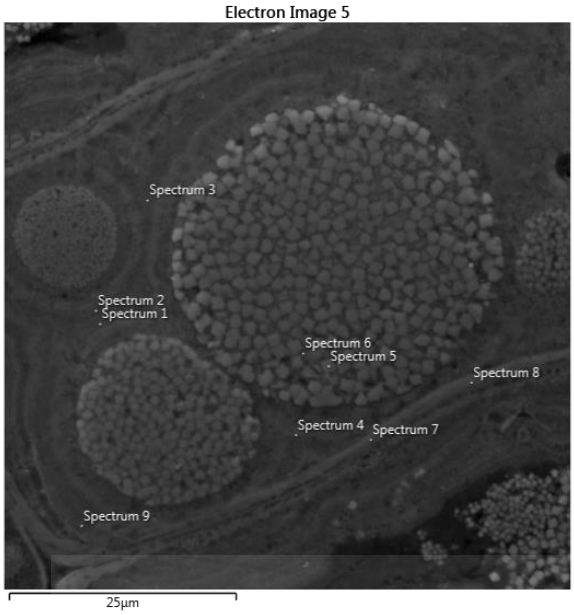

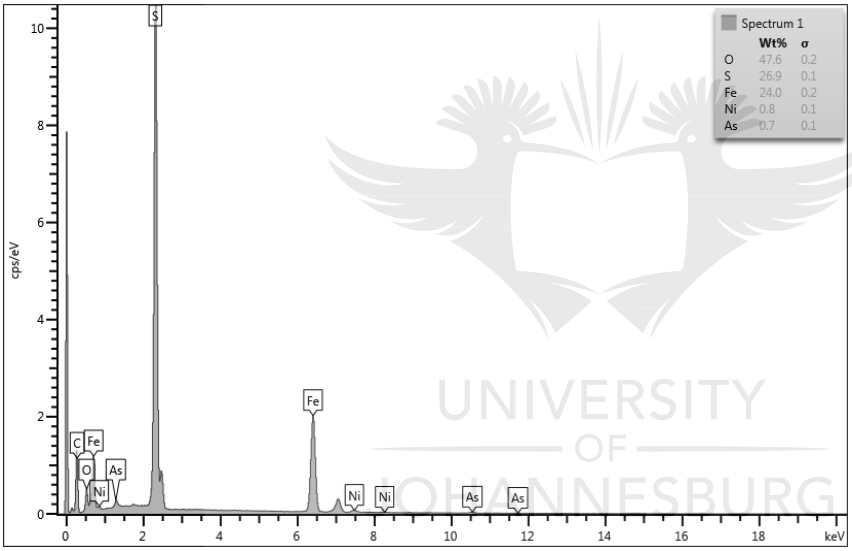

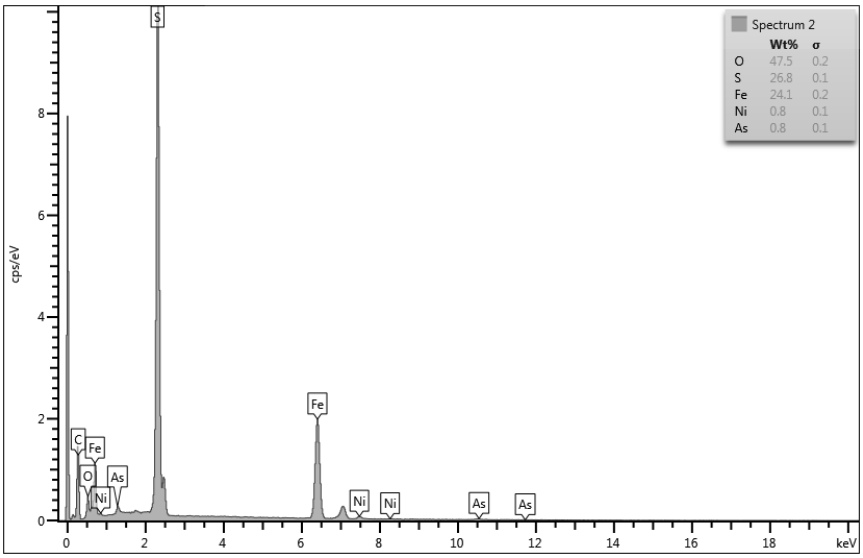

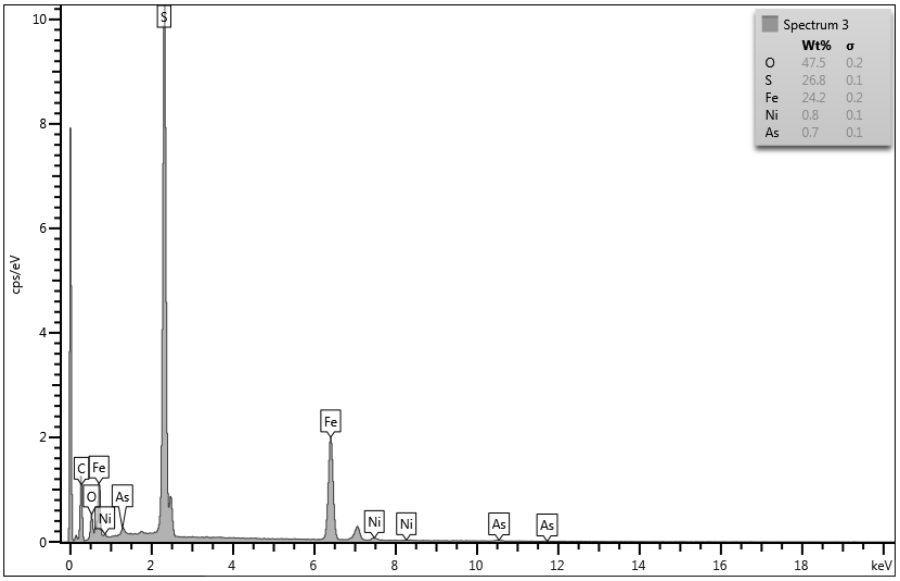

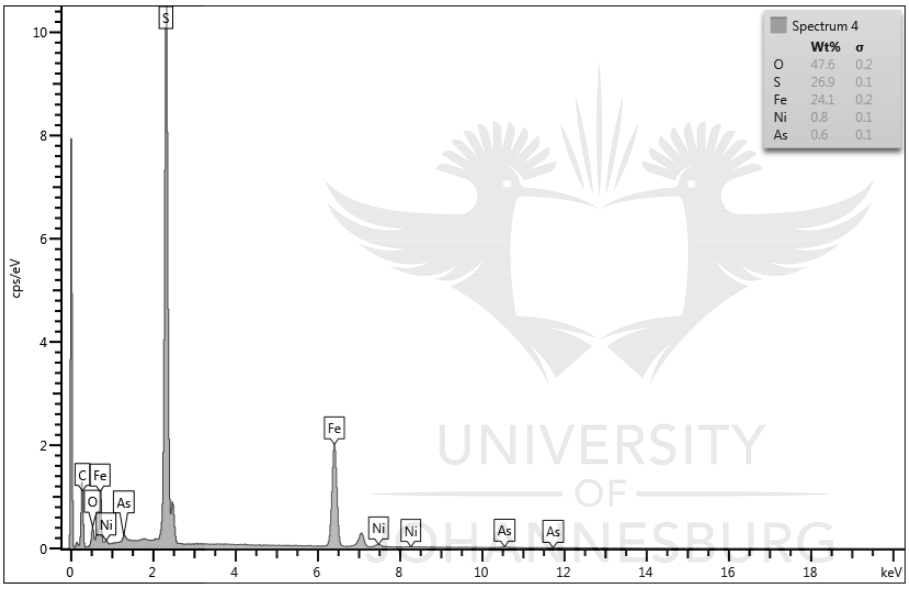

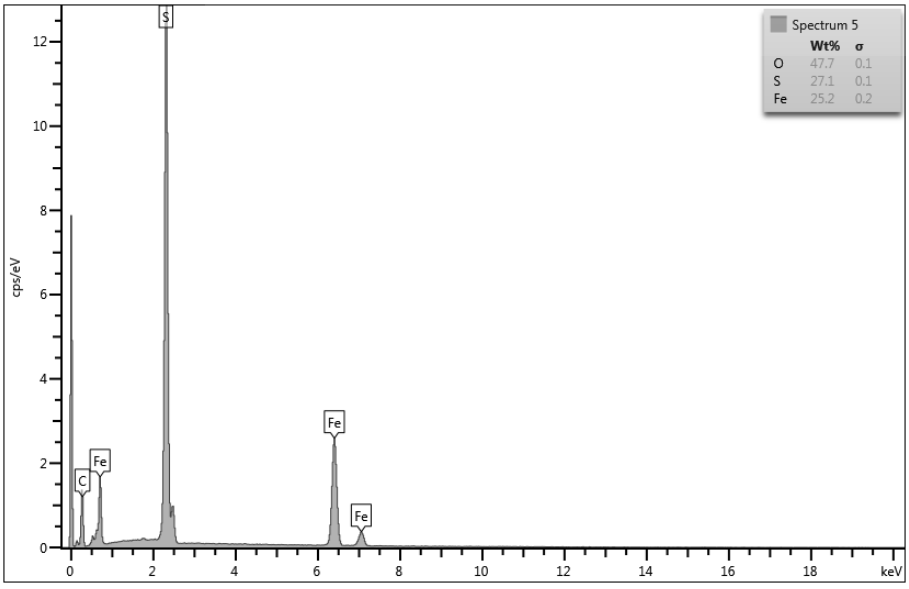

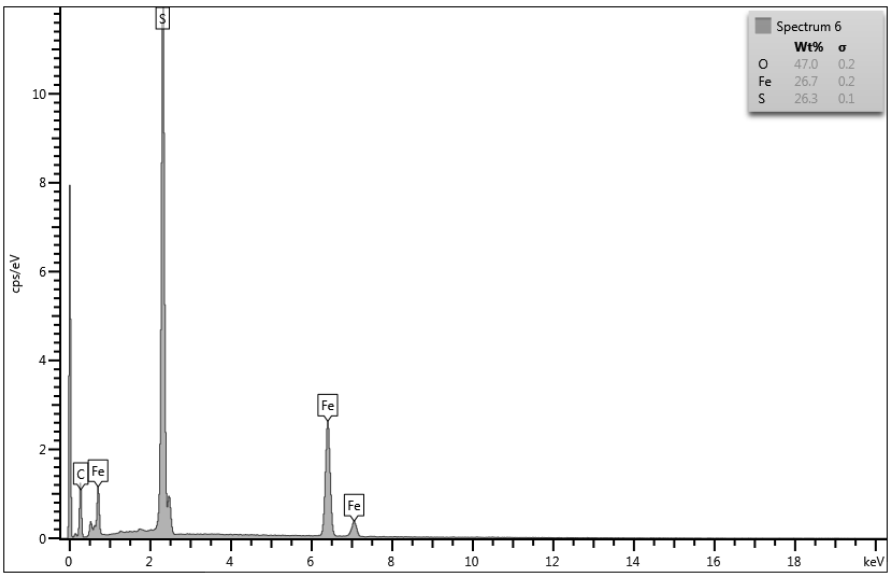

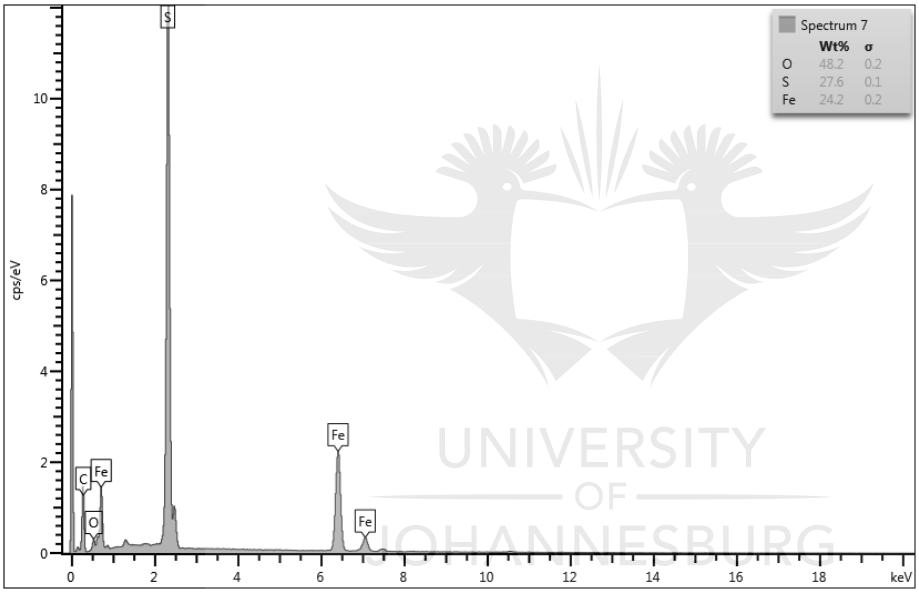

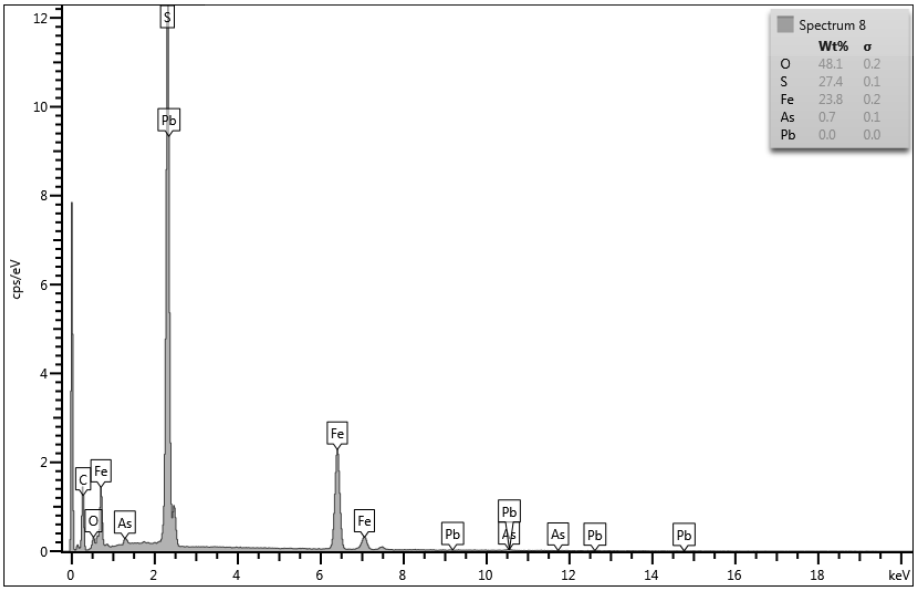

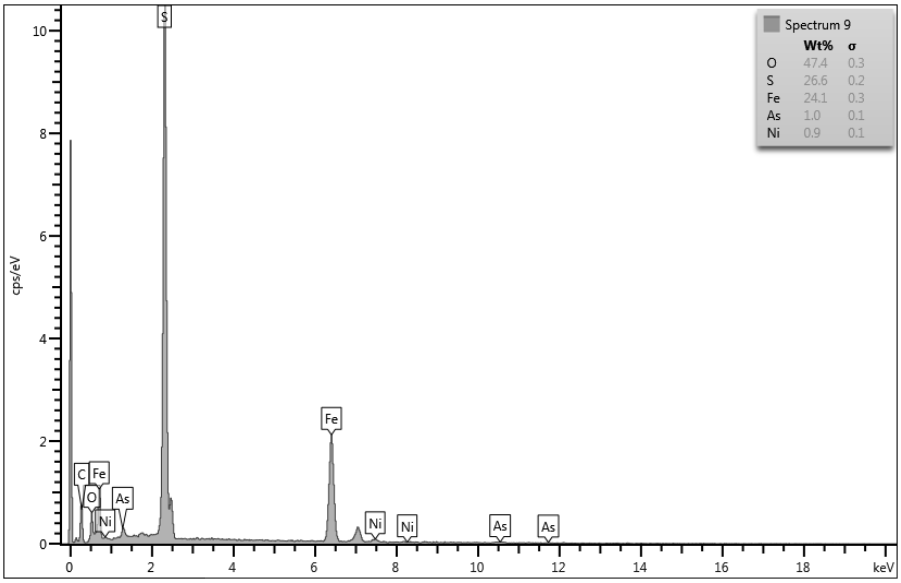

Figure C.2: SEM-EDS spectra peaks for botryoidal pyrite

C.3. EMPA for different carbonates

Table C.1.2: EMPA data for carbonates (wt. %) NS= nodular siderite, TS=Trigonal siderite AC= ankerite cleats

Sample No	15148	15148	15148	15148	15148	15148	15148	15148	15148	15148
Sample id	NS	NS	NS	NS	NS	NS	NS	NS	NS	NS
CaO	5.70	3.86	2.78	2.98	2.08	3.34	4.73	2.50	2.65	6.11
MgO	2.82	3.08	2.05	2.38	1.64	2.53	3.50	1.80	2.23	3.65
SrO	0.01	0.04	0.00	0.00	0.02	0.00	0.00	0.00	0.00	0.03
SiO2	0.11	0.09	0.04	0.23	0.93	0.84	0.06	0.04	0.08	0.31
Al2O3	0.04	0.11	0.05	4.53	0.34	0.51	0.07	0.05	0.05	0.15
FeO	48.13	51.03	53.72	52.56	37.34	51.65	51.09	53.95	52.74	48.86
MnO	2.32	1.32	1.53	1.99	0.47	1.55	0.36	1.53	1.58	0.13
BaO	0.04	0.00	0.04	0.12	0.05	0.00	0.00	0.04	0.04	0.00
ZnO	0.05	0.00	0.01	0.19	0.00	0.00	0.00	0.06	0.02	0.02
CO2	40.78	40.47	39.78	35.02	57.10	39.54	40.13	40.01	40.61	40.73
Total	100.00	99.99	99.99	99.99	99.97	99.97	99.94	99.99	100.00	99.99
Number of ions on the basis of 6O										
Ca	0.223	0.128	0.111	0.122	0.069	0.132	0.186	0.100	0.105	0.238
Mg	0.154	0.156	0.114	0.136	0.075	0.140	0.192	0.100	0.122	0.198
Sr	0.00	0.000	0.000	0.000	0.000	0.000	0.000	0.000	0.000	0.001
Si	0.004	0.031	0.001	0.009	0.029	0.031	0.002	0.002	0.003	0.011
Al	0.002	0.022	0.002	0.204	0.012	0.022	0.003	0.002	0.002	0.006
Fe	1.471	1.598	1.674	1.684	0.962	1.596	1.572	1.679	1.626	1.485
Mn	0.072	0.038	0.048	0.065	0.012	0.048	0.011	0.048	0.049	0.004
Ba	0.001	0.000	0.001	0.002	0.001	0.000	0.000	0.001	0.001	0.000
Zn	0.001	0.000	0.000	0.005	0.000	0.000	0.000	0.002	0.001	0.000
C	2.034	2.024	2.023	1.831	2.402	1.994	2.015	2.033	2.044	2.021
Total	3.961	3.997	3.974	4.058	3.563	3.964	3.981	3.965	3.952	3.965

Table C.1.2 continued: EMPA data for carbonates (wt. %)

Sample No	15148	15148	15148	15148	15143	15143	15143
Sample id	TS	TS	TS	TS	AC	AC	AC
CaO	1.11	1.30	0.59	0.55	31.13	30.16	30.35
MgO	0.55	0.92	0.58	0.39	13.65	12.49	14.68
SrO	0.02	0.00	0.03	0.00	0.07	0.04	0.05
SiO2	0.04	0.04	0.04	0.06	0.09	0.11	0.18
Al2O3	0.00	0.01	0.03	0.04	0.17	0.08	0.10
FeO	58.53	54.57	58.69	59.14	9.36	11.70	8.90
MnO	1.38	3.70	0.63	0.53	0.10	0.06	0.10
BaO	0.00	0.05	0.00	0.00	0.04	0.04	0.07
ZnO	0.02	0.00	0.01	0.00	0.02	0.00	0.03
CO2	38.28	39.36	39.39	39.26	45.36	45.25	45.55
Total	99.93	99.96	100.00	99.96	100.00	99.93	100.00
Number of ions on the basis of 6O							
Ca	0.045	0.053	0.024	0.022	1.076	1.050	1.044
Mg	0.032	0.052	0.033	0.022	0.656	0.605	0.703
Sr	0.000	0.000	0.001	0.000	0.001	0.001	0.001
Si	0.002	0.002	0.002	0.002	0.003	0.003	0.006
Al	0.000	0.000	0.001	0.002	0.006	0.003	0.004
Fe	1.874	1.721	1.854	1.873	0.252	0.318	0.239
Mn	0.045	0.118	0.020	0.017	0.003	0.002	0.003
Ba	0.000	0.001	0.000	0.000	0.001	0.001	0.001
Zn	0.001	0.000	0.000	0.000	0.001	0.000	0.001
C	2.000	2.026	2.031	2.029	1.997	2.007	1.996
Total	3.998	3.972	3.966	3.967	3.996	3.988	3.996

C.4. SEM data for carbonates

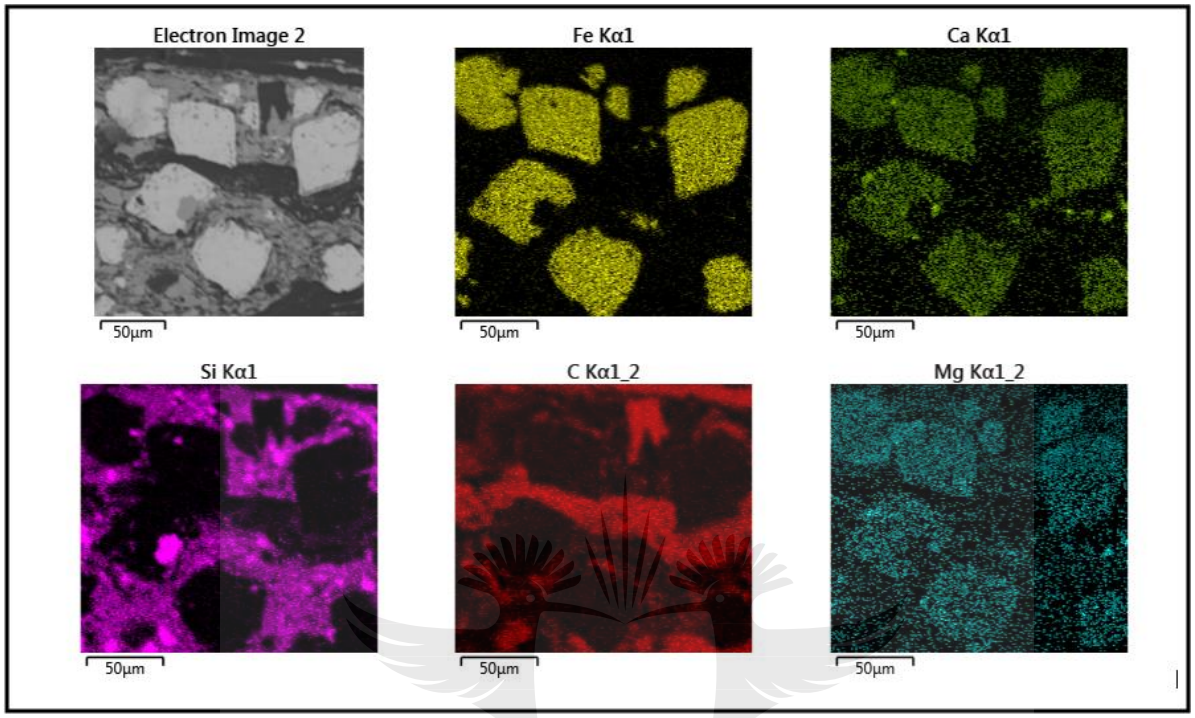

Figure C.3: SEM-EDS elemental maps of botryoidal pyrite. The pyrite shows enrichment of Pb element. The caα shows the cleats associated with the botryoidal pyrite.